

# Microscopic and spectroscopic analysis of biogenic aerosols

Dissertation

zur Erlangung des Grades eines  
'Doktor rerum naturalium (Dr. rer. nat.)' der Fachbereiche:  
08 - Physik, Mathematik und Informatik,  
09 - Chemie, Pharmazie und Geowissenschaften,  
10 - Biologie,  
Universitätsmedizin

verfasst und vorgelegt von

Christopher Pöhlker

geboren am 20. Oktober 1983  
in Lippe-Detmold

Max Planck Graduate Center  
mit der Johannes Gutenberg-Universität Mainz

angefertigt am Max-Planck-Institut für Chemie

Mainz, 2013



Max Planck **Graduate Center**  
mit der Johannes Gutenberg-Universität Mainz





I hereby declare that I wrote the dissertation submitted without any unauthorized external assistance and used only sources acknowledged in the work. All textual passages which are appropriated verbatim or paraphrased from published and unpublished texts as well as all information obtained from oral sources are duly indicated and listed in accordance with bibliographical rules. In carrying out this research, I complied with the rules of standard scientific practice as formulated in the statutes of the Johannes Gutenberg University Mainz to insure standard scientific practice.

Mainz, 19. February 2013, Christopher Pöhlker



### *Der Kreisel*

*Ein Philosoph trieb sich immer dort herum, wo Kinder spielten. Und sah er einen Jungen, der einen Kreisel hatte, so lauerte er schon. Kaum war der Kreisel in Drehung, verfolgte ihn der Philosoph, um ihn zu fangen. Dass die Kinder lärmten und ihn von ihrem Spielzeug abzuhalten suchten, kümmerte ihn nicht, hatte er den Kreisel, solange er sich noch drehte, gefangen, war er glücklich, aber nur einen Augenblick, dann warf er ihn zu Boden und ging fort. Er glaubte nämlich, die Erkenntnis jeder Kleinigkeit, also zum Beispiel auch eines sich drehenden Kreisels, genüge zur Erkenntnis des Allgemeinen. Darum beschäftigte er sich nicht mit den großen Problemen, das schien ihm unökonomisch. War die kleinste Kleinigkeit wirklich erkannt, dann war alles erkannt, deshalb beschäftigte er sich nur mit dem sich drehenden Kreisel. Und immer wenn die Vorberreitungen zum Drehen des Kreisels gemacht wurden, hatte er Hoffnung, nun werde es gelingen, und drehte sich der Kreisel, wurde ihm im atemlosen Laufen nach ihm die Hoffnung zur Gewissheit, hielt er aber dann das dumme Holzstück in der Hand, wurde ihm übel und das Geschrei der Kinder, das er bisher nicht gehört hatte und das ihm jetzt plötzlich in die Ohren fuhr, jagte ihn fort, er taumelte wie ein Kreisel unter einer ungeschickten Peitsche.*

*Franz Kafka*



# Abstract

Aerosol particles are important actors in the Earth's atmosphere and climate system. They scatter and absorb sunlight, serve as nuclei for water droplets and ice crystals in clouds and precipitation, and are a subject of concern for public health. Atmospheric aerosols originate from both natural and anthropogenic sources, and emissions resulting from human activities have the potential to influence the hydrological cycle and climate. An assessment of the extent and impacts of this human force requires a sound understanding of the natural aerosol background. This dissertation addresses the composition, properties, and atmospheric cycling of biogenic aerosol particles, which represent a major fraction of the natural aerosol burden. The main focal points are: (i) Studies of the autofluorescence of primary biological aerosol particles (PBAP) and its application in ambient measurements, and (ii) X-ray microscopic and spectroscopic investigations of biogenic secondary organic aerosols (SOA) from the Amazonian rainforest.

Autofluorescence of biological material has received increasing attention in atmospheric science because it allows real-time monitoring of PBAP in ambient air, however it is associated with high uncertainty. This work aims at reducing the uncertainty through a comprehensive characterization of the autofluorescence properties of relevant biological materials. Fluorescence spectroscopy and microscopy were applied to analyze the fluorescence signatures of pure biological fluorophores, potential non-biological interferences, and various types of reference PBAP. Characteristic features and fingerprint patterns were found and provide support for the operation, interpretation, and further development of PBAP autofluorescence measurements. Online fluorescence detection and offline fluorescence microscopy were jointly applied in a comprehensive bioaerosol field measurement campaign that provided unprecedented insights into PBAP-linked biosphere-atmosphere interactions in a North-American semi-arid forest environment. Rain showers were found to trigger massive bursts of PBAP, including high concentrations of biological ice nucleators that may promote further precipitation and can be regarded as part of a bioprecipitation feedback cycle in the climate system.

In the pristine tropical rainforest air of the Amazon, most cloud and fog droplets form on biogenic SOA particles, but the composition, morphology, mixing state and origin of these particles is hardly known. X-ray microscopy and spectroscopy (STXM-NEXAFS) revealed distinctly different types of secondary organic matter (carboxyl- vs. hydroxy-rich) with internal structures that indicate a strong influence of phase segregation, cloud and fog processing on SOA formation, and aging. In addition, nanometer-sized potassium-rich particles emitted by microorganisms and vegetation were found to act as seeds for the condensation of SOA. Thus, the influence of forest biota on the atmospheric abundance of cloud condensation nuclei appears to be more direct than previously assumed. Overall, the results of this dissertation suggest that biogenic aerosols, clouds and precipitation are indeed tightly coupled through a bioprecipitation cycle, and that advanced microscopic and spectroscopic techniques can provide detailed insights into these mechanisms.





# Zusammenfassung

Aerosolpartikel spielen eine wichtige Rolle in der Erdatmosphäre, mit starkem Einfluss auf das Klima. Sie streuen und absorbieren Strahlung, wirken als Keime für die Bildung von Wassertropfen und Eiskristallen in Wolken und Niederschlag und sind des Weiteren assoziiert mit einer Vielzahl von Gesundheitsaspekten. Aerosolpartikel stammen aus natürlichen und anthropogenen Quellen, wobei menschliche Emissionen einen starken Einfluss auf die atmosphärische Wasserzirkulation und das Klima ausüben können. Im Rahmen einer Abschätzung des Ausmaßes und der Relevanz dieses menschlichen Einflusses, ist eine genaue Kenntnis des natürlichen Hintergrundaerosols unerlässlich. Die vorliegende Dissertation adressiert die Zusammensetzung, Eigenschaften und atmosphärische Zirkulation biogener Aerosolpartikel, als eine der Hauptkomponenten des genannten Hintergrundaerosols. Die Schwerpunkte dieser Arbeit sind: (i) Studien zur Autofluoreszenz primärer biologischer Aerosolpartikel (PBAP) und ihre Anwendung im Rahmen von Feldmessungen sowie (ii) Röntgenmikroskopische und -spektroskopische Untersuchungen an sekundären organischen Aerosolpartikeln (SOA) biogenen Ursprungs aus dem tropischen Regenwald im Amazonasgebiet.

Die Autofluoreszenz biologischen Materials wird in der Atmosphärenwissenschaft mit gesteigertem Interesse diskutiert, da sie Echtzeitmessungen von PBAP in der Atmosphäre ermöglicht, auch wenn zurzeit noch mit großer Unsicherheit behaftet. Ziel dieser Arbeit ist es, mittels einer eingehenden Untersuchung der Autofluoreszenzeigenschaften relevanter biologischer Materialien, jene Unsicherheit zu mindern. Hierzu wurden Fluoreszenzspektroskopie und -mikroskopie genutzt, um die spektralen Signaturen reiner biologischer Fluorophore, potentieller nichtbiologischer Interferenzen und verschiedener Typen von Referenz-PBAP zu analysieren. Es wurden charakteristische „spektrale Fingerabdrücke“ gefunden, welche die Anwendung, Interpretation und Weiterentwicklung von PBAP-Messungen mittels Autofluoreszenz unterstützen können. Ferner wurden Echtzeit-Fluoreszenzmessungen und Fluoreszenzmikroskopie zusammen in einer umfangreichen Bioaerosol-Feldmesskampagne eingesetzt und erlaubten neuartige Einblicke in PBAP-vermittelte Biosphären-Atmosphären-Austauschprozesse in einem nordamerikanischen, semiariden Waldökosystem. Es wurde festgestellt, dass Niederschläge einen massiven Anstieg der PBAP-Konzentration bedingen, begleitet von erhöhten Konzentrationen biologischer Eiskeime, die ihrerseits weitere Niederschläge initiieren können. Im Klimasystem kann dieser Mechanismus als Variante einer direkten Biosphären-Niederschlags-Rückkopplung angesehen werden.

In der unbelasteten Atmosphäre des Amazonasregenwaldes wird die Mehrzahl der Regen- und Nebeltröpfchen auf biogenen SOA-Partikeln gebildet, deren Zusammensetzung, Morphologie, Mischungszustand und Ursprung noch wenig gekannt sind. Röntgenmikroskopie und -spektroskopie (STXM-NEXAFS) haben das Vorkommen von zwei unterschiedlichen SOA-Typen (carboxyl- vs. hydroxyreich) erwiesen und weiterhin partikelinterne Strukturen offenbart, die auf atmosphärische Alterung, Wolkenprozessierung und Phasentmischungseffekte schließen lassen. Weiterhin wurde das Vorkommen nanometergroßer, von Mikroorganismen und Vegetation emittierter, kaliumreicher

Partikel gefunden, die als Keime für die Kondensation von SOA-Partikeln fungieren. Dies zeigt, dass der Einfluss des Waldökosystems auf das Vorkommen atmosphärischer Wolkentropfen unmittelbarer ist, als zunächst angenommen. Abschließend zeigen die Ergebnisse dieser Dissertation, dass biogene Aerosole mit Wolkenbildung und Niederschlag in einer engen Biosphären-Niederschlags-Rückkopplung verknüpft sind und dass moderne mikroskopische und spektroskopische Techniken hier detaillierte Einblicke erlauben.

# Table of Contents

<b>Abstract</b>	<b>v</b>
<b>Zusammenfassung</b>	<b>vii</b>
<b>1 Introduction and motivation</b>	<b>1</b>
1.1 Aerosols in the Earth system	1
1.2 Primary biological aerosol particles	2
1.3 Biogenic secondary organic aerosols	4
1.4 Knowledge gaps and research objectives	6
1.4.1 Autofluorescence of primary biological aerosol particles	6
1.4.2 Microspectroscopic studies of Amazonian organic aerosols	7
<b>2 Results and conclusions</b>	<b>9</b>
2.1 Autofluorescence of primary biological aerosol particles	9
2.1.1 Biological fluorophores and potential interferences	9
2.1.2 Biological standard particles and aspects of selectivity	10
2.1.3 Ambient measurements and bioprecipitation	10
2.2 Microspectroscopic studies of Amazonian organic aerosols	11
<b>3 References</b>	<b>13</b>
<b>Appendix A List of related publications and presentations</b>	<b>19</b>
<b>Appendix B Selected publications</b>	<b>21</b>
B.1 Pöhlker et al. Atmos. Meas. Tech., 2012	23
Supplementary material	60
B.2 Pöhlker et al. to be submitted, 2013	69
Supplementary material	110
B.3 Huffman et al. Atmos. Chem. Phys. Discuss., 2013	115
Supplementary material	131
B.4 Pöhlker et al. Science, 2012	153
Supplementary material	159
<b>Acknowledgments</b>	<b>xi</b>
<b>Curriculum Vitae</b>	<b>xiii</b>



## Chapter 1

# Introduction and motivation

### 1.1 Aerosols in the Earth system

Global Change has become a topic of great importance in scientific, social, economic, and political debates. The term *Global Change* summarizes our awareness that human civilization is profoundly and enduringly perturbing the biogeochemical cycling and the ecological networks of the Earth. To emphasize that this “anthropogenic force” is of a geohistorical dimension and that the vividly discussed *Climate Change* is only the “tip of the iceberg”, Paul Crutzen has coined the term *Anthropocene*, defined as the geological epoch humankind has recently entered (Steffen et al., 2011). The changing Earth system is being investigated by a variety of scientific disciplines that address the interactions among the atmosphere, biosphere, hydrosphere, lithosphere, cryosphere, and human activities. The present study belongs to this wide field of Earth system science and is located at the interface between the atmosphere and biosphere. It focusses on the role and impacts of *biogenic aerosol particles* in atmospheric and biological cycling.

Atmospheric aerosols originate from natural and anthropogenic sources and comprise a diverse mixture of different particle classes, such as mineral and soil dust, sea spray, soot and other combustion residues, volcanic ash, organic and biological aerosols, as well as ammonium, nitrate and sulfate salts (Pöschl, 2005). *Primary* particles are directly emitted into the atmosphere from biomass burning and industrial combustion, desert dust storms, marine and biological activity, and other sources (e.g., Goudie and Middleton, 2001; O'Dowd et al., 2004). *Secondary* particles are formed in the atmosphere in the course of the oxidation and subsequent nucleation of sulfur and nitrogen gases as well as volatile organic compounds (VOC) (Junge, 1960; Hallquist et al., 2009). The diverse mixture of airborne particles encounters atmospheric aging and processing which can substantially alter their chemical and physical appearance (e.g., Robinson et al., 2007; Zhang et al., 2008). Aerosol properties and effects span a wide range on spatial, temporal, and chemical scales and therefore challenge the analytical capabilities of Earth system sciences.

Aerosols are important actors in the climate system, atmospheric chemistry, public health as well as in biological and ecological networks. They influence the Earth's radiative budget via the absorption and scattering of solar and terrestrial radiation (*direct effect*) (Satheesh and Moorthy, 2005) and via their role as nuclei for the formation of cloud water droplets and ice crystals (*indirect effect*) (Andreae and Rosenfeld, 2008; Hoose and Möhler, 2012). Both, the direct and indirect effects, constitute the largest uncertainty in our current understanding of climate change (Solomon et al., 2007). Moreover, aerosol particles can act as substrates for heterogeneous chemical reactions and therefore alter the concentration of certain trace gases in the air (e.g., Ammann et al., 1998). Regarding human health, aerosols are commonly recognized as causative agents of infectious disease, asthma, and allergies (Peccia et al., 2011). They also spread diseases to and between animals and plants, which has emerged as an important issue in modern agriculture and ecosystem stability

(e.g., Combes, 1996; Herfst et al., 2012). Aerosols can spread microorganisms intercontinentally with profound ecological and evolutionary implications (e.g., Kellogg and Griffin, 2006; Gorbushina and Broughton, 2009).

In the pre-human epoch cloud-mediated atmospheric cycling was driven by *natural* aerosols from diverse sources as illustrated in Figure 1 (Andreae and Crutzen, 1997). Currently, the natural aerosol burden is strongly “contaminated” by *anthropogenic* emissions and there is hardly a place on Earth without this human signature (Andreae, 2007). An assessment of the anthropogenic perturbation of atmospheric processes and the climate system in terms of aerosol effects requires a profound understanding of the “natural atmospheric scenery”. *Biogenic* particulate matter constitutes a substantial fraction of the background aerosol content and can be subdivided into a supermicrometer fraction, which mainly comprises *primary biological aerosol* particles, and a submicrometer fraction, which mainly consists of biogenic *secondary organic aerosol* particles.

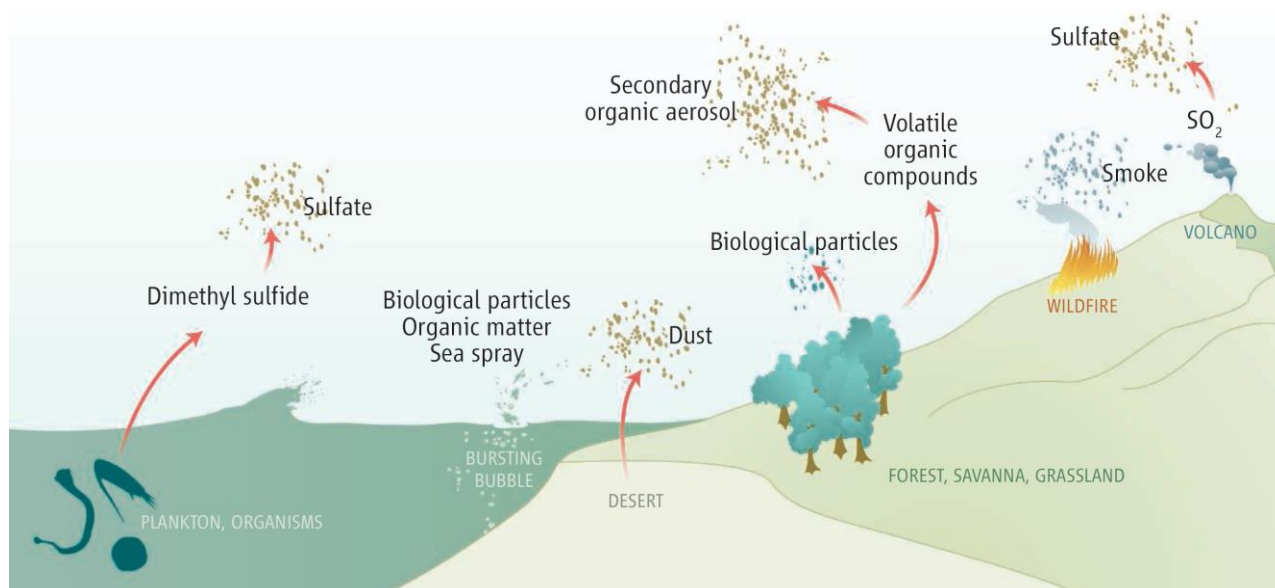


**Figure 1.** Sources of natural atmospheric aerosols. Biogenic aerosols constitute a major fraction and occur as secondary organic aerosols and primary biological particles. Figure from Andreae (2007).

## 1.2 Primary biological aerosol particles

Primary biological aerosol particles (PBAP), also referred to as bioaerosols, are a diverse mixture of biological material, which is directly released from the biosphere into the atmosphere. It comprises whole organisms (e.g., bacteria, algae), reproductive units (e.g., fungal spores, pollen), as well as fragments and excretions from plants and animals (e.g., plant debris, biopolymers, and excrements) (Després et al., 2012). PBAP can be living or dead material. They span a wide size range from few nanometers (e.g., viruses) up to hundreds of micrometers (e.g., plant fragments) with average atmospheric residence times between minutes and weeks (Burrows et al., 2009a; 2009b). There is increasing awareness that PBAP are important players in atmospheric processes, and the field of related research is growing (e.g., Georgakopoulos et al., 2009; Pearce et al., 2009; Xu et al., 2011; Després et al., 2012). The following paragraphs briefly emphasize the role of PBAP as ice

nuclei (IN) in cloud formation and as particulate outdoor pollutants and aeroallergens in public health.

The crystallization of ice is an important process in cloud formation and hydrological cycling, and most precipitation worldwide originates from ice containing clouds (DeMott et al., 2010). In the atmosphere, heterogeneous freezing at temperatures warmer than about  $-38\text{ }^{\circ}\text{C}$  is initiated by a small number of atmospheric IN, which play a key role in this process (e.g. Rogers et al., 2001). Compared to other aerosol types, PBAP (i.e., bacteria, fungal spores, and pollen) are known as the most efficient IN with freezing onset temperatures between  $-2\text{ }^{\circ}\text{C}$  and  $-10\text{ }^{\circ}\text{C}$  (Hoose and Möhler, 2012). Thus, PBAP are discussed as being crucial actors in cloud glaciation and precipitation initiation (e.g., Morris et al., 2004). The term *bio-precipitation* has been coined for such direct atmosphere-biosphere feedback processes (Sands et al., 1982). The current opinion is that on a global scale the comparatively low abundance of biological aerosols prevents them from being important IN (Hoose et al., 2010). In fact, mineral dust and soot account for the majority of IN. However, PBAP may dominate ice nucleation on local and regional scales, particularly in remote vegetated or marine regions where competing non-biological IN are lacking (e.g., Christner et al., 2008; Prenni et al., 2009; Burrows et al., 2012).

Gaseous and particulate outdoor pollutants can cause adverse respiratory effects, such as diseases, inflammatory reactions, and allergies, which is an issue of major public concern (Bartra et al., 2007). PBAP, such as pollen and fungal spores, constitute main aeroallergens making them important for atmosphere-related epidemiologic research (Traidl-Hoffmann et al., 2003; Bernstein et al., 2004; Yamamoto et al., 2012). The complex allergic mechanisms are poorly understood, and no effective therapies or treatments are available yet for susceptible individuals. Instead, pollen calendars and forecasts help preventively to avoid exposure. The most severe biological aeroallergens are pollen from grasses, ragweed, and *Parietaria*, which alone can cause strong allergenic responses to sensitive persons (D'Amato, 2000). However, there is evidence that the natural allergenicity is potentiated by the interaction of allergens and combustion-related air pollutants (i.e., ozone and nitrogen oxides) (e.g., Franze et al., 2005; Shiraiwa et al., 2011).

In spite of the growing attention that PBAP have obtained during recent years, they are usually not included in global atmospheric chemistry and climate models (Burrows et al., 2013). This can be attributed to a lack of standardized and quantitative PBAP measurements as well as to the complexity of the atmospheric PBAP burden. Bioaerosols have been investigated since the 19<sup>th</sup> century (e.g., Pasteur, 1861), however the *traditional* analytical methods (e.g., cultivation, light microscopy) still in use, suffer from substantial drawbacks (Burrows et al., 2009b). In particular, they rarely provide quantitative and real-time information, which is necessary for understanding global PBAP fluxes. Recently, the development and improvement of analytical techniques from various fields has revolutionized the investigation of biological aerosols. These *modern* approaches comprise *off-line* techniques, such as molecular, genetic, and sophisticated microscopy analyses (e.g., Axelrod, 2001; Després et al., 2007; Bauer et al., 2008), and quantitative *online* techniques which rely on optical or mass spectrometric principles (e.g., Fergenson et al., 2004; Pan et al., 2010). These methods have helped to increase our knowledge about biological aerosols tremendously.

A very promising approach to measure PBAP concentrations, emission patterns, and temporal variability in real-time relies on the *autofluorescence* of biological material (Figure 2). Autofluorescence, also called intrinsic fluorescence, is a photoluminescence process which originates from a certain set of fluorescent biological molecules, called fluorophores allowing the discrimination between biological and non-biological aerosol particles (Hill et al., 2009; Andrade-Eiroa et al., 2013). Bioaerosol detectors that are based on laser/light induced fluorescence (LIF) were mainly developed by military research facilities in the context of bio-warfare agent detection (e.g., Jeys et al., 2007). For several years, LIF instruments have received increasing attention in atmospheric science and have produced important insights into PBAP cycling (e.g., Huffman et al., 2010; 2012). The main advantages of LIF instruments are their quick, non-invasive and quantitative detection process, their operational stability for long-term field measurements, and their comparatively cheap maintenance. However, their application is still associated with uncertainty which is one subject of this thesis.

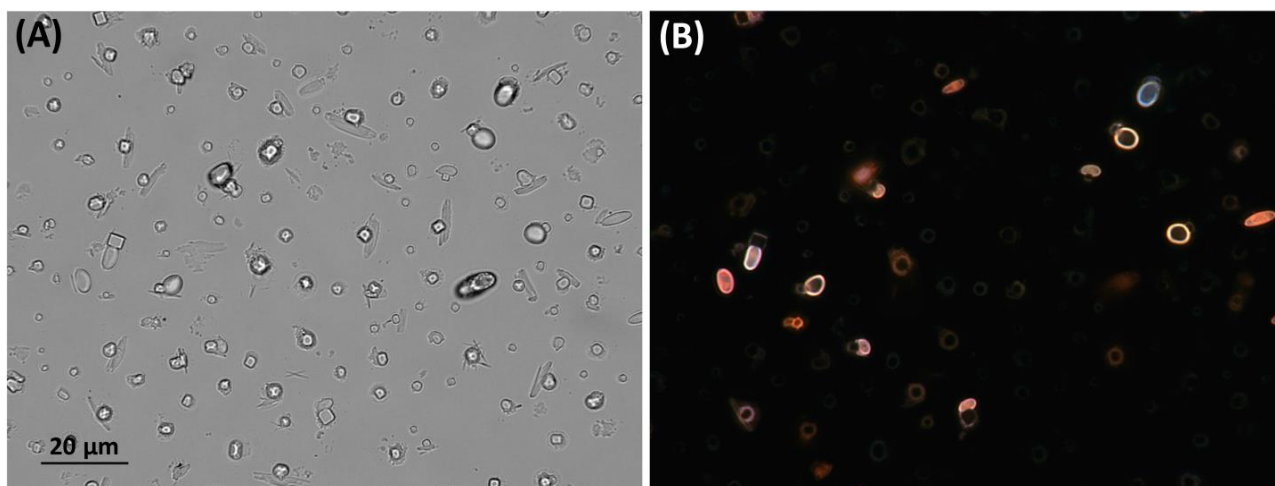


**Figure 2.** Light microscopy images of ambient aerosol particles in (A) bright field and (B) fluorescence mode. The images illustrate a strongly fluorescent PBAP fraction on top of a non-fluorescent non-biological background.

### 1.3 Biogenic secondary organic aerosols

The oxidation of volatile organic compounds (VOC) with the subsequent gas-to-particle partitioning of low- and semi-volatile oxidation products accounts for a major fraction of secondary particulate matter in the atmosphere, commonly referred to as secondary organic aerosol (SOA) (Hallquist et al., 2009). Atmospheric VOC consists of myriads of different compounds from biogenic and anthropogenic sources (Kesselmeier et al., 2000; Goldstein and Galbally, 2007). The oxidative degradation of the highly diverse VOC burden generates a similarly complex aerosol phase which encounters continuous chemical transformation in the atmosphere (Jimenez et al., 2009). Thus, SOA is regarded as a “metastable and dynamic component” in atmospheric cycling (Andreae, 2009; Kroll et al., 2011). Due to their large number concentrations and their diameters, which span the atmospherically relevant size ranges of Mie scattering and CCN activity, SOA particles are key players in the direct and indirect effects of the Earth’s climate system (Kanakidou et al., 2005). However, sources, transformation, and atmospheric effects of SOA are still poorly understood.



Due to its high biological activity and intense atmospheric photochemistry, the tropical rainforest in the Amazon Basin represents an interesting ecosystem for which to analyze the formation and properties of biogenic SOA particles. During the rainy season, the Amazon is one of the few vegetated continental places on Earth which approximate natural and pre-industrial atmospheric conditions. Several studies have shown that during this time of the year, biogenic SOA in the fine mode and PBAP in the coarse mode dominate the aerosol burden (Chen et al., 2009; Pöschl et al., 2010; Huffman et al., 2012). Clean conditions prevail during the rainy season, but are episodically interrupted by long range transport of African desert dust and biomass burning emissions, marine aerosols, and intracontinental anthropogenic influences (Martin et al., 2010). Under clean conditions, the Amazonian atmosphere can be characterized as a *biogeochemical reactor*, due to the fact that biogenic aerosols account for the majority of CCN and IN and therefore directly influence the formation of clouds and precipitation (Figure 3) (Pöschl et al., 2010).

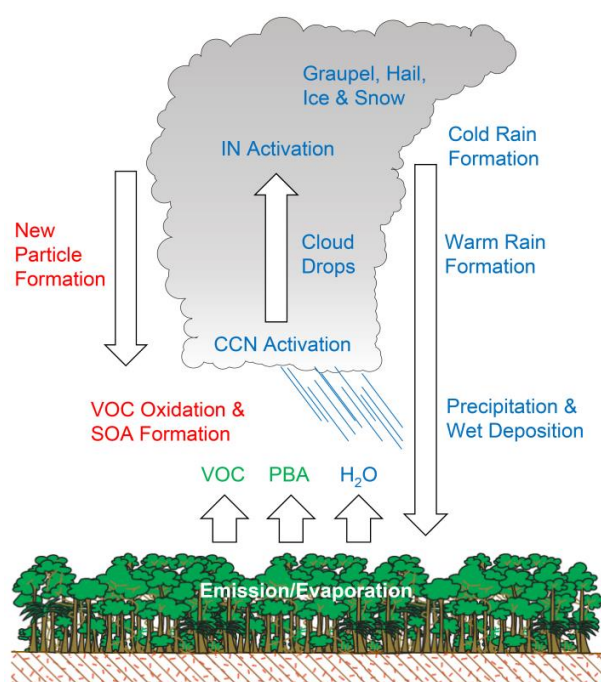


**Figure 3.** Bioprecipitation cycle in the pristine Amazonian atmosphere. SOA particles from the photooxidation of biogenic VOC and PBA particles account for the majority of CCN and IN, and thus directly influence cloud development and precipitation formation. Figure from Pöschl et al. (2010).

A wide variety of instrumentation has been utilized for the analysis of SOA (Jacobson et al., 2000; Hoffmann et al., 2011). Online techniques, such as mass spectrometry and chromatography, have become important tools in laboratory and field applications and provide valuable information about SOA composition, properties, and atmospheric abundance (e.g., Kalberer et al., 2004; Ng et al., 2010). Recently, single particle analysis of organic aerosols based on *microspectroscopic* techniques contributed important insights into SOA microstructure, mixing state, and reactivity (e.g., McIntire et al., 2010; Baustian et al., 2012). Particularly, STXM-NEXAFS provides high morphological and chemical sensitivity and is therefore an appropriate technique for organic aerosol analysis. It has been applied to SOA in a growing number of studies (e.g., Maria et al., 2004; Moffet et al., 2010a; 2010b; Takahama et al., 2010) and represents the second focal point of this dissertation.

## 1.4 Knowledge gaps and research objectives

This thesis presents two focal points in the field of biogenic aerosol research: (i) Studies on the autofluorescence of primary biological aerosol particles (PBAP) and its application in ambient measurements, and (ii) X-ray microscopic and spectroscopic investigations of biogenic secondary organic aerosols (SOA) from the Amazonian rainforest. The projects are presented independently in separate sections.

### 1.4.1 Autofluorescence of primary biological aerosol particles

Autofluorescence based techniques are regarded as a promising approach for addressing manifold yet unknown aspects in bioaerosol cycling, however, their application is still associated with uncertainty. From a methodological perspective, a sound understanding of the *selectivity* that autofluorescence can provide in the analysis of PBAP is yet missing, however, this is required for any application. From the perspective of PBAP analysis, further ambient measurements with LIF instruments are desired to extend our knowledge on ambient bioaerosol cycling in different ecosystems and under variable environmental conditions. This work addresses the following specific knowledge gaps:

- PBAP fluorescence originates from a mixture of many biological fluorophores, which differ in their identity, abundance, spectral properties, and light accessibility. For instance, the fluorescence *signature* of bacteria is dominated by proteins and coenzymes (e.g., Hill et al., 1999; Hill et al., 2009). In contrast, the constitutive fluorophores in fungal spores, pollen and other PBAP types are as of yet not clearly identified (Hill et al., 2009). For a reliable application of fluorescence techniques to the complex and highly variable atmospheric bioaerosol content, a systematic survey of all PBAP-relevant fluorophores, including their identity, spectral properties, and relative abundances, is required.
- LIF techniques detect *fluorescent* biological aerosol particles (FBAP) which is a subset of PBAP. The precise relationship between FBAP and PBAP is still unknown and comprises uncertainties, such as the occurrence of positive artifacts (fluorescent non-biological particles) and negative artifacts (non-fluorescent biological particles). According to Pan et al. (2007), there is “general agreement” that LIF can discriminate between biological and non-biological particles, in most cases. However, there is also evidence that LIF detection *overlooks* a certain yet unspecified fraction of weakly fluorescent bioparticles and that FBAP is therefore a lower limit of PBAP (Brosseau et al., 2000; Huffman et al., 2010). Furthermore, the counted FBAP concentration is surely dependent on specific instrument parameters and the sampled aerosol types (e.g., Healy et al., 2013). Thus, the relationship between FBAP and PBAP is yet to be quantified with regard to different spectral settings. Particularly, the inherent fluorescence properties of major bioaerosol types (e.g. bacteria vs. fungal spores vs. pollen) and their response to different optical configurations require a systematic analysis.
- The *first* and simplest level of selectivity that LIF instruments can provide is the discrimination between biological and non-biological particles, which allows FBAP quantification in ambient air, albeit without further information about FBAP identity. On a *second* level of selectivity, several studies have shown that more elaborate LIF instruments can classify standard and ambi-

ent bioaerosols into *meta-classes* with distinct fluorescence signatures (e.g., Pan et al., 2009). On a *third* level of selectivity, autofluorescence-based identification of individual PBA particles (e.g., allergenic pollen species) is desired, however not yet realized. A few studies report that a certain degree of identification is accessible under special circumstances (e.g., Mitsumoto et al., 2010), but in most cases species-specific identification appears to be beyond the scope of LIF-based bioaerosol analysis (Hill et al., 1999; Pan et al., 2007; Courvoisier et al., 2008). Ultimately, what the limits of discrimination and identification for LIF techniques in ambient applications are remains an open question.

- The number of studies that report medium- to long-term FBAP measurements in ambient air is still comparably small, although growing (e.g., Huffman et al., 2012 and references therein). Therefore, further field experiments, ideally in yet unexplored ecosystems, are highly desired and will add to our understanding of ambient PBAP cycling. Particularly, field measurements with comprehensive sets of instrumentation for bioaerosol analysis are promising because they allow the exploration and quantification of the responsiveness of LIF instruments to PBAP in synergistic comparison with other techniques.

#### 1.4.2 Microspectroscopic studies of Amazonian organic aerosols

The Amazonian rainforest is a predestinated region for studying the interaction between the biosphere and atmosphere under pristine conditions. A number of studies have addressed the atmospheric processes in the Amazon (e.g., Chen et al., 2009; Prenni et al., 2009; Pöschl et al., 2010). However, many uncertainties remain and the following specific knowledge gaps are addressed in this work:

- About 70 - 90 % of the fine mass fraction in the Amazon is usually dominated by SOA particles that are formed in the rainforest ecosystem (Fuzzi et al., 2007; Pöschl et al., 2010). The chemical composition of the biogenic SOA is not yet clearly characterized, however. Knowledge about the chemical constituents in the SOA particles would help to identify the major VOC sources and to better understand the atmospheric fate of SOA in terms of aging and processing.
- The morphology and mixing state of Amazonian aerosol particles in fine and coarse mode is largely unknown. During pristine periods when biogenic sources prevail and particularly when out-of-Basin influences mix with the biogenic in-Basin aerosol burden, knowledge about mixing (internal vs. external) and agglomeration of individual particles is of interest for estimating the influence of atmospheric and hydrological cycling. Moreover, morphology (i.e., liquid vs. semi-solid vs. solid) and liquid-liquid phase separation processes in SOA particles have received increasing attention (e.g., Virtanen et al., 2010; Bertram et al., 2011; Song et al., 2012). Such effects potentially have strong influence on the physical and chemical properties of SOA particles, but have not yet been analyzed for Amazon SOA aerosols.
- New particle formation is the main origin of SOA particles in many vegetated regions worldwide (Kulmala et al., 2004). In contrast, new particle formation is not observed in the Amazonian rainforest and therefore, the origin of biogenic SOA particles in the Amazon has remained enigmatic.



# Results and conclusions

## 2.1 Autofluorescence of primary biological aerosol particles

### 2.1.1 Biological fluorophores and potential interferences

As a first approach, the complex field of bioaerosol autofluorescence was investigated on the level of pure fluorophores and a systematic survey of biological fluorescent compounds was conducted. This bottom-up study aims to clarify the molecular basis of PBAP autofluorescence in order to identify the most relevant biofluorophore classes. The aim of this study is to collect data and knowledge from *offline* fluorescence measurements, which can help in understanding the levels of selectivity of *online* LIF techniques in ambient applications. The study consists of two parts: (i) a systematic synthesis of literature knowledge on biological fluorophores and (ii) a section with complementary fluorescence spectroscopy measurements.

The literature synthesis section summarizes knowledge about the identity and properties of relevant biological fluorophores, which can be divided into six main categories: (i) amino acids and proteins, (ii) cofactors, coenzymes and vitamins, (iii) structural biopolymers and cell wall compounds, (iv) pigments, (v) secondary metabolites, and (vi) others. Their relative importance for bioaerosol detection is estimated based on their spectral properties and abundance in PBAP. This review section is designed to serve as a “go-to reference” for researchers in bioaerosol autofluorescence and related fields. It suggests that a substantial number of different fluorescent compounds shape the fluorescence signals in bioaerosols. Moreover, certain PBAP types, such as bacteria, fungal spores, and pollen are associated with specific sets of fluorophores. Thus, this study emphasizes that focusing on protein and coenzyme fluorescence, which mostly is what is done in current literature, is too simplistic to explain the fluorescence properties of the entire atmospheric PBAP burden.

The experimental section provides results from complementary fluorescence spectroscopy measurements on selected biological fluorophores. Excitation emission matrices (EEMs) are utilized as a valuable tool to visualize the *fingerprint-like* autofluorescence properties of a variety of individual compounds. The EEMs show pronounced and overlapping signals from different fluorophores at the excitation wavelengths of  $\sim 280$  nm and  $\sim 360$  nm, which confirms the suitability of light sources commonly used for online FBAP detection. However, it also highlights the difficulty in making molecular determination of the fluorescence origin. In direct comparison to the fluorescence signatures from biofluorophores, EEMs of potentially interfering non-biological compounds were recorded, which generally exhibit only low levels of fluorescent emission. Ultimately, this study strengthens the hypothesis that autofluorescence can reliably be utilized for the discrimination of biological and non-biological aerosols in ambient air. However, it also shows that the identity of the biofluorophores in PBAP is difficult to determine and that detected fluorescence usually represents mixed emissions from different compounds.

For details, see: Pöhlker, et al., *Atmos. Meas. Tech.* (2012a): Autofluorescence of atmospheric bioaerosols – fluorescent biomolecules and potential interferences.

### 2.1.2 Biological standard particles and aspects of selectivity

This study follows up on Pöhlker et al. (2012a) and extends the analytical scope from pure fluorophores to whole biological particles. Pollen were chosen as illustrative bioaerosol type and systematically analyzed with fluorescence microscopy and spectroscopy. Our aim is (i) to give a general and comprehensive picture of the autofluorescence properties of native pollen, and (ii) to explore the limits of selectivity that autofluorescence can provide in PBAP detection.

Our study shows that pollen exhibit a characteristic and reproducible autofluorescence signature. Moreover, it indicates that the pollen cell wall efficiently prevents light from penetrating into the cytosol and that therefore the cell wall pigments dominate the fluorescence of entire pollen grains. Differences in light accessibility of the fluorophores can substantially shape the fluorescent appearance of biological aerosols, however, this aspect has so far not been adequately discussed in current literature. The main fluorescence signals are assigned to cell wall associated phenolic and carotenoid compounds as well as smaller contributions from proteins and chlorophyll pigments.

Across all pollen species analyzed we found a characteristic spectral signature due to specific fluorophores in the complex and thick pollen cell wall. The predominance of cell wall fluorophores in pollen is a distinctive feature and results in pollen fluorescence differing from other PBAP types. Moreover, the mixture of cell wall associated fluorophores shows species specificity and, therefore, fluorescence reflects a certain degree of taxonomic selectivity at the family level. These observations suggest that, in principle, autofluorescence is selective enough to discriminate pollen from other PBAP types. Moreover, the taxonomic trends in cell wall associated fluorescence indicate that a further level of selectivity - namely the discrimination of certain pollen families - is, in principle, practicable. This underlines the fact that autofluorescence-based techniques are promising candidates for automated and specific pollen monitoring in ambient air. Moreover, we suggest that the fluorescence signatures reported in this study can serve as “roadmaps” for the development of LIF instrumentation designed for pollen aeroallergen monitoring. A companion study builds on these findings and addresses the influence of environmental factors, such as humidity, on the pollen morphology and autofluorescence signature (Pöhlker et al., 2013a).

For details, see: Pöhlker, et al., *to be submitted* (2013): Autofluorescence of atmospheric bioaerosols – the spectral fingerprint and taxonomic trends of native pollen.

### 2.1.3 Ambient measurements and bioprecipitation

In addition to the offline laboratory experiments on PBAP autofluorescence, this study addresses the online application for ambient measurements. Here, we present results from a comprehensive bioaerosol campaign in a semiarid forest ecosystem in Northern America. Among a variety of other techniques for bioaerosol analysis, the autofluorescence-based bioaerosol detector, ultraviolet aerodynamic particle sizer (UV-APS), was operated continuously to monitor the concentration of FBAP

with high time and size resolution. The combination of online and offline instruments provided insights into the bioaerosol identity, cycling, and atmospheric effects.

We observed a low bioaerosol background during dry conditions, which was repeatedly interrupted by dramatic increases in PBAP concentrations during and after rain showers. This contrasts with the traditional view that aerosol concentrations decrease during rain due to efficient wet deposition, and indicates the presence of strong rain-triggered PBAP sources, which so far remain unidentified. Starting at the onset of rain, elevated PBAP concentrations prevail through extended post-precipitation periods with high surface wetness. Moreover, the rain-triggered bursts in PBAP abundance strongly correlate with similarly strong increases of atmospheric IN concentrations. There are strong indications that the majority of the observed IN is biological, which is consistent with the identification of efficient ice nucleating bacteria and fungal spores in the rain-triggered PBAP populations.

Our findings provide unprecedented insights into atmosphere-biosphere interactions with regard to bioaerosol cycling. The observation of the rain-triggered emission of large numbers of PBAP, including an IN-active fraction that potentially impacts the next generation of clouds, can be regarded as a bioprecipitation cycle. Moreover, the strong impact of rain on biota in a rain-limited ecosystem raise a number of evolutionary and ecological questions, which await being addressed in further studies. A further aspect of this study relates to the frequently observed increase of respiratory diseases after strong thunderstorms. Increased PBAP concentrations after rain may be part of the explanation, however, follow-up studies are needed.

For details, see: Huffman, et al., *Atmos. Chem. Phys. Discuss.* (2013): High concentrations of biological aerosol particles and ice nuclei during and after rain.

## 2.2 Microspectroscopic studies of Amazonian organic aerosols

This study presents the first application of X-ray microscopy and absorption spectroscopy (STXM-NEXAFS) to the analysis of organic aerosols from the pristine Amazonian atmosphere. Our study reveals the predominance of biogenic aerosols in the fine and coarse mode from the rainforest ecosystem and the absence of external influences, such as mineral dust and anthropogenic aerosols, during the sampling period. We found distinctly different types of secondary organic matter (carboxylic-acid- vs. hydroxy-rich), and internal structures that indicate a strong influence of cloud and fog processing on organic particle formation and aging.

An unexpected discovery was the observation of potassium in almost all organic aerosol particles. Moreover, the potassium mass fraction shows a clear size dependence, which indicates that primary and nanometer-sized potassium-rich salt particles are seeding the formation of SOA, with decreasing potassium content upon particle growth. In pristine rainforest air, we conclude that the observed potassium-rich particles are biogenic and suggest microorganisms and vegetation as plausible sources. Our findings provide an answer to the old riddle of why new particle formation is not observed in pristine Amazonian rainforest air, although the submicron aerosol particles consist mostly of secondary organic material formed by oxidation of gaseous precursors in the atmosphere.

This study extends our knowledge of the biosphere-atmosphere interaction in the Amazon and shows that rainforest biota have a much more direct influence on the hydrological cycle and climate

than previously thought. In addition to the SOA seeding by potassium salts, a number of other aspects, such as the composition and atmospheric aging of Amazonian SOA, are reported in this work, albeit without in-depth analysis. These aspects are the subject of a systematic follow up study (Pöhlker et al., 2013b). Moreover, the identification of the biological potassium source is the subject of ongoing work.

For details, see: Pöhlker, et al., *Science* (2012b): Biogenic potassium salt particles as seeds for secondary organic aerosol in the Amazon.



# References

- Ammann, M., Kalberer, M., Jost, D. T., Tobler, L., Rossler, E., Piguët, D., Gaggeler, H. W. and Baltensperger, U.: Heterogeneous production of nitrous acid on soot in polluted air masses, *Nature*, 395, 157-160, 10.1038/25965, 1998.
- Andrade-Eiroa, A., Canle, M. and Cerda, V.: Environmental Applications of Excitation-Emission Spectrofluorimetry: An In-Depth Review I, *Applied Spectroscopy Reviews*, 48, 1-49, 10.1080/05704928.2012.692104, 2013.
- Andreae, M. O. and Crutzen, P. J.: Atmospheric aerosols: Biogeochemical sources and role in atmospheric chemistry, *Science*, 276, 1052-1058, 1997.
- Andreae, M. O.: Aerosols before pollution, *Science*, 315, 50-51, 10.1126/science.1136529, 2007.
- Andreae, M. O. and Rosenfeld, D.: Aerosol-cloud-precipitation interactions. Part 1. The nature and sources of cloud-active aerosols, *Earth-Science Reviews*, 89, 13-41, 10.1016/j.earscirev.2008.03.001, 2008.
- Andreae, M. O.: A New Look at Aging Aerosols, *Science*, 326, 1493-1494, 10.1126/science.1183158, 2009.
- Axelrod, D.: Total internal reflection fluorescence microscopy in cell biology, *Traffic*, 2, 764-774, 10.1034/j.1600-0854.2001.21104.x, 2001.
- Bartra, J., Mollot, J., del Cuívillo, A., Davila, I., Ferrer, M., Jauregui, I., Montoro, J., Sastre, J. and Valero, A.: Air pollution and allergens, *Journal of Investigational Allergology and Clinical Immunology*, 17, 3-8, 2007.
- Bauer, H., Claeys, M., Vermeylen, R., Schueller, E., Weinke, G., Berger, A. and Puxbaum, H.: Arabitol and mannitol as tracers for the quantification of airborne fungal spores, *Atmospheric Environment*, 42, 588-593, 10.1016/j.atmosenv.2007.10.013, 2008.
- Baustian, K. J., Cziczo, D. J., Wise, M. E., Pratt, K. A., Kulkarni, G., Hallar, A. G. and Tolbert, M. A.: Importance of aerosol composition, mixing state, and morphology for heterogeneous ice nucleation: A combined field and laboratory approach, *Journal of Geophysical Research-Atmospheres*, 117, 10.1029/2011jd016784, 2012.
- Bernstein, J. A., Alexis, N., Barnes, C., Bernstein, I. L., Nel, A., Peden, D., Diaz-Sanchez, D., Tarlo, S. M. and Williams, P. B.: Health effects of air pollution, *Journal of Allergy and Clinical Immunology*, 114, 1116-1123, 10.1016/j.jaci.2004.08.030, 2004.
- Bertram, A. K., Martin, S. T., Hanna, S. J., et al.: Predicting the relative humidities of liquid-liquid phase separation, efflorescence, and deliquescence of mixed particles of ammonium sulfate, organic material, and water using the organic-to-sulfate mass ratio of the particle and the oxygen-to-carbon elemental ratio of the organic component, *Atmospheric Chemistry and Physics*, 11, 10995-11006, 10.5194/acp-11-10995-2011, 2011.
- Brosseau, L. M., Vesley, D., Rice, N., Goodell, K., Nellis, M. and Hairston, P.: Differences in detected fluorescence among several bacterial species measured with a direct-reading particle sizer and fluorescence detector, *Aerosol Science and Technology*, 32, 545-558, 2000.
- Burrows, S. M., Butler, T., Jockel, P., Tost, H., Kerkweg, A., Pöschl, U. and Lawrence, M. G.: Bacteria in the global atmosphere - Part 2: Modeling of emissions and transport between different ecosystems, *Atmospheric Chemistry and Physics*, 9, 9281-9297, 2009a.
- Burrows, S. M., Elbert, W., Lawrence, M. G. and Pöschl, U.: Bacteria in the global atmosphere - Part 1: Review and synthesis of literature data for different ecosystems, *Atmospheric Chemistry and Physics*, 9, 9263-9280, 2009b.
- Burrows, S. M., Hoose, C., Pöschl, U. and Lawrence, M. G.: Ice nuclei in marine air: bioparticles or dust?, *Atmospheric Chemistry and Physics Discussions*, 12, 4373-4416, 2012.
- Burrows, S. M., Rayner, P. J., Butler, T. and Lawrence, M. G.: Impact of modelled particle characteristics on emissions inferred by inversion of tracer transport, *Atmospheric Chemistry and Physics Discussions*, 13, 4391-4432, 10.5194/acpd-13-4391-2013, 2013.

- Chen, Q., Farmer, D. K., Schneider, J., et al.: Mass spectral characterization of submicron biogenic organic particles in the Amazon Basin, *Geophysical Research Letters*, 36, L20806, L20806 10.1029/2009gl039880, 2009.
- Christner, B. C., Morris, C. E., Foreman, C. M., Cai, R. M. and Sands, D. C.: Ubiquity of biological ice nucleators in snowfall, *Science*, 319, 1214-1214, 10.1126/science.1149757, 2008.
- Combes, C.: Parasites, biodiversity and ecosystem stability, *Biodiversity and Conservation*, 5, 953-962, 10.1007/bf00054413, 1996.
- Courvoisier, F., Bonacina, L., Boutou, V., et al.: Identification of biological microparticles using ultrafast depletion spectroscopy, *Faraday Discussions*, 137, 37-49, 10.1039/b615221j, 2008.
- D'Amato, G.: Urban air pollution and plant-derived respiratory allergy, *Clinical and Experimental Allergy*, 30, 628-636, 2000.
- DeMott, P. J., Prenni, A. J., Liu, X., Kreidenweis, S. M., Petters, M. D., Twohy, C. H., Richardson, M. S., Eidhammer, T. and Rogers, D. C.: Predicting global atmospheric ice nuclei distributions and their impacts on climate, *Proceedings of the National Academy of Sciences of the United States of America*, 107, 11217-11222, 10.1073/pnas.0910818107, 2010.
- Després, V. R., Nowoisky, J. F., Klose, M., Conrad, R., Andreae, M. O. and Pöschl, U.: Characterization of primary biogenic aerosol particles in urban, rural, and high-alpine air by DNA sequence and restriction fragment analysis of ribosomal RNA genes, *Biogeosciences*, 4, 1127-1141, 2007.
- Després, V. R., Huffman, J. A., Burrows, S. M., et al.: Primary biological aerosol particles in the atmosphere: a review, *Tellus B*, 64, 2012.
- Ferguson, D. P., Pitesky, M. E., Tobias, H. J., et al.: Reagentless detection and classification of individual bioaerosol particles in seconds, *Analytical Chemistry*, 76, 373-378, 10.1021/ac034467e, 2004.
- Franze, T., Weller, M. G., Niessner, R. and Pöschl, U.: Protein nitration by polluted air, *Environmental Science & Technology*, 39, 1673-1678, 10.1021/es0488737, 2005.
- Fuzzi, S., Decesari, S., Facchini, M. C., et al.: Overview of the inorganic and organic composition of size-segregated aerosol in Rondonia, Brazil, from the biomass-burning period to the onset of the wet season, *Journal of Geophysical Research-Atmospheres*, 112, 10.1029/2005jd006741, 2007.
- Georgakopoulos, D. G., Després, V., Fröhlich-Nowoisky, J., Psenner, R., Ariya, P. A., Posfai, M., Ahern, H. E., Moffett, B. F. and Hill, T. C. J.: Microbiology and atmospheric processes: biological, physical and chemical characterization of aerosol particles, *Biogeosciences*, 6, 721-737, 2009.
- Goldstein, A. H. and Galbally, I. E.: Known and unexplored organic constituents in the Earth's atmosphere, *Environmental Science & Technology*, 41, 1514-1521, 10.1021/es072476p, 2007.
- Gorbushina, A. A. and Broughton, W. J.: Microbiology of the Atmosphere-Rock Interface: How Biological Interactions and Physical Stresses Modulate a Sophisticated Microbial Ecosystem, *Annual Review of Microbiology*, 431-450, 2009.
- Goudie, A. S. and Middleton, N. J.: Saharan dust storms: Nature and consequences, *Earth-Science Reviews*, 56, 179-204, 10.1016/s0012-8252(01)00067-8, 2001.
- Hallquist, M., Wenger, J. C., Baltensperger, U., et al.: The formation, properties and impact of secondary organic aerosol: Current and emerging issues, *Atmospheric Chemistry and Physics*, 9, 5155-5236, 2009.
- Healy, D. A., Huffman, J. A., O'Connor, D. J., Pöhlker, C., Pöschl, U. and Sodeau, J. R.: Ambient measurements of biological aerosol particles near Killarney, Ireland: a comparison between fluorescence and optical microscopy approaches, *in preparation*, 2013.
- Herfst, S., Schrauwen, E. J. A., Linster, M., et al.: Airborne Transmission of Influenza A/H5N1 Virus Between Ferrets, *Science*, 336, 1534-1541, 10.1126/science.1213362, 2012.
- Hill, S. C., Pinnick, R. G., Niles, S., et al.: Real-time measurement of fluorescence spectra from single airborne biological particles, *Field Analytical Chemistry and Technology*, 3, 221-239, 1999.

Hill, S. C., Mayo, M. W. and Chang, R. K.: Fluorescence of bacteria, pollens, and naturally occurring airborne particles: excitation/emission spectra, Army report, ARL-TR-4722, 2009.

Hoffmann, T., Huang, R.-J. and Kalberer, M.: Atmospheric Analytical Chemistry, *Analytical Chemistry*, 83, 4649-4664, 10.1021/ac2010718, 2011.

Hoose, C., Kristjansson, J. E. and Burrows, S. M.: How important is biological ice nucleation in clouds on a global scale?, *Environmental Research Letters*, 5, 10.1088/1748-9326/5/2/024009, 2010.

Hoose, C. and Möhler, O.: Heterogeneous ice nucleation on atmospheric aerosols: A review of results from laboratory experiments, *Atmospheric Chemistry and Physics*, 12, 9817-9854, 10.5194/acp-12-9817-2012, 2012.

Huffman, J. A., Treutlein, B. and Pöschl, U.: Fluorescent biological aerosol particle concentrations and size distributions measured with an Ultraviolet Aerodynamic Particle Sizer (UV-APS) in Central Europe, *Atmospheric Chemistry and Physics*, 10, 3215-3233, 2010.

Huffman, J. A., Sinha, B., Garland, R. M., Snee-Pollmann, A., Gunthe, S. S., Artaxo, P., Martin, S. T., Andreae, M. O. and Pöschl, U.: Biological aerosol particle concentrations and size distributions measured in pristine tropical rainforest air during AMAZE-08, *Atmospheric Chemistry and Physics*, 12, 25181-25236, 2012.

Huffman, J. A., Pöhlker, C., Prenni, A. J., et al.: High concentrations of biological aerosol particles and ice nuclei during and after rain, *Atmospheric Chemistry and Physics Discussions*, 13, 1767-1793, 10.5194/acpd-13-1767-2013, 2013.

Jacobson, M. C., Hansson, H. C., Noone, K. J. and Charlson, R. J.: Organic atmospheric aerosols: Review and state of the science, *Reviews of Geophysics*, 38, 267-294, 10.1029/1998rg000045, 2000.

Jeys, T. H., Herzog, W. D., Hybl, J. D., Czerwinski, R. N. and Sanchez, A.: Advanced trigger development, *Lincoln Laboratory Journal*, 17, 29-62, 2007.

Jimenez, J. L., Canagaratna, M. R., Donahue, N. M., et al.: Evolution of Organic Aerosols in the Atmosphere, *Science*, 326, 1525-1529, 10.1126/science.1180353, 2009.

Junge, C. E.: Sulfur in the atmosphere, *Journal of Geophysical Research*, 65, 227-237, 10.1029/JZ065i001p00227, 1960.

Kalberer, M., Paulsen, D., Sax, M., et al.: Identification of polymers as major components of atmospheric organic aerosols, *Science*, 303, 1659-1662, 10.1126/science.1092185, 2004.

Kanakidou, M., Seinfeld, J. H., Pandis, S. N., et al.: Organic aerosol and global climate modelling: A review, *Atmospheric Chemistry and Physics*, 5, 1053-1123, 2005.

Kellogg, C. A. and Griffin, D. W.: Aerobiology and the global transport of desert dust, *Trends in Ecology & Evolution*, 21, 638-644, 10.1016/j.tree.2006.07.004, 2006.

Kesselmeier, J., Kuhn, U., Wolf, A., et al.: Atmospheric volatile organic compounds (VOC) at a remote tropical forest site in central Amazonia, *Atmospheric Environment*, 34, 4063-4072, 10.1016/s1352-2310(00)00186-2, 2000.

Kroll, J. H., Donahue, N. M., Jimenez, J. L., et al.: Carbon oxidation state as a metric for describing the chemistry of atmospheric organic aerosol, *Nature Chemistry*, 3, 133-139, 10.1038/nchem.948, 2011.

Kulmala, M., Vehkamäki, H., Petaja, T., Dal Maso, M., Lauri, A., Kerminen, V. M., Birmili, W. and McMurry, P. H.: Formation and growth rates of ultrafine atmospheric particles: A review of observations, *Journal of Aerosol Science*, 35, 143-176, 10.1016/j.jaerosci.2003.10.003, 2004.

Maria, S. F., Russell, L. M., Gilles, M. K. and Myneni, S. C. B.: Organic aerosol growth mechanisms and their climate-forcing implications, *Science*, 306, 1921-1924, 10.1126/science.1103491, 2004.

Martin, S. T., Andreae, M. O., Artaxo, P., et al.: Sources and properties of Amazonian aerosol particles, *Reviews of Geophysics*, 48, RG2002, Rg2002 10.1029/2008rg000280, 2010.

McIntire, T. M., Ryder, O. S., Gassman, P. L., Zhu, Z., Ghosal, S. and Finlayson-Pitts, B. J.: Why ozonolysis may not increase the hydrophilicity of particles, *Atmospheric Environment*, 44, 939-944, 2010.

- Mitsumoto, K., Yabusaki, K., Kobayashi, K. and Aoyagi, H.: Development of a novel real-time pollen-sorting counter using species-specific pollen autofluorescence, *Aerobiologia*, 26, 99-111, 10.1007/s10453-009-9147-1, 2010.
- Moffet, R. C., Henn, T. R., Tivanski, A. V., et al.: Microscopic characterization of carbonaceous aerosol particle aging in the outflow from Mexico City, *Atmospheric Chemistry and Physics*, 10, 961-976, 2010a.
- Moffet, R. C., Tivanski, A. V. and Gilles, M. K.: Scanning transmission X-ray microscopy - Applications in atmospheric aerosol research, in: *Fundamentals and applications in aerosol spectroscopy*, edited by: Signorell, R. and Reid, J., CRC Press Taylor & Francis Group, Boca Raton, 2010b.
- Morris, C. E., Georgakopoulos, D. G. and Sands, D. C.: Ice nucleation active bacteria and their potential role in precipitation, *Journal de Physique IV*, 121, 87-103, 10.1051/jp4:2004121004, 2004.
- Ng, N. L., Canagaratna, M. R., Zhang, Q., et al.: Organic aerosol components observed in Northern Hemispheric datasets from Aerosol Mass Spectrometry, *Atmospheric Chemistry and Physics*, 10, 4625-4641, 10.5194/acp-10-4625-2010, 2010.
- O'Dowd, C. D., Facchini, M. C., Cavalli, F., Ceburnis, D., Mircea, M., Decesari, S., Fuzzi, S., Yoon, Y. J. and Putaud, J. P.: Biogenically driven organic contribution to marine aerosol, *Nature*, 431, 676-680, 10.1038/nature02959, 2004.
- Pan, Y.-L., Hill, S. C., Pinnick, R. G., Huang, H., Bottiger, J. R. and Chang, R. K.: Fluorescence spectra of atmospheric aerosol particles measured using one or two excitation wavelengths: Comparison of classification schemes employing different emission and scattering results, *Optics Express*, 18, 12436-12457, 10.1364/oe.18.012436, 2010.
- Pan, Y. L., Eversole, J. D., Kaye, P. H., et al.: Bio-aerosol fluorescence - Detecting and characterising bio-aerosols via UV light-induced fluorescence spectroscopy, in: *Optics of Biological Particles*, edited by: Hoekstra, A., Maltsev, V. and Videen, G., NATO Science Series, Human Press / Springer, Dordrecht, 63-163, 2007.
- Pan, Y. L., Pinnick, R. G., Hill, S. C. and Chang, R. K.: Particle-Fluorescence Spectrometer for Real-Time Single-Particle Measurements of Atmospheric Organic Carbon and Biological Aerosol, *Environmental Science & Technology*, 43, 429-434, 10.1021/es801544y, 2009.
- Pasteur, L.: Mémoire sur les corpuscles organisés qui existent dans l'atmosphère. Examen de la doctrine des générations spontanées., *Annales des Science Naturelles (partie zoologique)*, 16, 5-98, 1861.
- Pearce, D. A., Bridge, P. D., Hughes, K. A., Sattler, B., Psenner, R. and Russell, N. J.: Microorganisms in the atmosphere over Antarctica, *Fems Microbiology Ecology*, 69, 143-157, 10.1111/j.1574-6941.2009.00706.x, 2009.
- Peccia, J., Hospodsky, D. and Bibby, K.: New Directions: A revolution in DNA sequencing now allows for the meaningful integration of biology with aerosol science, *Atmospheric Environment*, 45, 1896-1897, 10.1016/j.atmosenv.2010.11.037, 2011.
- Pöhlker, C., Huffman, J. A. and Pöschl, U.: Autofluorescence of atmospheric bioaerosols - fluorescent biomolecules and potential interferences, *Atmos. Meas. Tech.*, 5, 37-71, 10.5194/amt-5-37-2012, 2012a.
- Pöhlker, C., Wiedemann, K. T., Sinha, B., et al.: Biogenic Potassium Salt Particles as Seeds for Secondary Organic Aerosol in the Amazon, *Science*, 337, 1075-1078, 10.1126/science.1223264, 2012b.
- Pöhlker, C., Huffman, J. A., Förster, J.-D. and Pöschl, U.: Autofluorescence of atmospheric bioaerosols – water influence on pollen morphology and autofluorescence. *in preparation*, 2013a.
- Pöhlker, C., Wiedemann, K. T., Saturno, J., et al.: STXM-NEXAFS analysis of Amazonian aerosols, *in preparation*, 2013b.
- Pöschl, U.: Atmospheric aerosols: Composition, transformation, climate and health effects, *Angewandte Chemie-International Edition*, 44, 7520-7540, 10.1002/anie.200501122, 2005.
- Pöschl, U., Martin, S. T., Sinha, B., et al.: Rainforest Aerosols as Biogenic Nuclei of Clouds and Precipitation in the Amazon, *Science*, 329, 1513-1516, 10.1126/science.1191056, 2010.
- Prenni, A. J., Petters, M. D., Kreidenweis, S. M., Heald, C. L., Martin, S. T., Artaxo, P., Garland, R. M., Wollny, A. G. and Pöschl, U.: Relative roles of biogenic emissions and Saharan dust as ice nuclei in the Amazon basin, *Nature Geoscience*, 2, 401-404, 10.1038/ngeo517, 2009.

- Robinson, A. L., Donahue, N. M., Shrivastava, M. K., Weitkamp, E. A., Sage, A. M., Grieshop, A. P., Lane, T. E., Pierce, J. R. and Pandis, S. N.: Rethinking organic aerosols: Semivolatile emissions and photochemical aging, *Science*, 315, 1259-1262, 10.1126/science.1133061, 2007.
- Rogers, D. C., DeMott, P. J. and Kreidenweis, S. M.: Airborne measurements of tropospheric ice-nucleating aerosol particles in the Arctic spring, *Journal of Geophysical Research-Atmospheres*, 106, 15053-15063, 10.1029/2000jd900790, 2001.
- Sands, D. C., Langhans, V. E., Scharen, A. L. and de Smet, G.: The association between bacteria and rain and possible resultant meteorological implications, *Journal of the Hungarian Meteorological Service*, 86, 148-152, 1982.
- Satheesh, S. K. and Moorthy, K. K.: Radiative effects of natural aerosols: A review, *Atmospheric Environment*, 39, 2089-2110, 10.1016/j.atmosenv.2004.12.029, 2005.
- Shiraiwa, M., Sosedova, Y., Rouviere, A., Yang, H., Zhang, Y. Y., Abbatt, J. P. D., Ammann, M. and Pöschl, U.: The role of long-lived reactive oxygen intermediates in the reaction of ozone with aerosol particles, *Nature Chemistry*, 3, 291-295, 10.1038/nchem.988, 2011.
- Solomon, S., Qin, D., Manning, Z., Chen, Z., Marquis, M., Avery, K. B., Tignor, M. and Miller, H. L. E.: IPCC 4th Assessment Report, Cambridge Univ. Press, Cambridge, 2007.
- Song, M., Marcolli, C., Krieger, U. K., Zuend, A. and Peter, T.: Liquid-liquid phase separation and morphology of internally mixed dicarboxylic acids/ammonium sulfate/water particles, *Atmospheric Chemistry and Physics*, 12, 2691-2712, 10.5194/acp-12-2691-2012, 2012.
- Steffen, W., Grinevald, J., Crutzen, P. and McNeill, J.: The Anthropocene: conceptual and historical perspectives, *Philosophical Transactions of the Royal Society a-Mathematical Physical and Engineering Sciences*, 369, 842-867, 10.1098/rsta.2010.0327, 2011.
- Takahama, S., Liu, S. and Russell, L. M.: Coatings and clusters of carboxylic acids in carbon-containing atmospheric particles from spectromicroscopy and their implications for cloud-nucleating and optical properties, *Journal of Geophysical Research-Atmospheres*, 115, D01202, 10.1029/2009jd012622, 2010.
- Traidl-Hoffmann, C., Kasche, A., Menzel, A., Jakob, T., Thiel, M., Ring, J. and Behrendt, H.: Impact of pollen on human health: More than allergen carriers?, *International Archives of Allergy and Immunology*, 131, 1-13, 10.1159/000070428, 2003.
- Virtanen, A., Joutsensaari, J., Koop, T., et al.: An amorphous solid state of biogenic secondary organic aerosol particles, *Nature*, 467, 824-827, 10.1038/nature09455, 2010.
- Xu, Z., Wu, Y., Shen, F., Chen, Q., Tan, M. and Yao, M.: Bioaerosol Science, Technology, and Engineering: Past, Present, and Future, *Aerosol Science and Technology*, 45, 1337-1349, 10.1080/02786826.2011.593591, 2011.
- Yamamoto, N., Bibby, K., Qian, J., Hospodsky, D., Rismani-Yazdi, H., Nazaroff, W. W. and Peccia, J.: Particle-size distributions and seasonal diversity of allergenic and pathogenic fungi in outdoor air, *Isme Journal*, 6, 1801-1811, 10.1038/ismej.2012.30, 2012.
- Zhang, R., Khalizov, A. F., Pagels, J., Zhang, D., Xue, H. and McMurry, P. H.: Variability in morphology, hygroscopicity, and optical properties of soot aerosols during atmospheric processing, *Proceedings of the National Academy of Sciences of the United States of America*, 105, 10291-10296, 10.1073/pnas.0804860105, 2008.



## Appendix A

### List of related publications and presentations

#### Peer-reviewed publications

- Pöhlker, C., Huffman, J. A., Pöschl, U., Autofluorescence of atmospheric bioaerosols – fluorescent biomolecules and potential interferences. **Atmospheric Measurement Techniques**, 5, 37-71, 2012.
- Pöhlker, C., Wiedemann, K. T., Sinha, B., Shiraiwa, M., Gunthe, S. S., Smith, M., Su, H., Artaxo, P., Chen, Q., Cheng, Y., Elbert, W., Gilles, M. K., Kilcoyne, A. L. D., Moffet, R. C., Weigand, M., Martin, S. T., Pöschl, U., Andreae, M. O., Biogenic potassium salt particles as seeds for secondary organic aerosol in the Amazon. **Science**, 337, 1075-1078, 2012.
- Huffman, J. A., Pöhlker, C., Prenni, A. J., DeMott, P. J., Mason, R. H., Robinson, N. H., Fröhlich-Nowoisky, J., Tobo, Y., Després, V. R., Garcia, E., Gochis, D. J., Harris, E., Müller-Germann, I., Ruzene, C., Schmer, B., Sinha, B., Day, D. A., Andreae, M. O., Jimenez, J. L., Gallagher, M., Kreidenweis, S. M., Bertram, A. K., Pöschl, U., High concentrations of biological aerosol particles and ice nuclei during rain. **Atmospheric Chemistry and Physics Discussion** 13, 1767-1793, 2013.
- Prenni, A. J., Tobo, Y., Garcia, E., DeMott, P. J., Huffman, J. A., McCluskey, C. S., Kreidenweis, S. M., Prenni, J. E., Pöhlker, C., Pöschl, U., The impact of rain on ice nuclei populations at a forested site in Colorado. **Geophysical Research Letters**, 40(1), 227-231, 2013.
- Pöhlker, C., Huffman, J. A., Förster, J.-D., Pöschl, U., Autofluorescence of atmospheric bioaerosols – the spectral fingerprint and taxonomic trends of native pollen. **Atmospheric Measurement Techniques Discussion to be submitted**, 2013.
- Healy, D. A., Huffman, J. A., O'Connor, D. J., Pöhlker, C., Pöschl, U., Sodeau, J. R., Ambient measurements of biological aerosol particles near Killarney, Ireland: a comparison between fluorescence and optical microscopy approaches, *in preparation*, 2013.
- Pöhlker, C., Wiedemann, K. T., Saturno, J., Förster, J.-D., Krüger, M., Shiraiwa, M., Artaxo, P., Kilcoyne, A. L. D., Weigand, M., Pöschl, U., Andreae, M. O., STXM-NEXAFS analysis of Amazonian aerosols, *in preparation*, 2013.
- Pöhlker, C., Huffman, J. A., Förster, J.-D., Pöschl, U., Autofluorescence of atmospheric bioaerosols – water influence on pollen morphology and autofluorescence, *in preparation*, 2013.
- Sinha, B. W., Pöhlker, C., Wiedemann, K. T., Harris, E., Hoppe, P., Kilcoyne, A. L. D., Andreae, M. O., Gunthe, S. S., Pöschl, U., Borrmann, S., Investigating the chemical composition and mixing state of secondary aerosol particles using NanoSIMS, *in preparation*, 2013.

## Selected oral presentations

Pöhlker, C., Huffman, J. A., Pöschl, U., Fluoreszenz von Biopartikeln: On-Line-Detektion und Mikroskopie. TSI Seminar on aerosol measurement techniques, Berlin, Germany, April 2010.

Pöhlker, C., Wiedemann, K. T., Sinha, B., Smith, M., Artaxo, P., Gilles, M. K., Kilcoyne, A. L. D., Moffet, R. C., Martin, S. T., Pöschl, U., Andreae, M. O., STXM-NEXAFS investigations of laboratory secondary organic aerosols and Amazonian background aerosols. EGU General Assembly, Vienna, Austria, May 2011.

Pöhlker, C., Wiedemann, K. T., Sinha, B., Shiraiwa, M., Gunthe, S. S., Smith, M., Su, H., Artaxo, P., Chen, Q., Cheng, Y., Elbert, W., Gilles, M. K., Kilcoyne, A. L. D., Moffet, R. C., Weigand, M., Martin, S. T., Pöschl, U., Andreae, M. O., Composition and formation of organic aerosol particles in the Amazon. EGU General Assembly, Vienna, Austria, April 2012.

Pöhlker, C., Wiedemann, K. T., Sinha, B., Shiraiwa, M., Gunthe, S. S., Smith, M., Su, H., Artaxo, P., Chen, Q., Cheng, Y., Elbert, W., Gilles, M. K., Kilcoyne, A. L. D., Moffet, R. C., Weigand, M., Martin, S. T., Pöschl, U., Andreae, M. O., Composition and formation of organic aerosol particles in the Amazon. European Aerosol Conference, Granada, Spain, September 2012.

Pöhlker, C., et al., Single particle studies on biogenic aerosols. Chemistry seminar, University of Pretoria, Pretoria, South Africa, February 2013.

## Selected poster presentations

Pöhlker, C., Huffman, J. A., Pöschl, U., Bioaerosol analysis by online fluorescence detection and fluorescence microscopy. EGU Assembly, Vienna, Austria, May 2010.

Pöhlker, C., Huffman, J. A., Pöschl, U., Fluorescence of bioparticles: on-line detection and microscopy. International Aerosol Conference (IAC), Helsinki, Finland, August 2010.

Pöhlker, C., Huffman, J. A., Pöschl, U., Autofluorescence of bioaerosol standards - characterization by fluorescence spectroscopy and microscopy. EGU Assembly, Vienna, Austria, May 2011.

Pöhlker, C., Wiedemann, K. T., Sinha, B., Shiraiwa, M., Gunthe, S. S., Smith, M., Su, H., Artaxo, P., Chen, Q., Cheng, Y., Elbert, W., Gilles, M. K., Kilcoyne, A. L. D., Moffet, R. C., Weigand, M., Martin, S. T., Pöschl, U., Andreae, M. O., STXM-NEXAFS investigations of laboratory secondary organic aerosols and Amazonian background aerosols. European Aerosol Conference (EAC), Manchester, UK, September 2011.

Pöhlker, C., Huffman, J. A., Pöschl, U., Autofluorescence of bioaerosol standards - characterization by fluorescence spectroscopy and microscopy. EGU Assembly, Vienna, Austria, April 2012.

Pöhlker, C., Huffman, J. A., Förster, J.-D., Pöschl, U., Autofluorescence of atmospheric bioaerosols – fluorescent biomolecules, biological standard particles and potential interferences. European Aerosol Conference (EAC), Granada, Spain, September 2012.



## Appendix B

### Selected publications

- B1. Pöhlker, C., Huffman, J. A., Pöschl, U., Autofluorescence of atmospheric bioaerosols – fluorescent biomolecules and potential interferences. **Atmospheric Measurement Techniques** 5, 37-71, 2012.
- B2. Pöhlker, C., Huffman, J. A., Förster, J.-D., Pöschl, U., Autofluorescence of atmospheric bioaerosols – the spectral fingerprint and taxonomic trends of native pollen. **Atmospheric Measurement Techniques Discussion** *to be submitted*, 2013.
- B3. Huffman, J. A., Pöhlker, C., Prenni, A. J., DeMott, P. J., Mason, R. H., Robinson, N. H., Fröhlich-Nowoisky, J., Tobo, Y., Després, V. R., Garcia, E., Gochis, D. J., Harris, E., Müller-Germann, I., Ruzene, C., Schmer, B., Sinha, B., Day, D. A., Andreae, M. O., Jimenez, J. L., Gallagher M., Kreidenweis, S. M., Bertram, A. K., Pöschl, U., High concentrations of biological aerosol particles and ice nuclei during rain. **Atmospheric Chemistry and Physics Discussion** 13, 1767-1793, 2013.
- B4. Pöhlker, C., Wiedemann, K. T., Sinha, B., Shiraiwa, M., Gunthe, S. S., Smith, M., Su, H., Artaxo, P., Chen, Q., Cheng, Y., Elbert, W., Gilles, M. K., Kilcoyne, A. L. D., Moffet, R. C., Weigand, M., Martin, S. T., Pöschl, U., Andreae, M. O., Biogenic potassium salt particles as seeds for secondary organic aerosol in the Amazon. **Science**, 337, 1075-107



**B1. Pöhlker et al., Atmos. Meas. Tech., 2012**

**Autofluorescence of atmospheric bioaerosols –  
fluorescent biomolecules and potential interferences**

Christopher Pöhlker<sup>1</sup>, J. Alex Huffman<sup>2</sup>, and Ulrich Pöschl<sup>1</sup>

*1 Max Planck Institute for Chemistry, Biogeochemistry Department, Mainz, Germany*

*2 University of Denver, Department of Chemistry and Biochemistry, Denver, Colorado, USA*

**Atmospheric Measurement Techniques 5, 37-71, 2012.**





# Autofluorescence of atmospheric bioaerosols – fluorescent biomolecules and potential interferences

C. Pöhlker<sup>1</sup>, J. A. Huffman<sup>1,2</sup>, and U. Pöschl<sup>1</sup>

<sup>1</sup>Max Planck Institute for Chemistry, Biogeochemistry Department, P.O. Box 3060, 55020 Mainz, Germany

<sup>2</sup>University of Denver, Department of Chemistry and Biochemistry, 2190 E. Illif, Denver, Colorado, 80208, USA

Correspondence to: J. A. Huffman (alex.huffman@du.edu)

Received: 12 July 2011 – Published in Atmos. Meas. Tech. Discuss.: 16 September 2011

Revised: 16 December 2011 – Accepted: 19 December 2011 – Published: 9 January 2012

**Abstract.** Primary biological aerosol particles (PBAP) are an important subset of air particulate matter with a substantial contribution to the organic aerosol fraction and potentially strong effects on public health and climate. Recent progress has been made in PBAP quantification by utilizing real-time bioaerosol detectors based on the principle that specific organic molecules of biological origin such as proteins, coenzymes, cell wall compounds and pigments exhibit intrinsic fluorescence. The properties of many fluorophores have been well documented, but it is unclear which are most relevant for detection of atmospheric PBAP. The present study provides a systematic synthesis of literature data on potentially relevant biological fluorophores. We analyze and discuss their relative importance for the detection of fluorescent biological aerosol particles (FBAP) by online instrumentation for atmospheric measurements such as the ultraviolet aerodynamic particle sizer (UV-APS) or the wide issue bioaerosol sensor (WIBS).

In addition, we provide new laboratory measurement data for selected compounds using bench-top fluorescence spectroscopy. Relevant biological materials were chosen for comparison with existing literature data and to fill in gaps of understanding. The excitation-emission matrices (EEM) exhibit pronounced peaks at excitation wavelengths of ~280 nm and ~360 nm, confirming the suitability of light sources used for online detection of FBAP. They also show, however, that valuable information is missed by instruments that do not record full emission spectra at multiple wavelengths of excitation, and co-occurrence of multiple fluorophores within a detected sample will likely confound detailed molecular analysis. Selected non-biological

materials were also analyzed to assess their possible influence on FBAP detection and generally exhibit only low levels of background-corrected fluorescent emission. This study strengthens the hypothesis that ambient supermicron particle fluorescence in wavelength ranges used for most FBAP instruments is likely to be dominated by biological material and that such instrumentation is able to discriminate between FBAP and non-biological material in many situations. More detailed follow-up studies on single particle fluorescence are still required to reduce these uncertainties further, however.

## 1 Introduction

### 1.1 Primary biological aerosol particles

Primary biological aerosol particles (PBAP), also referred to as bioaerosols, are a diverse collection of small pieces of material emitted directly from the biosphere into the atmosphere (Després et al., 2012). They are globally ubiquitous, in some cases can dominate suspended particle concentrations, and comprise a diverse selection of particle types, including: whole organisms (e.g. bacteria, algae), reproductive entities (e.g. pollen, spores from fungi, bacteria, ferns, mosses), biopolymers (e.g. DNA, chitin, cellulose and other polysaccharides), plant debris, insect parts, and decaying biomass (e.g. Gregory, 1973; Madelin, 1994; Cox and Wathes, 1995; Andreae and Crutzen, 1997; Jones and Harrison, 2004; Jaenicke, 2005; Pöschl, 2005; Elbert et al., 2007; Jaenicke et al., 2007; Bauer et al., 2008; Pöschl et al., 2010; Després et al., 2012). PBAP can span several orders

of magnitude in particle diameter, from a few nanometers (e.g. viruses) to hundreds of micrometers (e.g. plant debris), making analysis challenging. A number of studies have indicated that PBAP may comprise large fractions of ambient particulate matter (PM) in many environments. Microscopic investigations have shown that PBAP can account for up to ~30 % of fine (<1  $\mu\text{m}$ ) and up to ~70 % of coarse (>1  $\mu\text{m}$ ) PM in rural and rain forest air, and estimates of PBAP emissions range from ~60  $\text{Tg a}^{-1}$  of fine PM to ~1000  $\text{Tg a}^{-1}$  in all size ranges (Penner, 1994; Jaenicke, 2005; Elbert et al., 2007). Fungal spores in particular account for a large proportion of PBAP with typical mass concentrations of ~1  $\mu\text{g m}^{-3}$  in continental boundary layer air and estimated global emissions in the order of ~50  $\text{Tg a}^{-1}$  (Elbert et al., 2007).

The aerial dispersal and transport of biological aerosols, particularly reproductive material such as spores and pollen, is an important pathway for the spread of organisms within and across ecosystems (Gregory, 1973; Elbert et al., 2007). Bioaerosols may act as giant cloud condensation nuclei (CCN) and ice nuclei (IN) (e.g. Dingle, 1966; Schnell and Vali, 1972; Lohmann and Feichter, 2005; Sun and Ariya, 2006; Möhler et al., 2007; Christner et al., 2008), thus influencing global climate by affecting cloud formation and precipitation. They also play a crucial role in public health by spreading disease to humans (e.g. tuberculosis, influenza), animals (e.g. anthrax, brucellosis) and crops (e.g. rust, smut) and by causing allergies (e.g. Lacey and Dutkiewicz, 1994; Linskens and Cresti, 2000; Brown and Hovmoller, 2002; Douwes et al., 2003; Franze et al., 2005). As a result, quantification of local PBAP concentrations and identification of individual species or classes is essential for diverse scientific fields such as climatology, atmospheric science, human health, crop science and agriculture, biogeography, and others. Within the last two decades, especially, the detection of bioaerosols used as biological warfare agents (BWA) has also become important, both on the battlefield and with respect to domestic terrorism (e.g. Hill et al., 1995; Pinnick et al., 1995; Primmerman, 2000; Ho, 2002; Lim et al., 2005; Manninen et al., 2008).

Existing methods for PBAP measurement have historically been off-line techniques which suffer from poor time resolution (hours to days), requiring costly and time consuming sample analysis (Griffiths and Decosemo, 1994). As a result, much work has been done to report qualitative and semi-quantitative observations of certain ambient bioaerosol classes, but systematic efforts to quantify PBAP as a whole have been limited (e.g. Lighthart and Shaffer, 1995; Matthias-Maser et al., 2000). Counting methods based on cultivation of viable airborne organisms cause certain methodologically difficulties that make comparison with other techniques difficult. For example, the “great plate count anomaly” describes the well known problem that only a small fraction (typically <10 %, often <1 %) of airborne microorganisms form colonies on a typical culture media (Amann et al., 1995; Heidelberg et al., 1997; Chi

and Li, 2007), thus leading to a significant underestimation of the actual viable airborne bioaerosol concentration. The vast remaining number of airborne microorganisms can be described as viable but non-culturable (VBNC), indicating very low metabolic activity or resting dormant state (Roszak and Colwell, 1987). Even non-viable PBAP can be important for atmospheric, biological, and human health concerns, however.

Cultivation methods only attempt to count full, viable (living) organisms, while other physical or chemical techniques are able to selectively analyze non-viable cells or fragments of biological material. In recent years virtually every available chemical, biological, and physical technique of analysis has been applied to the measurement of ambient PBAP, and a full review of these attempts is well beyond the scope of this manuscript (e.g. Spurny, 1994; Ho, 2002; Georgakopoulos et al., 2009; Després et al., 2012; Xu et al., 2011). Mass spectrometry (MS), in its various forms, has been successful at detecting PBAP with high time resolution and detailed chemical identification of analyzed particles (e.g. Parker et al., 2000; Fergenson et al., 2004; van Wuijckhuijse et al., 2005). Among modern microbiological methods, polymerase chain reaction (PCR) and quantitative PCR (qPCR) are promising tools for identification and quantification of cells from a specific organism via identification of sampled DNA, although the techniques are not capable of providing an estimate of the total PBAP concentration (e.g. Després et al., 2007; Bowers et al., 2009; Fröhlich-Nowoisky et al., 2009; Bowers et al., 2011). Epifluorescence microscopy, particularly in combination with the use of fluorescent dyes, has been a frequently utilized technique for PBAP quantification and refers to the microscopic imaging of the distribution of fluorescent compounds in cells or tissue (e.g. Hobbie et al., 1977; Kepner and Pratt, 1994). By staining specific cell constituents (e.g. DNA, proteins, cell walls) PBAP can be analyzed regardless of the metabolic state of the organism, thus overcoming the problem of poor culturability. The commercial availability of a wide selection of fluorescent dyes allows a flexible and selective quantification of many classes of microorganisms (McFeters et al., 1995; Li et al., 2004). The method suffers from the need for time-consuming and, therefore, costly sample analysis, however. Instruments able to discriminate biological content in real-time based on the emission of laser-induced fluorescence (LIF) have recently become commercially available and are among the most promising techniques for ambient atmospheric PBAP analysis (e.g. Pinnick et al., 1995; Hairston et al., 1997; Kaye et al., 2000). While these do not offer the molecular specificity or detailed imaging capabilities of microscopy, many instruments are able to provide an estimate of PBAP properties in real-time, with high time and size resolution (e.g. Huffman et al., 2010).

## 1.2 Physical principles of fluorescence

Spectroscopy refers to a wide class of analytical techniques where an analyte is selectively interrogated through interaction with a region of the electromagnetic radiation, and has been widely applied to virtually every scientific field, including the measurement of biological aerosols. For the purpose of clarifying arguments later in the paper we present a brief overview of key spectroscopic principles here. Analyte molecules exposed to incident radiation can either absorb or scatter incoming photons. If photons are absorbed or inelastically scattered, energy is imparted to a molecule that can be dissipated either radiatively, non-radiatively, or through a combination of both (e.g. fluorescence, phosphorescence). Molecular fluorescence can be seen mechanistically as an inelastic light scattering process (i.e. energy is imparted to the molecule) with three distinct electronic steps: (I) Photon absorption causes an electron to transition from the lowest vibrational state of the electronic ground state of the molecule to a higher vibrational state of an excited electronic state. (II) This is followed by dissipation of energy through non-radiative decay (heat) and transition of the electron to the lowest vibrational level of the excited electronic state. (III) The electron can then return to the electronic ground state by radiative emission (fluorescence) or through a variety of non-radiative processes (quenching), depending largely on the local molecular environment. Many different quenching mechanisms are possible, such as collision quenching (i.e. by oxygen or water) and concentration quenching (i.e. self-quenching and inner-filtering effects) (Sinski and Exner, 2007). Phosphorescence is mechanistically similar to fluorescence, except that a spin change occurs due to an intersystem conversion in the excited electronic state. This leads to the practical distinction that the timescale of radiative emission for fluorescence (ns) is up to several orders of magnitude shorter than for phosphorescence ( $\mu\text{s}$ -ms) (RichardsKortum and SeavickMuraca, 1996).

Both excitation ( $\lambda_{\text{ex}}$ ) and emission wavelengths ( $\lambda_{\text{em}}$ ) are characteristic for a given fluorophore, and the most likely electron transition pathways for that molecule are determined by the overlap integral of the corresponding vibrational wave functions. Usually spontaneous fluorescent emission is specific for a certain fluorophore and its molecular environment and occurs at relatively narrow, defined  $\lambda_{\text{em}}$ . Molecular excitation, however, can occur over a comparatively wide spectral range due to several accessible electron transition pathways, but is still an important piece of information for fluorophore assignment. The spectral difference between  $\lambda_{\text{ex}}$  and  $\lambda_{\text{em}}$  is referred to as the Stokes shift ( $\Delta\lambda_{\text{Stokes}}$ ). An important feature of fluorescence is the independence of  $\lambda_{\text{em}}$  with respect to  $\lambda_{\text{ex}}$  which means that the qualitative appearance of the emission peak is similar for different excitation wavelengths. This is due to the fact that all non-radiative decay processes end in the lowest vibrational level of the first excited electronic state from where fluorescent

relaxation occurs. For further details see Lakowicz (1999), Kunnil (2005) and Ramanujam (2006).

The fluorescence properties of a molecule can be characterized by parameters of steady state fluorescence spectroscopy, such as  $\lambda_{\text{ex}}$  and  $\lambda_{\text{em}}$  or the quantum yield  $\Phi$  (fluorescent emission events per photons absorbed). Time resolved measurements also analyze the lifetime  $\tau$  of the excited state (average time the electron spends in the excited electronic state until it returns to the ground state). Large polymers, heterocyclic aromatic compounds, or molecules with conjugated double bonds are among classes of molecules known to be especially efficient at emitting fluorescence, particularly when nitrogenous substitutions are present. The incident light in the ultraviolet (UV) to visible range predominantly promotes electronic  $\pi - \pi^*$  transitions. Accordingly the size of the conjugated  $\pi$ -bond system and the identity of adjacent electron donating or withdrawing groups determine the spectral properties of the fluorescence process.

Fluorescence spectroscopy and imaging have become tools of enormous analytical importance, especially within biological research. The techniques can be divided into the general classes of extrinsic and intrinsic fluorescence. Extrinsic fluorescence refers to the addition of exogenous fluorophores to a set of analyte molecules in order to highlight biological components not easily distinguishable otherwise. This is achieved by insertion of a synthetic fluorescent probe into an organism or material in order to perform selective labeling of a certain target. As a result of its wide use, a large variety of fluorescent probes have become commercially available for selective labeling of macromolecules, cell parts or tissue and for subsequent analysis by various imaging techniques. For example fluorescent dyes such as 4',6-diamidino-2-phenylindole (DAPI) are useful tools to visualize DNA and RNA. Fluorescence in-situ hybridization (FISH) allows the labeling of complete DNA sequences in order to selectively detect and quantify specific organisms. In molecular biology the gene of the green fluorescent protein (GFP) has been introduced in many organisms where GFP is expressed for selective in vivo labeling of certain cell parts. These methods are powerful, in part, because they enable the combination of highly selective labeling of a target molecule with tools for quick, quantitative and non-invasive detection of fluorescence signals within tissue and biological material. Intrinsic fluorescence, or autofluorescence, in contrast, is caused by fluorescent molecules (fluorophores) which exist as a natural component of the analyte material. A large number of biological molecules and compounds are known to exhibit fluorescence light emission. Certain amino acids and coenzymes are among the most commonly analyzed biofluorophores, but numerous other metabolites and biogenic molecules emit fluorescence. Biological samples most often contain a multi-component mixture of biofluorophores, and, accordingly, the overall fluorescent emission often comprises a superposition of individual signals.

Intrinsic fluorescence has been extensively utilized in various fields such as tissue diagnostic (e.g. Koenig and Schneck-enburger, 1994; Andersson Engels et al., 1997), bioprocess monitoring (e.g. Marose et al., 1998; Pons et al., 2004), plant physiology (e.g. Roshchina, 2003, 2004), and environmental studies (e.g. Hudson et al., 2007; Wedborg et al., 2007).

### 1.3 History of online detection of fluorescent aerosols

While the use of fluorescence techniques to image biological specimens under a microscope is well established, the application of fluorescence to biological aerosol measurement has received significant attention only within the last decades and increasingly so recently. In particular, much effort has been placed on the use of laser/light-induced fluorescence (LIF) for online particle detection, because it allows the non-invasive, in-situ detection of particles with high temporal resolution. Most of the progress in this field has been a result of scientific communities focused on the detection of biological warfare agents (BWA) (e.g. Hill et al., 1995; Cheng et al., 1999; Seaver et al., 1999; Kaye et al., 2000; Ho, 2002). BWA sensors are designed to detect suspicious agents reliably, even in low concentrations, with a low false-positive rate and with short response. Especially challenging is the rapid and selective recognition of specific organisms on top of a diverse and variable ambient aerosol background. Naturally occurring PBAP such as pollen and fungal spores as well as certain non-biogenic aerosols (e.g. soot, industrial plumes) could, in some cases, mimic the BWA signal and trigger a false-alarm. Reliable distinction of analyzed particles is not possible by single-wavelength LIF, and so many instrument developers have added the ability to monitor additional optical properties of the sampled particles, such as: LIF at a second wavelength (dual-wavelength LIF), optical size, shape factor or light absorption.

Most BWA agents are bacteria and bacterial spores (*Bacillus anthracis*, *Yersinia pestis*), viruses (Ebola virus, Marburg virus) and toxins (Ricin, Botulinum toxin) (Hawley and Eitzen, 2001; Kamboj et al., 2006). It has been shown that amino acids (i.e. tryptophan) and some coenzymes (i.e. NAD(P)H, flavins, vitamin B<sub>6</sub> and B<sub>9</sub> compounds) dominate the fluorescence properties of these agents, particularly bacteria (Dalterio et al., 1987; Kopczyński et al., 2005; Johansson and Liden, 2006; Włodarski et al., 2006), thus simplifying the list of molecules desired for online detection. Viable bacteria usually exhibit a coenzyme signal due to increased metabolic activity and an amino acid signal due to proteins and peptides. In contrast, viruses and peptide toxins exclusively show a protein signal. Accordingly, BWA sensors are individually optimized to match the spectral properties of these agents.

Decades of research by military agencies interested in detecting BWA have recently led to the development and commercialization of several instruments now available for civilian use and that have begun to contribute to atmospheric

measurement and research. The ultraviolet aerodynamic particle sizer (UV-APS), for example, provides aerodynamic particle sizing and fluorescence information via single-wavelength LIF by a pulsed Nd:YAG laser ( $\lambda_{\text{ex}} = 355 \text{ nm}$ ;  $\lambda_{\text{em}} = 420\text{--}575 \text{ nm}$ ) (Hairston et al., 1997; Brosseau et al., 2000) and is sold by TSI, Inc. (Shoreview, MN, USA). The University of Hertfordshire wide issue bioaerosol sensor (WIBS) optically provides particle sizing, an estimate of particle sphericity, and fluorescence information based on dual-wavelength LIF by a Xe-flashlamp ( $\lambda_{\text{ex},1} = 280 \text{ nm}$ ,  $\lambda_{\text{ex},2} = 370 \text{ nm}$ ;  $\lambda_{\text{em}} = 310\text{--}400$  and  $400\text{--}600 \text{ nm}$ ) (Kaye et al., 2000; Stanley et al., 2011). The Bristol Industrial and Research Associates Limited (BIRAL) aerosol fluorescence sensor (AFS) provides particle size and sphericity based on light scattering and fluorescence information after excitation from a UV flash lamp ( $\lambda_{\text{ex}} = 280 \text{ nm}$ ;  $\lambda_{\text{em}} = 330\text{--}650$  and  $420\text{--}600 \text{ nm}$ ). Both, UV-APS and WIBS have been utilized for ambient measurements in urban European (Huffman et al., 2010; Gabey, 2011) and in pristine rainforest (Gabey et al., 2010; Pöschl et al., 2010; Huffman et al., 2011) environments. These instruments have provided the first continuous and quantitative measurements of fluorescent biological aerosol particles (FBAP) with both high temporal and size resolution, thus providing a lower limit of PBAP concentrations (Huffman et al., 2010). Similar future experiments will help provide crucial input estimates of PBAP flux for global transport models (e.g. Burrows et al., 2009; Heald and Spracklen, 2009; Hoose et al., 2010).

### 1.4 Fluorescence spectral maps and online FBAP detectors

Wavelength-dependent fluorescence emission spectra, recorded as a function of excitation wavelength, can be plotted as a three-dimensional landscape and thus referred to as an excitation-emission matrix (EEM). Such plots, accordingly, relay a broad collection of information about the steady-state autofluorescence properties of a compound and can be regarded as a unique, sample-specific fingerprint. Similar spectral summaries have been applied as valuable tools in various scientific fields, such as environmental (Kunnil, 2005; Hudson et al., 2007; Wedborg et al., 2007) and medical science (DaCosta et al., 2003; Chang et al., 2005), because they allow a quick, quantitative and non-invasive in-situ characterization with high sensitivity (detection limit:  $10^{-8}\text{--}10^{-9} \text{ M}$ ) (Miao et al., 2003). EEMs may also help facilitate the qualitative assignment of spectral modes to known fluorophores, thus providing insights into the molecular origin of fluorescence. This kind of analysis in the laboratory, in complement to ambient PBAP detection, is particularly necessary for the identification of fluorophores responsible for fluorescence within atmospheric biological particles, and consequently may also allow the estimation of the fluorophore selectivity of a given real-time instrument.



Light scattering effects can complicate peak assignment of fluorescence spectra and, in particular, quantification of fluorescence. Three types of light scattering are typically important for laboratory fluorescence measurements. Rayleigh scattering can originate from both sample and solvent (i.e. water) molecules, which are smaller than the incident wavelength, and Tyndall scattering is a strongly wavelength-dependent reflection process from particulate matter in a suspension (Zepp et al., 2004). Both are types of elastic scattering, meaning that the incident wavelength is identical to the emitted or reflected wavelength ( $\lambda_{em} = \lambda_{ex}$ ). Inelastic Raman scattering from solvent molecules (i.e. water O-H stretching mode) is a much weaker process and appears at slightly longer wavelengths than the elastic scattering signal in solution-phase samples (Ewald et al., 1983; Zepp et al., 2004; Bhartia et al., 2008). If present, each scattering effect can appear as peak in a given emission spectrum and can be further distorted by non-idealities in the spectrometer wavelength dispersion or filtering. For example, elastic scattering of 350 nm incident light will exhibit a sharp peak at the same wavelength in the emission spectrum, referred to as a first order effect ( $\lambda_{em} = \lambda_{ex}$ ), but diffraction gratings can also introduce peaks at emission wavelengths of diffraction orders. Thus second order diffraction would allow the same 350 nm incident photons to appear at 700 nm ( $\lambda_{em} = 2 \lambda_{ex}$ ) in the emission spectra. Higher order (e.g. 2nd, 3rd) diffraction, as well as 0-th order diffraction are also possible, but less intense. Imperfect wavelength filtering also allows photons with shorter or longer wavelength than desired to pass through the instrument optics and this is referred to as a form of “light leakage”. This phenomenon broadens the incoming wavelength peak and is noticeable by size of the tail of elastic scattering signal. For samples in solution the emission spectrum of pure solvent can be subtracted to reduce the influence of these interferences. No similar subtraction is possible for suspended or solid-phase samples, however, and scattering effects can, therefore, introduce artificial features to spectra.

Because fluorescence is an inelastic light scattering process, emitted radiation is by definition red-shifted with respect to the incident radiation ( $\lambda_{em} > \lambda_{ex}$ ). The Stokes shift is, therefore, also by definition positive. Typical  $\Delta\lambda_{Stokes}$  values of naturally occurring fluorophores are usually approximately 10–200 nm, which means that fluorescence signals usually appear between the 1st and 2nd order diffraction peaks of elastically scattered light (Lakowicz, 1999). As an example, contour plots of three frequently investigated biological fluorophores (tryptophan, NADPH and riboflavin) are shown in Fig. 1. Fluorescence modes usually occur as broad and relatively featureless peaks. As discussed in Sect. 1.2, electron transition can occur to different vibrational energy levels. The resulting vibrational fine structure can be seen for samples in the gas phase where fewer molecular collisions occur, but are usually not resolvable for condensed phase samples. Instead, the appearance of multiple distinct excitation modes (i.e. for riboflavin) is due to different electron

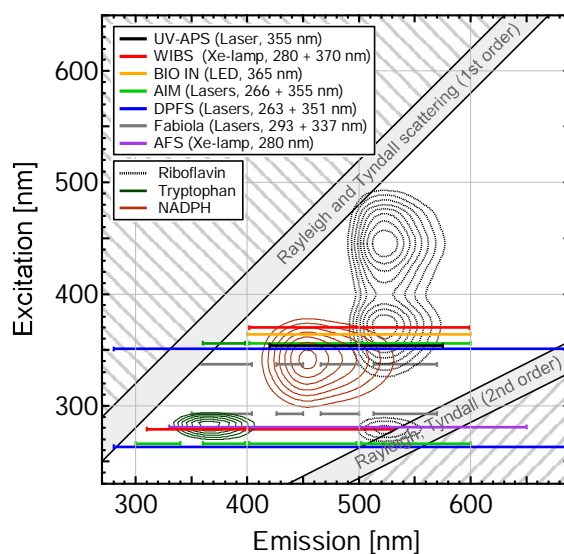


**Fig. 1.** Conceptual EEM displaying: (a) fluorescence data area (white), areas strongly influenced by Rayleigh and Tyndall light scattering (grey diagonal bars), areas without meaningful data (grey stripes); (b) contour lines for the fluorophores tryptophan, NADPH and riboflavin; (c) operational range of selected bioaerosol detectors represented by horizontal colored lines. Length of individual lines indicates measured emission band for a certain excitation wavelength shown as sharp line for purpose of clarity. Single-wavelength detectors are represented by one line, dual-wavelength detectors by two lines. Instruments shown with spectral specification: UV-APS (laser,  $\lambda_{ex} = 355$  nm,  $\lambda_{em} = 420$ – $575$  nm) (Hairston et al., 1997); WIBS (Xe-lamps,  $\lambda_{ex,1} = 280$ ,  $\lambda_{em,280} = 310$ – $400$ ,  $400$ – $600$ ;  $\lambda_{ex,2} = 370$ ,  $\lambda_{em,370} = 400$ – $600$ ) (Foot et al., 2008; Gabey, 2011); DPFS (lasers,  $\lambda_{ex,1} = 263$ ,  $\lambda_{em,263} = 280$ – $700$ ;  $\lambda_{ex,2} = 351$ ,  $\lambda_{em,351} = 280$ – $700$ ) (Pan et al., 2011); AIM (lasers,  $\lambda_{ex,1} = 266$ ,  $\lambda_{em,266} = 300$ – $340$ ,  $360$ – $400$ ,  $400$ – $500$ ,  $500$ – $600$ ;  $\lambda_{ex,2} = 355$ ,  $\lambda_{em,355} = 360$ – $400$ ,  $400$ – $500$ ,  $500$ – $600$ ) (Sivaprakasam et al., 2004, 2009); Fabiola (lasers,  $\lambda_{ex,1} = 293$ ,  $\lambda_{em,293} = 350$ – $404$ ,  $426$ – $450$ ,  $466$ – $500$ ,  $513$ – $570$ ;  $\lambda_{ex,2} = 337$ ,  $\lambda_{em,337} = 350$ – $404$ ,  $426$ – $450$ ,  $466$ – $500$ ,  $513$ – $570$ ) (Feugnet et al., 2008); SPFA (laser,  $\lambda_{ex} = 266$ ,  $\lambda_{em,266} = 300$ – $400$ ,  $400$ – $600$ ) (Snyder et al., 2004); BIO IN ( $\lambda_{ex} = 365$ ,  $\lambda_{em,365} = 400$ – $600$ ) (Bundke et al., 2010); AFS ( $\lambda_{ex} = 280$ ,  $\lambda_{em,280} = 330$ – $650$ ,  $420$ – $650$ ).

transition pathways (Lakowicz, 1999). Figure 1 also conceptually shows how EEMs can be utilized in this context. According to Thygesen et al. (2004) three different areas can be distinguished in an EEM: (I) the fluorescence data area (white), (II) areas dominated by strong light scattering interferences (gray diagonal bars), and (III) an area that lacks physical meaning because  $\lambda_{em} < \lambda_{ex}$  (gray stripes in upper left corner). Additionally, we have removed data from the lower right corner of each EEM for data shown here. In this region spurious peaks may appear which are caused by second order diffraction of the fluorescent light at the emission grating. As mentioned, the Raman signal of solvents can also be observed in certain situations and would appear in Fig. 1

as a weak diagonal signal whose slope is 0.75 times that of the 1st order elastic scattering line. Raman scattering was not directly observed in any measurements reported here, however, and will not be discussed further.

Figure 1 also summarizes the spectral ranges over which several current bioaerosol instruments detect FBAP. Though somewhat independent in terms of instrument design, only two relatively narrow ranges of excitation ( $\sim 280$  nm and  $\sim 360$  nm) have been utilized for most FBAP detectors. Excitation at  $\sim 280$  nm has typically been chosen to highlight the presence of tryptophan as a marker for proteins, and has therefore been used to estimate the total biological fraction in environmental samples. Excitation at  $\sim 360$  nm has typically been chosen to highlight NAD(P)H as a measure for the viable biological fraction, because they are directly linked to the cellular energy metabolism. These assumptions could potentially be problematically simplistic, as will be discussed further. Several dual-wavelength biodetectors have been designed to provide fluorescence from multiple wavelengths of excitation in an attempt to quantify both the whole FBAP fraction and an estimate of its viable subset (i.e. Kaye et al., 2005; Pan et al., 2010).

Selectivity, or the ability to separate fluorophore types within analyzed particles, is a key issue in the design of bioaerosol detectors. A reliable estimate of PBAP concentration requires clear distinction between biological and non-biological particles. It has been suggested that FBAP can be seen as a lower limit estimate for PBAP, because not all biofluorophores will fluoresce at a given wavelength, leading to an underestimation of PBAP concentration (Huffman et al., 2010). However, the exact relationship of FBAP and PBAP is complicated and still unknown. In addition, the ability to discriminate between viable and non-viable organisms based on LIF of key metabolic coenzymes (e.g. NADH) has been a key assumption in the development of many FBAP detectors. This separation and distinction has been successfully shown under certain defined conditions (e.g. in bioreactors and for aerosolized laboratory bacteria) but is highly uncertain under complex atmospheric conditions (Marose et al., 1998; Agranovski et al., 2003; Johansson and Liden, 2006; Li et al., 2011). Based on the amount of biological fluorophores that also fluoresce at wavelengths typically used to determine cell viability (see Table 1 and following discussion) it is almost certain that the signal at  $\sim 360$  nm, typically assumed to indicate the presence of NAD(P)H, reflects more than just viable FBAP. In all cases, however, detailed EEM plots can be a helpful tool to visualize the combination of fluorophores emission signals and the instruments operational range.

### 1.5 Motivation of fluorophore literature synthesis

As discussed, much work has been performed by the BWA community and more recently by researchers interested in ambient PBAP analysis to utilize autofluorescence for the

search of bioaerosols in the atmosphere, taking advantage of the fact that biological material contains characteristic intrinsic fluorophores. Both biological and non-biological material can exhibit intrinsic fluorescence, however, and so the challenge of discriminating between the two requires a firm knowledge of the corresponding fluorophores. Amino acids with aromatic residues (tryptophan, tyrosine, phenylalanine) and several coenzymes (e.g. NAD(P)H, flavins, and vitamin B<sub>9</sub> compounds) have been generally used by these communities as the most important fluorophores in biological cells and particles (i.e. Davitt et al., 2005; Kaye et al., 2005; Wlodarski et al., 2006; Pan et al., 2010). Whereas amino acids occur in all organisms as building blocks of proteins, coenzymes such as NADH and flavins have only been shown to occur in actively metabolizing organisms and therefore may be specific markers for living cells. Living bacteria actively metabolize and are an important subset of ambient PBAP, but other essential constituents, such as fungal and bacterial spores as well as pollen, do not exhibit measureable metabolic activity (Setlow and Setlow, 1977). As such, they may not contain significant concentrations of NADH, though this is not well agreed upon within the scientific community and we are not aware that the concentration of NADH has even been measured with individual fungal spores or pollen grains (Sivaprakasam et al., 2004; Hill et al., 2009).

This paper investigates the identity and properties of biogenic fluorophores that are most likely responsible for autofluorescence within FBAP. Understanding of the molecular origin of bioaerosol autofluorescence is critical to the development of and measurements with real-time FBAP instrumentation. Moreover a detailed understanding of commonly occurring fluorophores will aid the estimation of the selectivity that can be achieved by FBAP measurement. Some initial studies provide fluorescence spectroscopic data for different classes of PBAP, pure fluorophores and interferences (Campbell et al., 2005; Kopczyński et al., 2005; Wlodarski et al., 2006; Jeys et al., 2007; Hill et al., 2009; O'Connor et al., 2011). In this study we provide a synthesis of literature data as well as original laboratory measurements, designed to give a broad overview of intrinsic fluorophores most likely to be important within ambient aerosols. While subsets of information regarding intrinsic fluorescence of classes of biological molecules have been previously reviewed elsewhere (see Sec. 2), each from a certain perspective, the current synthesis comprehensively summarizes material relevant to atmospheric aerosol research for the first time. Fluorophores are characterized by their steady state fluorescence properties and discussed in relation to a collection of current fluorescent bioaerosol detectors. Moreover, we estimate the relative importance of these fluorophores to atmospheric measurement, using fluorescence characteristics and atmospheric abundance as primary metrics. We also provide fluorescent EEM maps measured with a bench-top spectrofluorometer both for a variety of bulk solid-, suspended-, and solution-phase biological fluorophores and for selected non-biological

compounds which could be considered as important interfering species for FBAP detection and quantification in certain ambient situations. This combination of information will be crucial in the future investigation of the fluorescent properties of standard bioaerosol particles in the laboratory under varied environmental conditions.

## 2 Literature synthesis

Many fields of science have utilized intrinsic fluorescence for study of biological molecules. The following section serves as an overview of existing knowledge about biological fluorophores that have potential atmospheric relevance. Several existing reviews have collected similar information from the perspective of disparate scientific fields such as biology (Billinton and Knight, 2001; Roshchina, 2003, 2005), medical science (Koenig and Schneckenburger, 1994; Richards-Kortum and Sevick-Muraca, 1996; Ramanujam, 2000; Da-Costa et al., 2003) and defense research (Kopczyński et al., 2005; Włodarski et al., 2006; Pan et al., 2010). Most of these overviews, however, are shorter and less exhaustive. For this reason we provide in this section a synthesis of literature values and knowledge that represent an extensive collection of fluorophores specifically relevant to atmospheric PBAP detection. Table 1 gives a summary of key parameters for each compound and a short characterization of the major fluorophore groups is given in the corresponding text section. Information about  $\lambda_{\text{ex}}$  and  $\lambda_{\text{em}}$  are based on data from different studies which are merged here into representative spectral ranges. Depending on data availability and measurement conditions, this can be seen as a general, but not exhaustive, characterization of the fluorescence properties of key fluorophores and classes. Moreover, as a first approach for general orientation the relevance of individual fluorophores for FBAP detection is estimated based on its fluorescence properties (category 1) and atmospheric abundance (category 2). Fluorophores were ranked as highly relevant if they show both intense fluorescence emission and are considered by the authors to be very abundant in PBAP. Fluorophores were ranked with medium relevance if one of the two categories was rated high and the other was considered weak/low. Low relevance means molecules are weakly fluorescent and show rare occurrence. While the terms listed here are uncertain and potentially contentious, we feel this language provides a qualitative means for discussion.

### 2.1 Group I – amino acids

Amino acids are the basic structural constituent of proteins and peptides in all organisms. Three amino acids with aromatic side chains – tryptophan (Trp), tyrosine (Tyr) and phenylalanine (Phe) – are known to UV or blue visible fluorescent emission when excited in the UV range of the

electromagnetic spectrum. All three are relatively rare in proteins (Trp: 1.1 % of total amino acid groups, average; Tyr: 3.5 %; Phe: 3.5 %) <sup>1</sup>, though still structurally important and of sufficient concentration to cause the omnipresent intrinsic fluorescence of proteins (Klapper, 1977; Creed, 1984a,b). However, it is known that tryptophan is the dominant fluorophore in proteins (causing approx. 90 % of the signal), due to a relatively high quantum yield ( $\Phi = 0.13\text{--}0.20$ , depending on microenvironment) and efficient (non-radiative) resonance energy transfer (RET) from phenylalanine and tyrosine to tryptophan (energy transfer quenching of Phe and Tyr fluorescence). Tyrosine is the major source of fluorescence for proteins and peptides without tryptophan, whereas phenylalanine is of only minor importance in all cases due to its low quantum yield ( $\Phi = \sim 0.02$ ) and efficient RET. Consequently, in most cases emission of fluorescence from proteins is dominated by tryptophan, though specific properties are also highly sensitive to the protein's molecular environment (i.e. conformational transitions, substrate binding, denaturation which leads to variations in emission maximum and quantum yield between proteins) (Dalterio et al., 1987; Permyakov, 1993; Lakowicz, 1999; Ladokhin, 2000).

### 2.2 Group II – coenzymes and vitamins

This group summarizes fluorophores that can be assigned to coenzymes (free or bound to an enzyme) and vitamins. They frequently exhibit fluorescence due to heterocyclic aromatic rings within their molecular structures. The major classes of fluorescent coenzymes are the pyridines, pteridines, pyridoxines and structurally related flavins, among which NAD(P)H and flavins are most frequently studied (Dalterio et al., 1987; Lakowicz, 1999; Włodarski et al., 2006).

Two pyridine nucleotides, nicotinamide adenine dinucleotide (NADH) and nicotinamide adenine dinucleotide phosphate (NADPH), are well known fluorescent coenzymes which are often utilized as intrinsic fluorescent probes in various scientific fields (Bigio and Mourant, 1997; Huang et al., 2002). While similar in structure, the two coenzymes appear in different biochemical mechanisms. NADH is the universal coenzymatic redox carrier in the energy metabolism of cells, whereas NADPH is a ubiquitous reductant in biosynthesis processes (Klingenberg and Bucher, 1960; Michal, 1999; Voet and Voet, 2004). In contrast to the oxidized form NAD(P)<sup>+</sup>, only the reduced form NAD(P)H is fluorescent and can be utilized for an optical assessment of cell metabolic status (Eng et al., 1989; Li et al., 1991; Farabegoli et al., 2003; Wos and Pollard, 2006). Excitation occurs either at  $\sim 340$  nm (direct excitation of the coenzyme) or at  $\sim 295$  nm (light absorption by protein and RET to bound NAD(P)H) (Li and Lin, 1996). NADH and NADPH both show an emission signal at  $\sim 460$  nm and thus cannot be spectrally separated. For this reason the two molecules are often represented

<sup>1</sup>Based on sequences from 207 non-related proteins.

**Table 1.** Summary of atmospherically relevant biological fluorophores. Within the table the molecules are organized in six subgroups: (I) amino acids, (II) coenzymes and vitamins, (III) structural biopolymers and cell wall compounds, (IV) pigments, (V) secondary metabolites and (VI) others. Every fluorophore or family of fluorophores, respectively, is characterized by means of its natural occurrence (organism and metabolic function), its fluorescence properties (especially  $\lambda_{\text{ex}}$  and  $\lambda_{\text{em}}$  and quantum yield  $\Phi$  if available) and an estimation of its importance (high, medium or low) to ambient FBAP detection. The selection is focused on the main constituents of PBAP (in particular, microorganisms and debris from larger organisms). References are listed below table.

Fluorophore	Organism	Cell part/ Metabolic function	$\lambda_{\text{ex}}$ [nm]	$\lambda_{\text{em}}$ [nm]	Remarks	Role in FBAP detection ( <i>Estimated relevance</i> )
<i>I. Amino acids</i>						
Tryptophan (Trp)	All	Proteins	280–295 <sup>2–6</sup> 286 <sup>1</sup>	340–353 <sup>2–6</sup> 363 <sup>1</sup>	Amino acid (AA) with highest fluorescence in native proteins – responsible for ~90% of signal; $\Phi = 0.13–0.2$ ; Efficient RET from Tyr and Phe to Trp <sup>2–4,7</sup>	Most important AA for FBAP detection; used as indicator for total biomass; protein fluorescence resembles Trp signal; main target for many FBAP detectors ( <i>High</i> )
Tyrosine (Tyr)	All	Proteins	275 <sup>2–6</sup> 280 <sup>1</sup>	300–304 <sup>2–6</sup> 307 <sup>1</sup>	Signal in native proteins often quenched (RET: Tyr to Trp); responsible for ~10% of proteins fluorescence; $\Phi = 0.1–0.14$ <sup>2–4,7</sup>	Responsible for protein fluorescence when no Trp present; in presence of Trp, signal usually not detectable ( <i>Medium</i> )
Phenylalanine (Phe)	All	Proteins	260 <sup>2–6</sup> 270 <sup>1</sup>	280–282 <sup>2–6</sup> 296 <sup>1</sup>	Signal in native proteins often quenched (RET: Phe to Trp); Weakly fluorescent; $\Phi = 0.02–0.04$ <sup>2–4,7</sup>	Negligible for proteins overall fluorescence ( <i>Low</i> )
<i>II. Cofactors, coenzymes, vitamins</i>						
Pyridine nucleotides: NADH and NADPH (Nicotinamide adenine dinucleotide (phosphate))	All	NADH: Ubiquitous coenzymatic redox carrier  NADPH: Reductant in biosynthesis	290–295, 340–366 <sup>2–5,8,9</sup> 341 <sup>1</sup>	440–470 <sup>2–5,8,9</sup> 454 <sup>1</sup>	Only reduced form NAD(P)H fluorescent oxidized form NAD(P) <sup>+</sup> non-fluorescent, higher (fourfold) fluorescence intensity when bound to protein; spectral parameters sensitive to local environment <sup>2,10,11</sup>	Major contribution to fluorescence of metabolizing cells; used as indicator for viability main target for many FBAP detectors ( <i>High</i> )
Flavins: Riboflavin, Flavin mononucleotide (FMN), Flavin adenine dinucleotide (FAD)	All	Ubiquitous coenzymatic redox carrier (in most organisms) and photoreceptor (in plants, fungi)	380, 450–488 <sup>4,5,8,12,13</sup> 280, 373, 445 <sup>1</sup>	520–560 <sup>4,5,8,12,13</sup> 523 <sup>1</sup>	Only oxidized form fluorescent; $\Phi \sim 0.3$ ; Riboflavin and FMN show strong fluorescence, whereas FAD and flavoproteins (flavin non-covalently bound to protein) exhibit weak signal <sup>2,4,10,14</sup>	Indicator for cell metabolism; supposed to be a major source of cellular autofluorescence; target for many FBAP detectors ( <i>High</i> )
Vitamin B <sub>6</sub> compounds: Pyridoxine, Pyridoxamine, Pyridoxal, 4-Pyridoxic acid, Pyridoxal-5'- phosphate	All	Key coenzymes in amino acid, protein, carbohydrate, lipid and nucleic acid metabolism	315–345 <sup>5,8,15,16</sup> 280, 320–360 <sup>1</sup>	350–425 <sup>5,8,15,16</sup> 391–394 <sup>1</sup>	Fluorescence very sensitive to molecular environment and conditions (i.e. pH, ionization state, solvent polarity) <sup>10,15,17</sup>	Very abundant; strongly fluorescent; used as indicator for metabolic state in combination with other fluorophores ( <i>High</i> )

Table 1. Continued.

Fluorophore	Organism	Cell part/ Metabolic function	$\lambda_{\text{ex}}$ [nm]	$\lambda_{\text{em}}$ [nm]	Remarks	Role in FBAP detection ( <i>Estimated relevance</i> )
Pteridine compounds: Folic acid (vitamin B <sub>9</sub> ), Pterin, Biopterin, Neopterin, Lumazine	e.g. microorganisms, plants, archaea, mammals	Various metabolic functions (i.e. oxygenation reactions, cellular electron transport, growth factor)	331–361 <sup>4,18</sup> 335–355 <sup>1</sup>	373–458 <sup>4,18</sup> 446–454 <sup>1</sup>	Significant contribution to autofluorescence of various organisms; properties highly influenced by conditions <sup>4,10,12,19,20</sup>	Ubiquitous coenzymes; highly fluorescent; used as specific marker fluorophores; considered as particularly important for microorganisms ( <i>High</i> )
Vitamin A (retinol)	e.g. plants, mammals	Many, i.e. gene transcription, photodetection	327–340 <sup>5,8</sup>	490–510 <sup>5,8,21</sup>	Belongs to carotenoid compounds	Rarely mentioned in context of autofluorescence ( <i>Low</i> )
Vitamin C (ascorbic acid)	e.g. plants, algae, fungi, mammals	Many, i.e. involved in various biological redox reactions	350 <sup>8</sup>	430 <sup>8</sup>	Non-aromatic compound showing weak fluorescence	Rarely mentioned in context of autofluorescence; weakly fluorescent ( <i>Low</i> )
Vitamin D compounds: i.e. sterols: calciferol, ergosterol	e.g. plants, fungi, mammals	Many, i.e. involved in Ca <sup>2+</sup> and phosphate metabolism; cell wall components	390 <sup>5,8</sup>	470–480 <sup>5,8</sup>	Many sterol compounds known to be fluorescent; important cell wall fluorophores <sup>22,23</sup>	Ergosterol used as tracer for fungal spores; considered to be relative weakly fluorescent ( <i>Low</i> )
Vitamin K and quinones: i.e. phyloquinone, menaquinone, anthraquinone	e.g. plants, bacteria, mammals	Many, i.e. involved in photosynthetic processes	335 <sup>5</sup>	480 <sup>5</sup>	n/a	Rarely mentioned in context of autofluorescence ( <i>Low</i> )
<i>III. Structural biopolymers and cell wall compounds</i>						
Cellulose	Plants, algae, bacteria, oomycetes	Structural component of primary cell wall	250–350 <sup>24–26</sup> ~250, ~340 <sup>1</sup>	350–500 <sup>24–26</sup> 410–460 <sup>1</sup>	Nature of molecular fluorophores in cellulose not unequivocally identified; main contributor to cell wall fluorescence; weakly fluorescent compared to other fluorophores (i.e. secondary metabolites) <sup>24–27</sup>	Very abundant biopolymer (also in atmosphere); fluorescent emission over wide wavelength range; cell wall fluorescence common feature of FBAP ( <i>Medium</i> )
Chitin	Fungi, algae, arthropods, crustaceans, mollusks, insects	Principal cell wall compound	335 <sup>28–30</sup> 254, 373 <sup>1</sup>	413 <sup>28–30</sup> 452–458 <sup>1</sup>	Very abundant; i.e. occurrence in many fungi; brightly fluorescent <sup>28–30</sup>	Referred to as main fluorophore in fungal spore cell walls ( <i>High</i> )
Lignin	Plants, algae, (fungi)	Cell wall component; chief component of woody tissue support and protection	240–320 <sup>8,25,31</sup> 282, 331–345 <sup>1</sup>	360, 470–510 <sup>8,25,31</sup> 419–458 <sup>1</sup>	Polyphenolic macromolecule based on coniferyl, coumaryl, and sinapyl alcohols; $\lambda_{\text{ex}}$ and $\lambda_{\text{em}}$ dependent on organism and microenvironment of fluorophores; potential fluorophores: ferulic acid, phenylcoumarones, <i>cis</i> -stilbene, quimines <sup>32–34</sup>	Fluorescent emission over broad spectral range; highly abundant in nature; occurrence in plant debris ( <i>Medium</i> )

Table 1. Continued.

Fluorophore	Organism	Cell part/ Metabolic function	$\lambda_{ex}$ [nm]	$\lambda_{em}$ [nm]	Remarks	Role in FBAP detection (Estimated relevance)
Sporopollenin	Pollen, fungal spores, microspores	Cell wall constituent in exine	300–550 <sup>35–37</sup>	400–650 <sup>35–37</sup>	Complex biopolymer containing mixture of fluorescent compounds (i.e. phenolics, carotenoids, azulene) <sup>35–38</sup>	Origin of intense fluorescence from pollen (High)
Collagen and elastin	Mammals	Fibrous proteins; collagen: major extracellular matrix component; elastin: major component of elastic fibers	290, 325 <sup>3,5</sup>	340, 400 <sup>3,5</sup>	Cross links are origin of fluorescence (i) collagen: hydroxyllysyl pyridoline and lysyl pyridinoline; (ii) for elastin: tricarboxylic triannio pyridinium <sup>5</sup>	No occurrence in microorganisms; low abundance in FBAP (Low)
Suberin and cutin	Plants	Suberin: cell wall constituents of underground organs; Cutin: waxy polymer coating outer call walls	n/a	n/a	Three-dimensional hydrophobic network based on functionalized fatty acids and phenolic compounds; related to lignin <sup>32</sup>	Rarely mentioned in context of autofluorescence (Low)
Phospholipid	All	Major component of cell membranes	436 <sup>5</sup>	540, 560 <sup>5</sup>	Cell wall component in all cells	Rarely mentioned in context of autofluorescence (Low)
<i>IV. Pigments</i>						
Lipofuscin and ceroid (age-related pigments)	i.e. plants (pollen), bacteria, algae, fungi, mammals	Heterogeneous granules in residual body-type lysosomes in cytosol	260–280, 340–490 <sup>39,40</sup>	430–670 <sup>39,40</sup>	Strongly cross-linked lipid-protein pigmented substance; generated due to age, oxidative stress, antioxidant deficiency, UV-induced lipidic peroxidation <sup>41–43</sup>	Ubiquitous in biology; lipofus- cinogenesis induced by ozone or UV-light, known as fluorophore in pollen (Medium)
Advanced glycation end-products (AGEs) (age-related pigments)	i.e. mammals	Pigments caused by aging and oxidative stress	320–370 <sup>8,41</sup>	385–450 <sup>8,41</sup>	Products of non-enzymatic glycosylation (Maillard reaction); family of nitrogenous, cyclic and conjugated compounds <sup>8,41</sup>	(Low-medium)
Melanin	Mammals, fungi, bacteria	Accumulated in cell wall; protective response against adverse environmental conditions	469–471 <sup>44</sup>	543–548 <sup>44</sup>	Polymerized phenolic and/or indolic compounds, when non-oxidized: non-fluorescent, when oxidized (i.e. by ozone): shows bright fluorescence <sup>44,45</sup>	Ubiquitous in biology; in some cells highly concentrated; relatively low fluorescence intensity (Low)
Chlorophyll and pheopigments	Plants, cyanobacteria, purple and green bacteria, algae, cryptomonads	Photopigment for microbial and plant photosynthesis	390–470 <sup>46–48</sup>	630–730 <sup>46–48</sup>	Chlorophylls strongly fluorescent; pheopigments = chlorophyll degradation products; fluorescence of pheopigments weaker than of parent chlorophyll <sup>7,32,46</sup>	Very abundant in various organisms; (Medium)

Table 1. Continued.

Fluorophore	Organism	Cell part/ Metabolic function	$\lambda_{\text{ex}}$ [nm]	$\lambda_{\text{em}}$ [nm]	Remarks	Role in FBAP detection ( <i>Estimated relevance</i> )
Phycobiliproteins: i.e. phycoerythrin, phycocyanin, allophycocyanin	Plants, cyano- bacteria (= blue- green algae), red algae, cryptomonads	Photopigment in light-harvesting antenna complex for microbial and plant photosynthesis	480–650 <sup>49</sup>	580–660 <sup>49</sup>	High molar absorption coefficient ( $\sim 10^6 \text{ M}^{-1} \text{ cm}^{-1}$ ); high quantum yield (up to 0.98); broad excitation range <sup>49</sup>	Highly fluorescent; very abundant in algae and cyanobacteria – sometimes highly enriched (up to 40% of proteins in cells) ( <i>Medium</i> )
Flavonoids: i.e. anthocyanins, flavones, flavonols, isoflavones	Plants	Defense, attraction of pollinators, UV-shielding	365 <sup>36,50</sup>	440–610 <sup>36,50</sup>	Major class of colored pigments; oligophenolic compounds; spectral properties (coloration) span over wide range depending on functionalization; wide occurrence in plants <sup>32,51</sup>	Flavonol accumulated in pollen (2–4% of dry weight); known to be major fluorescent component in pollen ( <i>High</i> )
Carotenoids: i.e. carotenes, xanthophylls, retinoids	Plants, algae, bacteria, fungi	Accessory pigment in photosynthesis; UV-protection	400–500 <sup>36,50</sup>	520–560 <sup>36,50</sup>	Major compound family of colored pigments; (tetra)terpenoid compounds <sup>32,51</sup>	Widely distributed in plants; enriched in outer pollen wall ( <i>High</i> )
<i>V. Secondary metabolites</i>						
Alkaloids: i.e. amino acid based, purine and polyketide alkaloids	e.g. plants, fungi, bacteria, insects, animals	Many, i.e. defense agents against predators and pathogens	360–380 <sup>36,37,52</sup>	410–600 <sup>36,37,52</sup>	Heterocyclic nitrogenous compounds; structurally highly diverse compound class; $\lambda_{\text{em}}$ spans broad spectral range <sup>32,36,52</sup>	Occurrence in many (micro)- organisms; strongly autofluorescent ( <i>High–medium</i> )
Phenolics: Simple compounds (i.e. coumarins), oligophenolics (i.e. flavonoids), polyphenolics (i.e. tannins)	e.g. plants, fungi, bacteria,	Many, i.e. defense agents, pollinator attractors, UV- shielding, constituent of supporting tissue	300–380 <sup>36,52</sup>	400–500 <sup>36,52</sup>	Chemically highly heterogeneous group; fluorescence mostly in blue range, although variety of structures <sup>32,36,52</sup>	Wide occurrence particularly in plants; many compounds fluoresce – some with high intensity; crucial for cell wall fluorescence; ( <i>High–medium</i> )
Terpenoids: i.e. monoterpenes (e.g. menthol), sesquiterpenes (e.g. azulenes), diterpenes	e.g. plants, fungi	Many, i.e. pigments, growth factors, messengers, toxins	250–395 <sup>36</sup>	400–725 <sup>36,37</sup>	Fluorescent over wide spectral range depending on structure <sup>2,36,52</sup>	Very abundant; some compounds known to be highly fluorescent ( <i>Medium</i> )
Other secondary metabolites: i.e. mycotoxins, siderophores, cytokinines, Mycosporine-like amino acids (MAAs)	Plants, bacteria, fungi	Various metabolic functions	n/a	n/a	Many heterocyclic aromatic compounds, hence potentially highly fluorescent; very broad range of reported fluorescence properties <sup>52</sup>	High diversity of compounds; individual compounds can be highly fluorescent and relevant for FBAP detection ( <i>Medium</i> )

Table 1. Continued.

Fluorophore	Organism	Cell part/ Metabolic function	$\lambda_{ex}$ [nm]	$\lambda_{em}$ [nm]	Remarks	Role in FBAP detection ( <i>Estimated relevance</i> )
<i>VI. Others</i>						
Dipicolinic acid (DPA) and salts CaDPA, NaDPA	Unique constituents of bacterial endospores	Accumulated in spore core; supposed role in dormancy, heat- and UV- resistance	278, 300–360 <sup>53, 54</sup>	400–440 <sup>53, 54</sup>	DPA = 2-6-pyridine-dicarboxylic acid (C <sub>7</sub> H <sub>5</sub> N <sub>2</sub> O <sub>4</sub> ); 5–17% of dry weight; highly fluorescent after UV- exposure and/or when dry <sup>53, 54</sup>	Highly fluorescent; high concentration in spores as important bacterial propagation vector in atmosphere ( <i>Medium</i> )
DNA/RNA	All	Storage for genetic information	260 <sup>52, 55</sup>	334 <sup>52, 55</sup>	Quantum yield 100 times lower than for Trp <sup>52, 56–58</sup>	Ubiquitous in organisms but weak fluorescence emission ( <i>Low</i> )

<sup>1</sup> This report; <sup>2</sup> Lakowicz (1999); <sup>3</sup> Richards Kortum and Seviak Murua (1996); <sup>4</sup> Kopezyński et al. (2005); <sup>5</sup> Ramaniyam (2000); <sup>6</sup> Teale and Weber (1957); <sup>7</sup> Voet and Voet (2004); <sup>8</sup> Billinton and Knight (2001); <sup>9</sup> Avi-Dor et al. (1962); <sup>10</sup> Michal (1999); <sup>11</sup> Li and Lin (1996); <sup>12</sup> Włodarski et al. (2006); <sup>13</sup> Benson et al. (1979); <sup>14</sup> Albani et al. (1999); <sup>15</sup> Bridges et al. (1966); <sup>16</sup> Bueno and Enriñas (2003); <sup>17</sup> Li et al. (1991); <sup>18</sup> Dalerio et al. (1987); <sup>19</sup> Tyagi and Penzkofer (2010); <sup>20</sup> Rembold and Gyure (1972); <sup>21</sup> Zipfel et al. (2003); <sup>22</sup> McInosh et al. (2008); <sup>23</sup> Rosenheim (1927); <sup>24</sup> Olmstead and Gray (1993); <sup>25</sup> Olmstead and Gray (1997); <sup>26</sup> Castellani et al. (2007); <sup>27</sup> Jabagiare et al. (1984); <sup>28</sup> Bontanietasolo et al. (1990); <sup>29</sup> Viehellig et al. (1999); <sup>30</sup> Dreyer et al. (2006); <sup>31</sup> He et al. (1999); <sup>32</sup> Tairz and Zäiger (2010); <sup>33</sup> Donaldson et al. (1999); <sup>34</sup> Albinsson et al. (1999); <sup>35</sup> Roshchina et al. (1997); <sup>36</sup> Roshchina (2003); <sup>37</sup> Roshchina et al. (2004); <sup>38</sup> Brooks and Shaw (1978); <sup>39</sup> Eldred et al. (1982); <sup>40</sup> Andersson et al. (1998); <sup>41</sup> Ym (1996); <sup>42</sup> Tsuchida et al. (1987); <sup>43</sup> Roshchina and Karnaukhov (1999); <sup>44</sup> Kayatz et al. (2001); <sup>45</sup> Gomez and Nosanchuk (2003); <sup>46</sup> French et al. (1956); <sup>47</sup> Welschmeyer (1994); <sup>48</sup> Moberg et al. (2001); <sup>49</sup> Glazer (1994); <sup>50</sup> Roshchina and Mel'nikova (2001); <sup>51</sup> Wiernann and Vieh (1983); <sup>52</sup> Roshchina (2008); <sup>53</sup> Alimova et al. (2003); <sup>54</sup> Sarasandarajah et al. (2005); <sup>55</sup> Leblanc and Dufour (2002); <sup>56</sup> Pan et al. (2009); <sup>57</sup> Ammor et al. (2004); <sup>58</sup> Ammor (2007)



by a short-hand NAD(P)H form, referring to both molecules at once. It has been shown that the fluorescence contribution of NADH dominates that of NADPH, due to differences in cellular concentration and fluorescence characteristics. Furthermore the NADH signal is highly influenced by the metabolic status whereas the weaker NADPH signal is rather constant (Vishwasrao et al., 2005). The excited electronic state is quenched by two mechanisms: collisional deactivation and stacking of the fluorescent nicotinamide ring to the adenine moiety. The extent of quenching is decreased when NAD(P)H is bound to a protein, thus explaining the fourfold increase in fluorescence intensity as compared to free NAD(P)H in solution (Li and Lin, 1996). Because of its links to active cell metabolism, NAD(P)H has often been used in the search for viable airborne microorganisms (i.e. Hairston et al., 1997; Bundke et al., 2010). Cell death is accompanied by NADH and NADPH depletion within the temporal range of hours (2–10 h) depending on various intracellular processes and extracellular conditions (Petit et al., 2001; Liang et al., 2007).

Riboflavin (vitamin B<sub>2</sub>) is the precursor for both cofactors flavin mononucleotide (FMN) and flavin adenine dinucleotide (FAD), which are prosthetic groups of flavoenzymes (Benson et al., 1979). Flavins are ubiquitous redox carriers in the energy metabolism of all organisms and act also as photoreceptors in plants and fungi (Galland and Senger, 1988; Billinton and Knight, 2001). In contrast to NAD(P)H, only the oxidized form of flavins is fluorescent and shows light emission at ~525 nm when excited at ~450 nm, although excitation has also been observed at ~280 nm and ~380 nm (Hill et al., 2009). It is known that riboflavin and FMN show intense fluorescence, whereas FAD and especially flavoproteins exhibit only a weak fluorescence signal (Albani et al., 1999). Flavins are also connected to the metabolic status of cells, but at different rates than other coenzymes. Accordingly it has been suggested that the ratio of fluorescence emission of NAD(P)H to flavins can be used as indicator for the cellular metabolic rate (Chance et al., 1979; Siano and Mutharasan, 1989; Heikal, 2010).

Vitamin B<sub>6</sub> acts as precursor for the coenzyme pyridoxine and related compounds (i.e. pyridoxal 5'-phosphate, pyridoxamine 5'-phosphate). Pyridoxine and related coenzymes are required by many enzymes that are involved in amino acid, protein, carbohydrate, lipid and nucleic acid metabolism in all organisms (Martell, 1989; Voet and Voet, 2004). Pyridoxine compounds comprise a substituted pyridine ring as structural fluorophore and its spectral characteristics are highly sensitive to its molecular environment (i.e. pH, ionization state, solvent polarity). Accordingly fluorescence occurs in a relatively broad spectral ranges depending on the conditions ( $\lambda_{\text{ex}} = 315\text{--}345\text{ nm}$ ,  $\lambda_{\text{em}} = 350\text{--}425\text{ nm}$ ) (Bridges et al., 1966; Bueno and Encinas, 2003). Pyridoxine compounds are key metabolites and along with NAD(P)H and flavins have been commonly utilized as indicators for metabolic activity, often in combination with other intrinsic

fluorophores (i.e. Trp, NAD(P)H) (Siano and Mutharasan, 1989; Li et al., 1991; Heikal, 2010).

Pteridine compounds are ubiquitous within most organisms and as a group are comprised by: folic acid (vitamin B<sub>9</sub>), pterins, and lumazines, among others. They are involved in various biochemical processes, such as oxygenase reactions, single carbon transfer reactions and cellular electron transport. The bicyclic ring system is structurally related to purine and exhibits strong fluorescent emission (Rembold and Gyure, 1972). Pteridines have been considered as responsible for significant autofluorescence within bacterial cells (Dalterio et al., 1987; Kopczynski et al., 2005; Włodarski et al., 2006), fungi (Hohl et al., 1992; Galland and Tolle, 2003) and other microorganisms (Galland et al., 1990; Uchiyama et al., 1997). Pteridines emit fluorescence peaking at ~450 nm when excited at ~350 nm, though this is partially dependent on environmental conditions such as pH and ionization state (Dalterio et al., 1987; Tyagi and Penzkofer, 2010).

Other vitamins, such as vitamin A, C, D and K, are sometimes mentioned in the context of cellular fluorescence (Billinton and Knight, 2001; Ramanujam, 2006). However, most of these are considered to comprise only minor contributions, due to low concentration, weak fluorescent emission, or both. In particular ergosterol (sterol compound, precursor for vitamin D) can be found in the cells wall of fungi and yeasts and has often been used as a tracer for fungal spores (Lau et al., 2006; Burshtein et al., 2011). Ergosterol and other sterols are known to fluoresce, though usually weakly, and this has been utilized in some cases for their detection (e.g. This work, Fig. 2l; Rosenheim, 1927; McIntosh et al., 2008).

### 2.3 Group III – structural biopolymers and cell wall compounds

In addition to fluorophores which actively participates in cellular metabolism, various structural compounds also emit fluorescent radiation. The biopolymers cellulose, chitin, lignin and sporopollenin are structural compounds crucial to many microorganisms and are abundant within the atmosphere (Kunit and Puxbaum, 1996; Winiwarter et al., 2009). The protein polymers elastin and collagen also exhibit fluorescent emission, however, they are regarded as of minor importance due to their absence in microorganisms.

Cellulose ( $\beta$  (1,4)-linked homopolymer of D-glucose) is one of the most abundant organic compounds in nature and, in particular, is an essential constituent in the cell wall of various organisms (such as bacteria, fungi, algae, plants) (Cannon and Anderson, 1991; Niklas, 2004; Voet and Voet, 2004). Cellulosic materials exhibit fluorescence over a broad spectral range with an emission maximum at ~420 nm and efficient excitation in the UV range (250–350 nm) (Olmstead and Gray, 1993, 1997; Castellan et al., 2007). The spectral properties of cellulose from different sources are well

characterized, however the molecular origin of the fluorescence is still debated (Olmstead and Gray, 1993). The fluorescence of cellulose is known to be highly increased by phenolic residues (e.g. ferulic acid) (Roshchina, 2008).

Chitin ( $\beta$  (1,4)-linked homopolymer of N-acetylglucosamine) is a highly abundant cell wall compounds which occurs in all fungi, various microorganisms and insects (Lenardon et al., 2010). It shows maximum fluorescent emission  $\sim 410$  nm and an excitation maximum  $\sim 335$  nm (Jabajihare et al., 1984). Several studies refer to chitin as a major fluorophore in fungal cell walls (Bonfantefasolo et al., 1990; Vierheilig et al., 1999; Dreyer et al., 2006).

Lignin is the chief compound in woody tissue and the most abundant polymer in nature, along with cellulose. It is a polyphenolic, branched, and disordered macromolecule derived by polymerization of monolignols in the cell wall of plants and algae (Donaldson, 2001; Boerjan et al., 2003). Lignin exhibits intense fluorescent emission of blue and green light when excited by radiation in the UV or blue spectral range, respectively (Harris and Hartley, 1976; He et al., 1999; Donaldson, 2001). It is assumed that light is absorbed by a number of chromophores (light-absorbing molecules) followed by intramolecular energy transfer to certain emission sinks (i.e. phenylcoumarone, stilbene) (Olmstead and Gray, 1997; Albinsson et al., 1999). In general, the fluorescence properties of these structural compounds are rather undefined and distributed over a broad spectral range, depending on organism and conditions (Billinton and Knight, 2001).

Sporopollenin is a rigid and complex biopolymer comprising a main constituent of the outer cell wall (exine) of pollen (Brooks and Shaw, 1978). Its intense fluorescent emission over a broad spectral range is caused by a mixture of different fluorophores, such as phenolic compounds ( $\lambda_{em} = \sim 460$  nm), carotenoids ( $\lambda_{em} = \sim 530$  nm), azulene ( $\lambda_{em} = \sim 450$  nm), anthocyanin ( $\lambda_{em} = \sim 460$  and  $620$  nm) and other compounds (Roshchina et al., 1997, 2003, 2004). However, the exact chemical composition of sporopollenin, including its fluorescence properties, is not well known.

The structural proteins collagen and elastin are important fluorophores within mammalian tissue which are frequently used for fluorescence-based tissue investigation. Both show similar fluorescent properties, respectively:  $\lambda_{ex} = \sim 325$  nm and  $\lambda_{em} = \sim 400$  nm (Billinton and Knight, 2001; Ramanujam, 2006). Due to their exclusive occurrence in mammalian tissues, however, these molecules are not expected to bare much significance on atmospheric FBAP.

## 2.4 Group IV – pigments

Two compound classes are summarized as fluorescent pigments in the following section: age-related pigments (i.e. lipofuscin, ceroid and melanin) and pigments that are involved in photoreceptor, photosynthesis and light

harvesting processes (i.e. (bacterio)chlorophylls, phycobiliproteins, flavonoids and carotenoids).

The following intracellular and extracellular compounds are usually summarized as age related pigments: lipofuscin, ceroid, advanced glycation end-products (AGEs) and age pigment-like fluorophores (APFs). The formation of these yellow-brown pigments is based on oxidation and peroxidation of lipids, proteins, nucleic acids, carbohydrates and other biomolecules, followed by cross-linking of the secondary oxidation products (particularly unsaturated carbonyls) with amino compounds (i.e. primary amines, amino acids). The generated fluorophores are mainly nitrogenous conjugated and cyclic compounds and polymers (Tsuchida et al., 1987; Yin, 1996). Fluorescent emission has been observed in a broad spectral range, when excited by UV or blue light. Usually fluorescent emission of cellular age related pigments is located between 450 and 640 nm, depending on the identity of the fluorophores, cellular environment and concentration (Eldred et al., 1982; Andersson et al., 1998).

Melanins are dark-colored hydrophobic pigments of high molecular weight which are assumed to consist of polymerized phenolic and indolic compounds. They are ubiquitous in nature and occur in various organisms, particularly fungi and bacteria have been found to show a high melanin content which is associated with microbial pathogenesis (Gomez and Nosanchuk, 2003; Nosanchuk and Casadevall, 2003). Compared to the other age-related pigments, melanin is regarded to show only a relatively weak fluorescence, but it has been shown that oxidation significantly increases fluorescence with a emission maximum at  $\sim 540$  nm when excited at  $\sim 470$  nm (Kayatz et al., 2001).

Fluorescent light emission from tetrapyrrolic compounds (i.e. protoporphyrin IX, chlorophylls, phycobilins) is well known and utilized in various applications (i.e. Lichtenhaler et al., 1986). Photosynthetic chlorophyll pigments such as chlorophyll-*a*, *b*, *c* and *d* in plants, many algae and cyanobacteria show fluorescent emission  $\sim 650$  nm. Pheopigments are chlorophyll degradation products obtained by acidification which show fluorescent emission (630–730 nm) with weaker intensity than the parent chlorophylls (French et al., 1956; Welschmeyer, 1994; Moberg et al., 2001). Another important class of fluorescent tetrapyrrolic pigments are phycobiliproteins and bilins as their prosthetic groups. They are known to show intense fluorescent emission of red light (580–660 nm) with high quantum yields (up to 0.98) (Glazer, 1994).

Carotenoids and flavonoids comprise the most important colored pigments in plants (Mantoura and Llewellyn, 1983). Flavonoids are polyphenolic and carotenoids are terpene compounds. Because of their pronounced fluorescence characteristics and importance in FBAP detection, they are each listed here as independent fluorophore classes. Both pigments are known to be enriched in certain plant parts, particularly in pollen ( $\mu\text{g kg}^{-1}$ ), constituting a main origin of

pollen autofluorescence (Roshchina and Karnaukhov, 1999, 2003; Taiz and Zeiger, 2010).

## 2.5 Group V – secondary metabolites

In addition to the given metabolites and intermediates (i.e. amino acids, sugars, nucleotides) in the primary metabolism (growth and development) of organisms, myriads of highly structurally diverse organic compounds, called secondary metabolites, are known, but which have no direct role in basic anabolic or catabolic processes. They are distinctive products with relatively narrow distribution among small groups of species and are active players in highly specialized metabolic processes of survival and competition: i.e. mycotoxins in fungi, terpenoids as attractants for pollinators, or metal-chelating siderophores in bacteria (Vining, 1990; Theis and Lerdau, 2003; Keller et al., 2005; Taiz and Zeiger, 2010). Secondary metabolites usually comprise complex chemical structures, often with conjugated heterocycles containing oxygen atoms (O) or nitrogen atoms (N), or both. Many tend to be autofluorescent and are known to show a significantly higher intensity compared to structural fluorophores in cell walls and primary metabolites (Roshchina, 2003, 2008). In the following paragraph main classes of secondary metabolites and their autofluorescence properties (if known) are discussed.

Alkaloids are one of the most diverse groups of secondary metabolites and occur in plants, fungi, bacteria, insects and other organisms, though every species shows a specific genetically determined alkaloid pattern. Most of these compounds serve as defense agents against predators and pathogens. Alkaloids are defined as cyclic compounds containing N in low oxidation states and can be subdivided based on their molecular origin into four groups: alkaloids based on amino acids, purine alkaloids, aminated terpenes and polyketide alkaloids (Roberts, 1998). The high structural diversity is reflected into highly diverse spectral properties. According to Roshchina (2003, 2005) a wide spectral range (410–600 nm) of fluorescent emission is covered by plant alkaloids. For UV excitation (360–380 nm) emission in the shorter wavelength range (410–520 nm) has been found for structurally smaller alkaloids (e.g. atropine) whereas larger compounds (e.g. sanguinarine) exhibit further red-shifted emission (585–600 nm).

Phenolic compounds comprise a large variety of chemically heterogeneous substances including simple molecules (e.g. benzoic acid derivatives, coumarins), oligophenolics (e.g. flavonoids) and complex polyphenolics (e.g. lignin, tannins). The unifying chemical feature is a multiple hydroxyl functionalization of conjugated and non-conjugated aromatic structures. They serve as UV shielding, defense against pathogens and mechanically supportive tissue. Many phenolics are well known fluorophores which usually emit blue fluorescence light (400–500 nm) when excited in the UV range (Roshchina, 1997).

Terpenes (or terpenoids) comprise a diverse class of lipophilic secondary metabolites synthesized by plants. Structurally based on isoprene ( $C_5$ ) units, this group includes monoterpenes ( $C_{10}$  compounds), sesquiterpenes ( $C_{15}$ ), diterpenes ( $C_{20}$ ) and other even larger compounds. They play important roles in various metabolic processes for examples as accessory pigments in photosynthesis (carotenoids,  $C_{20}$ ), deterrent toxins (pyrethroids,  $C_{10}$ ) or insect repellents (mono- and sesquiterpenes) (Theis and Lerdau, 2003; Taiz and Zeiger, 2010). For several monoterpenes Roshchina (2003) reports fluorescent emission in the blue range of the electromagnetic spectrum (405–430 nm) when excited with UV light (310–380 nm). For larger terpenes fluorescent emission occurs red-shifted, depending on the size of the conjugated  $\pi$ -bond system.

In addition to the previously mentioned large classes of secondary metabolites several other families of compounds such as mycotoxins, siderophores, quinones and mycosporin-like amino acids (MAAs) are known to autofluoresce, although details are in most cases not yet understood. In certain cases these compounds can be relevant for the autofluorescence of an organism even in low concentrations. In general secondary metabolites can be considered as a highly structurally diverse class of compounds comprising autofluorescent emission over a wide spectral range. Depending on their occurrence and concentration in certain species they can act as important or even dominant fluorophores.

## 2.6 Group VI – other fluorophores

Fluorophores that do not fit in the previous groups are summarized here. The most important compounds here are DNA and RNA as well as dipicolinic acid (DPA). The genetic information of all organisms is stored in the sequence of purin and pyrimidine bases in deoxyribonucleic acid (DNA). In the expression of genes and in the biosynthesis of peptides and proteins ribonucleic acid (RNA) is responsible for the information transfer from the genome to the proteome. The nucleic acids DNA and RNA are known to be fluorescent due to their constitutive nitrogenous and heterocyclic bases adenine, cytosine, guanine and thymine. Different studies report about DNA and RNA autofluorescence in microorganisms. When excited at 260 nm DNA fluorescence can be observed at 330–335 nm, although the signal is merged with the protein emission peak (e.g. Leblanc and Dufour, 2002; Roshchina, 2008). Biological aromatic molecules tend to be fluorescent due to energetically accessible  $\pi - \pi^*$  transitions, however, some heterocyclic aromatic compounds (i.e. the bases of DNA and RNA) are known to be very weakly fluorescent (Pan et al., 2009). The quantum yield of DNA/RNA is 100-times lower than tryptophan (Leblanc and Dufour, 2002; Estes et al., 2003; Ammor et al., 2004, 2007), however, and thus the overall relevance of DNA autofluorescence is considered to be negligible.

Dipicolinic acid (DPA or 2,6-pyridine-dicarboxylic acid) and its salts are synthesized during bacterial spore formation and enriched in the spore core (>10% of dry weight), where these compounds are assumed to be involved in affecting spore dormancy, heat resistance, and UV radiation protection (Paidhungat et al., 2000; Slieman and Nicholson, 2001). Medium fluorescence is observed for pure DPA in the dry state which is increased by UV-light exposure. The emission occurs around 440 nm, with an excitation maximum at 360 nm. The calcium salt CaDPA is also known to be fluorescent with peak emission at approximately 410 nm, when excited between 280 and 340 nm (Alimova et al., 2003; Sarasanandarajah et al., 2005). Since DPA occurs exclusively in bacterial endospores, it has been used as a spectral signature for spore detection (Bronk et al., 2000).

### 2.7 Possible interfering, non-biological compounds

Fluorescence is a widespread phenomenon common to a wide variety of chemical compounds and materials. As such it is not unique for biological materials, and aerosol of both anthropogenic and natural origin may also show emission of fluorescent radiation. This must be considered when performing fluorescence measurements on atmospheric samples, because certain non-biological compounds have the potential to cause positive fluorescence measurement artifacts and an overestimation of actual FBAP concentrations. We discuss here a selection of possible interferences in this context: (I) humic-like substances (HULIS), (II) secondary organic aerosols (SOA), (III) minerals/mineral dust, (IV) polycyclic aromatic hydrocarbons (PAH) and (V) soot. The following section briefly characterizes the fluorescence properties of each class, but is not represented in Table 1.

HULIS is a complex mixture of poorly defined heterogeneous compounds formed by biological material broken down through natural decay mechanisms and after subsequent atmospheric oxidation (Andreae and Gelencser, 2006; Graber and Rudich, 2006). It is terrestrially ubiquitous, but also constitutes an important subset of the organic aerosol fraction. While not chemically identical, humic and fulvic acids are generally considered to be appropriate HULIS surrogates. Various studies have investigated the fluorescence properties of humic and fulvic acids by means of EEMs. In particular the soluble fraction, referred to as dissolved organic matter (DOM), has been investigated in natural waters from rivers and oceans (Coble, 1996; Hudson et al., 2007) as well as rain and fog droplets (Duarte et al., 2004; Kieber et al., 2006; Birdwell and Valsaraj, 2010). Because humic-like material extracted from complex natural matter is not chemically pure it contains a mixture of many fluorophores. It has been shown that EEMs of DOM show two types of fluorescence modes: for humic-like and protein-like fluorescence, respectively. Humic-like fluorescence has been observed in three characteristic spectral positions ( $\lambda_{\text{ex}}/\lambda_{\text{em}}$ ) at: (i) 237–260/380–460

(humic-like, UV excitation), (ii) 300–370/400–500 (humic-like, visible excitation), (iii) 312/380–420 (marine humic-like). Protein- or amino acid-like fluorescence, however, occurs at 275/310 (tyrosine-like) and at 275/340 (tryptophan-like) (Coble, 1996; Hudson et al., 2007; Muller et al., 2008). Occurrence, spectral properties, and relative intensity of these five modes are highly dependent on molecular identity and chemical properties of the sample, however, and vary from sample to sample. It is reported that the fluorescence spectra, particularly EEMs, of humic and fulvic acids provide chemical and structural information such as conformation and functional groups (Chen et al., 2003), molecular weight (Stewart and Wetzel, 1980), aromatic character (Miano et al., 1988) and oxidation state (Klapper et al., 2002). HULIS isolated from aerosols or cloud water tends to show farther blue-shifted fluorescence when compared to terrestrial samples and thus is more similar to marine humic-like material (e.g. Krivacsy et al., 2001; Duarte et al., 2004). This may indicate aerosol HULIS contains a lower molecular weight and a smaller content of aromatic and conjugated  $\pi$ -bond structures compared with terrestrial HULIS (Graber and Rudich, 2006).

Secondary organic aerosol (SOA) is also an important constituent of atmospheric particulate matter, dominating sub-micron aerosol in many environments and also capable of condensing as a liquid layer onto larger particles (Pöschl, 2005; Jimenez et al., 2009; Pöschl et al., 2010). SOA forms as a result of the atmospheric oxidation of ubiquitous volatile organic compounds (VOCs) generating myriads of differently functionalized organic molecules. Bones et al. (2010) investigated the autofluorescence properties of lab-generated limonene and  $\gamma$ -terpinene SOA which exhibits strongly increased fluorescent emission when aged in the presence of ammonium compounds or amino acids. They found four major fluorescence modes (280/420, 300/360, 340/440, 425/490 nm, respectively) similar to the autofluorescence characteristics of HULIS. In particular this study indicates that nitrogen-containing SOA could be an important source of autofluorescence within certain SOA. In a related study Chang et al. (2010) found fluorescent emission within 325–425 nm when excited at 280 nm for photooxidation products of various phenolic compounds.

Mineral dust is also a major constituent of the global atmospheric aerosol, occurring in both fine and coarse mode and dominating total particle mass concentrations at locations worldwide (Gillette and Walker, 1977; Andreae and Rosenfeld, 2008; Monks et al., 2009). The photoluminescence of minerals is a well known phenomenon, and this allows the analysis of the presence and identity of so-called luminescence centers within given minerals (i.e. transition metal cations, rare-earth cations, biological impurities, trapped electron-hole pairs). A variety of different naturally occurring minerals (e.g. silicate, carbonate, phosphate and sulfate minerals) have been found to show clearly resolved, narrow emission modes at  $\sim$ 500 and  $\sim$ 700 nm when excited at

different wavelengths, for example 266 or 355 nm, in which particularly transition metal cations such as  $\text{Mn}^{2+}$ ,  $\text{Eu}^{2+}$  and/or  $\text{Ti}^{3+}$  originate these characteristic emission bands (Bozlee et al., 2005). The lifetime of these processes have been found to span a wide range from nanoseconds ( $10^{-9}$  s) to milliseconds ( $10^{-3}$  s), indicating the occurrences of both fluorescence and phosphorescence processes (Reisfeld et al., 1996; Gaft et al., 2001; Bozlee et al., 2005). The luminescence processes in minerals are not yet well understood due to complex atomic interactions within the crystal structures. However, because many isolated minerals have been shown to be capable of fluorescent emission they may contribute to fluorescence of certain types of dust within atmospheric aerosols and, therefore, should be considered as possibly introducing interference for FBAP detection in some situations. In many cases the timescale of emission (i.e. for phosphorescence) may be longer than detectable by online instrumentation, however, and so would not contribute significantly to detected FBAP numbers in these cases (e.g. Reisfeld et al., 1996).

PAHs are omnipresent in the environment and are known to have severe impacts on human health (e.g. Dix and Marnett, 1983; Nielsen et al., 1984). In the atmosphere they can occur primarily in the gas-phase as products of incomplete combustion (highly volatile 2-ring compounds, i.e. naphthalene), absorbed on organic aerosol particles such as soot, (low-volatile 5-ring compounds, i.e. benzo[*a*]pyrene) or as semi-volatile species present in both gas and particle phases (3- and 4-ring compounds, i.e. phenanthrene) (e.g. Finlayson-Pitts and Pitts, 2000; Slowik et al., 2007). LIF and a number of other methods have been utilized to identify and quantify PAHs in atmospheric aerosols (e.g. Niessner and Krupp, 1991; Panne et al., 2000). Pure PAHs are known to be highly fluorescent (quantum yields up to 1.0) over a wide spectral range (300–460/310–540). In the natural environment they usually occur as mixture of different compounds and produce complex EEMs (Kumke et al., 1995). PAHs are also known to be particularly enriched on the surface of soot particles from biomass burning and fuel combustion. When excited by strong laser light the mixture of PAHs in combustion aerosols can be analyzed and quantified (Aizawa and Kosaka, 2008, 2010). However, it has also been observed that fluorescent emission by PAH coatings on organic aerosols is weak due to efficient quenching by the bulk material (Lewitzka and Niessner, 1995; Panne et al., 2000).

### 3 Materials and methods

#### 3.1 Chemicals and materials

Samples of humic acid (2S101H) and fulvic acid (1S101F) were purchased from International Humic Substance Standards (IHSS; St. Paul, MN, USA). Arizona test dust

(ISO 12103-1) was obtained from Powder Technology Inc (Burnsville, MN, USA). Kaolin was purchased from Sigma Aldrich (K7375). Ash was obtained from wood burning (spruce, specially designed wood burning facility). Diesel soot (SRM 2975) was purchased from National Institute of Standards and Technology (NIST; Gaithersburg, MD, USA). Biomass burning soot was obtained by burning a sample of spruce and directly sampling the black smoke on a clean glass cover slide held at approximately 10 cm away from the flame in direct flow of the smoke. *Saccharomyces cerevisiae* was purchased as baker's yeast from a local supermarket and used immediately (within one day). Solvents were obtained from Merck (Darmstadt, Germany). All other chemicals were purchased from Sigma Aldrich. All purchased chemicals were used as delivered.

#### 3.2 Fluorescence spectroscopy

All fluorescence spectra were recorded on a LS 45 Luminescence Spectrometer (Perkin Elmer, Inc.; Waltham, MA, USA). The instrument is equipped with a pulsed xenon lamp, two Monk-Gillieson-type grating monochromators<sup>2</sup>, and a gated photomultiplier tube (PMT) detector. Wavelength-dependent variation in light source intensity (*I*) was corrected by an internal reference light path with dedicated PMT. Measurements were initiated after a minimum of approximately 30 min of instrument warm-up time to ensure lamp stability. The instrument was operated using FL WinLab software (Perkin Elmer, Inc.) and its performance was controlled (every ~10th spectrum analyzed) by means of a software validation utilizing Raman and Rayleigh signal positions as well as the signal-to-noise ratio. All spectra were recorded at a PMT voltage of 650 V, a scan speed of 600 nm min<sup>-1</sup>, and using excitation and emission slit widths of 10 nm at room temperature. EEMs were recorded for excitation wavelengths from 230–650 nm (5 nm increments) and emission wavelengths from 270–700 nm (0.5 nm increments). To avoid detector saturation for highly fluorescent samples a blocking filter (Perkin Elmer, Inc.) was utilized to reduce the emission intensity. This filter is a metal plate with holes bored through to allow 1 % of light to be transmitted, but without introducing wavelength-dependent effects. Spectral analysis was performed using Igor Pro (Wavemetrics, Inc.; Portland, OR, USA).

Samples were investigated in the solid (powder), solution, or suspension states. Solvated and suspended samples were placed in a 10 × 10 × 40 mm UV quartz cuvette (Hellma Analytics, Müllheim, Germany) and measured immediately (within 15 min). The concentration of fluorophore within solution or suspension was deliberately low in order to avoid inner filtering and concentration-related quenching effects. For highly dilute samples the concentration is linearly correlated with fluorescence intensity according to the

<sup>2</sup>e.g. <http://gratings.newport.com/information/handbook/chapter6.as>

Beer-Lambert law. Suspensions of insoluble materials were prepared by adding fluorophore analyte ( $0.2\text{--}0.4\text{ mg ml}^{-1}$ ) to phosphate-buffered saline (PBS) at pH 7.2. PBS was prepared from ultrapure water (MilliQ,  $18.2\text{ M}\Omega$ ) and purified by sterile filtration before use. A magnetic stirrer was utilized to stir the sample in the cuvette during the measurement to avoid sedimentation. Solutions of most soluble fluorophores were prepared in PBS, however, pyrene, naphthalene, phenanthrene and chlorophyll-*b* were solvated in *n*-hexane due to their hydrophobicity. The concentration of analyte used was  $3\text{ }\mu\text{mol l}^{-1}$ , but was increased by a factor of 10 or 100 for weakly fluorescent samples until fluorescent emission was detectable. Background correction of solvated or suspended samples was performed by taking the difference of fluorescence spectra of solvent with and without sample.

Powdered materials were analyzed with a Front Surface Accessory for the spectrometer (Perkin Elmer, Inc.). With this technique several milligrams of powder were placed onto the black surface holder and placed as a vertical plane into the spectrometer such that the illumination angle shining horizontally onto the sample surface shows maximum fluorescence intensity. The illumination spot size on the samples was  $\sim 60\text{ mm}^2$ . For weakly fluorescent powders, which exhibited no clear emission peaks, fluorescence properties were qualitatively dominated by light leakage (e.g. NaCl, Fig. S6 in the Supplement) and appear as steep-walled valleys of emission between the 1st and 2nd order elastic scattering lines. The magnitude of “emission” on the left and right of the 1st order scattering peak are similar, however, confirming that most of the signal in the fluorescence region is spurious. The magnitude of this effect correlated with the color of the sample powder, with white samples exhibiting a higher background than colored samples. This suggests that light absorption within the samples reduces internal reflection and mitigates the background effect. We, therefore, assume that all radiation arriving to the detector at wavelengths shorter than the incident wavelength is due either to stray background light, or light leakage past the monochromators. EEMs of dry powder samples were normalized by the intensity of light leakage in order to provide a comparable scale of fluorescence intensity across all solid samples. Often fluorescence spectra of this type are normalized to the height of the 1st order scattering peak, but this was not possible here, because the PMT was saturated at this wavelength for some samples. For each EEM, a constant normalization factor (NF) was determined by taking the mean of the measured light leakage intensity values along a line 40 nm above the center of the excitation line (as shown in Fig. S1 in the Supplement) and dividing the entire matrix by this NF. Doing so preserves all qualitative features within measured EEMs, but normalizes the absolute intensity of fluorescence for comparison. Each 1-D spectrum shown with single excitation wavelength (Fig. 6) was extracted from the normalized EEMs.

As a result of differing normalization procedure quantitative comparison of emitted fluorescence intensity between

wet and dry samples is not possible by this technique, while qualitative features are consistent and comparable. Further details concerning the normalization procedure can be found in the supplement (Fig. S1 in the Supplement) along with examples of non-normalized spectra (Figs. S4 and S5 in the Supplement).

### 3.3 Fluorescence microscopy

The fluorescence microscopy images were taken on a BZ-9000 Fluorescence Microscope (Keyence, Inc., Osaka, Japan). The instrument was equipped with a super-high-compression mercury lamp (120 W) and a 2/3-inch, 1.5 mega pixel monochrome CCD. The following fluorescence filters were used to take images in different spectral ranges: OP-66834 DAPI-BP ( $\lambda_{\text{ex}} = 360/20\text{ nm}$ ,  $\lambda_{\text{Dichroic}} = 400\text{ nm}$ ,  $\lambda_{\text{Absorp}} = 460/25$ ), OP-66836 GFP-BP ( $\lambda_{\text{ex}} = 470/20\text{ nm}$ ,  $\lambda_{\text{Dichroic}} = 495\text{ nm}$ ,  $\lambda_{\text{Absorp}} = 535/25$ ), OP-66838 TexasRed ( $\lambda_{\text{ex}} = 560/20\text{ nm}$ ,  $\lambda_{\text{Dichroic}} = 595\text{ nm}$ ,  $\lambda_{\text{Absorp}} = 630/30$ ). Filter specifications are represented as wavelength and peak width ( $\lambda/\text{FWHM}$ ).

### 3.4 Ambient sampling

Ambient samples of airborne particulate matter were taken using a single stage impactor (PIXE International Corp. Tallahassee, FL, USA; nozzle diameter 0.65 mm, distance between nozzle and impaction plate 3 mm, flow rate  $1\text{ l min}^{-1}$ , cut-point  $\sim 0.6\text{ }\mu\text{m}$ ) (Russell et al., 2002). Samples were taken on the roof of the Max Planck Institute for Chemistry building on the university campus in Mainz, Germany. Sampling was performed on a clean round glass cover slide (diameter 15 mm, thickness 0.13–0.15 mm) and immediately used for microscopy investigation.

## 4 Results and discussion

### 4.1 EEMs of pure biological standards

Following on the summary presented in Table 1 we applied fluorescence spectroscopy to a selection of pure biological fluorophores, particularly those molecules that are considered to be most relevant within ambient PBAPs. Figure 2 shows EEMs for a selection of biological fluorophores, and spectra for further compounds can be found in Fig. S2 in the Supplement. The selection covers protein autofluorescence by means of all three fluorescent amino acids and two common proteins: bovine serum albumin (BSA) and ovalbumin (OVA). Coenzymes constitute a diverse class of highly fluorescent compounds and are represented by several examples (i.e. pyridoxine, NADPH, folic acid and riboflavin). The major biopolymers are represented by cellulose and chitin as well as ferulic acid as a proxy for lignin. As an example for vitamins the sterol compound ergosterol

is shown. Chlorophyll-*b* is an example of the group of porphyrin fluorophores.

It is well known that the fluorescence properties of a fluorophore (i.e. spectral parameters and intensity) are highly depended on its molecular environment, particularly: pH, fluorophore concentration and interaction with other compounds. All measurements in the present study were, therefore, performed under consistent, defined conditions. Pure compounds were utilized for solid state investigations. For samples in solution or suspension, defined pH and fluorophore concentrations were chosen to ensure comparability of the spectral parameters (see Sect. 3.2 for more details). The molecular environment within biological samples, such as cells and tissue, is much more dynamic and complex than in a defined test environment. As a result the position and intensity of fluorescence modes shown may differ from in situ measurements within actual biological samples. Bearing this complexity in mind, however, we suggest that the presented results can be seen as a general characterization and overview, providing a collection of fluorescence landmarks for different compounds relevant to atmospheric PBAP.

Under atmospheric conditions aerosols can contain wide ranges of moisture content, from extremely dry particles to nuclei suspended in cloud water droplets. Hydration state has also been found to significantly influence the fluorescence properties of a fluorophore (Lakowicz, 1999; Pöhlker et al., 2012). Accordingly, spectra for most materials in this study were each recorded in solid, solution, and suspension phases, respectively. All EEMs of solvated or suspended samples show clearly defined fluorescence modes with only weak interference by light scattering effects. In EEMs of solid state compounds fluorescence modes, by contrast, are usually less clearly resolved and exhibit stronger light scattering, broader fluorescence modes, and an elevated fluorescent background. This background effect is more pronounced in white samples with very weak fluorescence modes, and we propose that the light detected as fluorescence is simply a function of light leakage (i.e. the tails of the 1st and 2nd order elastic scattering peaks cause a significant enhancement in signal in the absence of true molecular fluorescence). For this reason, the absolute intensity of all powdered samples have been normalized, as discussed in Sect. 3.2. Moreover a shift in location of emission peaks from solid- and solution-phase samples (e.g. cellulose in Figs. 2m and S2k in the Supplement, riboflavin in Figs. 2f and S2f in the Supplement) was also observed.

Molecular fluorescence generally provides less characteristic spectra than other methods of spectroscopy, making detailed chemical analysis impossible in most cases. Mixing of emission peaks from different fluorophores has been particularly well described for bacteria (Marose et al., 1998). Different compounds also exhibit large variations in the intensity of fluorescent emission. Compounds such as pyridoxine and neopterin emit intensely even in low concentrations, for example, whereas fluorescent emission of

phenylalanine and ferulic acid exhibited weak emission in all cases. The intensity of fluorophores frequently discussed within the bioaerosol detection community, such as tryptophan, NADPH and riboflavin, can be characterized among the compounds shown as having a medium level of fluorescent emission. However, fluorescence intensity is a complex function of various parameters such as concentration, extinction coefficient at  $\lambda_{\text{ex}}$  and quantum yield at  $\lambda_{\text{em}}$  as well as influences by the molecular environment. Accordingly, only semi-quantitative comparison of intensity levels is possible based on the presented results.

## 4.2 Spectral mapping of biological fluorophores

As a way of summarizing the properties of key biofluorophores, Fig. 3 highlights fluorescent emission peaks (and corresponding mode widths), but ignores differences in intensity among the compounds. Most compounds chosen exhibit peaks at relatively short ( $<500$  nm) wavelengths of excitation and emission and appear in the lower left of Fig. 3 (i.e.  $\lambda_{\text{ex}} = 250\text{--}400$  nm,  $\lambda_{\text{em}} = 300\text{--}500$  nm). Riboflavin and chlorophyll-*b*, however, uniquely exhibit significantly larger  $\Delta\lambda_{\text{Stokes}}$  (i.e. the right side of the plot). Furthermore, it is obvious that the modes of many fluorophores cluster in two “emission hotspots”. Hotspot I ( $\lambda_{\text{ex}} \approx 280$  nm;  $\lambda_{\text{em}} = 300\text{--}530$  nm) is dominated by amino acids and proteins, biopolymers such as cellulose and chitin, and several coenzymes (i.e. pyridoxamine, riboflavin). Hotspot II ( $\lambda_{\text{ex}} = 330\text{--}360$  nm;  $\lambda_{\text{em}} = 390\text{--}460$  nm) shows emission from the majority of coenzymes (i.e. NADPH, pyridoxine, folic acid), the proxies for lignin (ferulic acid, phenylcoumarin) and DPA. Note that experimental data for DPA are not available through the present study, but were added to Fig. 3 from Sarasanandarajah et al. (2005) because of its importance in bacterial spores. Both emission hotspots directly correspond with the operational range of most bioaerosol detectors, as shown in Fig. 1. Excitation at  $\sim 280$  and  $\sim 360$  nm are particularly important wavelengths to excite many atmospherically important biofluorophores. Beyond these established excitation bands, however, the development of relatively cheap diodes lasers for consumer electronic technology (e.g. Blu-Ray Disc<sup>TM</sup>,  $\lambda_{\text{ex}} = 405$  nm) within the last several years has opened up new possibilities for the design of FBAP detection instrumentation. Extensive laboratory studies have not yet been performed to validate the use of these new sources for FBAP detection and will be necessary before interpretation of complex aerosol samples will be meaningful. Figure 3 shows that the 405 nm excitation band is located in a spectral region where only relatively few biofluorophores (e.g. riboflavin, chlorophyll-*b* and chitin) are efficiently excited (see also Fig. S6 in the Supplement). Riboflavin, however, is ubiquitous within PBAP and the relative selectivity of  $\lambda_{\text{ex}} = 405$  nm may eventually prove particularly successful at PBAP detection.

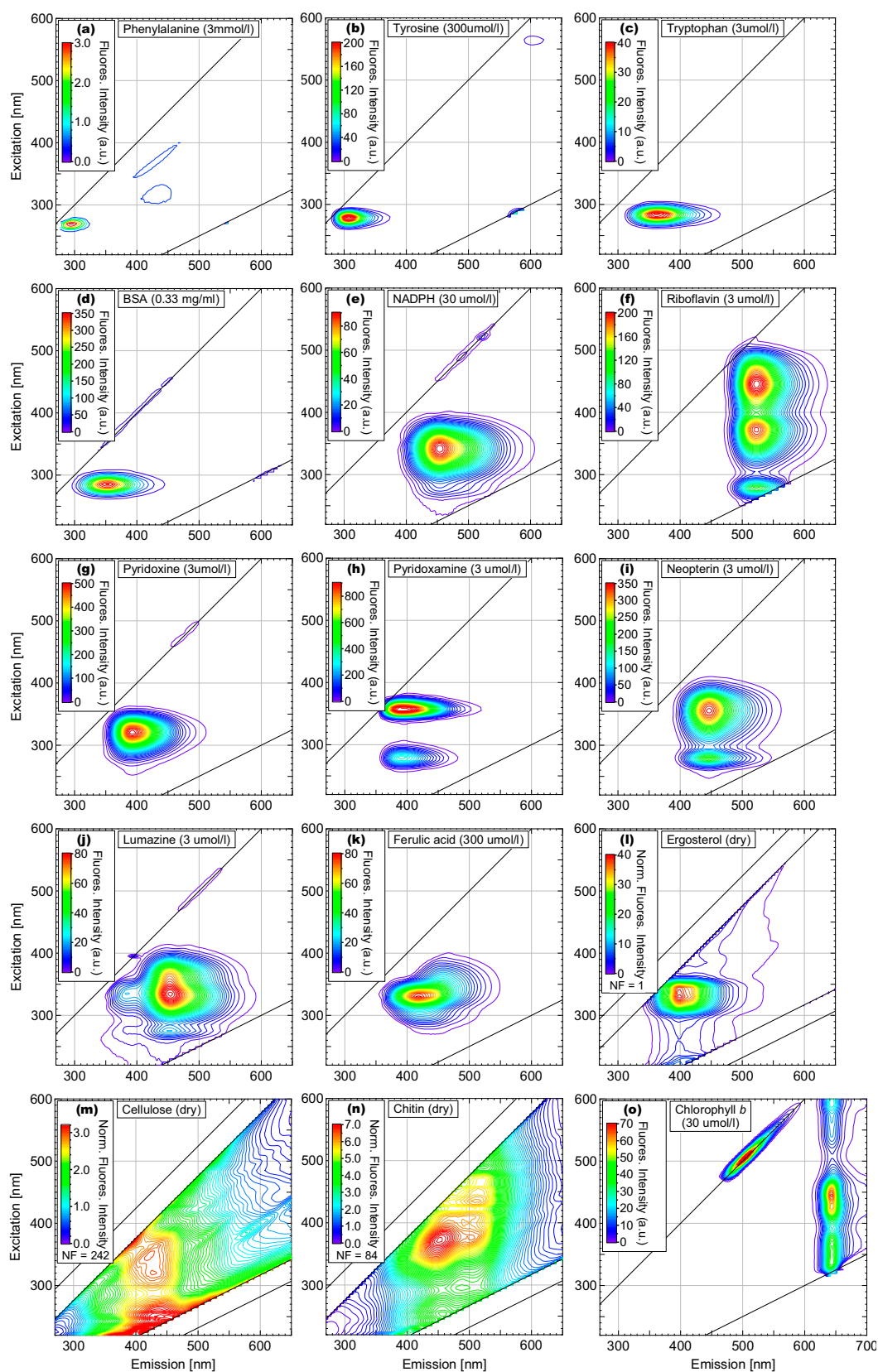


**Fig. 2.** EEM contour profiles for selected pure biological fluorophores in solid or solvated state. Intensity color scale has been adjusted to intensity of individual components. All EEMs are normalized as discussed in text (Sect. 3.2). Normalization factor (NF) is reported for each solid-state sample. Lower NF indicates higher fluorescence intensity. Note change in x-axis scale for chlorophyll-*b*.



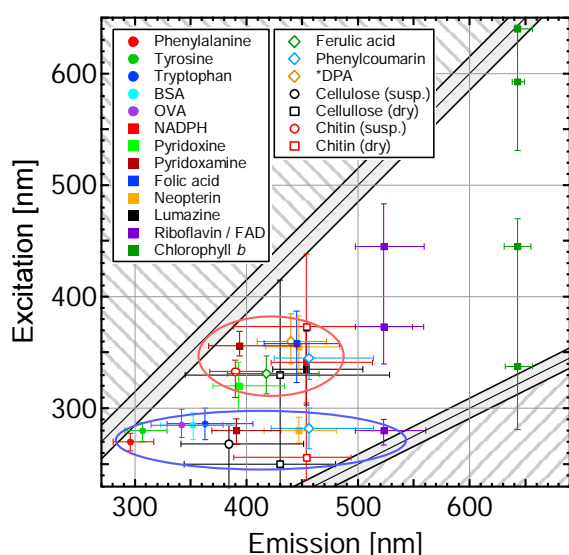


**Fig. 3.** Overview EEM mapping the spectral position of biological fluorophores. Protein fluorophores are represented by solid circular markers, coenzyme fluorophores by solid square markers and structural fluorophores by open markers. Full width half max (FWHM) of emission peaks is represented by horizontal and vertical bars. Differences in relative fluorescence intensity are neglected. For multimodal fluorophores all modes are shown. Data refer to measurements of solvated fluorophores in PBS. For cellulose and chitin results of solid state and suspension state spectra are shown. \* Data for DPA are taken from Sarasanandarajah et al. (2005).

Accordingly, a variety of fluorophores within atmospheric particles are potential targets for these instruments. It is clear that PBAPs comprise potentially many different fluorescent constituents at the same time (see Table 1). For example, bacteria have been shown to contain a mixture of fluorescent coenzymes such as pyridine, flavin, pyridoxine and pteridine compounds (Dalterio et al., 1987; Wlodarski et al., 2006). It can thus be assumed that ambient FBAP detection based on autofluorescence usually detects a mixed signal from potentially many different fluorophores. In contrast to technical applications where autofluorescence of NADH is directly used to monitor the metabolic status of yeast or bacteria in bioreactors (Marose et al., 1998; Johansson and Liden, 2006), the high diversity of organisms, debris and other compounds in the atmosphere makes a selective assignment of the measured fluorescence to a certain fluorophores difficult. This suggestion is not new, however, and several groups have investigated the use of varied post-detection techniques (e.g. principle component analysis) to elucidate further information from ambient PBAP (e.g. Pinnick et al., 2004; Pan et al., 2010, 2011). The only coenzyme which is largely free from interference by other biofluorophore is riboflavin and related flavoproteins (Koenig and Schneckenburger, 1994).

Figure 3 also shows that the fluorescence signal of the proteins sampled (BSA, OVA) is very similar to the tryptophan

signal. Because the fluorescent emission of tyrosine and phenylalanine have a smaller  $\Delta\lambda_{\text{Stokes}}$  than tryptophan this may suggest that these amino acids do not contribute significantly to the overall fluorescence signal in native proteins where they occur (BSA: 30 Phe residues, 21 Tyr, 3 Trp; Hirayama et al., 1990; OVA: 15 Phe, 10 Tyr, 3 Trp; Nisbet et al., 1981). In addition, it can be seen that the modes of BSA and OVA are slightly red-shifted with respect to tryptophan, which is due to the specific influence of the microenvironment of the folded protein (Lakowicz, 1999). The position of each individual fluorescence mode in Fig. 3 is determined by the structural nature of the corresponding fluorophore, such as the extent of  $\pi$ -bond conjugation or influence of electron donating or withdrawing groups. Aizawa et al. (2008) provides an overview EEM map showing the spectral position of PAHs depends on the size of their  $\pi$ -bond system. Figure 3 displays a similar map for biofluorophores presented here. Sampled compounds that contain small monocyclic fluorophore groups such as phenyl (phenylalanine), phenol (tyrosine) and indol (tryptophan) are excited by radiation in the UV and blue visible range ( $\lambda_{\text{ex}} = 260\text{--}290\text{ nm}$ ;  $\lambda_{\text{em}} = 290\text{--}370\text{ nm}$ ). Compounds with larger fluorophores such as pyridine (i.e. pyridoxine and dipicolinic acid), nicotinamide (NAD(P)H) and pteridine (i.e. folic acid, lumazine) are spectrally more red-shifted ( $\lambda_{\text{ex}} = 280\text{--}370\text{ nm}$ ;  $\lambda_{\text{em}} = 390\text{--}470\text{ nm}$ ). Compounds containing large aromatic structures such as flavins and porphyrins (chlorophyll-*b*) are even further red-shifted ( $\lambda_{\text{ex}} = 280\text{--}640\text{ nm}$ ;  $\lambda_{\text{em}} = 510\text{--}660\text{ nm}$ ). In addition, increasing the size of the  $\pi$ -bond system opens more potential excitation pathways for electron transition, thus extending the fluorescence band over a much broader range of excitation wavelengths (i.e. for riboflavin and chlorophyll-*b*).

In addition to the investigation of fluorescence properties of pure fluorophores, the analysis of biological standard compounds (i.e. bacteria and pollen) promises to help to explain the selectivity of online FBAP detection. A full investigation of microorganism fluorescence is beyond the scope of this text, but *Saccharomyces cerevisiae* (baker's yeast) is shown in Fig. 4 as an example of an actively metabolizing organism and surrogate for atmospheric PBAP. The fluorescence properties of this organism are well described, due to its various industrial applications. According to Marose et al. (1998) tryptophan, NAD(P)H, pyridoxine, pyridoxal 5'-phosphate and flavins are the dominating fluorophores in *S. cerevisiae*. The ratio of their relative emission intensities has been used to monitor the metabolic status of the cells and to estimate the overall biomass. The EEM in Fig. 4 shows a fluorescence pattern corresponding with several of the previously mentioned fluorophores. A strong peak at 285/350 nm ( $\lambda_{\text{ex}}/\lambda_{\text{em}}$ ) is likely caused by proteins, particularly tryptophan residues, whereas the signal at 230/350 nm appears to be also protein fluorescence due to deep UV excitation (Bhartia et al., 2008). An emission signal occurs at 350/450 nm that is most probably NAD(P)H, although pteridin coenzymes may also

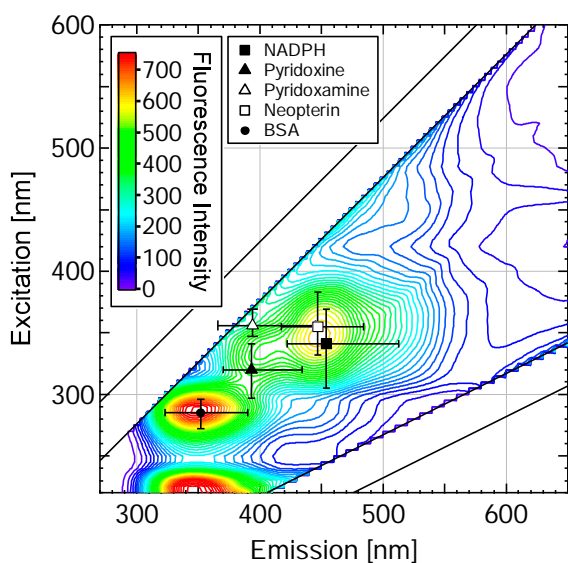


**Fig. 4.** EEM contour profile for *Saccharomyces cerevisiae* (baker's yeast). Spectral positions of selected pure fluorophores are shown for comparison. BSA is chosen as a general proxy for protein.

contribute to this signal (Michal, 1999; Kopczynski et al., 2005). A shoulder at 340/410 nm is likely caused by pyridoxine coenzymes. However, no flavin signal was observed. For purpose of illustration the spectral positions of the corresponding fluorophores (based on the measurements in Fig. 2) are projected into the EEM. In further studies EEMs will be used to characterize the fluorescence properties of various bioaerosol standard particles.

#### 4.3 EEMs of potential interferences

In order to estimate the relative interfering potential of the compound types discussed in Sect. 2.7 fluorescence spectra of HULIS (humic and fulvic acid), PAHs (pyrene, naphthalene, phenanthrene, fluoranthene), mineral dust (kaolin and Arizona test dust) and soot (biomass burning and diesel soot) were investigated. Figure 5 shows EEMs of selected compounds, with additional samples shown in Fig. S3 in the Supplement, and can be grouped into two qualitatively distinct categories: (I) EEMs with clearly resolved fluorescence modes (e.g. all solutions and suspensions, dry PAHs) and (II) EEMs without clear modes, but with significant light emission over a wide spectral “plateau” (all dry samples with the exception of PAHs).

EEMs of HULIS surrogates which show defined fluorescence modes are consistent with results from DOM analysis. Humic and fulvic acids in solution exhibit broad modes (390/490, 450/520), but with relatively low intensity and resemble fluorescence behavior of DOM (e.g. Chen et al., 2003; Wedborg et al., 2007). In contrast, PAH compounds show strongly fluorescent emission, the peak location of which corresponds to the size of the  $\pi$ -bond

system. In general, PAH samples in the solid state can be excited efficiently over a wide wavelength range (230–390 nm), whereas samples in solution show relatively narrow, defined excitations.

In contrast to compounds that show well defined modes of fluorescent emission, EEMs of dry powders such as mineral dust (kaolin and Arizona test dust) and HULIS (humic and fulvic acid) exhibit broad, featureless emission over an extended spectral area (230–500/350–600) with steep increase near the 1st and 2nd order scattering signals. We observed that the relative intensity level of this plateau correlates with the visible color of the samples. For example, the broad emission intensity of kaolin (white, Fig. S5h in the Supplement) is higher than that of fulvic acid (yellow, Fig. S5b in the Supplement), which is higher still than that of humic acid (brown, Fig. S5a in the Supplement). We further tested additional white powder compounds (i.e. NaCl and glass microspheres) not expected to show any classical fluorescent emission in this range. These also exhibit EEMs that are qualitatively almost identical with the other dry powder samples, with intensity levels similar to that of the white kaolin powder. This suggests that the featureless emission observed from these powder samples is spurious and does not originate as molecular fluorescence. We thus suggest that the “plateau” effect is a result of light leakage due to imperfect monochromators within the spectrofluorometer and that light arriving at the detector at wavelengths in between the dominant scattering lines largely represents the transmission tails of the elastic scattering signals. The presence of this elevated fluorescence background is minimal for compounds that exhibit defined fluorescence modes, is magnified in powdered samples with high surface area for reflection, and is highest in samples whose color reduces light absorption. In order to qualitatively eliminate these effects from EEMs of dry materials the spectra have been normalized as described in Sect. 3.2. Normalized spectra are shown in Figs. 5 and S3 in the Supplement, while a selection of raw EEMs can be found in Figs. S4 and S5 in the Supplement. According to De Souza Sierra et al. (1994) it is critical to correct fluorescence spectra of solid particulate matter for stray light transmitted by the excitation monochromator and scattered by the sample to ensure comparability. These normalized spectra offer the ability to semi-quantitatively compare fluorescent intensities from different materials. While quantitative comparisons within the list of dry materials or within the list of wet materials (solution, suspension) is possible, differences in normalization procedure between the two is quantitatively challenging by this technique.

#### 4.4 Comparison of autofluorescence from biofluorophores and interfering species

Figure 6 shows a summary of selected biological and non-biological compounds, excited at one of two wavelengths: either 280 nm (Fig. 6a and c) or 355 nm (Fig. 6b and d). These

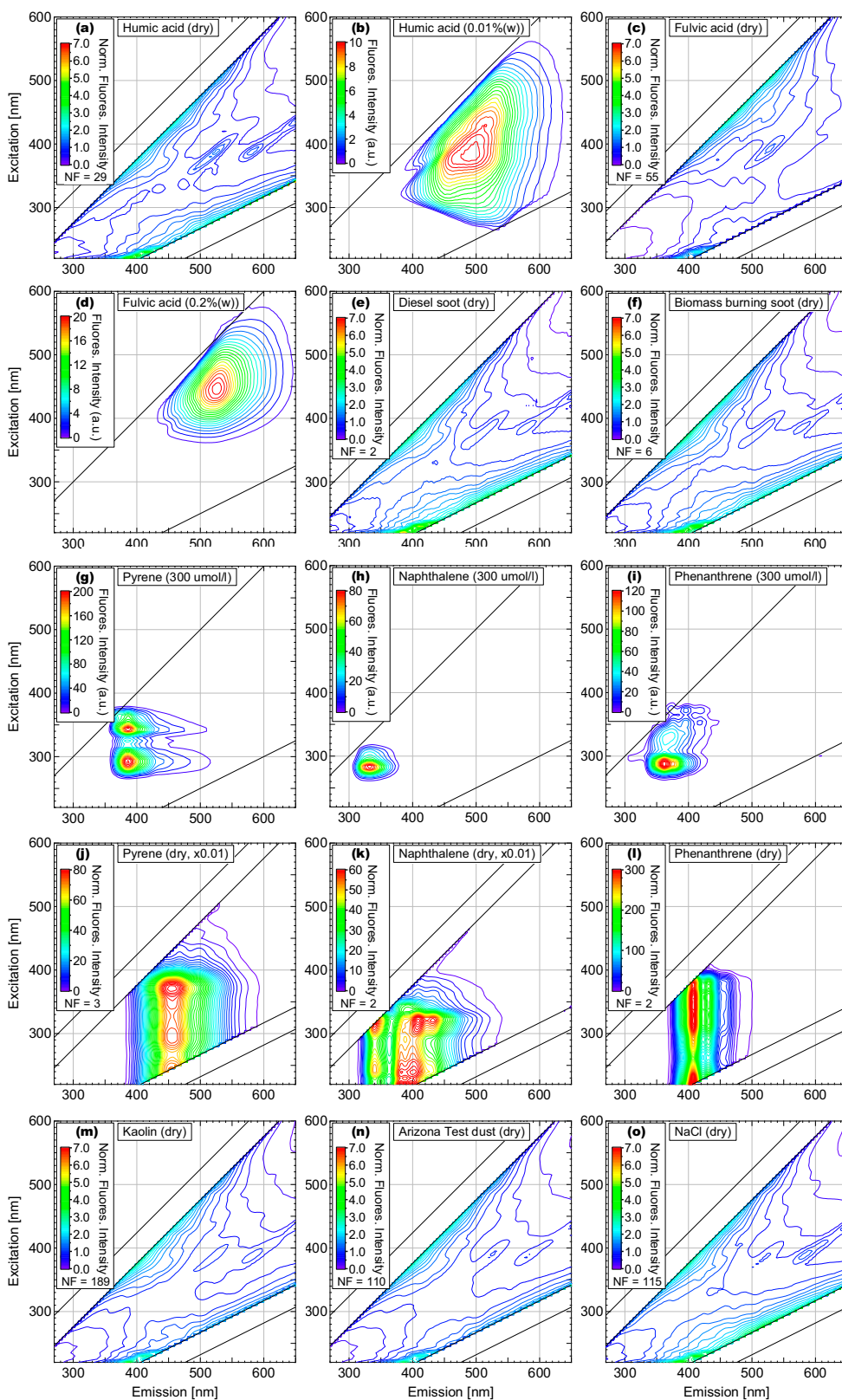


**Fig. 5.** Normalized EEM contour profiles for selected interferences in solid state and/or solution. Intensity color scale has been adjusted to intensity of individual components. All EEMs are normalized as discussed in text (Sect. 3.2). Normalization factor (NF) is reported for each solid-state sample. Lower NF indicates higher fluorescence intensity.

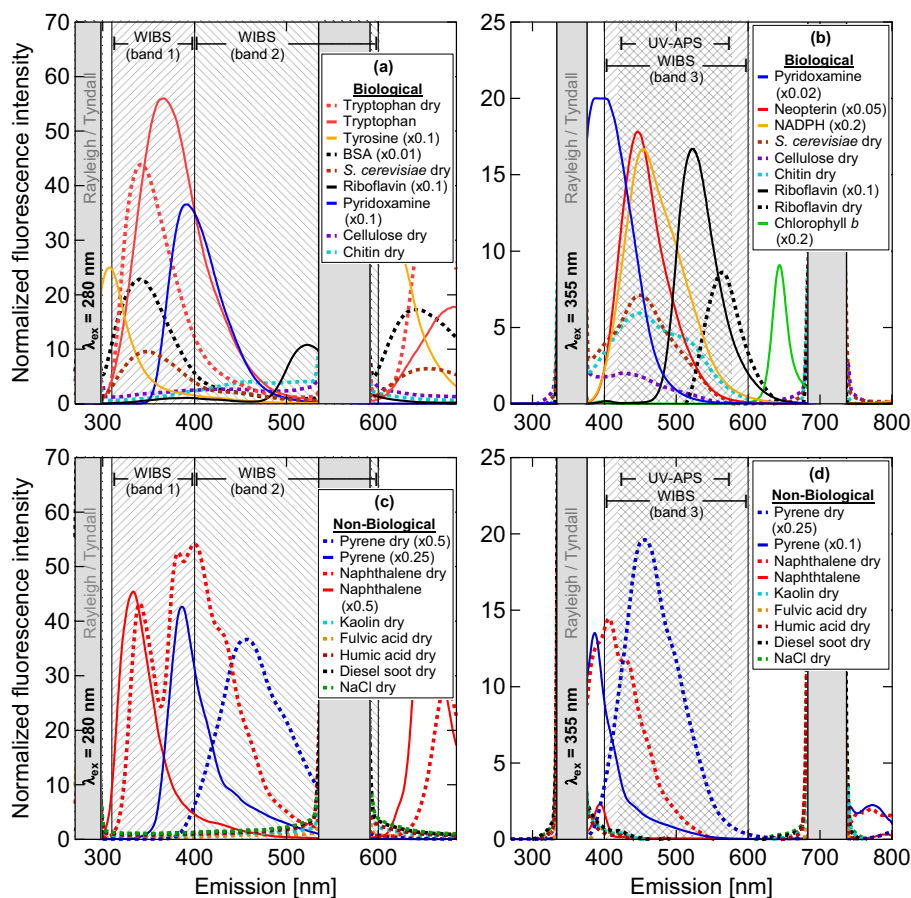


**Fig. 6.** Normalized fluorescence emission spectra of biofluorophores and potential interferences for selected excitation wavelengths  $\lambda_{\text{ex}}$ ; (a) emission spectra of biological fluorophores at  $\lambda_{\text{ex}} = 280$  nm; (b) emission spectra of biological fluorophores at  $\lambda_{\text{ex}} = 355$  nm; (c) emission spectra of potential interferences at  $\lambda_{\text{ex}} = 280$  nm; (d) emission spectra of potential interferences at  $\lambda_{\text{ex}} = 355$  nm. Dashed lines indicate samples in dry state, solid lines indicate samples in solution. Spectra were scaled in some cases to fit on same y-axis. For example, pyridoxamine in (a) peaks at  $\sim 350$  a.u., and not  $\sim 35$  a.u. as shown.

wavelengths of excitation were chosen to highlight observed fluorescent emission within the two primary bands of fluorophores discussed in Sects. 4.1–4.2 and because they represent or approximate the excitation sources of two commercially available FBAP-detection instruments (UV-APS and WIBS). Detected emission ranges for both instruments are shown by shaded regions on the plot, although it is important to note that the second WIBS excitation source produces radiation at 370 nm and not at 355 nm (corresponding to UV-APS) as shown in Fig. 6b and d. Colored traces show individual fluorophores selected to represent key molecules for FBAP detection from Table 1. This set of summary plots enables a semi-quantitative comparison of fluorophore importance, in particular regarding the influence of potential interferences. Fluorescence properties of certain biofluorophores have been investigated in various studies, however, much less information is available regarding the intercomparison between very different compound types (in particular biofluorophores and non-biological fluorophores). Figure 6 provides a simple approach to fill this gap.

In the raw (non-normalized) spectra (Figs. S4, 5 in the Supplement) the “plateau-like” emission of materials such as fulvic acid, kaolin, NaCl, and cellulose can be easily seen, while the normalized spectra of such materials (Fig. 6) show only weak fluorescence. The normalized spectra of NaCl can be used as a surrogate post-normalization background, because it is not expected to fluoresce at wavelengths used here and because it exhibits the most fluorescence intensity of the “non-fluorescent” powders. As such, the emission spectrum for NaCl retains a measureable background when excited at 280 nm, increasing from a minimum  $I \sim 1.0$  at  $\lambda_{\text{em},350}$  to  $\sim 2.0$  at  $\lambda_{\text{em},550}$ , while it exhibits a steep valley profile when excited by 355 nm radiation, but with  $I < 0.5$  for all emission between 400 and 650 nm. Small peaks in emission spectra of weakly fluorescing compounds can consistently be seen at  $\sim 340$ , 422, 459, and 485 nm for  $\lambda_{\text{ex},280}$  and at 420 and 485 nm for  $\lambda_{\text{ex},355}$ . The most prominent of these appear as subtle diagonal lines between the 1st and 2nd order elastic scattering lines on EEMs of weakly fluorescing dry powders (e.g. Figs. 2m and 5a,c,m–o). These

do not appear for fluorescent compounds, however, and are assumed to be a product of weakly interfering elastic scattering processes. In contrast to weakly fluorescing molecules, emission by biofluorophores and PAH compounds show clearly resolved peaks before and after normalization, and we roughly categorize these to be fluorescent in all cases. In general it can be stated that position and linewidth of fluorescence emission peaks in EEMs are independent of  $\lambda_{\text{ex}}$  due to radiative electron relaxation from the lowest vibrational level of the first excited electronic state (Sect. 1.2). Thus, fluorescence signals are indicated by vertical lines or individual peaks in EEMs as presented here. Further, the only parameter that varies along the excitation axis (vertical) is the fluorescence intensity, which does so as a function of the absorption spectrum of the fluorophore. In contrast, signals of other light scattering effects (i.e. Rayleigh, Tyndall and Raman) are a function of  $\lambda_{\text{ex}}$  and accordingly can be seen as diagonal lines within the EEMs (Coble et al., 1990).

Figure 6a and b highlight the fact that a wide variety of molecules associated with biological organisms fluoresce. Moreover the compounds shown in Fig. 6, which were chosen to represent larger groups of molecules from Table 1, underline the previously mentioned suggestion that a large variety of fluorophores contribute to the overall fluorescence signal detected by online FBAP instrumentation. Among the nine biomolecules chosen, fluorescence is generally high. The only exceptions to this are cellulose and chitin. Cellulose shows essentially no fluorescence (similar emission profile of NaCl) at  $\lambda_{\text{ex},280}$ , but weak fluorescence at  $\lambda_{\text{ex},355}$  ( $I \sim 1$  at  $\lambda_{\text{em},426}$ ). Chitin shows only marginally increased fluorescence for  $\lambda_{\text{ex},280}$  compared to cellulose, but significant emission for  $\lambda_{\text{ex},355}$  ( $I \sim 5.9$  at  $\lambda_{\text{em},426}$  and  $\sim 4.2$  at  $\lambda_{\text{em},515}$ ). All other samples of biological fluorophores and material chosen exhibit relatively high intensity peaks in each emission spectrum shown in Fig. 6. Amino acid peaks, especially tryptophan, showed fluorescent emission among the most intense of compounds sampled. Samples of isolated protein and of the *S. cerevisiae* each showed similar peak placement with tryptophan indicating that tryptophan is the major and crucial fluorophore in proteins.

In contrast, most of the seven non-biological samples shown in Fig. 6c and d show very weak fluorescence. Pyrene and naphthalene, shown here as examples of PAH fluorescence, are the only exceptions to this trend and show sharp peaks in the range of 333–456 nm in the emission spectra for both excitation wavelengths, where  $I$ : 54–172 for  $\lambda_{\text{ex},280}$  and 2–140 for  $\lambda_{\text{ex},355}$ . Strong fluorescent emission of pyrene is observed for  $\lambda_{\text{ex},280}$  and  $\lambda_{\text{ex},355}$  whereas naphthalene shows only fluorescence when excited at 280 nm. Moreover, large differences in  $\lambda_{\text{em}}$  can be observed between solid state and solution samples, for example pyrene in *n*-hexane exhibits  $\lambda_{\text{em},280} = 387$  nm, while in the solid state exhibits  $\lambda_{\text{em},280} = 457$  nm. As mentioned, NaCl is expected to exhibit no emission of classically-termed fluorescence, but four of the other compounds chosen show fluorescent emission

levels at or below the level of NaCl for each excitation wavelength chosen in Fig. 6. This indicates that, while mineral dust has been shown to fluoresce in some circumstances, kaolin fluorescence is insignificantly weak compared with the intensity of the biofluorophores measured here. Fulvic and humic acids analyzed in this study also exhibited very weak fluorescence. This could indicate that HULIS may not cause significant interference within FBAP measurements because of a comparatively low level of fluorescent intensity compared to biological material. However, these effects are complicated and contain a high degree of uncertainty (see Sect. 2.7). In particular, fluorescence from single particles may exhibit different trends from that of the bulk. While pure PAH compounds were observed to fluoresce intensely, diesel and biomass burning soot that likely contain PAH molecules both show emission levels below the surrogate NaCl background. While still a preliminary determination, the spectra of these soot samples corroborate suggestions by Lewitzka and Niessner (1995) and Panne et al. (2000) that soot exhibits only weak fluorescence due to inner quenching effects.

For excitation at 355 nm fluorophores such as NAD(P)H, pyridoxamine, neopterin, riboflavin, chitin and cellulose likely contribute to wavelength-integrated fluorescence detection by UV-APS ( $\lambda_{\text{em}} = 420\text{--}575$  nm) and WIBS ( $\lambda_{\text{em}} = 400\text{--}600$  nm) instruments, but this depends largely on exact instrumental optics and operational emission thresholds. Moreover a large number of other molecules (i.e. secondary metabolites) emit in the same spectral region, as discussed in Sect. 2. Accordingly we suggest that within this spectral range an integrated fluorescence signal provides no clear selectivity for certain coenzymes (e.g. NAD(P)H) as indicators for viability, and users of such instrumentation should avoid the assumption that these molecules dominate the fluorescence signal in all cases. Neither UV-APS nor WIBS instrument is likely to detect chlorophyll, because of its large  $\Delta\lambda_{\text{Stokes}}$ . The WIBS channels measuring emission after  $\lambda_{\text{ex},280}$  may be more sensitive to influence from PAHs when the molecular environment in the sampled atmospheric particle approximates that of the solution-phase PAHs presented here. However, for excitation at 280 nm, the region exemplified by the first WIBS emission band ( $\lambda_{\text{em}} = 310\text{--}400$  nm) suggests that fluorophores such as proteins and particularly tryptophan-containing proteins will dominate the emission signal in most cases, with some coenzymes (i.e. pyridoxamine, riboflavin) also important. The region exemplified by the second WIBS emission band ( $\lambda_{\text{em}} = 400\text{--}600$  nm) at  $\lambda_{\text{ex},280}$  will also likely detect protein and coenzyme fluorescence, however, to a lower extent.

The emission spectrum observed for *S. cerevisiae* suggests by extrapolation that viable PBAP can, not surprisingly, be expected to exhibit clear signals in both FBAP instruments. Given the fluorescence spectra shown, however, the WIBS may be more likely to see higher intensity for this organism in the first of two channels at  $\lambda_{\text{ex},280}$ .

## 5 Conclusions and outlook

In this study a systematic literature survey of key biological fluorophores which are relevant for atmospheric science is presented. The individual compounds are organized into major fluorophore classes and characterized by their biological role and abundance as well as by certain fluorescence properties. As a first approach the relative atmospheric importance of individual fluorophores or classes of fluorophores have been estimated. In addition, emission spectra have been measured as a function of excitation wavelength for various representative compounds. An overview of individual fluorophores shows that unique autofluorescence properties can indeed be useful for discrimination of biological material by online FBAP methods. Moreover key biological fluorophores can be collected into two relatively narrow excitation bands ( $\sim 280$  and  $\sim 360$  nm). Each of these bands has been utilized by designers of FBAP instruments for bioaerosol detection.

Amino acids and proteins are among the most important fluorophores at  $\lambda_{\text{ex},280}$ , while some coenzymes (e.g. pyridoxamine, riboflavin) are also potentially important. Coenzymes such as NAD(P)H, pyridoxine compounds and pteridines are among the most highly fluorescent compounds at  $\lambda_{\text{ex},355}$ , but structural biopolymers (e.g. chitin, lignin) are also important. The complexity of overlapping spectra for fluorophores expected to be present in many classes of PBAP highlights the difficulty in making molecular determination of fluorescence origin from spectrally integrated signals detected in broad emission bands. Care should be taken, therefore, not to assume molecular identity from signals from instruments such as the UV-APS and WIBS. Further, the ability to determine cell viability for an unknown biological particle arriving at a detector may be difficult by single wavelength fluorescence alone, as has been suggested in depth previously (e.g. Pinnick et al., 2004). More work investigating standard particles in the laboratory are needed before uncertainties in these suggestions can be reduced, however.

A collection of atmospherically relevant non-biological compounds have also been analyzed and presented here. These data suggest that some non-biological materials could potentially contribute to fluorescence at wavelengths used by FBAP detectors (e.g. PAHs and SOA), whereas the majority of compounds suggested to cause interference (e.g. HULIS, mineral dust, soot) are less likely to contribute signal due to extremely weak intensity. SOA were not investigated here, because experimental procedures for producing oxidized aerosol in environmental chambers are beyond the scope of this text. Lab-generated SOA have been shown to fluoresce under certain conditions (Bones et al., 2010), though this has not been documented systematically within scientific literature. While SOA can dominate submicron particle concentrations, its contribution to supermicron particle mass is probably small. As such, its influence on the fluorescence signal of supermicron FBAP is likely also very

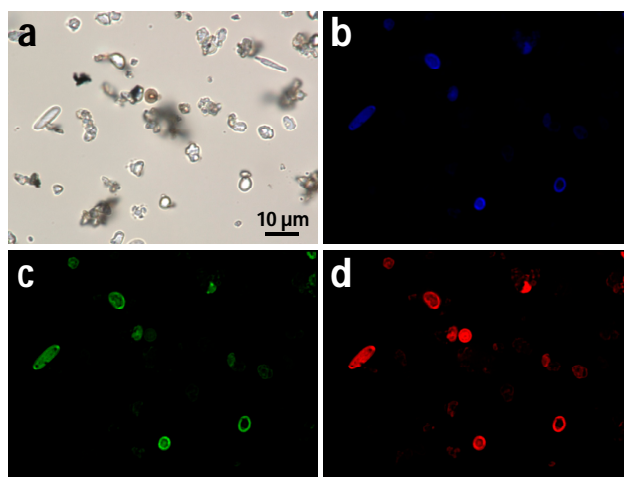


**Fig. 7.** Microscopy pictures of ambient aerosol sample. Illumination source: (a) brightfield, (b)  $\lambda_{\text{ex}} = 340\text{--}380$  nm,  $\lambda_{\text{em}} = 435\text{--}485$ , (c)  $\lambda_{\text{ex}} = 465\text{--}495$  nm,  $\lambda_{\text{em}} = 510\text{--}560$ , (d)  $\lambda_{\text{ex}} = 540\text{--}580$  nm,  $\lambda_{\text{em}} = 600\text{--}660$ .

small, although this should be investigated further. PAHs, which often are intensely fluorescent, are largely present in atmospheric aerosols on the surface of soot particles, but the complex chemical environments of soot have been shown to largely quench fluorescence. As a result of this and the fact that soot also often peaks at submicron sizes PAHs are considered to contribute only minimally to FBAP number, though they could cause potential interference in some cases. Despite uncertainties based on this bottom-up approach of addressing fluorescent properties of selected compounds the results of this laboratory study suggest that fluorescent properties of ambient FBAP are likely to be dominated by biological material in most cases. However, the authors are aware of the fact that the results presented in this study can only serve as a first general approach to aspects of selectivity in FBAP detection. In particular, further investigation must address differences between bulk and single particle fluorescence (Hill et al., 2009), the characteristic fluorescence fingerprints of authentic bioparticles and the impact of different atmospheric conditions and aging.

As a proof of concept study we collected ambient aerosol in Mainz, Germany and other locations for investigation of autofluorescence via fluorescence microscopy. Initial observations show that particles that fluoresce most strongly also exhibit characteristic biological morphologies, based on visual evidence presented here (Fig. 7). These ambient studies need to be furthered in much greater detail, but again provide a similar conclusion as given by the laboratory fluorescence study presented here that ambient FBAP appear to be comprised at least heavily of particles from biological origin, consistent with previous observations reported by Pöschl et al. (2010) and Huffman et al. (2012). Further work is necessary and forthcoming in order to fill in important gaps in

understanding. For example, the fluorescence properties of standard microorganism types have been investigated in the laboratory under varying environmental conditions and will be presented in a follow-up study.

#### List of frequently used acronyms.

Acronym	Description
AA	amino acid
AFS	aerosol fluorescence sensor
AGE	advanced glycation end-product
APF	age pigment-like fluorophore
BP	band-pass
BSA	bovine serum albumin
BWA	biological warfare agent
CCN	cloud condensation nuclei
DAPI	4',6-diamidino-2-phenylindole
DNA	deoxyribonucleic acid
DOM	dissolved organic matter
DPA/CaDPA	dipicolinic acid/calcium dipicolinic acid
EEM	excitation-emission matrix
FAD	flavin adenine dinucleotide
FBAP	fluorescent biological aerosol particles
FISH	fluorescence in-situ hybridization
FMN	flavin mononucleotide
FWHM	full width half max
GFP	green fluorescent protein
HULIS	humic-like substances
IN	ice nuclei
LIF	light/laser-induced fluorescence
MAA	mycosporin-like amino acid
MS	mass spectrometry
NADH	nicotinamide adenine dinucleotide
NADPH	nicotinamide adenine dinucleotide phosphate
NAD(P)H	NADH and NADPH
Nd:YAG	neodymium-doped yttrium aluminium garnet
NF	normalization factor
OVA	ovalbumin
PAH	polycyclic aromatic hydrocarbons
PBAP	primary biological aerosol particles
PBS	phosphate-buffered saline
PCR/qPCR	polymerase chain reaction/quantitative polymerase chain reaction
Phe	phenylalanine
PM	particulate matter
PMT	photomultiplier tube
RET	resonance energy transfer
RNA	ribonucleic acid
SOA	secondary organic aerosols
Trp	tryptophan
Tyr	tyrosine

UV	ultraviolet
UV-APS	ultraviolet aerodynamic particle sizer
VBNC	viable but non-culturable
VOC	volatile organic compound
WIBS	wide issue bioaerosol sensor

#### Supplementary material related to this article is available online at:

<http://www.atmos-meas-tech.net/5/37/2012/amt-5-37-2012-supplement.pdf>.

*Acknowledgements.* This work has been funded by the Max Planck Society, the Max Planck Graduate Center and the LEC Geocycles Mainz. The authors gratefully acknowledge support by M. O. Andreae, J. Schneider, K. Selzle and W. Elbert and helpful conversation with D. R. Huffman, M. Shiraiwa, H. Su and M. Ermel.

The service charges for this open access publication have been covered by the Max Planck Society.

Edited by: J. Curtius

#### References

- Agranovski, V., Ristovski, Z., Hargreaves, M., Blackall, P. J., and Morawska, L.: Performance evaluation of the UVAPS: influence of physiological age of airborne bacteria and bacterial stress, *J. Aerosol Sci.*, 34, 1711–1727, doi:10.1016/s0021-8502(03)00191-5, 2003.
- Aizawa, T. and Kosaka, H.: Investigation of early soot formation process in a diesel spray flame via excitation-emission matrix using a multi-wavelength laser source, *Int. J. Eng. Res.*, 9, 79–96, doi:10.1243/14680874jer01407, 2008.
- Aizawa, T. and Kosaka, H.: Effects of Fischer-Tropsch diesel fuel on soot formation processes in a diesel spray flame, *Int. J. Eng. Res.*, 11, 79–87, doi:10.1243/14680874jer04709, 2010.
- Albani, J. R., Sillen, A., Engelborghs, Y., and Gervais, M.: Dynamics of flavin in flavocytochrome b(2): A fluorescence study, *Photochem. Photobiol.*, 69, 22–26, 1999.
- Albinsson, B., Li, S. M., Lundquist, K., and Stomberg, R.: The origin of lignin fluorescence, *J. Mol. Struct.*, 508, 19–27, 1999.
- Alimova, A., Katz, A., Savage, H. E., Shah, M., Minko, G., Will, D. V., Rosen, R. B., McCormick, S. A., and Alfano, R. R.: Native fluorescence and excitation spectroscopic changes in *Bacillus subtilis* and *Staphylococcus aureus* bacteria subjected to conditions of starvation, *Appl. Optics*, 42, 4080–4087, 2003.
- Amann, R. I., Ludwig, W., and Schleifer, K. H.: Phylogenetic identification and in-situ detection of individual microbial-cells without cultivation, *Microbiol. Rev.*, 59, 143–169, 1995.
- Ammor, M. S.: Recent advances in the use of intrinsic fluorescence for bacterial identification and characterization, *J. Fluoresc.*, 17, 455–459, doi:10.1007/s10895-007-0180-6, 2007.
- Ammor, S., Yaakoubi, K., Chevallier, I., and Dufour, E.: Identification by fluorescence spectroscopy of lactic acid bacteria isolated from a small-scale facility producing traditional dry sausages, *J. Microbiol. Meth.*, 59, 271–281, doi:10.1016/j.mimet.2004.07.014, 2004.

- Andersson, H., Baechi, T., Hoehchl, M., and Richter, C.: Autofluorescence of living cells, *J. Microsc.-Oxford*, 191, 1–7, 1998.
- Andersson Engels, S., af Klinteberg, C., Svanberg, K., and Svanberg, S.: In vivo fluorescence imaging for tissue diagnostics, *Phys. Med. Biol.*, 42, 815–824, 1997.
- Andreae, M. O. and Crutzen, P. J.: Atmospheric aerosols: Biogeochemical sources and role in atmospheric chemistry, *Science*, 276, 1052–1058, 1997.
- Andreae, M. O. and Gelencsér, A.: Black carbon or brown carbon? The nature of light-absorbing carbonaceous aerosols, *Atmos. Chem. Phys.*, 6, 3131–3148, doi:10.5194/acp-6-3131-2006, 2006.
- Andreae, M. O. and Rosenfeld, D.: Aerosol-cloud-precipitation interactions, Part 1, The nature and sources of cloud-active aerosols, *Earth-Sci. Rev.*, 89, 13–41, doi:10.1016/j.earscirev.2008.03.001, 2008.
- Avidor, Y., Doherty, M. D., Olson, J. M., and Kaplan, N. O.: Fluorescence of pyridine nucleotides in mitochondria, *J. Biol. Chem.*, 237, 2377–2383, 1962.
- Bauer, H., Schueller, E., Weinke, G., Berger, A., Hitzengerger, R., Marr, I. L., and Puxbaum, H.: Significant contributions of fungal spores to the organic carbon and to the aerosol mass balance of the urban atmospheric aerosol, *Atmos. Environ.*, 42, 5542–5549, doi:10.1016/j.atmosenv.2008.03.019, 2008.
- Benson, R. C., Meyer, R. A., Zaruba, M. E., and McKhann, G. M.: Cellular autofluorescence – is it due to flavins, *J. Histochem. Cytochem.*, 27, 44–48, 1979.
- Bhartia, R., Hug, W. F., Salas, E. C., Reid, R. D., Sijapati, K. K., Tsapin, A., Abbey, W., Neelson, K. H., Lane, A. L., and Conrad, P. G.: Classification of Organic and Biological Materials with Deep Ultraviolet Excitation, *Appl. Spectrosc.*, 62, 1070–1077, 2008.
- Bigio, I. J. and Mourant, J. R.: Ultraviolet and visible spectroscopies for tissue diagnostics: Fluorescence spectroscopy and elastic-scattering spectroscopy, *Phys. Med. Biol.*, 42, 803–814, 1997.
- Billinton, N. and Knight, A. W.: Seeing the wood through the trees: A review of techniques for distinguishing green fluorescent protein from endogenous autofluorescence, *Anal. Biochem.*, 291, 175–197, 2001.
- Birdwell, J. E. and Valsaraj, K. T.: Characterization of dissolved organic matter in fogwater by excitation-emission matrix fluorescence spectroscopy, *Atmos. Environ.*, 44, 3246–3253, doi:10.1016/j.atmosenv.2010.05.055, 2010.
- Boerjan, W., Ralph, J., and Baucher, M.: Lignin biosynthesis, *Annu. Rev. Plant Biol.*, 54, 519–546, doi:10.1146/annurev.arplant.54.031902.134938, 2003.
- Bones, D. L., Henricksen, D. K., Mang, S. A., Gonsior, M., Bateman, A. P., Nguyen, T. B., Cooper, W. J., and Nizkorodov, S. A.: Appearance of strong absorbers and fluorophores in limonene-O-3 secondary organic aerosol due to NH<sub>4</sub><sup>+</sup>-mediated chemical aging over long time scales, *J. Geophys. Res.-Atmos.*, 115, D05203, doi:10.1029/2009jd012864, 2010.
- Bonfante-fasolo, P., Faccio, A., Perotto, S., and Schubert, A.: Correlation between chitin distribution and cell-wall morphology in the mycorrhizal fungus *glomus-versiforme*, *Mycol. Res.*, 94, 157–165, 1990.
- Bowers, R. M., Lauber, C. L., Wiedinmyer, C., Hamady, M., Hallar, A. G., Fall, R., Knight, R., and Fierer, N.: Characterization of Airborne Microbial Communities at a High-Elevation Site and Their Potential To Act as Atmospheric Ice Nuclei, *Appl. Environ. Microbiol.*, 75, 5121–5130, doi:10.1128/aem.00447-09, 2009.
- Bowers, R. M., McLetchie, S., Knight, R., and Fierer, N.: Spatial variability in airborne bacterial communities across land-use types and their relationship to the bacterial communities of potential source environments, *ISME J.*, 5, 601–612, 2011.
- Bozlee, B. J., Misra, A. K., Sharma, S. K., and Ingram, M.: Remote Raman and fluorescence studies of mineral samples, *Spectroc. Acta Pt. A-Molec. Biomolec. Spectr.*, 61, 2342–2348, doi:10.1016/j.saa.2005.02.033, 2005.
- Bridges, J. W., Davies, D. S., and Williams, R. T.: Fluorescence studies on some hydroxyridines including compounds of vitamin B6 group, *Biochem. J.*, 98, 451–468, 1966.
- Bronk, B. V., Shoaibi, A., Nudelman, R., and Akinyemi, A.: Physical perturbation for fluorescent characterization of microorganism particles, in: *Chemical and Biological Sensing*, edited by: Gardner, P. J., Proceedings of the Society of Photo-Optical Instrumentation Engineers – Spie, Spie-Int Soc Optical Engineering, Bellingham, 169–180, 2000.
- Brooks, J. and Shaw, G.: Sporopollenin in a review of its chemistry paleochemistry and geochemistry, *Grana*, 17, 91–98, 1978.
- Brosseau, L. M., Vesley, D., Rice, N., Goodell, K., Nellis, M., and Hairston, P.: Differences in detected fluorescence among several bacterial species measured with a direct-reading particle sizer and fluorescence detector, *Aerosol Sci. Tech.*, 32, 545–558, 2000.
- Brown, J. K. M. and Hovmoller, M. S.: Epidemiology – Aerial dispersal of pathogens on the global and continental scales and its impact on plant disease, *Science*, 297, 537–541, 2002.
- Bueno, C. and Encinas, M. V.: Photophysical and photochemical studies of pyridoxamine, *Helv. Chim. Acta*, 86, 3363–3375, 2003.
- Bundke, U., Reimann, B., Nillius, B., Jaenicke, R., and Bingermer, H.: Development of a Bioaerosol single particle detector (BIO IN) for the Fast Ice Nucleus Chamber FINCH, *Atmos. Meas. Tech.*, 3, 263–271, doi:10.5194/amt-3-263-2010, 2010.
- Burrows, S. M., Butler, T., Jöckel, P., Tost, H., Kerkweg, A., Pöschl, U., and Lawrence, M. G.: Bacteria in the global atmosphere – Part 2: Modeling of emissions and transport between different ecosystems, *Atmos. Chem. Phys.*, 9, 9281–9297, doi:10.5194/acp-9-9281-2009, 2009.
- Burshtein, N., Lang-Yona, N., and Rudich, Y.: Ergosterol, arabinol and mannitol as tracers for biogenic aerosols in the eastern Mediterranean, *Atmos. Chem. Phys.*, 11, 829–839, doi:10.5194/acp-11-829-2011, 2011.
- Campbell, S. D., Tremblay, D. P., Daver, F., and Cousins, D.: Wavelength comparison study for bioaerosol detection, in: *Sensors, and Command, Control, Communications, and Intelligence*, edited by: Carapezza, E. M., Proceedings of the Society of Photo-Optical Instrumentation Engineers – Spie, Spie-Int Soc Optical Engineering, Bellingham, 130–138, 2005.
- Cannon, R. E. and Anderson, S. M.: Biogenesis of bacterial cellulose, *Crit. Rev. Microbiol.*, 17, 435–447, 1991.
- Castellan, A., Ruggiero, R., Frollini, E., Ramos, L. A., and Chirat, C.: Studies on fluorescence of celluloses, *Holzforchung*, 61, 504–508, doi:10.1515/hf.2007.090, 2007.



- Chance, B., Schoener, B., Oshino, R., Itshak, F., and Nakase, Y.: Oxidation-reduction ratio studies of mitochondria in freeze-trapped samples – NADH and flavoprotein fluorescence signals, *J. Biol. Chem.*, 254, 4764–4771, 1979.
- Chang, J. L. and Thompson, J. E.: Characterization of colored products formed during irradiation of aqueous solutions containing H<sub>2</sub>O<sub>2</sub> and phenolic compounds, *Atmos. Environ.*, 44, 541–551, doi:10.1016/j.atmosenv.2009.10.042, 2010.
- Chang, S. K., Mirabal, Y. N., Atkinson, E. N., Cox, D., Malpica, A., Follen, M., and Richards-Kortum, R.: Combined reflectance and fluorescence spectroscopy for in vivo detection of cervical pre-cancer, *J. Biomed. Opt.*, 10, 024031, doi:10.1117/1.1899686, 2005.
- Chen, J., LeBoef, E. J., Dai, S., and Gu, B. H.: Fluorescence spectroscopic studies of natural organic matter fractions, *Chemosphere*, 50, 639–647, 2003.
- Cheng, Y. S., Barr, E. B., Fan, B. J., Hargis, P. J., Rader, D. J., O'Hern, T. J., Torczynski, J. R., Tisone, G. C., Preppernau, B. L., Young, S. A., and Radloff, R. J.: Detection of bioaerosols using multiwavelength UV fluorescence spectroscopy, *Aerosol Sci. Tech.*, 30, 186–201, 1999.
- Chi, M. C. and Li, C. S.: Fluorochrome in monitoring atmospheric bioaerosols and correlations with meteorological factors and air pollutants, *Aerosol Sci. Tech.*, 41, 672–678, doi:10.1080/02786820701383181, 2007.
- Christner, B. C., Morris, C. E., Foreman, C. M., Cai, R. M., and Sands, D. C.: Ubiquity of biological ice nucleators in snowfall, *Science*, 319, 1214–1214, doi:10.1126/science.1149757, 2008.
- Coble, P. G.: Characterization of marine and terrestrial DOM in seawater using excitation emission matrix spectroscopy, *Mar. Chem.*, 51, 325–346, 1996.
- Coble, P. G., Green, S. A., Blough, N. V., and Gagosian, R. B.: Characterization of dissolved organic-matter in the black-sea by fluorescence spectroscopy, *Nature*, 348, 432–435, 1990.
- Cox, C. S. and Wathes, C. M.: *Bioaerosols handbook*, Lewis, Boca Raton, 1995.
- Creed, D.: The photophysics and photochemistry of the near-UV absorbing amino-acids – 2. Tyrosine and its simple derivatives, *Photochem. Photobiol.*, 39, 563–575, 1984a.
- Creed, D.: The photophysics and photochemistry of the near-UV absorbing amino-acids – 1. Tryptophan and its simple derivatives, *Photochem. Photobiol.*, 39, 537–562, 1984b.
- DaCosta, R. S., Andersson, H., and Wilson, B. C.: Molecular fluorescence excitation-emission matrices relevant to tissue spectroscopy, *Photochem. Photobiol.*, 78, 384–392, 2003.
- Dalterio, R. A., Nelson, W. H., Britt, D., Sperry, J. F., Tanguay, J. F., and Suib, S. L.: The steady-state and decay characteristics of primary fluorescence from live bacteria, *Appl. Spectrosc.*, 41, 234–241, 1987.
- Davitt, K., Song, Y. K., Patterson, W. R., Nurmikko, A. V., Gherasimova, M., Han, J., Pan, Y. L., and Chang, R. K.: 290 and 340 nm UV LED arrays for fluorescence detection from single airborne particles, *Opt. Express*, 13, 9548–9555, 2005.
- Després, V. R., Nowojsky, J. F., Klose, M., Conrad, R., Andreae, M. O., and Pöschl, U.: Characterization of primary biogenic aerosol particles in urban, rural, and high-alpine air by DNA sequence and restriction fragment analysis of ribosomal RNA genes, *Bio-geosciences*, 4, 1127–1141, doi:10.5194/bg-4-1127-2007, 2007.
- Després, V. R., Huffman, J. A., Burrows, S. M., Hoose, C., Safatov, A. S., Buryak, G. A., Fröhlich-Nowojsky, J., Elbert, W., Andreae, M. O., Pöschl, U., and Jaenicke, R.: *Primary Biological Aerosol Particles in the Atmosphere: A Review*, Tellus B, in press, 2012.
- Dingle, A. N.: Pollens as condensation nuclei, *Journal de Recherches Atmospheriques*, 2, 231–237, 1966.
- Dix, T. A. and Marnett, L. J.: Metabolism of polycyclic aromatic hydrocarbon derivatives to ultimate carcinogens during lipid-peroxidation, *Science*, 221, 77–79, 1983.
- Donaldson, L. A.: Lignification and lignin topochemistry – an ultrastructural view, *Phytochemistry*, 57, 859–873, 2001.
- Donaldson, L. A., Singh, A. P., Yoshinaga, A., and Takabe, K.: Lignin distribution in mild compression wood of *Pinus radiata*, *Can. J. Bot.-Rev. Can. Bot.*, 77, 41–50, 1999.
- Douwes, J., Thorne, P., Pearce, N., and Heederik, D.: Bioaerosol health effects and exposure assessment: Progress and prospects, *Ann. Occup. Hyg.*, 47, 187–200, doi:10.1093/annhyg/meg032, 2003.
- Dreyer, B., Morte, A., Perez-Gilbert, M., and Honrubia, M.: Autofluorescence detection of arbuscular mycorrhizal fungal structures in palm roots: an underestimated experimental method, *Mycol. Res.*, 110, 887–897, doi:10.1016/j.mycres.2006.05.011, 2006.
- Duarte, R., Pio, C. A., and Duarte, A. C.: Synchronous scan and excitation-emission matrix fluorescence spectroscopy of water-soluble organic compounds in atmospheric aerosols, *J. Atmos. Chem.*, 48, 157–171, 2004.
- Elbert, W., Taylor, P. E., Andreae, M. O., and Pöschl, U.: Contribution of fungi to primary biogenic aerosols in the atmosphere: wet and dry discharged spores, carbohydrates, and inorganic ions, *Atmos. Chem. Phys.*, 7, 4569–4588, doi:10.5194/acp-7-4569-2007, 2007.
- Eldred, G. E., Miller, G. V., Stark, W. S., and Feeneyburns, L.: Lipofuscin – Resolution of discrepant fluorescence data, *Science*, 216, 757–759, 1982.
- Eng, J., Lynch, R. M., and Balaban, R. S.: Nicotinamide adenine-dinucleotide fluorescence spectroscopy and imaging of isolated cardiac myocytes, *Biophys. J.*, 55, 621–630, 1989.
- Estes, C., Duncan, A., Wade, B., Lloyd, C., Ellis, W., and Powers, L.: Reagentless detection of microorganisms by intrinsic fluorescence, *Biosens. Bioelectron.*, 18, 511–519, doi:10.1016/s0956-5663(03)00008-3, 2003.
- Ewald, M., Belin, C., Berger, P., and Weber, J. H.: Corrected fluorescence-spectra of fulvic-acids isolated from soil and water, *Environ. Sci. Technol.*, 17, 501–504, 1983.
- Farabegoli, G., Hellinga, C., Heijnen, J. J., and van Loosdrecht, M. C. M.: Study on the use of NADH fluorescence measurements for monitoring wastewater treatment systems, *Water Res.*, 37, 2732–2738, doi:10.1016/s0043-1354(03)00064-2, 2003.
- Ferguson, D. P., Pitesky, M. E., Tobias, H. J., Steele, P. T., Czerwieniec, G. A., Russell, S. C., Lebrilla, C. B., Horn, J. M., Coffee, K. R., Srivastava, A., Pillai, S. P., Shih, M. T. P., Hall, H. L., Ramponi, A. J., Chang, J. T., Langlois, R. G., Estacio, P. L., Hadley, R. T., Frank, M., and Gard, E. E.: Reagentless detection and classification of individual bioaerosol particles in seconds, *Anal. Chem.*, 76, 373–378, doi:10.1021/ac034467e, 2004.

- Feugnet, G., Lallier, E., Grisard, A., McIntosh, L., Hellstrom, J. E., Jelger, P., Laurell, F., Albano, C., Kaliszewski, M., Wlodarski, M., Mlyneczek, J., Kwasny, M., Zawadzki, Z., Mierczyk, Z., Kopczynski, K., Rostedt, A., Putkiranta, M., Marjamaki, M., Keskinen, J., Enroth, J., Janka, K., Reinivaara, R., Holma, L., Humppi, T., Battistelli, E., Iliakis, E., and Gerolimos, G.: Improved laser-induced fluorescence method for bio-attack early warning detection system, *Proc. SPIE – Int. Soc. Opt. Eng.*, 7116, 71160C, doi:10.1117/12.799151, 2008.
- Finlayson-Pitts, B. J. and Pitts, J. N.: *Chemistry of the upper and lower atmosphere*, Academic press, San Diego, USA, 2000.
- Foot, V. E., Kaye, P. H., Stanley, W. R., Barrington, S. J., Gallagher, M., and Gabey, A.: Low-cost real-time multi-parameter bio-aerosol sensors, *Proc. SPIE - Int. Soc. Opt. Eng.*, 7116, 711601, doi:10.1117/12.800226, 2008.
- Franze, T., Weller, M. G., Niessner, R., and Pöschl, U.: Protein nitration by polluted air, *Environ. Sci. Technol.*, 39, 1673–1678, doi:10.1021/es0488737, 2005.
- French, C. S., Smith, J. H. C., Virgin, H. I., and Airth, R. L.: Fluorescence-spectrum curves of chlorophylls, pheophytins, phycoerythrins, phycocyanins and hypericin, *Plant Physiol.*, 31, 369–374, 1956.
- Fröhlich-Nowoisky, J., Pickersgill, D. A., Després, V. R., and Pöschl, U.: High diversity of fungi in air particulate matter, *P. Natl. Acad. Sci. USA*, 106, 12814–12819, doi:10.1073/pnas.0811003106, 2009.
- Gabey, A. M., Gallagher, M. W., Whitehead, J., Dorsey, J. R., Kaye, P. H., and Stanley, W. R.: Measurements and comparison of primary biological aerosol above and below a tropical forest canopy using a dual channel fluorescence spectrometer, *Atmos. Chem. Phys.*, 10, 4453–4466, doi:10.5194/acp-10-4453-2010, 2010.
- Gabey, A. M., Stanley, W. R., Gallagher, M. W., and Kaye, P. H.: The fluorescence properties of aerosol larger than 0.8  $\mu\text{m}$  in urban and tropical rainforest locations, *Atmos. Chem. Phys.*, 11, 5491–5504, doi:10.5194/acp-11-5491-2011, 2011.
- Gaft, M., Panczer, G., Reisfeld, R., and Uspensky, E.: Laser-induced time-resolved luminescence as a tool for rare-earth element identification in minerals, *Phys. Chem. Miner.*, 28, 347–363, 2001.
- Galland, P. and Senger, H.: The role of flavins as photoreceptors, *J. Photochem. Photobiol. B*, 1, 277–294, 1988.
- Galland, P. and Tolle, N.: Light-induced fluorescence changes in *Phycomyces*: evidence for blue light-receptor associated flavo-semiquinones, *Planta*, 217, 971–982, doi:10.1007/s00425-003-1068-6, 2003.
- Galland, P., Keiner, P., Dornemann, D., Senger, H., Brodhun, B., and Hader, D. P.: Pterin-like and flavin-like fluorescence associated with isolated flagella of *euglena-gracilis*, *Photochem. Photobiol.*, 51, 675–680, 1990.
- Georgakopoulos, D. G., Després, V., Fröhlich-Nowoisky, J., Psenner, R., Ariya, P. A., Pósfai, M., Ahern, H. E., Moffett, B. F., and Hill, T. C. J.: Microbiology and atmospheric processes: biological, physical and chemical characterization of aerosol particles, *Biogeosciences*, 6, 721–737, doi:10.5194/bg-6-721-2009, 2009.
- Gillette, D. A. and Walker, T. R.: Characteristics of airborne particles produced by wind erosion of sandy soil, high plains of west Texas, *Soil Sci.*, 123, 97–110, 1977.
- Glazer, A. N.: Phycobiliproteins – A family of valuable, widely used fluorophores, *J. Appl. Phycol.*, 6, 105–112, 1994.
- Gomez, B. L. and Nosanchuk, J. D.: Melanin and fungi, *Curr. Opin. Infect. Dis.*, 16, 91–96, doi:10.1097/01.aco.0000065076.06965.04, 2003.
- Graber, E. R. and Rudich, Y.: Atmospheric HULIS: How humic-like are they? A comprehensive and critical review, *Atmos. Chem. Phys.*, 6, 729–753, doi:10.5194/acp-6-729-2006, 2006.
- Gregory, P. H.: *The Microbiology of the Atmosphere*, Wiley, New York, 1973.
- Griffiths, W. D. and Decosemo, G. A. L.: The Assessment of Bioaerosols – A Critical Review, *J. Aerosol Sci.*, 25, 1425–1458, 1994.
- Hairston, P. P., Ho, J., and Quant, F. R.: Design of an instrument for real-time detection of bioaerosols using simultaneous measurement of particle aerodynamic size and intrinsic fluorescence, *J. Aerosol Sci.*, 28, 471–482, 1997.
- Harris, P. J. and Hartley, R. D.: Detection of bound ferulic acid in cell-walls of gramineae by ultraviolet fluorescence microscopy, *Nature*, 259, 508–510, 1976.
- Hawley, R. J. and Eitzen, E. M.: Biological weapons – A primer for microbiologists, *Annu. Rev. Microbiol.*, 55, 235–253, 2001.
- He, X. Q., Li, S. W., Hu, Y. X., and Lin, J. X.: Microspectrofluorometric analysis of autofluorescence in the cell walls of *Phyllostachys pubescens* Culm, *Acta Bot. Sin.*, 41, 711–714, 1999.
- Heald, C. L. and Spracklen, D. V.: Atmospheric budget of primary biological aerosol particles from fungal spores, *Geophys. Res. Lett.*, 36, L09806, doi:10.1029/2009gl037493, 2009.
- Heidelberg, J. F., Shahamat, M., Levin, M., Rahman, I., Stelma, G., Grim, C., and Colwell, R. R.: Effect of aerosolization on culturability and viability of gram-negative bacteria, *Appl. Environ. Microbiol.*, 63, 3585–3588, 1997.
- Heikal, A. A.: Intracellular coenzymes as natural biomarkers for metabolic activities and mitochondrial anomalies, *Biomark. Med.*, 4, 241–263, doi:10.2217/bmm.10.1, 2010.
- Hill, S. C., Pinnick, R. G., Nachman, P., Chen, G., Chang, R. K., Mayo, M. W., and Fernandez, G. L.: Aerosol-fluorescence spectrum analyzer – Real-time measurement of emission-spectra of airborne biological particles, *Appl. Optics*, 34, 7149–7155, 1995.
- Hill, S. C., Mayo, M. W., and Chang, R. K.: Fluorescence of bacteria, pollens, and naturally occurring airborne particles: excitation/emission spectra Army report, ARL-TR-4722, 2009.
- Hirayama, K., Akashi, S., Furuya, M., and Fukuhara, K.: Rapid confirmation and revision of the primary structure of bovine serum-albumin by ESIMS and FRIT-FAB LC MS, *Biochem. Biophys. Res. Commun.*, 173, 639–646, 1990.
- Ho, J.: Future of biological aerosol detection, *Anal. Chim. Acta*, 457, 125–148, 2002.
- Hobbie, J. E., Daley, R. J., and Jasper, S.: Use of nucleopore filters for counting bacteria by fluorescence microscopy, *Appl. Environ. Microbiol.*, 33, 1225–1228, 1977.
- Hohl, N., Galland, P., and Senger, H.: Altered pterin patterns in photobehavioral mutants of *phycomyces-blakesleanus*, *Photochem. Photobiol.*, 55, 239–245, 1992.
- Hoose, C., Kristjansson, J. E., and Burrows, S. M.: How important is biological ice nucleation in clouds on a global scale?, *Environ. Res. Lett.*, 5, 024009, doi:10.1088/1748-9326/5/2/024009, 2010.

- Huang, S. H., Heikal, A. A., and Webb, W. W.: Two-photon fluorescence spectroscopy and microscopy of NAD(P)H and flavo-protein, *Biophys. J.*, 82, 2811–2825, 2002.
- Hudson, N., Baker, A., and Reynolds, D.: Fluorescence analysis of dissolved organic matter in natural, waste and polluted waters – A review, *River Res. Appl.*, 23, 631–649, doi:10.1002/rra.1005, 2007.
- Huffman, J. A., Treutlein, B., and Pöschl, U.: Fluorescent biological aerosol particle concentrations and size distributions measured with an Ultraviolet Aerodynamic Particle Sizer (UV-APS) in Central Europe, *Atmos. Chem. Phys.*, 10, 3215–3233, doi:10.5194/acp-10-3215-2010, 2010.
- Huffman, J. A., Sinha, B., Garland, R. M., Gunthe, S., Artaxo, P., Martin, S., Andreae, M. O., and Pöschl, U.: Fluorescent biological aerosol particle concentrations and size distributions measured in pristine tropical rainforest air during AMAZE-08, *Atmos. Chem. Phys.*, in preparation, 2012.
- Jabajihare, S. H., Perumalla, C. J., and Kendrick, W. B.: Autofluorescence of vesicles, arbuscules, and intercellular hyphae of a versicular-arbuscular fungus in leek (*Allium porrum*) roots, *Can. J. Bot.-Rev. Can. Bot.*, 62, 2665–2669, 1984.
- Jaenicke, R.: Abundance of cellular material and proteins in the atmosphere, *Science*, 308, 73, doi:10.1126/science.1106335, 2005.
- Jaenicke, R., Matthias-Maser, S., and Gruber, S.: Omnipresence of biological material in the atmosphere, *Environ. Chem.*, 4, 217–220, doi:10.1071/en07021, 2007.
- Jeys, T. H., Herzog, W. D., Hybl, J. D., Czerwinski, R. N., and Sanchez, A.: Advanced trigger development, *Linc. Lab. J.*, 17, 29–62, 2007.
- Jimenez, J. L., Canagaratna, M. R., Donahue, N. M., Prevot, A. S. H., Zhang, Q., Kroll, J. H., DeCarlo, P. F., Allan, J. D., Coe, H., Ng, N. L., Aiken, A. C., Docherty, K. S., Ulbrich, I. M., Grieshop, A. P., Robinson, A. L., Duplissy, J., Smith, J. D., Wilson, K. R., Lanz, V. A., Hueglin, C., Sun, Y. L., Tian, J., Laaksonen, A., Raatikainen, T., Rautiainen, J., Vaattovaara, P., Ehn, M., Kulmala, M., Tomlinson, J. M., Collins, D. R., Cubison, M. J., Dunlea, E. J., Huffman, J. A., Onasch, T. B., Alfarra, M. R., Williams, P. I., Bower, K., Kondo, Y., Schneider, J., Drewnick, F., Borrmann, S., Weimer, S., Demerjian, K., Salcedo, D., Cottrell, L., Griffin, R., Takami, A., Miyoshi, T., Hatakeyama, S., Shimojo, A., Sun, J. Y., Zhang, Y. M., Dzepina, K., Kimmel, J. R., Sueper, D., Jayne, J. T., Herndon, S. C., Trimborn, A. M., Williams, L. R., Wood, E. C., Middlebrook, A. M., Kolb, C. E., Baltensperger, U., and Worsnop, D. R.: Evolution of Organic Aerosols in the Atmosphere, *Science*, 326, 1525–1529, doi:10.1126/science.1180353, 2009.
- Johansson, L. and Liden, G.: A study of long-term effects on plasmid-containing *Escherichia coli* in carbon-limited chemostat using 2D-fluorescence spectrofluorimetry, *Biotechnol. Prog.*, 22, 1132–1139, doi:10.1021/bp060061m, 2006.
- Jones, A. M. and Harrison, R. M.: The effects of meteorological factors on atmospheric bioaerosol concentrations – a review, *Sci. Total Environ.*, 326, 151–180, doi:10.1016/j.scitotenv.2003.11.021, 2004.
- Kamboj, D. V., Goel, A. K., and Singh, L.: Biological warfare agents, *Def. Sci. J.*, 56, 495–506, 2006.
- Kayatz, P., Thumann, G., Luther, T. T., Jordan, J. F., Bartz-Schmidt, K. U., Esser, P. J., and Schraermeyer, U.: Oxidation causes melanin fluorescence, *Invest. Ophthalmol. Vis. Sci.*, 42, 241–246, 2001.
- Kaye, P. H., Barton, J. E., Hirst, E., and Clark, J. M.: Simultaneous light scattering and intrinsic fluorescence measurement for the classification of airborne particles, *Appl. Optics*, 39, 3738–3745, 2000.
- Kaye, P. H., Stanley, W. R., Hirst, E., Foot, E. V., Baxter, K. L., and Barrington, S. J.: Single particle multichannel bio-aerosol fluorescence sensor, *Opt. Express*, 13, 3583–3593, 2005.
- Keller, N. P., Turner, G., and Bennett, J. W.: Fungal secondary metabolism – From biochemistry to genomics, *Nat. Rev. Microbiol.*, 3, 937–947, doi:10.1038/nrmicro1286, 2005.
- Kepner, R. L. and Pratt, J. R.: Use of fluorochromes for direct enumeration of total bacteria in environmental-samples – Past and present, *Microbiol. Rev.*, 58, 603–615, 1994.
- Kieber, R. J., Whitehead, R. F., Reid, S. N., Willey, J. D., and Seaton, P. J.: Chromophoric dissolved organic matter (CDOM) in rainwater, southeastern North Carolina, USA, *J. Atmos. Chem.*, 54, 21–41, doi:10.1007/s10874-005-9008-4, 2006.
- Klapper, L., McKnight, D. M., Fulton, J. R., Blunt-Harris, E. L., Nevin, K. P., Lovley, D. R., and Hatcher, P. G.: Fulvic acid oxidation state detection using fluorescence spectroscopy, *Environ. Sci. Technol.*, 36, 3170–3175, doi:10.1021/es0109702, 2002.
- Klapper, M. H.: Independent distribution of amino-acid near neighbor pairs into polypeptides, *Biochem. Biophys. Res. Commun.*, 78, 1018–1024, 1977.
- Klingenberg, M. and Bucher, T.: Biological oxidations, *Annu. Rev. Biochem.*, 29, 669–708, 1960.
- Koenig, K. and Schneckeburger, H.: Laser-induced autofluorescence for medical diagnosis, *J. Fluoresc.*, 4, 17–40, doi:10.1007/bf01876650, 1994.
- Kopczynski, K., Kwasny, M., Mierczyk, Z., and Zawadzki, Z.: Laser induced fluorescence system for detection of biological agents: European project FABIOLA, *Proc. SPIE – The International Society for Optical Engineering*, 5954, 0501–0512, doi:10.1117/12.623013, 2005.
- Krivacsy, Z., Gelencser, A., Kiss, G., Meszaros, E., Molnar, A., Hoffer, A., Meszaros, T., Sarvari, Z., Temesi, D., Varga, B., Baltensperger, U., Nyeki, S., and Weingartner, E.: Study on the chemical character of water soluble organic compounds in fine atmospheric aerosol at the Jungfraujoch, *J. Atmos. Chem.*, 39, 235–259, 2001.
- Kumke, M. U., Löhmannsröben, H. G., and Roch, T.: Fluorescence spectroscopy of polynuclear aromatic compounds in environmental monitoring, *J. Fluoresc.*, 5, 139–152, doi:10.1007/bf00727531, 1995.
- Kunit, M. and Puxbaum, H.: Enzymatic determination of the cellulose content of atmospheric aerosols, *Atmos. Environ.*, 30, 1233–1236, 1996.
- Kunnil, J.: Identification Studies of Bacillus Spores Using Fluorescence Spectroscopy, Doctor of Philosophy, Physics and Astronomy, University of Canterbury, New Zealand, Christchurch, 192 pp., 2005.
- Lacey, J. and Dutkiewicz, J.: Bioaerosols and occupational lung-disease, *J. Aerosol Sci.*, 25, 1371–1404, 1994.

- Ladokhin, A. S.: Fluorescence spectroscopy in peptide and protein analysis, in: *Encyclopedia of analytical chemistry*, edited by: Meyers, R. A., John Wiley & Sons, New York, 5762–5779, 2000.
- Lakowicz, J. R.: *Principles of Fluorescence Spectroscopy*, Plenum publishers, New York, 1999.
- Lau, A. P. S., Lee, A. K. Y., Chan, C. K., and Fang, M.: Ergosterol as a biomarker for the quantification of the fungal biomass in atmospheric aerosols, *Atmos. Environ.*, 40, 249–259, doi:10.1016/j.atmosenv.2005.09.048, 2006.
- Leblanc, L. and Dufour, E.: Monitoring the identity of bacteria using their intrinsic fluorescence, *FEMS Microbiol. Lett.*, 211, 147–153, 2002.
- Lenardon, M. D., Munro, C. A., and Gow, N. A. R.: Chitin synthesis and fungal pathogenesis, *Curr. Opin. Microbiol.*, 13, 416–423, doi:10.1016/j.mib.2010.05.002, 2010.
- Lewitzka, F. and Niessner, R.: Application of time-resolved fluorescence spectroscopy on the analysis of PAH-coated aerosols, *Aerosol Sci. Tech.*, 23, 454–464, 1995.
- Li, B. and Lin, S. X.: Fluorescence-energy transfer in human estradiol 17 beta-dehydrogenase-NADPH complex and studies on the coenzyme binding, *Eur. J. Biochem.*, 235, 180–186, 1996.
- Li, J. K., Asali, E. C., and Humphrey, A. E.: Monitoring cell concentration and activity by multiple excitation fluorometry, *Biotechnol. Prog.*, 7, 21–27, 1991.
- Li, W. H., Sheng, G. P., Lu, R., Yu, H. Q., Li, Y. Y., and Harada, H.: Fluorescence spectral characteristics of the supernatants from an anaerobic hydrogen-producing bioreactor, *Appl. Microbiol. Biotechnol.*, 89, 217–224, doi:10.1007/s00253-010-2867-x, 2011.
- Li, Y., Dick, W. A., and Tuovinen, O. H.: Fluorescence microscopy for visualization of soil microorganisms - a review, *Biol. Fert. Soils*, 39, 301–311, doi:10.1007/s00374-004-0722-x, 2004.
- Liang, J., Wu, W. L., Liu, Z. H., Mei, Y. J., Cai, R. X., and Shen, P.: Study the oxidative injury of yeast cells by NADH autofluorescence, *Spectrosc. Acta Pt. A*, 67, 355–359, doi:10.1016/j.saa.2006.07.035, 2007.
- Lichtenthaler, H. K., Buschmann, C., Rinderle, U., and Schmuck, G.: Application of chlorophyll fluorescence in ecophysiology, *Radiat. Environ. Biophys.*, 25, 297–308, 1986.
- Lighthart, B. and Shaffer, B. T.: Airborne bacteria in the atmospheric surface-layer – Temporal distribution above a grass seed field, *Appl. Environ. Microbiol.*, 61, 1492–1496, 1995.
- Lim, D. V., Simpson, J. M., Kearns, E. A., and Kramer, M. F.: Current and developing technologies for monitoring agents of bioterrorism and biowarfare, *Clin. Microbiol. Rev.*, 18, 583–607, doi:10.1128/cmr.18.4.583-607.2005, 2005.
- Linskens, H. F. and Cresti, M.: Pollen-allergy as an ecological phenomenon: a review, *Plant Biosyst.*, 134, 341–352, 2000.
- Lohmann, U. and Feichter, J.: Global indirect aerosol effects: a review, *Atmos. Chem. Phys.*, 5, 715–737, doi:10.5194/acp-5-715-2005, 2005.
- Madelin, T. M.: Fungal aerosols: A review, *J. Aerosol Sci.*, 25, 1405–1412, 1994.
- Manninen, A., Putkiranta, M., Rostedt, A., Saarela, J., Laurila, T., Marjamäki, M., Keskinen, J., and Hernberg, R.: Instrumentation for measuring fluorescence cross sections from airborne micro-sized particles, *Appl. Optics*, 47, 110–115, 2008.
- Mantoura, R. F. C. and Llewellyn, C. A.: The rapid-determination of algal chlorophyll and carotenoid-pigments and their breakdown products in natural-waters by reverse-phase high-performance liquid-chromatography, *Anal. Chim. Acta*, 151, 297–314, 1983.
- Marose, S., Lindemann, C., and Scheper, T.: Two-dimensional fluorescence spectroscopy: A new tool for on-line bioprocess monitoring, *Biotechnol. Prog.*, 14, 63–74, 1998.
- Martell, A. E.: Vitamin-B6 catalyzed-reactions of alpha-amino and alpha-keto acids – Model systems, *Accounts Chem. Res.*, 22, 115–124, 1989.
- Matthias-Maser, S., Obolkin, V., Khodzer, T., and Jaenicke, R.: Seasonal variation of primary biological aerosol particles in the remote continental region of Lake Baikal/Siberia, *Atmos. Environ.*, 34, 3805–3811, doi:10.1016/s1352-2310(00)00139-4, 2000.
- McFeters, G. A., Yu, F. P. P., Pyle, B. H., and Stewart, P. S.: Physiological assessment of bacteria using fluorochromes, *J. Microbiol. Meth.*, 21, 1–13, 1995.
- McIntosh, A., Atshaves, B., Huang, H., Gallegos, A., Kier, A., and Schroeder, F.: Fluorescence Techniques Using Dehydroergosterol to Study Cholesterol Trafficking, *Lipids*, 43, 1185–1208, doi:10.1007/s11745-008-3194-1, 2008.
- Miano, T. M., Sposito, G., and Martin, J. P.: Fluorescence spectroscopy of humic substances, *Soil Sci. Soc. Am. J.*, 52, 1016–1019, 1988.
- Miao, H., Rubakhin, S. S., and Sweedler, J. V.: Analysis of serotonin release from single neuron soma using capillary electrophoresis and laser-induced fluorescence with a pulsed deep-UV NeCu laser, *Anal. Bioanal. Chem.*, 377, 1007–1013, doi:10.1007/s00216-003-2191-8, 2003.
- Michal, G.: *Biochemical pathways*, Spectrum Akademischer Verlag, Berlin, 1999.
- Moberg, L., Robertsson, G., and Karlberg, B.: Spectrofluorimetric determination of chlorophylls and pheopigments using parallel factor analysis, *Talanta*, 54, 161–170, 2001.
- Möhler, O., DeMott, P. J., Vali, G., and Levin, Z.: Microbiology and atmospheric processes: the role of biological particles in cloud physics, *Biogeosciences*, 4, 1059–1071, doi:10.5194/bg-4-1059-2007, 2007.
- Monks, P. S., Granier, C., Fuzzi, S., Stohl, A., Williams, M. L., Akimoto, H., Amann, M., Baklanov, A., Baltensperger, U., Bey, I., Blake, N., Blake, R. S., Carslaw, K., Cooper, O. R., Dentener, F., Fowler, D., Fragkou, E., Frost, G. J., Generoso, S., Ginoux, P., Grewe, V., Guenther, A., Hansson, H. C., Henne, S., Hjorth, J., Hofzumahaus, A., Huntrieser, H., Isaksen, I. S. A., Jenkin, M. E., Kaiser, J., Kanakidou, M., Klimont, Z., Kulmala, M., Laj, P., Lawrence, M. G., Lee, J. D., Liou, S. C., Maione, M., McFiggans, G., Metzger, A., Mieville, A., Moussiopoulos, N., Orlando, J. J., O'Dowd, C. D., Palmer, P. I., Parrish, D. D., Petzold, A., Platt, U., Pöschl, U., Prevot, A. S. H., Reeves, C. E., Reimann, S., Rudich, Y., Sellegri, K., Steinbrecher, R., Simpson, D., ten Brink, H., Theloke, J., van der Werf, G. R., Vautard, R., Vestreng, V., Vlachokostas, C., and von Glasow, R.: Atmospheric composition change – global and regional air quality, *Atmos. Environ.*, 43, 5268–5350, doi:10.1016/j.atmosenv.2009.08.021, 2009.
- Muller, C. L., Baker, A., Hutchinson, R., Fairchild, I. J., and Kidd, C.: Analysis of rainwater dissolved organic carbon compounds using fluorescence spectrophotometry, *Atmos. Environ.*,

- 42, 8036–8045, doi:10.1016/j.atmosenv.2008.06.042, 2008.
- Nielsen, T., Seitz, B., and Ramdahl, T.: Occurrence of nitro-PAH in the atmosphere in a rural area, *Atmos. Environ.*, 18, 2159–2165, 1984.
- Niessner, R. and Krupp, A.: Detection and chemical characterization of polycyclic aromatic hydrocarbon aerosols by means of laser-induced fluorescence, *Part. Part. Syst. Charact.*, 8, 23–28, 1991.
- Niklas, K. J.: The cell walls that bind the tree of life, *Bioscience*, 54, 831–841, 2004.
- Nisbet, A. D., Saundry, R. H., Moir, A. J. G., Fothergill, L. A., and Fothergill, J. E.: The complete amino-acid-sequence of hen ovalbumin, *Eur. J. Biochem.*, 115, 335–345, 1981.
- Nosanchuk, J. D. and Casadevall, A.: The contribution of melanin to microbial pathogenesis, *Cell Microbiol.*, 5, 203–223, 2003.
- O'Connor, D. J., Iacopino, D., Healy, D. A., O'Sullivan, D., and Sodeau, J. R.: The intrinsic fluorescence spectra of selected pollen and fungal spores, *Atmos. Environ.*, 45, 6451–6458, doi:10.1016/j.atmosenv.2011.07.044, 2011.
- Olmstead, J. A. and Gray, D. G.: Fluorescence emission from mechanical pulp sheets, *J. Photochem. Photobiol. A*, 73, 59–65, 1993.
- Olmstead, J. A. and Gray, D. G.: Fluorescence spectroscopy of cellulose, lignin and mechanical pulps: A review, *J. Pulp Pap. Sci.*, 23, J571–J581, 1997.
- Paidhungat, M., Setlow, B., Driks, A., and Setlow, P.: Characterization of spores of *Bacillus subtilis* which lack dipicolinic acid, *J. Bacteriol.*, 182, 5505–5512, 2000.
- Pan, Y. L., Pinnick, R. G., Hill, S. C., and Chang, R. K.: Particle-Fluorescence Spectrometer for Real-Time Single-Particle Measurements of Atmospheric Organic Carbon and Biological Aerosol, *Environ. Sci. Technol.*, 43, 429–434, doi:10.1021/es801544y, 2009.
- Pan, Y.-L., Hill, S. C., Pinnick, R. G., Huang, H., Bottiger, J. R., and Chang, R. K.: Fluorescence spectra of atmospheric aerosol particles measured using one or two excitation wavelengths: Comparison of classification schemes employing different emission and scattering results, *Opt. Express*, 18, 12436–12457, doi:10.1364/oe.18.012436, 2010.
- Pan, Y.-L., Hill, S. C., Pinnick, R. G., House, J. M., Flagan, R. C., and Chang, R. K.: Dual-excitation-wavelength fluorescence spectra and elastic scattering for differentiation of single airborne pollen and fungal particles, *Atmos. Environ.*, 45, 1555–1563, doi:10.1016/j.atmosenv.2010.12.042, 2011.
- Panne, U., Knoller, A., Kotzick, R., and Niessner, R.: On-line and in-situ detection of polycyclic aromatic hydrocarbons (PAH) on aerosols via thermodesorption and laser-induced fluorescence spectroscopy, *Fresen. J. Anal. Chem.*, 366, 408–414, 2000.
- Parker, E. P., Trahan, M. W., Wagner, J. S., Rosenthal, S. E., Whitten, W. B., Gieray, R. A., Reilly, P. T. A., Lazar, A. C., and Ramsey, J. M.: Detection and classification of individual airborne microparticles using laser ablation mass spectroscopy and multivariate analysis, *Field Anal. Chem. Technol.*, 4, 31–42, 2000.
- Penner, J. E.: Carbonaceous aerosols influencing atmospheric radiation: Black and organic carbon, *Medium: P; Size: 35 p.*, 1994.
- Permyakov, E. A.: Luminescent spectroscopy of proteins, CRC Press, Boca Raton, 1993.
- Petit, P. X., Gendron, M. C., Schrantz, N., Metivier, D., Kroemer, G., Maciorowska, Z., Sureau, F., and Koester, S.: Oxidation of pyridine nucleotides during Fas- and ceramide-induced apoptosis in Jurkat cells: correlation with changes in mitochondria, glutathione depletion, intracellular acidification and caspase 3 activation, *Biochem. J.*, 353, 357–367, 2001.
- Pinnick, R. G., Hill, S. C., Nachman, P., Pendleton, J. D., Fernandez, G. L., Mayo, M. W., and Bruno, J. G.: Fluorescence Particle Counter for Detecting Airborne Bacteria and Other Biological Particles, *Aerosol Sci. Tech.*, 23, 653–664, 1995.
- Pinnick, R. G., Hill, S. C., Pan, Y. L., and Chang, R. K.: Fluorescence spectra of atmospheric aerosol at Adelphi, Maryland, USA: measurement and classification of single particles containing organic carbon, *Atmos. Environ.*, 38, 1657–1672, doi:10.1016/j.atmosenv.2003.11.017, 2004.
- Pöhlker, C., Huffman, J. A., and Pöschl, U.: Autofluorescence of Bioaerosol Standards, in preparation, 2012.
- Pöschl, U.: Atmospheric aerosols: Composition, transformation, climate and health effects, *Angew. Chem.-Int. Edit.*, 44, 7520–7540, doi:10.1002/anie.200501122, 2005.
- Pöschl, U., Martin, S. T., Sinha, B., Chen, Q., Gunthe, S. S., Huffman, J. A., Borrmann, S., Farmer, D. K., Garland, R. M., Helas, G., Jimenez, J. L., King, S. M., Manzi, A., Mikhailov, E., Pauliquevis, T., Petters, M. D., Prenni, A. J., Roldin, P., Rose, D., Schneider, J., Su, H., Zorn, S. R., Artaxo, P., and Andreae, M. O.: Rainforest Aerosols as Biogenic Nuclei of Clouds and Precipitation in the Amazon, *Science*, 329, 1513–1516, doi:10.1126/science.1191056, 2010.
- Pons, M. N., Le Bonte, S., and Potier, O.: Spectral analysis and fingerprinting for biomedica characterisation, *J. Biotechnol.*, 113, 211–230, doi:10.1016/j.jbiotec.2004.03.028, 2004.
- Primmerman, C. A.: Detection of biological agents, *Linc. Lab. J.*, 12, 3–32, 2000.
- Ramanujam, N.: Fluorescence spectroscopy of neoplastic and non-neoplastic tissues, *Neoplasia*, 2, 89–117, 2000.
- Ramanujam, N.: Fluorescence Spectroscopy In Vivo, *Encyclopedia of Analytical Chemistry*, John Wiley & Sons, Ltd, 2006.
- Reisfeld, R., Gaft, M., Boulon, G., Panczer, C., and Jorgensen, C. K.: Laser-induced luminescence of rare-earth elements in natural fluor-apatites, *J. Lumines.*, 69, 343–353, 1996.
- Rembold, H. and Gyure, W. L.: Biochemistry of pteridines, *Angew. Chem.-Int. Edit. Engl.*, 11, 1061–1072, 1972.
- RichardsKortum, R. and Sevick Muraca, E.: Quantitative optical spectroscopy for tissue diagnosis, *Annu. Rev. Phys. Chem.*, 47, 555–606, 1996.
- Roberts, M. F. W.: Alkaloids: Biochemistry, Ecology, and Medicinal Applications, Plenum Press, New York, 1998.
- Rosenheim, O.: Note on the induced fluorescence of ergosterol, *Biochem. J.*, 21, 1335, 1927.
- Roshchina, V. V.: Autofluorescence of plant secreting cells as a biosensor and bioindicator reaction, *J. Fluoresc.*, 13, 403–420, 2003.
- Roshchina, V. V.: Allelochemicals as fluorescent markers, dyes and probes, *Allelopathy J.*, 16, 31–46, 2005.
- Roshchina, V. V.: Fluorescing world of plant secreting cells, Science Publishers, 2008.
- Roshchina, V. V. and Karnaukhov, V. N.: Changes in pollen autofluorescence induced by ozone, *Biologia Plantarum*, 42, 273–278, 1999.

- Roshchina, V. V. and Mel'nikova, E. V.: Pollen chemosensitivity to ozone and peroxides, *Russ. J. Plant Physiol.*, 48, 74–83, 2001.
- Roshchina, V. V., Melnikova, E. V., and Kovaleva, L. V.: Changes in fluorescence during development of the male gametophyte, *Russ. J. Plant Physiol.*, 44, 36–44, 1997.
- Roshchina, V. V., Yashin, V. A., and Kononov, A. V.: Autofluorescence of developing plant vegetative microspores studied by confocal microscopy and microspectrofluorimetry, *J. Fluoresc.*, 14, 745–750, 2004.
- Rozsak, D. B. and Colwell, R. R.: Survival strategies of bacteria in the natural-environment, *Microbiol. Rev.*, 51, 365–379, 1987.
- Russell, L. M., Maria, S. F., and Myneni, S. C. B.: Mapping organic coatings on atmospheric particles, *Geophys. Res. Lett.*, 29, 1779, doi:10.1029/2002gl014874, 2002.
- Sarasanandarajah, S., Kunnil, J., Bronk, B. V., and Reinisch, L.: Two-dimensional multiwavelength fluorescence spectra of dipicolinic acid and calcium dipicolinate, *Appl. Optics*, 44, 1182–1187, 2005.
- Schnell, R. C. and Vali, G.: Atmospheric Ice Nuclei from Decomposing Vegetation, *Nature*, 236, 163–165, 1972.
- Seaver, M., Eversole, J. D., Hardgrove, J. J., Cary, W. K., and Roselle, D. C.: Size and fluorescence measurements for field detection of biological aerosols, *Aerosol Sci. Tech.*, 30, 174–185, 1999.
- Setlow, B. and Setlow, P.: Levels of oxidized and reduced pyridine nucleotides in dormant spores and during growth, sporulation, and spores germination of bacillus megaterium, *J. Bacteriol.*, 129, 857–865, 1977.
- Siano, S. A. and Mutharasan, R.: NADH and flavin fluorescence responses of starved yeast cultures to substrate additions, *Biotechnol. Bioeng.*, 34, 660–670, 1989.
- Sierra, M. M. D., Donard, O. F. X., Lamotte, M., Belin, C., and Ewald, M.: Fluorescence spectroscopy of coastal and marine waters, *Mar. Chem.*, 47, 127–144, 1994.
- Sinski, J. F. and Exner, J.: Concentration dependence in the spectra of polycyclic aromatic hydrocarbon mixtures by front-surface fluorescence analysis, *Appl. Spectrosc.*, 61, 970–977, 2007.
- Sivaprakasam, V., Huston, A. L., Scotto, C., and Eversole, J. D.: Multiple UV wavelength excitation and fluorescence of bioaerosols, *Opt. Express*, 12, 4457–4466, 2004.
- Sivaprakasam, V., Pletcher, T., Tucker, J. E., Huston, A. L., McGinn, J., Keller, D., and Eversole, J. D.: Classification and selective collection of individual aerosol particles using laser-induced fluorescence, *Appl. Optics*, 48, B126–B136, 2009.
- Slieman, T. A. and Nicholson, W. L.: Role of dipicolinic acid in survival of *Bacillus subtilis* spores exposed to artificial and solar UV radiation, *Appl. Environ. Microbiol.*, 67, 1274–1279, 2001.
- Slowik, J. G., Cross, E. S., Han, J. H., Kolucki, J., Davidovits, P., Williams, L. R., Onasch, T. B., Jayne, J. T., Kolb, C. E., and Worsnop, D. R.: Measurements of morphology changes of fractal soot particles using coating and denuding experiments: Implications for optical absorption and atmospheric lifetime, *Aerosol Sci. Tech.*, 41, 734–750, doi:10.1080/02786820701432632, 2007.
- Snyder, A. P., Maswadeh, W. M., Tripathi, A., Eversole, J., Ho, J., and Spence, M.: Orthogonal analysis of mass and spectral based technologies for the field detection of bioaerosols, *Anal. Chim. Acta*, 513, 365–377, doi:10.1016/j.aca.2004.03.003, 2004.
- Spurny, K. R.: On the chemical-detection of bioaerosols, *J. Aerosol Sci.*, 25, 1533–1547, 1994.
- Stanley, W. R., Kaye, P. H., Foot, V. E., Barrington, S. J., Gallagher, M., and Gabey, A.: Continuous bioaerosol monitoring in a tropical environment using a UV fluorescence particle spectrometer, *Atmos. Sci. Lett.*, 12, 195–199, doi:10.1002/asl.310, 2011.
- Stewart, A. J. and Wetzel, R. G.: Fluorescence – absorbance ratios – a molecular-weight tracer of dissolved organic-matter, *Limnol. Oceanogr.*, 25, 559–564, 1980.
- Sun, J. M. and Ariya, P. A.: Atmospheric organic and bio-aerosols as cloud condensation nuclei (CCN): A review, *Atmos. Environ.*, 40, 795–820, doi:10.1016/j.atmosenv.2005.05.052, 2006.
- Taiz, L. and Zeiger, E.: *Plant Physiology*, Sinauer Associates, Incorporated, 2010.
- Teale, F. W. J. and Weber, G.: Ultraviolet fluorescence of the aromatic amino acids, *Biochem. J.*, 65, 476–482, 1957.
- Theis, N. and Lerchau, M.: The evolution of function in plant secondary metabolites, *Int. J. Plant Sci.*, 164, S93–S102, 2003.
- Thygesen, L. G., Rinnan, A., Barsberg, S., and Møller, J. K. S.: Stabilizing the PARAFAC decomposition of fluorescence spectra by insertion of zeros outside the data area, *Chemometr. Intell. Lab. Syst.*, 71, 97–106, doi:10.1016/j.chemolab.2003.12.012, 2004.
- Tsuchida, M., Miura, T., and Aibara, K.: Lipofuscin and lipofuscin-like substances, *Chem. Phys. Lipids*, 44, 297–325, 1987.
- Tyagi, A. and Penzkofer, A.: Fluorescence spectroscopic behaviour of folic acid, *Chem. Phys.*, 367, 83–92, doi:10.1016/j.chemphys.2009.10.026, 2010.
- Uchiyama, S., Nagai, S., and Maruyama, K.: Lumazine-like fluorescence in a mass of spores of the cellular slime mold, *Diclyostelium discoideum*, *J. Plant Res.*, 110, 383–386, 1997.
- van Wuijckhuijse, A. L., Stowers, M. A., Kleefsman, W. A., van Baar, B. L. M., Kientz, C. E., and Marijnissen, J. C. M.: Matrix-assisted laser desorption/ionisation aerosol time-of-flight mass spectrometry for the analysis of bioaerosols: development of a fast detector for airborne biological pathogens, *J. Aerosol Sci.*, 36, 677–687, doi:10.1016/j.jaerosci.2004.11.003, 2005.
- Vierheilig, H., Bockenhoff, A., Knoblauch, M., Juge, C., Van Bel, A. J. E., Grundler, F., Piche, Y., and Wyss, U.: In vivo observations of the arbuscular mycorrhizal fungus *Glomus mosseae* in roots by confocal laser scanning microscopy, *Mycol. Res.*, 103, 311–314, 1999.
- Vining, L. C.: Functions of secondary metabolites, *Annu. Rev. Microbiol.*, 44, 395–427, 1990.
- Vishwasrao, H. D., Heikal, A. A., Kasischke, K. A., and Webb, W. W.: Conformational dependence of intracellular NADH on metabolic state revealed by associated fluorescence anisotropy, *J. Biol. Chem.*, 280, 25119–25126, doi:10.1074/jbc.M502475200, 2005.
- Voet, D. and Voet, J. G.: *Biochemistry*, Bd. 1, J. Wiley & Sons, 2004.
- Wedborg, M., Persson, T., and Larsson, T.: On the distribution of UV-blue fluorescent organic matter in the Southern Ocean, *Deep-Sea Res. Pt. I*, 54, 1957–1971, doi:10.1016/j.dsr.2007.07.003, 2007.
- Welschmeyer, N. A.: Fluorometric analysis of chlorophyll a in the presence of chlorophyll b and pheopigments, *Limnol. Oceanogr.*, 39, 1985–1992, 1994.
- Wiermann, R. and Vieth, K.: Outer pollen wall, an important accumulation site for flavonoids, *Protoplasma*, 118, 230–233, 1983.

- Winiwarter, W., Bauer, H., Caseiro, A., and Puxbaum, H.: Quantifying emissions of primary biological aerosol particle mass in Europe, *Atmos. Environ.*, 43, 1403–1409, doi:10.1016/j.atmosenv.2008.01.037, 2009.
- Wlodarski, M., Kaliszewski, M., Kwasny, M., Kopczyński, K., Zawadzki, Z., Mierczyk, Z., Mlynczak, J., Trafny, E., and Szpakowska, M.: Fluorescence excitation-emission matrices of selected biological materials, in: *Optically Based Biological and Chemical Detection for Defence III*, edited by: Carrano, J. C. and Zukauskas, A., Proceedings of the Society of Photo-Optical Instrumentation Engineers – Spie, Spie-Int Soc Optical Engineering, Bellingham, U18–U29, 2006.
- Wos, M. and Pollard, P.: Sensitive and meaningful measures of bacterial metabolic activity using NADH fluorescence, *Water Res.*, 40, 2084–2092, doi:10.1016/j.watres.2006.03.020, 2006.
- Xu, Z., Wu, Y., Shen, F., Chen, Q., Tan, M., and Yao, M.: *Bioaerosol Science, Technology, and Engineering: Past, Present, and Future*, *Aerosol Sci. Tech.*, 45, 1337–1349, doi:10.1080/02786826.2011.593591, 2011.
- Yin, D. Z.: Biochemical basis of lipofuscin, ceroid, and age pigment-like fluorophores, *Free Radic. Biol. Med.*, 21, 871–888, 1996.
- Zepp, R. G., Sheldon, W. M., and Moran, M. A.: Dissolved organic fluorophores in southeastern US coastal waters: correction method for eliminating Rayleigh and Raman scattering peaks in excitation-emission matrices, *Mar. Chem.*, 89, 15–36, doi:10.1016/j.marchem.2004.02.006, 2004.
- Zipfel, W. R., Williams, R. M., Christie, R., Nikitin, A. Y., Hyman, B. T., and Webb, W. W.: Live tissue intrinsic emission microscopy using multiphoton-excited native fluorescence and second harmonic generation, *P. Natl. Acad. Sci. USA*, 100, 7075–7080, doi:10.1073/pnas.0832308100, 2003.

## Supporting Online Material

Autofluorescence of atmospheric bioaerosols –  
Fluorescent biomolecules and potential interferences

Christopher Pöhlker<sup>1</sup>, J. Alex Huffman<sup>1,2\*</sup>, Ulrich Pöschl<sup>1</sup>

<sup>1</sup>*Max Planck Institute for Chemistry, Biogeochemistry Department, P.O. Box 3060, D-55020 Mainz, Germany*

<sup>2</sup>*University of Denver, Department of Chemistry and Biochemistry, 2190 E. Illif, Denver, Colorado 80208, USA*

*\*Corresponding author: alex.huffman@du.edu*

**Keywords:** Autofluorescence, Bioaerosols, Excitation-Emission-Matrix, Fluorescence Spectroscopy, Fluorophores



EEM normalization:

The intensity of all raw EEMs of solid state samples shown in this paper have been normalized as described in Section 3.2. Figure S1 shows tails of transmitted light on the left and right side of the Rayleigh scattering bands (1<sup>st</sup> and 2<sup>nd</sup> order) due to imperfect monochromators. In particular, this effect was magnified by the instrument settings utilized in this study, because the excitation and emission slit widths were fixed at relatively large values of 10 nm each. This setting allows a higher quantity of light to pass the slits, which provides the advantage of increased sensitivity. However, it also decreases spectral resolution and increases the spurious background light as discussed. Superposition of these spurious light effects leads to the elevated background signal ('plateau') that can be observed between the 1<sup>st</sup> and 2<sup>nd</sup> order Rayleigh lines.

Fluorescence spectra of solid state, powder samples in this study were corrected for spurious background light, which was observed to be significantly stronger for white (non-absorbing) materials than for materials of other colors. A normalization factor (NF) has been calculated as a function of the emitted light intensity to the left of 1<sup>st</sup> order Rayleigh scattering within an EEM. This light, by definition, cannot be considered fluorescent, because the wavelength of emission would be shorter than the wavelength of excitation. The NF was calculated as the mean "emission" signal on a line parallel to the 1<sup>st</sup> order Rayleigh signal, but separated by 40 nm vertically ( $\Delta$ ) in the EEM (thus in excitation). A  $\Delta$  value of 40 nm was utilized because it was found to be a compromise between two factors. Allowing the  $\Delta$  value to decrease caused an increase in the noise of the normalization due to the fact that the NF line became increasingly close to the steeply increasing 1<sup>st</sup> order Rayleigh scattering signal. Allowing the  $\Delta$  value to increase reduced the magnitude of the normalization as a function of the decreasing intensity of the light leakage tail. A large  $\Delta$  value also chopped data from the right side of each normalized EEM (high emission values), caused by corresponding reduction in vertical range (excitation) in the plot. In Figure S1 the lines for NF-calculation are shown for kaolin, chitin and humic acid (Fig. S1a-c). In Figure S1d the profiles of these lines are shown highlighting that the intensity background light strongly varies with  $\lambda_{em}$ . The highest intensities (e.g. for kaolin) were observed between 375 and 500 nm. Moreover NF show the highest values for white and highly reflecting materials (i.e.  $NF_{kaolin} = 189$ , white powder) and significantly lower values for darker and less reflecting materials (i.e.  $NF_{humic\ acid} = 29$ , dark brown powder).

Due to the wavelength dependence of the spurious light intensity along the normalization line attempts to normalize the EEM matrix based on individual excitation (horizontally) or emission (vertically) wavelengths, respectively, were performed. Two major problems were produced by this procedure, however. (I) Significant qualitative changes are reflected into the EEM by the peaking intensity of the normalization line. It has been found that these changes thus influence the characteristic fluorescence pattern in the EEMs ('shadowing effect'). (II). Moreover a certain area of the EEM cannot be normalized because the normalization line is accessible in vertical and horizontal direction only for a certain wavelength range. Accordingly for horizontal normalization the lower excitation wavelengths and for vertical normalization the upper emission wavelengths are chopped off.

For comparison with normalized EEMs a collection of non-normalized raw EEMs can be found in Figure S4 and S5.

**Figure S1.** Conceptual illustration of normalization for (a) kaolin, (b) chitin and (c) humic acid. Colored normalization lines for calculation of NF are shown in (d) for comparison.

**Figure S2.** Additional EEM contour profiles for selected pure biological fluorophores in solid, suspended or solvated state. Color intensity scale has been adjusted to intensity of individual components. All EEMs are normalized as discussed in text (Section 3.2). Normalization factor (NF) is reported for each solid-state sample. Lower NF indicates higher fluorescence intensity.

**Figure S3.** Additional EEM contour profiles for selected potential interferences in solid or solvated state. Intensity color scale has been adjusted to intensity of individual components. All EEMs are normalized as discussed in text (Section 3.2). Normalization factor (NF) is reported for each solid-state sample.

**Figure S4.** Raw EEM contour profiles for selected pure biological fluorophores in solid, suspended or solvated state. Intensity color scale has been adjusted to intensity of individual components.

**Figure S5.** Raw EEM contour profiles for selected potential interferences in solid, suspended or solved state. Intensity color scale has been adjusted to intensity of individual components.

**Figure S6.** Normalized fluorescence emission spectra of biofluorophores and potential interferences for selected excitation wavelanghts  $\lambda_{\text{ex}}$ ; (a) Emission spectra of biological fluorophores at  $\lambda_{\text{ex}} = 280$  nm; (b) Emission spectra of biological fluorophores at  $\lambda_{\text{ex}} = 355$  nm; (c) Emission spectra of biological fluorophores at  $\lambda_{\text{ex}} = 405$  nm; (d) Emission spectra of potential interferences at  $\lambda_{\text{ex}} = 280$  nm; (e) Emission spectra of potential interferences at  $\lambda_{\text{ex}} = 355$  nm; (f) Emission spectra of potential interferences at  $\lambda_{\text{ex}} = 405$  nm. Dashed lines indicate samples in dry state, solid lines indicate samples in solution. Spectra were scaled in some cases to fit on same y-axis.

**Figure S7.** Raw fluorescence emission spectra of biofluorophores and potential interferences for selected excitation wavelanghts  $\lambda_{\text{ex}}$ ; (a) Emission spectra of biological fluorophores at  $\lambda_{\text{ex}} = 280$  nm; (b) Emission spectra of biological fluorophores at  $\lambda_{\text{ex}} = 355$  nm; (c) Emission spectra of potential interferences at  $\lambda_{\text{ex}} = 280$  nm; (d) Emission spectra of potential interferences at  $\lambda_{\text{ex}} = 355$  nm. Dashed lines indicate samples in dry state, solid lines indicate samples in solution.

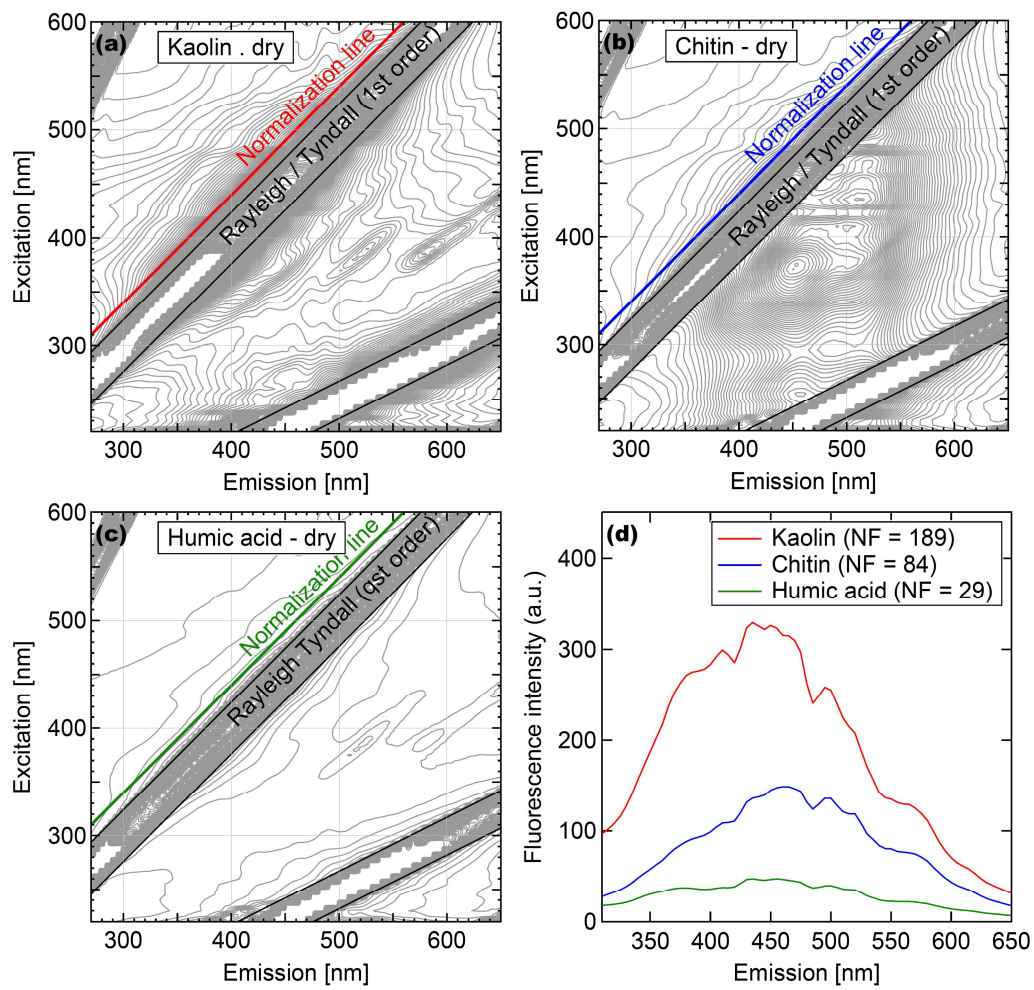


**Figure 1**

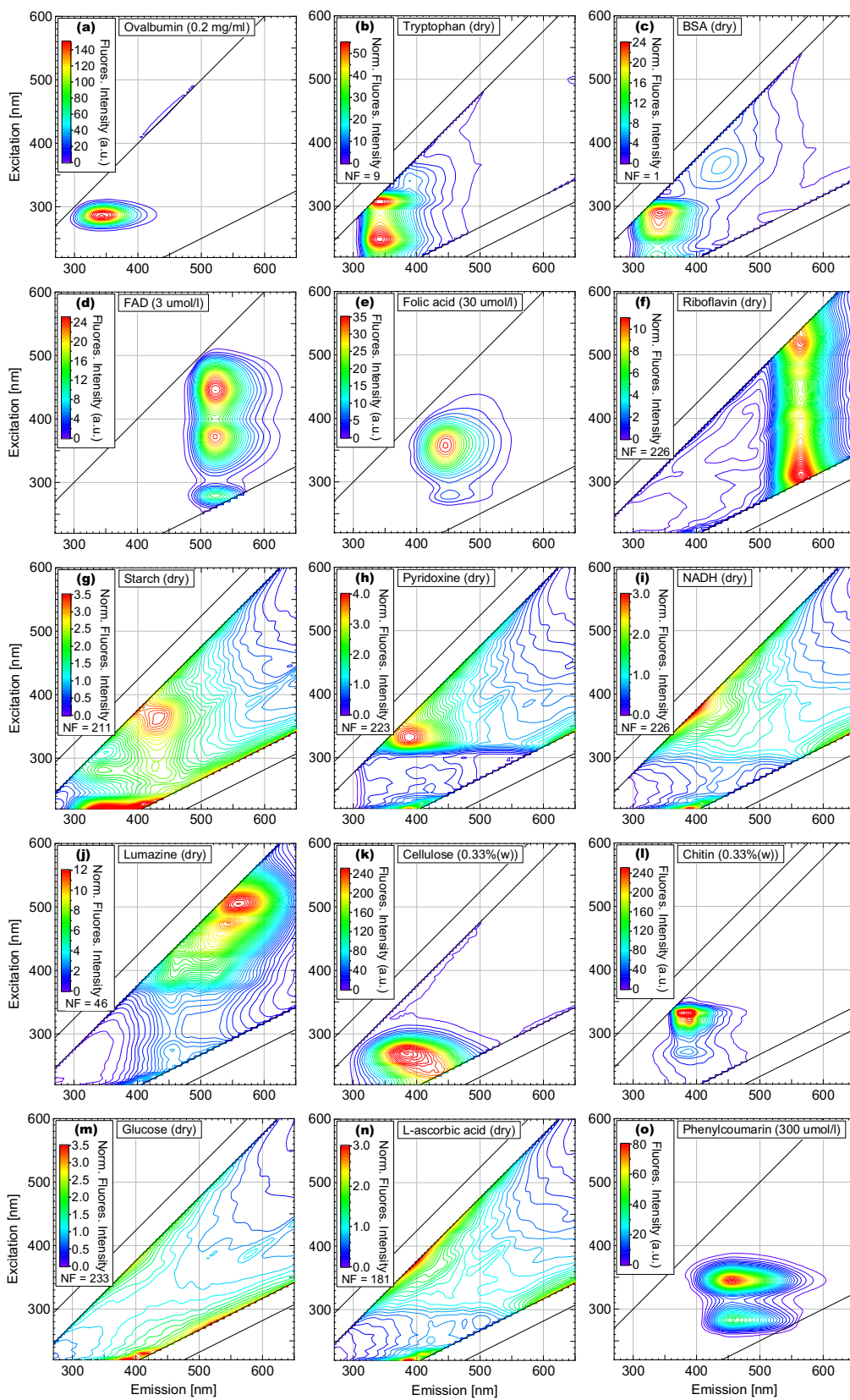
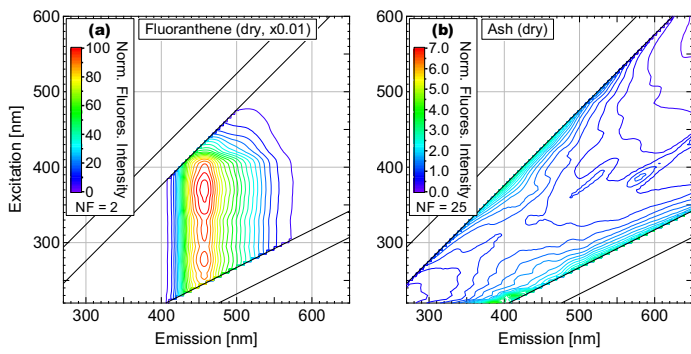
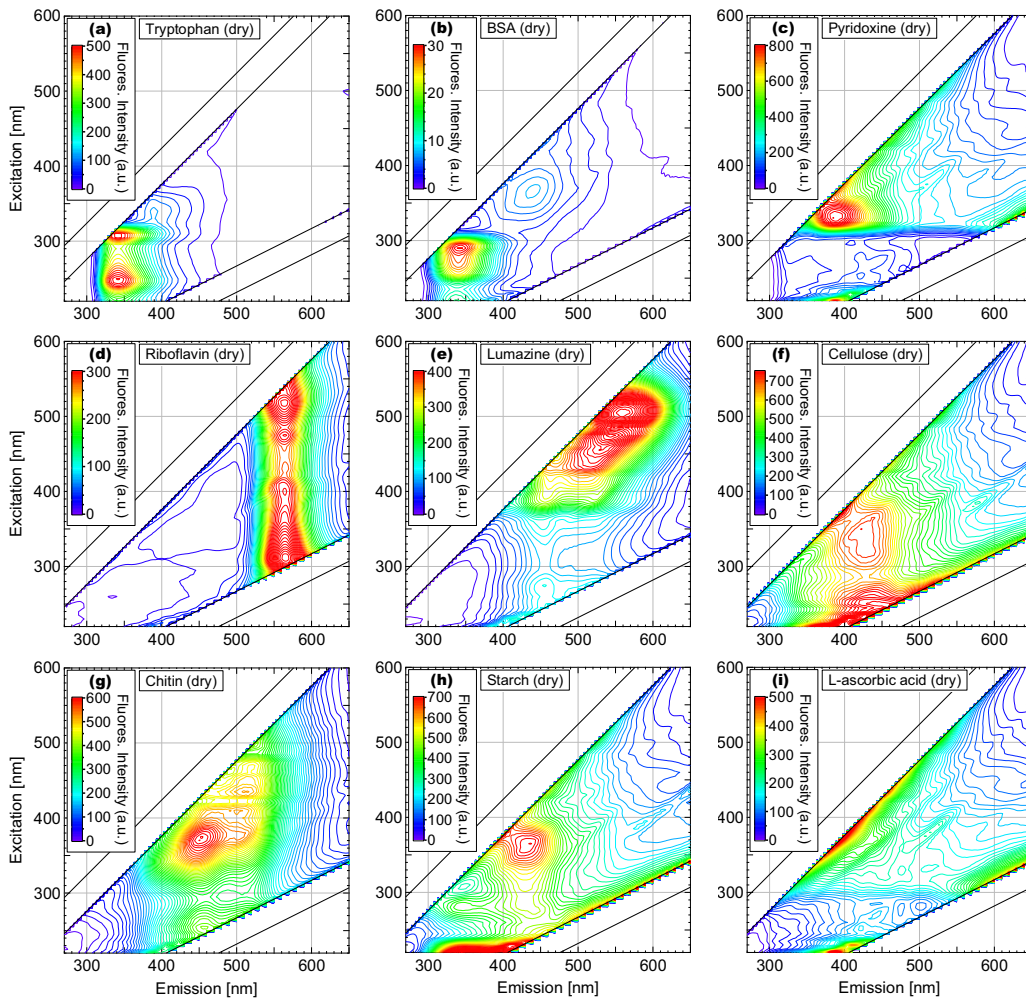


Figure S2.



**Figure S3.**



**Figure S4.**

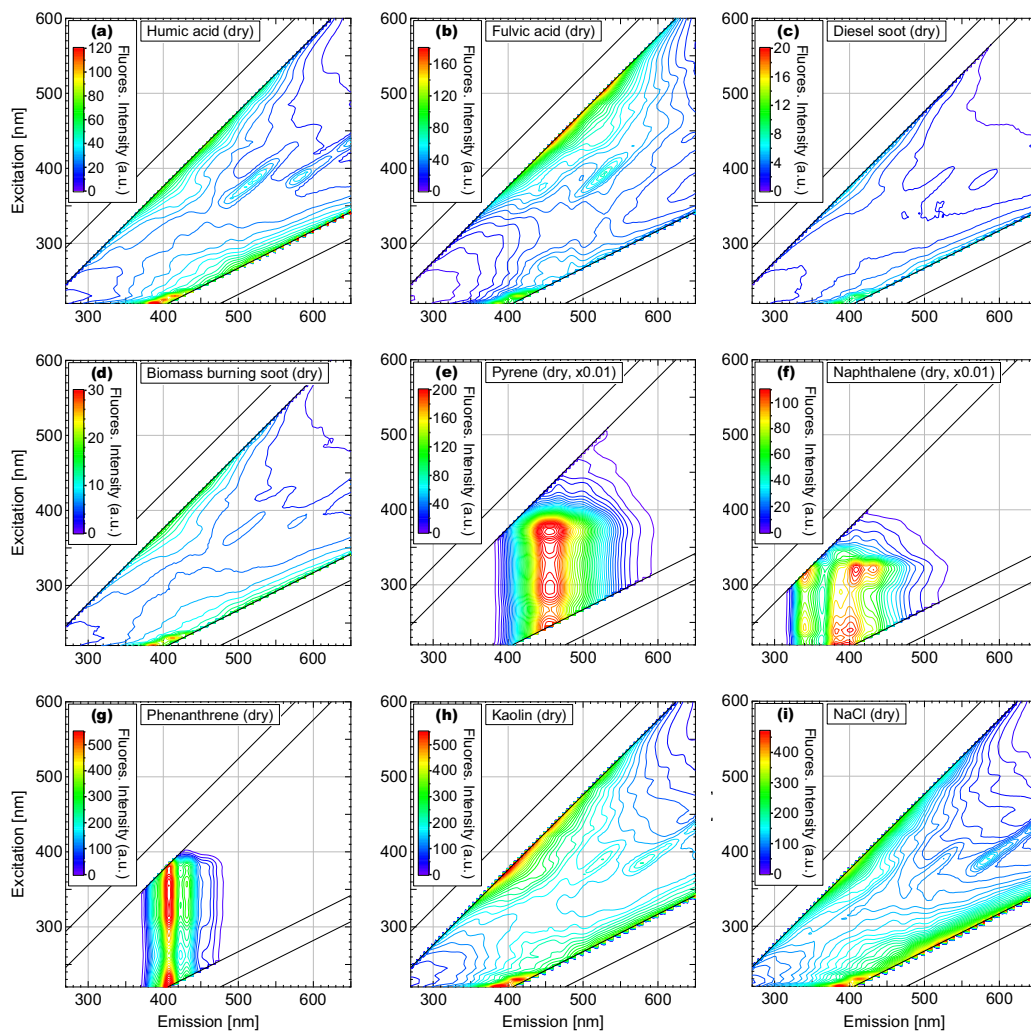


**Figure S5.**

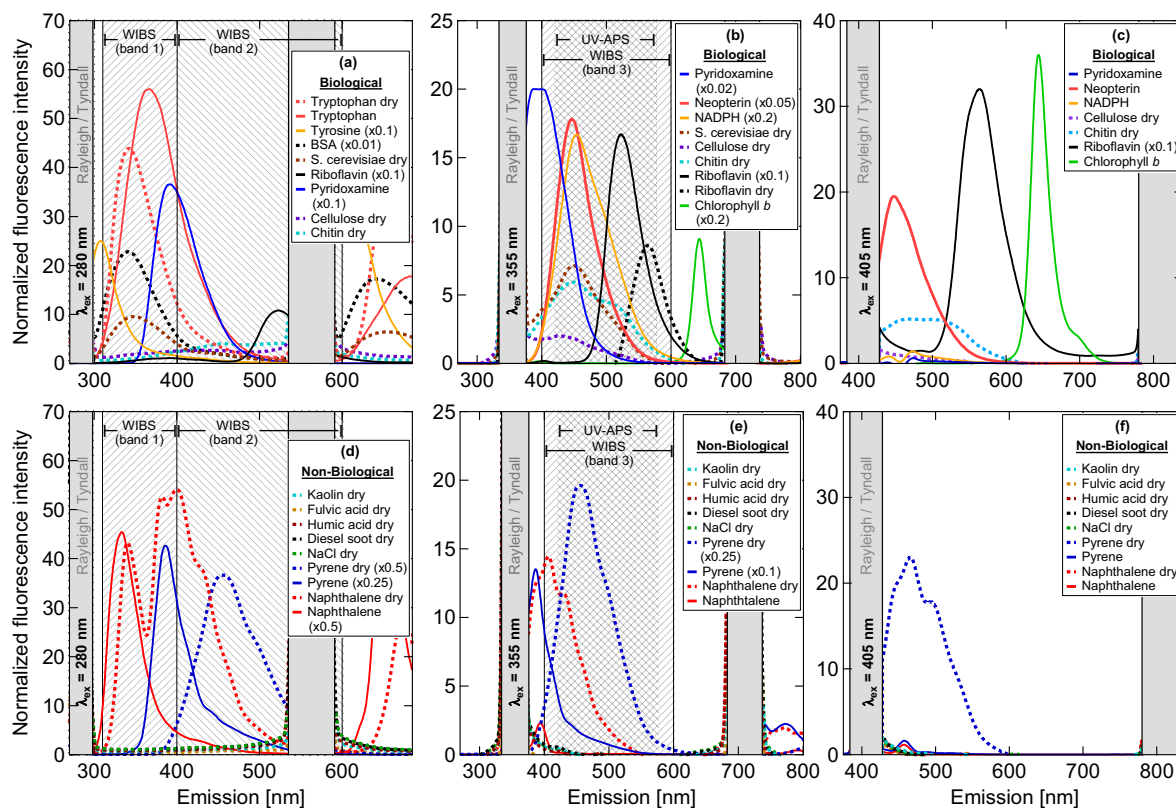


Figure S6.

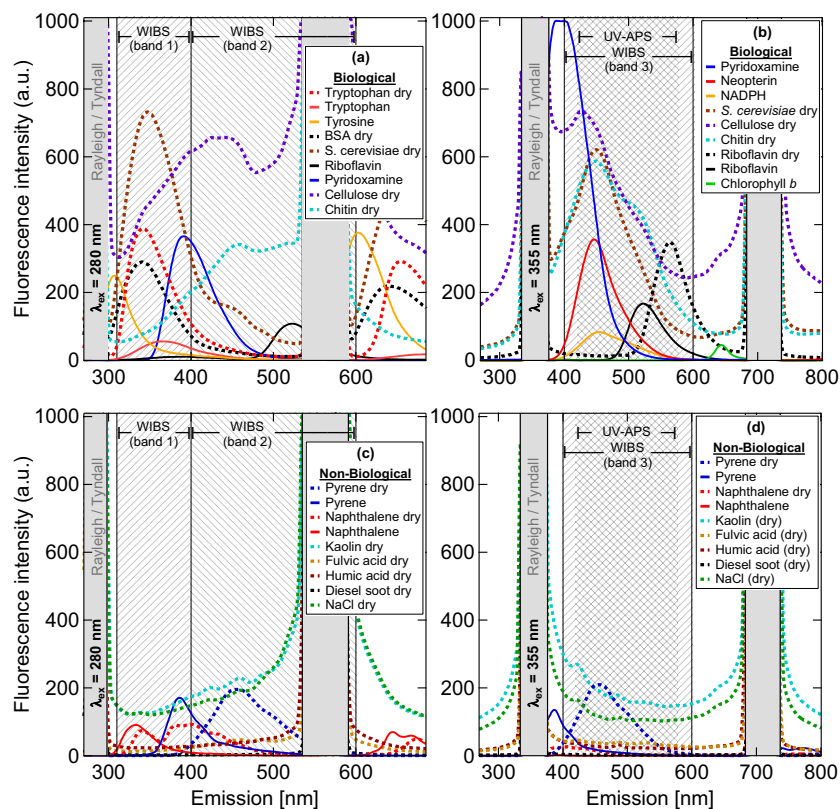


Figure S7.



**B2. Pöhlker et al., to be submitted**

**Autofluorescence of atmospheric bioaerosols –  
the spectral fingerprint and taxonomic trends of native pollen**

Christopher Pöhlker<sup>1</sup>, J. Alex Huffman<sup>2</sup>, Jan-David Förster<sup>1</sup>, and Ulrich Pöschl<sup>1</sup>

*1 Max Planck Institute for Chemistry, Biogeochemistry Department, Mainz, Germany*

*2 University of Denver, Department of Chemistry and Biochemistry, Denver, Colorado, USA*

**to be submitted**



# **Autofluorescence of atmospheric bioaerosols – the spectral fingerprint and taxonomic trends of native pollen**

Christopher Pöhlker<sup>1\*</sup>, J. Alex Huffman<sup>2\*</sup>, Jan-David Förster<sup>1</sup>, and Ulrich Pöschl<sup>1</sup>

<sup>1</sup>*Max Planck Institute for Chemistry, Biogeochemistry Department, P.O. Box 3060, D-55020 Mainz, Germany*

<sup>2</sup>*University of Denver, Department of Chemistry and Biochemistry, 2190 E. Illif, Denver, Colorado 80208, USA*

*\*Corresponding authors: alex.huffman@du.edu, c.pohlker@mpic.de*

to be submitted to Atmospheric Measurement Techniques Discussion

Keywords: Autofluorescence, bioaerosols, pollen, excitation-emission-matrix, fluorescence spectroscopy, fluorescence microscopy

## Abstract

Primary biological aerosol particles (PBAP) are important actors in atmospheric cycling, climate, and public health. Pollen is a major fraction of PBAP and has received increasing attention due to its high allergenic potential and the associated severe impacts on personal life quality and economy. Recently, autofluorescence-based techniques have proven to be valuable tools for *in situ* and real-time quantification and classification of PBAP. First studies suggest that the autofluorescence of pollen may be sufficiently selective to be utilized for an automated and real-time monitoring of pollen in ambient air. However, the degree of selectivity autofluorescence can provide is still in question and actively debated.

This study addresses the origin, properties, and selectivity of native pollen autofluorescence. The term *native* denotes undamaged and chemically untreated samples from fresh collection and commercial sources. The study provides fluorescence microscopy and spectroscopy measurements along with a systematic synthesis of related literature. We show that native and dry pollen reveals characteristic and reproducible autofluorescence signatures which are shaped by cell wall associated fluorophores, such as phenolic compounds and carotenoid pigments. In addition, fluorescence signals from proteins and chlorophyll *a* were observed occasionally. The abundance and intensity of the individual fluorescence signals show certain taxonomic trends. Principal component analysis was used to explore the discrimination potential of pollen autofluorescence and revealed a differentiation of pollen on family level. We suggest that the results reported here can support the development and application of autofluorescence-based detectors for a specific monitoring of allergenic pollen in the atmosphere. In general, our results help to explore the levels of selectivity that autofluorescence-based techniques can provide in PBAP analysis.

## 1. Introduction

### 1.1 Primary biological aerosol particles and atmospheric relevance

Primary biological aerosol particles (PBAP), also called bioaerosols, consist of a complex mixture of small biogenic particles, which are directly released from the biosphere into the atmosphere (Després et al., 2012). The major constituents of PBAP are microorganisms (e.g. bacteria and algae), reproductive units (e.g. pollen, fungal and bacterial spores), as well as fragments and excretions of various organisms (e.g. plant debris and bacterial vesicles) spanning a wide size range from a few nanometers to hundreds of micrometers (e.g. Kuehn and Kesty, 2005; Elbert et al., 2007; Burrows et al., 2009). Bioaerosols are globally ubiquitous and can dominate the coarse aerosol burden in certain ecosystems (e.g. Pöschl et al., 2010). PBAP have received increased attention in atmospheric science due to their impact on atmospheric chemistry and physics (Pöschl, 2005; Möhler et al., 2007), their important role in biogeochemical (Gorbushina and Broughton, 2009; Mahowald et al., 2011) and hydrological cycling (Morris et al., 2008; Huffman et al., 2013; Prenni et al., 2013), as well as their influence on public and agricultural health (D'Amato, 2000; Bernstein et al., 2004).

Pollen is the male gametophyte in the life-cycle of sexually reproducing plants and thus plays a crucial role in plant reproduction and ecology (Nepi and Franchi, 2000; Taiz and Zeiger, 2010). Pollen development in the plant stamen, its maturation and release as well as pollen-stigma recognition and pollen tube growth represent a highly specialized developmental process (e.g. Bedinger et al., 1994; Pacini, 2000; Boavida et al., 2005). Plants rely on either abiotic (i.e. wind-driven, called *anemophilous*) or biotic (i.e. insect mediated, called *entomophilous*) pollination methods (Sofiev et al., 2009). Pollen which are dispersed *anemophilously* are “optimized” for atmospheric transport (i.e. small physical and aerodynamic grain size, low density e.g. due to air bladders, lacking sticky coating) and account for ~10 % of all pollen species. *Anemophilous* pollen (range 10–100  $\mu\text{m}$ , average 20–30  $\mu\text{m}$ ) mark the upper size limit of airborne biological material with typical number concentrations around  $\sim 10\text{ m}^{-3}$  in ambient air (Wilson et al., 1973; Sofiev et al., 2006; 2009). Though generally less abundant in number than other classes of atmospheric bioaerosols, such as fungal spores at  $\sim 10^3\text{--}10^4\text{ m}^{-3}$  (Fröhlich-Nowoisky et al., 2009) or bacteria at  $\sim 10^4\text{--}10^5\text{ m}^{-3}$  (Burrows et al., 2009), pollen concentrations can increase to  $10^3\text{ m}^{-3}$  during strong pollination events (Siljamo et al., 2008). The number concentration of small PBAP could be underestimated in some cases, due to the fact that pollen can swell and burst after taking up water, releasing  $10^2\text{--}10^3$  particles (Taylor et al., 2007). Despite their relatively large physical diameter and high sedimentation velocities, intact pollen grains frequently undergo long distance dispersal (up to  $\sim 10^3$  km) (e.g. Kellogg and Griffin, 2006; Sofiev et al., 2006; Kuparinen et al., 2009), and thus may impact the biology of the destination and atmospheric properties *en route*. Thus, potential changes in pollination patterns due to climate change are discussed as a major uncertainty regarding biodiversity and ecosystem stability (Tylianakis et al., 2008; Zhang et al., 2013).

During the last few decades, pollen have received increased attention due to their extreme allergenicity and severe impacts on human health (e.g. Franze et al., 2005; Reid and Gamble, 2009; Sofiev et al., 2009). Between 10 and 25 % of the European population is affected by seasonal aller-

genic rhinitis causing substantial impact to personal life quality and to national economies as a result of lost work time (Traidl-Hoffmann et al., 2003; Scharring et al., 2006; Diethart et al., 2007). Therefore, substantial technical, financial and scientific effort has been invested in developing reliable aeroallergen monitoring and forecasting systems (e.g. Kalman et al., 1997; Ranzato et al., 2007; Scheifinger et al., 2013). However, quantification and identification of pollen is a demanding task due to highly diverse and variable pollen concentrations in the atmosphere, as well as influence of environmental conditions (e.g. relative humidity) and air pollutants (e.g. ozone and nitrogen oxides) (e.g. Franze et al., 2005; Shiraiwa et al., 2012). In particular, the role of small and respirable allergenic entities - so called *daughter allergens* or *paucimicronic particles* - which are released from the pollen surface and/or from the cytosol upon pollen grain bursting is poorly understood (e.g. D'Amato, 2000; Taylor et al., 2007; Wang et al., 2012). Furthermore, observations suggest that the atmospheric abundances of intact pollen and allergenic submicron particles, after pollen burst, are frequently “decoupled”, thus complicating efforts to develop a coherent allergen monitoring strategy. This suggests that a combination of direct-counting and immunodetection techniques may be necessary to adequately predict airborne allergen levels (Razmovski et al., 2000).

In addition to health related effects, pollen may impact atmospheric cycling and cloud microphysics (Möhler et al., 2007; Prenni et al., 2009; Hoose and Möhler, 2012). Pope (2010) showed that pollen can act as efficient cloud condensation nuclei (CCN), however, their low atmospheric number concentration prevents them from being important on a global scale. In contrast, many studies have reported the high ice nucleation activity (INA) of various pollen species and highlight their potential importance for mixed-phase clouds in biologically-influenced environments (Dingle, 1966; Diehl et al., 2001; 2002; von Blohn et al., 2005; Pummer et al., 2012). Although pollen are assumed to account only for a small fraction of IN on a global scale, their local and regional impact on cloud micro-physics could be substantial (Hoose et al., 2010).

## 1.2 Autofluorescence in bioaerosol detection

The term *autofluorescence*, or *intrinsic* fluorescence, denotes fluorescent light emission from a material based on the presence of fluorophores, for example cell constituents such as proteins and co-enzymes (Pöhlker et al., 2012; Andrade-Eiroa et al., 2013). The term is to be distinguished from *extrinsic* fluorescence achieved through the use of fluorescent stains applied to otherwise non-fluorescent material, such as biological cells allowed to interact with fluorescent dyes (e.g. Hawe et al., 2008). Among a large variety of techniques for the investigation of atmospheric PBAP, autofluorescence-based instruments have received increasing attention in the last few decades (e.g. Ho, 2002; Kaye et al., 2005; Hill et al., 2009; Sivaprakasam et al., 2009; Bundke et al., 2010). Such instruments utilize the emission of laser/light induced fluorescence (LIF) from biological material, providing a quantitative, non-destructive, and *in situ* detection of atmospheric biological particles in real-time. Thus, LIF instruments overcome certain drawbacks in traditional PBAP analysis, such as high labor cost, low time resolution and lack of quantitative information (Burrows et al., 2009).

The application of LIF to bioaerosol detection relies on the basic assumption that the intrinsic fluorescence within the measured spectral range of biological material exceeds that of potentially

interfering non-biological matter. This may be a valid assumption in many cases, suggesting that LIF techniques can, to a large degree, identify many types of biological aerosol particles on top of a complex and variable mixture of other atmospheric aerosol types. However, the exact relationship between the fraction of detected fluorescent biological aerosol particles (FBAP) and the fraction of all PBAP remains unclear and is surely dependent on specific instrument parameters and the sampled aerosol types. One reason is, that the fluorescence properties of biological and non-biological materials are not separated by a clear offset, but rather show overlapping properties (Hill et al., 2009; Huffman et al., 2012). Biological particles exhibiting weak fluorescence will not be counted by LIF instrumentation (Huffman et al., 2012; Pöhlker et al., 2012). As a further complication, small particles are prone to escape LIF detection because fluorescence intensity, as a function of fluorophore abundance in the cell, depends strongly on particles size (e.g. Sivaprakasam et al., 2004; Healy et al., 2012). Thus, it has been suggested that FBAP number is, in many cases, a lower limit of PBAP number (Huffman et al., 2010), but further work is needed to explore and quantify this relationship. It is also expected, for example, that certain non-biological aerosols could show elevated fluorescence (e.g. polycyclic aromatic hydrocarbons, PAH) and would thus represent false-positive counts. The concentration of PAH is expected to be low at supermicron particle sizes and would not contribute significantly to fluorescent particle number. Certain types of mineral dust and humic-like substances (HULIS) could also be detected as fluorescent, and this will undoubtedly confound FBAP interpretation. Comparing FBAP size distributions from a commercially available bioaerosol LIF instrument with contemporaneous filter samples analyzed via microscopy, Huffman et al. (2012) concluded that the LIF instrument was reliably able to provide lower-limit values of PBAP in a pristine rainforest location, but that more work was necessary to apply the same conclusions more broadly.

In the context of ambient bioaerosol detection, three major fields of LIF application can be distinguished: (I) the detection of biological warfare agents (BWA), (II) the analysis of PBAP in atmospheric science, and (III) the selective online monitoring of aeroallergens. (I) The development of LIF instruments for BWA detection has mainly been conducted by military research facilities. Their aim is to develop early warning systems for BWA treats, which requires a quick, reliable recognition of potentially harmful organisms (e.g. Jeys et al., 2007). (II) Commercialization of LIF instruments has triggered their application in the atmospheric science community for field-based PBAP analysis. Here, LIF is utilized to explore the concentration, composition, temporal and spatial variability as well as characteristic size and emission patterns of PBAP in different environments. A growing number of studies has been published which provide new and important insights into the PBAP cycling in the ambient atmosphere (e.g. Gabey et al., 2010; Huffman et al., 2010; Pöschl et al., 2010; Gabey, 2011; Huffman et al., 2012; Toprak and Schnaiter, 2013). Currently, applications in atmospheric science are designed primarily to quantify the total PBAP burden rather than to differentiate individual classes or species. (III) The development of a reliable monitoring infrastructure for major aeroallergens, such as pollen and molds, is a concern of high medical and societal interest (e.g. Scharring et al., 2006). LIF techniques feature real time detection capability

and certain taxonomical selectivity. Therefore promising efforts have begun to utilize LIF techniques for pollen monitoring (Ronneberger et al., 2002; Mitsumoto et al., 2009; 2010).

The quality of the discrimination ability between biological and non-biological aerosol particles is strongly depended on the spectral design of the LIF bioaerosol detector (i.e. excitation wavelengths and emission detection bands). Thus, the application of LIF for bioaerosol quantification and classification requires a sound knowledge of the fluorescence properties of the target bioaerosol particles. Accordingly, a number of studies have been conducted in the laboratory to characterize the LIF detection process and to understand it on a molecular level. One strategy utilizes laboratory-generated and well defined standard bioaerosols to analyze the corresponding response of online LIF instruments (Agranovski et al., 2003; Kanaani et al., 2008). Such experiments provide important information about the sensitivity and selectivity of instruments and their optical configurations. Another strategy uses offline techniques to measure and characterize the general autofluorescence signature of selected bioaerosol types. In some studies fluorescence microscopy is used to understand general fluorescence patterns and fluorophore locations in bioaerosol proxies (e.g. Roshchina et al., 2004; Herbrich et al., 2012). Other studies have applied fluorescence spectroscopy to understand characteristic emission signatures (e.g. O'Connor et al., 2011). Particularly, excitation-emission-matrices (EEMs) can be a useful tool for a systematic characterization of steady-state autofluorescence signatures (Satterwhite, 1990; Wlodarski et al., 2006; Hill et al., 2009; Mularczyk-Oliwa et al., 2012; Andrade-Eiroa et al., 2013). They can be used as “roadmaps” to identify spectral regions with high fluorescence levels, good signal-to-noise ratios and high degrees of selectivity (Pan et al., 2007).

### **1.3 Scope and aim of this study**

This paper follows our recent study on bioaerosol autofluorescence and therefore the studies can be regarded as part I (Pöhlker et al., 2012) and part II (this study). Part I provides a detailed introduction into the field of autofluorescence for PBAP detection and analysis. It addresses the question of whether the complex autofluorescence signals from bioaerosols can be traced back to individual biofluorophores on a molecular level. Therefore, part I provides a systematic summary of literature knowledge on (bio)fluorophores and a fluorescence spectroscopic characterization of the most important fluorophores in PBAP and non-biological interferences. Part I operates on the simple level of individual and pure biofluorophores and uses EEMs as an appropriate offline tool. Metrics, such as spectral properties, intensity and fluorophore abundance in PBAP, are utilized to explore bioaerosols autofluorescence on a molecular basis.

This part II study operates with the concepts introduced in part I and is motivated by the same scientific questions. However, here we extend the analytical scope from pure fluorescent molecules to whole biological particles, thus adding a layer of complexity. As outlined in the introduction, atmospheric PBAP is a very diverse mixture of suspended biological material. Ultimately, it is an open question of what type of information autofluorescence techniques may provide in atmospheric PBAP analysis. The present study aims to help to reduce the uncertainty associated with LIF applications in PBAP analysis, by means of a systematic analysis of standard biological particles. Here,



we focus on pollen as an adequate bioaerosol type. We suggest that this systematic investigation (i) gives a clear and general picture on the autofluorescence properties of native pollen and (ii) illustrates, by means of *one* standard particle type, how offline fluorescence techniques can support the application of LIF in ambient air. Beyond pollen, other major PBAP types, such as fungal spores and bacteria, still await a similar characterization in follow-up studies.

The choice of pollen is motivated by two main reasons. First, from an experimental point of view, we found that pollen represent ideal test particles because of their strong and diverse fluorescence signatures. Moreover, the large grain size supports microscopic analysis and allows the resolution of cellular details and autofluorescent “fine structure”. Therefore, within this first explorative study, pollen is appropriate to illustrate the scope and limits of the techniques. The second reason is, that pollen represents atmospheric particles of high relevance, particularly due to its high allergenic potential with severe social and economic impacts. Therefore, a reliable, selective, and automated pollen monitoring infrastructure which can be operated in real-time is highly desirable, but technically not yet practicable. Autofluorescence-based techniques have proven to be highly valuable tools for the analysis of atmospheric bioaerosols. Thus, autofluorescence is regarded as a promising candidate for a selective *in situ* monitoring of allergenic pollen in the air. Here, we aim to contribute to this discussion by systematically exploring the autofluorescence properties of pollen and to assess their applicability for ambient measurements.

## 2. Materials and methods

### 2.1 Chemicals and materials

Most pollen samples were purchased from commercial vendors: Allergon AB (Ängelholm, Sweden), Sigma Aldrich (St. Louis, MO, USA), Thermo Scientific (Waltham, MA, USA) and Polyscience (Niles, IL, USA) (see Table 1 for detailed information). On inquiry, the providers assured that their marketed standard pollen samples can be regarded as *native* which means that no chemical (e.g. dewaxing) or comparably harsh treatment was applied after harvest and that the pollen were stored under cool and dry conditions<sup>1</sup>. The purity of the purchased pollen samples was carefully checked by microscopy. In addition to standard pollen from commercial providers, various further samples were collected freshly in a local park in Mainz, Germany, during spring pollination season – three of these samples are included in this study for comparison (see Table 1). In the course of the manuscript, the term *native* pollen is used for both, freshly harvested and commercially obtained samples, which were collected without any post-processing, except sieving. All other chemicals were purchased from Sigma Aldrich and Merck (Darmstadt, Germany) and used as delivered.

The consistency of the pollen fluorescence properties across different sources was carefully evaluated. Two pollen species (*B. papyrifera* and *A. artemisiifolia*) were each obtained from two different providers, and EEMs were shown to be identical, irrespective of commercial source (Fig. S1). Moreover, fresh and purchased pollen showed similar appearance in fluorescence mi-

---

<sup>1</sup> The only exception is *A. stolonifera*. In this case, dewaxing with acetone was conducted after harvesting. No substantial differences in morphology and fluorescence to the untreated pollen samples were observed. Thus, *A. stolonifera* is included in the analysis, however, treated carefully and marked in Fig. S2.

croscopy analysis, further confirming their comparability (Fig. 2). In addition, the EEM of freshly collected *S. nigra* pollen (Fig. S2M) resembles the general fluorescence signatures of the commercial pollen samples. Based on these crosschecks we assume in following that the fluorescence properties of commercially obtained pollen are consistent with results from freshly harvested samples.

## 2.2 Fluorescence microscopy

Fluorescence microscopy images were taken on a BZ-9000 Fluorescence Microscope (Keyence, Inc., Osaka, Japan). The instrument was equipped with a super-high-compression mercury lamp (120 W) and a 2/3-inch, 1.5 mega pixel monochrome CCD. The following fluorescence filters were used to take images in different spectral ranges: OP-66834 DAPI-BP ( $\lambda_{\text{ex}} = 360/20$  nm,  $\lambda_{\text{Dichroic}} = 400$  nm,  $\lambda_{\text{Absorp}} = 460/25$  nm), OP-66836 GFP-BP ( $\lambda_{\text{ex}} = 470/20$  nm,  $\lambda_{\text{Dichroic}} = 495$  nm,  $\lambda_{\text{Absorp}} = 535/25$  nm), OP-66838 TexasRed ( $\lambda_{\text{ex}} = 560/20$  nm,  $\lambda_{\text{Dichroic}} = 595$  nm,  $\lambda_{\text{Absorp}} = 630/30$  nm). Filter specifications are represented as mode wavelength and peak width ( $\lambda/\text{FWHM}$ ;  $\text{FWHM} = \text{full width half max}$ ). The spectral characteristics of the microscope filters are illustrated in Fig. 1.

For microscopy analysis the pollen samples were placed between a specimen holder and a cover slide and fixed with one of the two following mounting media: (i) glycerol gelatin (Sigma Aldrich), which is an aqueous mounting medium, or (ii) Eukitt<sup>®</sup> (Sigma Aldrich), which is a polymethacrylate-based and quickly hardening medium. A small amount of pollen was placed on the specimen holder and one drop of the mounting medium was added. Glycerin gelatin was diluted with ~ 40 % (vol) of water and heated to ~ 60 °C to decrease its viscosity for easy handling. Pollen and mounting medium were carefully homogenized with a spatula and a cover slide was placed on top of the mixture. After ~ 20 minutes of hardening the samples were used for microscopy analysis. The aqueous medium of the glycerol gelatin allows the investigation of pollen grains in a *moist* state. This is due to the fact that dry pollen mounted in contact with glycerol gelatin quickly take up water and will thus swell within a matter of minutes before analysis (Reitsma, 1969; Praglowski, 1970). In contrast, the Eukitt<sup>®</sup> medium preserves the *dry* state of the pollen grains. Preparation in moist state was applied for most samples, whereas dry state preparation was chosen occasionally as outlined in Sect. 3.1. Glycerol gelatin also introduces weak background fluorescence in all three channels (mostly in blue), whereas no background was observed for Eukitt<sup>®</sup>.

The microscopy investigation was initiated immediately after samples preparation and pollen grains were exposed to the excitation radiation for as little time as possible to minimize photo-bleaching effects. The exposure time in all channels was adjusted to a maximum dynamic range by increasing the signal to just below the detector saturation threshold. Raw images were processed with software: BW Analyzer (Keyence, Inc.) and Adobe Photoshop (Adobe Systems Inc., San Jose, CA, USA). Fluorescence overlay images were prepared by merging individual images from three fluorescence channels. A histogram equalization was done for all channels by manually adjusting the dynamic range between the pixel of maximum brightness and the background which was set to black zero level. This procedure corrects for photo-bleaching-related intensity decrease. For low background fluorescence levels, this does not change the image's color balance.

Pollen grain sizes and axis aspect ratios in Table 1 were obtained as follows: Under the bright field microscope, a certain number of separated and dry pollen grains (50-150) was imaged and sizing was performed with the software BW Analyzer. The given diameters are the arithmetic mean values for all imaged grains, averaged over grain dimensions in x and y direction. Aspect ratios correspond to the measured major and minor axes of the pollen. Note that the orientation of individual grains on the specimen slide is not uniform and that the given aspect ratios are therefore approximations.

### 2.3 Fluorescence spectroscopy

Fluorescence spectra were recorded on a LS 45 Luminescence Spectrometer (Perkin Elmer, Inc., Waltham, MA, USA) and a detailed instrument description is given in our part I paper (Pöhlker et al., 2012). EEMs are measured in a spectral area of 220-650/270-700 nm ( $\Delta\lambda_{\text{ex}}/\Delta\lambda_{\text{em}}$ ) which covers most biofluorophores relevant to atmospheric PBAP and the detection ranges of most LIF bioaerosols detectors (Pöhlker et al., 2012). Figure 1 displays a conceptual overview-EEM illustrating the spectral realm of interest, elastic scattering interferences, and instrumental parameters. The dry pollen samples were analyzed with a Front Surface Accessory (Perkin Elmer, Inc.). Several milligrams of powder were placed onto the sample holder as homogeneous and thin layer. The resulting EEMs are processed and normalized as described in part I.

### 2.4 Principal component analysis

Principal component analysis (PCA) was used as a statistical tool to visualize taxonomic trends in pollen autofluorescence. PCA was performed using Origin 8.6 (OriginLab Corp., Northampton, Ma, USA) based on fluorescence spectroscopy data from 25 pollen species (Table 1). The following pollen features were used as PCA input data: (i) Intensities of the main fluorescence modes A ( $\lambda_{\text{ex}} = 280/\Delta\lambda_{\text{em}} = 440-460$ ), B (355/440-460), and C (460/510-530). Mode intensities are normalized to total fluorescence intensity. (ii) Total fluorescence intensity, as average of fluorescence from modes A - C. (iii) Pollen grains size as given in Table 1.

## 3 Results and Discussion

Pollen grains exhibit strong emission of autofluorescent light originating from both, their cytosol (intra-cell components) and their complex, multi-layered cell wall (e.g. Asbeck, 1955; Driessen et al., 1989; Castro et al., 2010). The natural fluorescence of pollen has been used as a valuable tool for quick and non-invasive *in situ* analyses of fresh and fossil pollen in diverse scientific fields, such as atmospheric science (e.g. Ronneberger et al., 2002; Mitsumoto et al., 2010; Pan et al., 2011), geology and palynology (e.g. Phillips, 1972; Yeloff and Hunt, 2005), as well as plant physiology and botany (e.g. Roshchina, 2003; Roshchina, 2008; Grienberger et al., 2009; Roshchina, 2012). The following sections characterize the autofluorescence of native pollen using fluorescence microscopy and spectroscopy.

### 3.1 Fluorescence microscopy

Common white light (or bright field) microscopy is an important and wide-spread technique for pollen characterization and counting (i.e. for routine pollen monitoring), and therefore a large body of pollen-related microscopy data<sup>2</sup> is available. Fluorescence microscopy, in contrast, has been applied only occasionally for the characterization of pollen. In addition to size and shape, it provides information about surface texture and internal structures as well as spectral properties (e.g. Asbeck, 1955; Driessen et al., 1989; Ronneberger et al., 2002; Roshchina et al., 2004; Scharring et al., 2006; Mitsumoto et al., 2009; Castro et al., 2010). Morphologically, it allows to localize the cellular origin and to estimate the relative contributions of fluorescence emission from different cellular regions (i.e. cell wall, organelles, cytosol). It also provides spectroscopic information about the predominant excitation and emission ranges and allows a pollen classification based on specific emission intensity ratios (Mitsumoto et al., 2009; Castro et al., 2010; Mitsumoto et al., 2010). Analyses utilizing micro-spectroscopic approaches even allow the analysis of fluorescence spectra for single pollen grains (e.g. Roshchina et al., 2004).

Previous studies have reported that the complex and multilayered pollen cell wall (sporoderm) is the main origin of pollen autofluorescence (e.g. Driessen et al., 1989; Roshchina et al., 1997; Grienenberger et al., 2009; Castro et al., 2010). The sporoderm is a unique feature of pollen and generally consists of two components: exine and intine. The intine forms the internal part of the sporoderm; it comprises cellulose and related compounds and it is chemically similar to the primary cell wall of plants (Bedinger et al., 1994). The exine is a chemically and morphologically unique biopolymer and comprises the outermost layer of the sporoderm showing a species-specific sculptured morphology (Brooks and Shaw, 1978; Scott, 1994). It consists of the exceptionally resistant biopolymer sporopollenin whose complex chemical composition is not fully characterized. Its biosynthesis is assumed to be based on a mixture of phenolic, fatty acid and probably carotenoid precursors (Bedinger et al., 1994). Moreover, the exine is usually coated with an oily substance called pollenkitt (up to 10-15% of total pollen mass), containing a mixture of lipids as well as carotenoid, flavonoid, and phenolic pigments (Wiermann and Vieth, 1983; Pacini and Hesse, 2005). The complexity of the pollen's sporoderm reflects the plurality of its functions, such as protection against harsh environmental conditions (Boavida et al., 2005), pollen-stigma interaction and recognition (Piffanelli et al., 1998), and regulation of the pollen's hydration state (Dickinson, 1995). One major function is UV-light shielding to avoid radiative damage to the DNA and physiological processes in the cell (Rozema et al., 2001; Jacobs et al., 2007). The UV-light reduction occurs via light reflection, absorption as well as fluorescence light conversion from UV to the visible spectral range and is mainly based on sporoderm pigments (Hoque and Remus, 1999).

Figures 2 and 3 show selected fluorescence microscopy images of pollen grains from different species. Figure 2 exhibits overview images of 12 selected pollen samples, providing a visual impression of their diverse autofluorescence appearance. Figure 3 focusses on individual grains from

---

<sup>2</sup> <http://www.polleninfo.org>  
[http://pollen.usda.gov/Light\\_Micrographs/LMicro.html](http://pollen.usda.gov/Light_Micrographs/LMicro.html)  
<http://oldweb.geog.berkeley.edu/ProjectsResources/PollenKey/pollen.html>  
<http://www.geo.arizona.edu/palynology/nsw/index.html>

6 species and shows cytological details with the highest resolution accessible for full-field light microscopy. Our aim in this fluorescence microscopy section is to highlight intra-cellular autofluorescent structures. We found that pollen in *moist* state are most appropriate for microscopy analysis, because cellular components are thus most visible, and the majority of pollen samples was prepared, accordingly (see Sect. 2.2). In few cases, *dry* sample preparation was preferred to highlight specific morphological aspects. We are aware the water uptake changes the pollen's morphology due to grain swelling (Diehl et al., 2001; Castro et al., 2010; Griffiths et al., 2012). This water effect has important atmospheric implications, but is beyond the scope of this study. A companion paper will address this and other aspects in more detail (Pöhlker et al., 2013).

In the course of our microscopy analysis, we made the following general observations: (i) Grains from all pollen species show fluorescent emission with cell wall *and* cytosolic contributions (e.g. Fig. 2G,H). (ii) The relative emission intensities of individual pollen grains of the same species can vary significantly, with fluorescence from few individual grains being much higher than the intensity of the majority (e.g. Fig. 2C,L; also Fig. 3E). (iii) Differences in emission wavelengths among pollen grains of the same species are common and observable qualitatively as different colors in the fluorescence overlay images (e.g. Fig. 2E,G; also Fig. 3E). (iv) In several cases, the fluorescence overlay images provide a better contrast and “perceptibility” of the pollen microarchitecture (i.e. patterns in the cell wall and internal cytosolic structures) than the corresponding bright-field images (e.g. Fig. 2I and Fig. 3A,C).

(i) Our results confirm that the pollen sporoderm contributes substantially to the overall fluorescence emission. As typical examples, the high-resolution images of *P. sylvestris*, *B. fontinalis* and *A. artemisiifolia* in Fig. 3A,C,E exhibit a thick exine ( $\sim 1\text{-}2\ \mu\text{m}$ ) which shows pronounced fluorescence. In these cases, the cell wall fluorescence occurred in the green-to-red spectral range of the visible light, however, the diversity of the cell wall appearance is high. In addition, many species show fluorescence contributions from other cell parts, such as the cytosol (e.g. Fig. 2G,J; also Fig. 3C,D), specific organelles (e.g. Fig. 3A,E), and the air bladders in *P. sylvestris* (Fig. 3A,B). The blue, sometimes red tinted, cytosolic fluorescence is observed for many pollen species. In many cases the cytosol emission appears homogeneously distributed (Fig. 2H,K) and for other samples contrasts with the embedded non-fluorescent vesicular bodies (e.g. Fig. 3C) which are usually filled with oils (mostly in *entomophilous* pollen) or starch (mostly in *anemophilous* pollen) and serve as energy reserve for germination (Piffanelli et al., 1998).

(ii) Previously, Castro et al. (2010) reported a heterogeneous fluorescence intensity of individual pollen grains and stated that this variability is caused by different hydration states. In our study a heterogeneous intensity has been found for several species, in which some pollen grains show strongly increased cytosolic fluorescence compared with the majority of grains (i.e. Fig. 2J,L and Fig. 3E). Alternatively, differences in metabolic state can also explain this observation. Roshchina et al. (1997; 2003) reported a threefold increased intensity for pollen which have lost their viability. They further suggested utilizing this relationship as a quick and non-invasive *in vivo* diagnosis of the pollen cell state. Interestingly, a very similar effect has been observed for the fluorescence

properties of fungal spores, which also show strongly increased emission intensities for non-viable compared to viable cells (Wu and Warren, 1984a, b).

(iii) In addition, the remarkable differences in emission wavelengths (visible as color differences) among grains of the same species may also be associated with differences in metabolic and maturation state, as reported by Roshchina et al. (2003). Some species show grains with very heterogeneous appearance (e.g. Fig. 2E,G), whereas others reveal more uniform properties (e.g. Fig. 2K). *Phleum pratense* in Fig. 3E represents a characteristic example with highly diverse fluorescence properties among grains which cannot be distinguished in the brightfield image. It has been shown that during their development and maturation the fluorescence properties of pollen undergo changes due to chemical and physiological transformations of the cell (Roshchina et al., 1997). Accordingly, the heterogeneity of pollen grains under the fluorescence microscope can be regarded as a visible reflection of such metabolic and maturational differences. This aspect is important for ambient PBAP detection as highlighted by Pinnick et al. (2013) because single particle fluorescence may substantially differ from bulk fluorescence of the same material. Accordingly, bulk fluorescence spectra, such as the EEMs presented in this study, provide an average characterization of fluorescent materials, however, differences on the level of individual cells (e.g. metabolic differences) are smeared.

(iv) The images in Fig. 3 are recorded with the maximum resolution of a full-field fluorescence microscope. They show individual pollen grains in great detail and allow cytological and histological insights. The high contrast of the overlay fluorescence images reveals much more fine features of the pollen micro-architecture than the corresponding bright field images. In particular, the pollen's cytosol reveals a complex internal structure with membranes, vacuoles, organelles and non-fluorescent vesicular bodies. For example, the central spot of bluish-white fluorescence in the cytosol of *P. sylvestris* probably reveals the location of the (vegetative) nucleus (Fig. 3A). Moreover, in Fig. 3B blue fluorescence shows a “foam-like” skeleton inside the air bladders of *P. sylvestris* and a thin red fluorescing membrane around them. In addition, details of the sporoderm are also resolved, such as an increased red fluorescence at the aperture in *P. sylvestris* (Fig. 3A) and a thickened cell wall at the apertures of *B. fontinalis* (Fig. 3C) with strong green fluorescence. *Ambrosia artemisiifolia* in Fig. 3F represents an interesting example of sporoderm fluorescence with a thick red tinted outer layer and a thin internal layer emitting bluish fluorescent light.

### 3.2 Fluorescence spectroscopy

The previous section discussed that fluorescence microscopy is a valuable technique to explore the morphological autofluorescence properties of individual pollen grains. The following section provides a spectral characterization of the steady-state autofluorescence properties of pollen and explains observed spectral signatures by assignment of individual fluorophores. EEMs were recorded for 25 different pollen species and Fig. 4 exhibits selected examples (for further EEMs see supplementary Figure S2). Pollen show pronounced fluorescence within a wide spectral range with strongest excitation at  $\lambda_{\text{ex}} = 220\text{-}550$  nm and with corresponding emission at  $\lambda_{\text{em}} = 380\text{-}600$  nm (Fig. 4). The presence of multiple distinguishable, but overlapping, modes indicates fluorescent

emission mixed from different fluorophores. The general fluorescence mode *signature* in the EEMs appears to be reproducible and characteristic across all analyzed pollen samples, as outlined below, suggesting a relatively few, but dominant, fluorophores common across most pollen species.

Among all dry pollen samples studied, three fluorescence modes appear most prominent: **(A)** a mode at  $\sim 280/450$  nm ( $\lambda_{\text{ex}}/\lambda_{\text{em}}$ ), **(B)** a mode at  $\sim 355/450$  nm, and **(C)** a mode at  $\sim 460/520$  nm. In addition to the modes A - C, two further signals at  $\sim 280/340$  nm **(D)** and at  $\sim 350\text{-}650/675$  nm **(E)** were observed for a smaller number of samples. Table 2 provides a summary, including fluorophore assignment, which is discussed in detail in the following paragraphs. As a first, coarse classification, the 25 pollen samples can be subdivided into two groups: A first group with 10 species, each showing a strong mode C with rather weak or even non-detectable modes A and B (e.g. *B. fontinalis*, Fig. 4D; *J. nigra*, Fig. 4G) and a second group with 15 species, each exhibits clear and strong modes A, B, and C (e.g. *A. vulgaris*, Fig. 4C; *L. perenne*, Fig. 4H). In addition to the major signals, five samples show also mode D which appears for *C. betulus* (Fig. 4F) as a pronounced peak and for other species as a weak shoulder (e.g. *P. pratense*, Fig. 4I). Six samples show the very weak and multimodal signal E (e.g. *A. vulgaris*; Fig. 4C).

Based on all EEMs in Fig. 4 and Fig. S2, a general autofluorescence signature for dry and native pollen was extracted and is shown in Fig. 5A. Here, the red markers represent the maxima of all clearly resolved modes in the individual pollen EEMs. The close clustering of the markers in the previously defined areas A - E indicates that the measured fluorescence is caused by a similar set of fluorescent compounds across the analyzed species. Moreover, a direct comparison with results from previous studies (Satterwhite, 1990; Wlodarski et al., 2006; Hill et al., 2009) underlines the characteristic clustering, particularly in the areas A - D (Fig. 5A). These results support the idea that dry and native pollen show consistent, *fingerprint-like* fluorescence signatures which can be used for fluorophore assignment (Pöhlker et al., 2012). Roshchina et al. (e.g. 1997; 2003; 2004) conducted a number of studies to analyze the autofluorescence of pollen and other secretory plant cells. Their experiments indicated that pollen fluorescence is dominated by sporoderm fluorophores and that phenolics ( $\lambda_{\text{em}} = 440\text{-}490$  nm), azulenes ( $\lambda_{\text{em}} = 440\text{-}460$  nm) and carotenoids ( $\lambda_{\text{em}} = 500\text{-}560$  nm) constitute the main classes.

In our experiments, emission at  $\sim 450$  nm (modes A and B; Fig. 5C,D) and  $\sim 520$  nm (mode C; Fig. 5B,C) represent the most obvious and reproducible fluorescence features. Fluorophores usually show rather sharp and characteristic emission wavelengths, whereas excitation can occur over a comparably wide spectral range (Pöhlker et al., 2012). Thus, we assume that the modes A and B are caused by the same fluorophore type which is excited over a wide range, but most efficiently at 280 and 350 nm (Fig. 5F). The emission at 450 nm is consistent with phenolic fluorescence which is observed in most plant cell walls (e.g. Harris and Hartley, 1980; Lang et al., 1991; Hutzler et al., 1998). In addition, various studies, including real-time LIF ambient measurements, reported a similar and characteristic signal at  $\sim 450$  nm for pollen, confirming its ubiquitous role (Hill et al., 1999; Roshchina et al., 2004; Kiselev et al., 2011; O'Connor et al., 2011; Pan et al., 2011). Phenolic compounds represent the most abundant class of secondary plant metabolites in nature and typical subclasses in plant tissue and pollen are: (i) hydroxylated cinnamic acid derivatives (e.g. ferulic, caf-

feic, *p*-coumaric and chlorogenic acid), (ii) flavonoid compounds (e.g. kaempferol and quercetin), and (iii) anthocyanins (e.g. cyanidin, malvidin) (Li et al., 2010; Taiz and Zeiger, 2010). The molecular skeleton of all these compounds comprises closely related conjugated structures of strongly oxygen-functionalized phenolic moieties. The structural and electronic similarity across these phenolic subclasses explains similar excitation (i.e. UV-range) and emission (i.e. blue spectral range) properties. Many cinnamic acids (i.e. ferulic and caffeic acid) are covalently bound to the cell walls (Lichtenthaler and Schweiger, 1998), whereas other phenolic fluorophores (e.g. trihydroxyferuloyl spermidine and many flavonoids in the pollen coat) are easily removed by washing (Wiermann and Vieth, 1983; Grienenberger et al., 2009). The large diversity of phenolic products in plants suggests that the pollen modes A and B are probably based on a mixture of fluorescent phenolic derivatives which exhibit similar emission at 450 nm and are “distributed” over a wide excitation range. However, Lichtenthaler and Schweiger (1998) suggest that among all fluorescent phenolics, ferulic acid plays a key role.

Mode C shows strong emission at ~ 520 nm which is consistent with carotenoid fluorescence (Roshchina, 2003). Carotenoid pigments are widespread in nature, such as in plant photosynthesis, where they act as light-harvesting pigments (Taiz and Zeiger, 2010). In cell walls (e.g. in pollen) they are part of the “natural sunscreen” providing UV-radiation protection and they also act as reactive oxygen species scavengers (Barrell et al., 2010). The pollen sporoderm is known as an accumulation site for carotenoid pigments, such as  $\alpha$ - and  $\beta$ -carotene and lutein (e.g. Prahl et al., 1985; Kano and Hamaguchi, 2006). Together with flavonoids they cause the typical yellow to orange color and their abundance in the pollen coat shows taxonomic specificity (Schulte et al., 2009). The reported absorption maximum of carotenoids is located at ~ 480 nm (here  $\lambda_{\text{ex,max}} = \sim 460$  nm) and therefore mode C is inefficiently excited by UV-light (Sufra et al., 1977). Accordingly, dual- or multi-wavelength excitation is most appropriate to address the carotenoid *and* phenolic features of pollen fluorescence. In contrast, single-wavelength excitation, usually in the UV-range, misses the main peak of the pollen carotenoid emission (compare Fig. 5E).

In addition to the strong and abundant signals A - C, the modes D (280/340) and E (350-650/675) occur in some pollen species. The weak mode E is attributed to chlorophyll *a* (chl *a*) fluorescence which has been found in pollen previously (O'Connor et al., 2011). The individual chlorophyll pigment types (i.e. chl *a*, chl *b*, chl *c*, and chl *d*) show different fluorescence properties (Welschmeyer, 1994; Moberg et al., 2001). For instance, chl *a* reveals its main emission at ~ 670 nm whereas chl *b* emits at ~ 650 nm (French et al., 1956). All of them reveal comparably wide excitation ranges (Pöhlker et al., 2012). We found chl *a* fluorescence in grass and weed pollen species (e.g. *A. vulgaris*, *L. perenne*), however, at a very low intensity level. One explanation for the presence of chlorophyll in pollen is the cytoplasmic inheritance of chloroplast DNA which is independent of the nuclear chromosomes and occurs via pollen dispersal for a number of species (McCauley et al., 2007; Miko, 2008). Thus, the presence of chloroplasts in the course of paternal cytoplasmic gene transmission can explain the presence of chlorophyll in some pollen species (e.g. Hipkins et al., 1994). Moreover, it has been shown that the presence of chlorophyll pigments de-



depends on the pollen maturation state, with higher chlorophyll abundance in immature pollen grains (Roshchina, 2003; 2004).

Mode D is attributed to protein fluorescence which is mainly caused by the amino acid tryptophan with emission at 280-295/340-353 nm (Pöhlker et al., 2012). For comparison, Fig. 5A shows the emission signals of the proteins bovine serum albumin (BSA) and ovalbumin (OVA) which clearly overlap with mode D. Protein autofluorescence is an omnipresent and characteristic feature in PBAP and has been observed for many organisms (e.g. Sivaprakasam et al., 2004; Kopczynski et al., 2005; Wlodarski et al., 2006; Hill et al., 2009). Furthermore, several bioaerosol detectors are designed to selectively excite and detect protein fluorescence (e.g. WIBS; compare Fig. 5D). It is therefore, perhaps, somewhat surprising that only one pollen type measured in the dry state (*C. betulus*, see Fig. 5D), among all analyzed 25 species, showed a clearly resolved protein mode, despite the fact that proteins and enzymes can constitute up to ~ 60% of dry pollen weight (e.g. Roulston and Cane, 2000; Andrada and Telleria, 2005). Four grass pollen species (e.g. *A. stolonifera* and *L. perenne*) also show a shoulder-like signal for mode D, indicating the presence of weak protein fluorescence (see Fig. 5D).

The absence of a clear protein signal can be related to UV-light shielding properties of the pollen sporoderm. About 95-99% of the incoming UV-radiation usually does not reach the cytosol because of sporoderm reflection (elastic scattering), fluorescence (inelastic scattering) and absorption (thermal energy dissipation). However, fluorescence and absorption can be regarded as linked processes which only differ in the extent the imparted energy is reemitted as radiative versus thermal energy (Lakowicz, 1999). Thus, in pollen grains with highly absorbing sporoderms, proteins and coenzymes which are located in the cytoplasm are not accessible to UV-excitation light. So, when measuring bulk properties of dry pollen by fluorescence spectroscopy, fluorescence from sporoderm pigments dominates EEM features, swamping any contribution from cytosolic fluorophores. In contrast, fluorescence microscopy of single pollen grains has the benefit of spatially resolving emission, thus showing the strong fluorescence from cell wall components, while also showing fluorescence from the cytosol (Sect. 3.1).

*Carpinus betulus* is the only observed exception to this trend because it shows a clear protein signal in its EEM (see Fig. 4F). The fluorescence microscopy image of *C. betulus* pollen in Fig. 6 provides a potential explanation for this “anomaly”. It can be seen that the larger pollen grains (~ 35 µm) which show a yellowish fluorescence occur as agglomerates with many smaller particles (~ 4 µm) showing strong bluish fluorescence. The fluorescence microscopic appearance of the larger *C. betulus* grains resembles the micrographs of other species in Fig. 2. Therefore, we assume that the “contaminating” small particles are causing the unusual protein signals on top of the pollen-related modes in the EEM. The origin and identity of the small adherent particles is unclear. They exhibit a biological morphology with a cell wall-like structure which is the main origin of the blue emission. A contamination with microorganisms (i.e. bacteria) appears to be unlikely because of the comparably large particle size. One explanation would be the presence of many small *immature* pollen grains, associated with the larger and mature ones. It is known that pollen fluorescence properties change during grain maturation and, particularly, with increasing contents of carotenoids

in the sporoderm (causing green-yellow fluorescence) which is consistent Fig. 6 (Roshchina, 2003). However, a detailed investigation of the identity of the adherent particles is beyond the scope of this study. It can be concluded that fluorescence from all analyzed pollen species lacks clear cytosol contributions (i.e. from proteins) and that the only exception to this general trend exhibits an obvious, and probably causative, morphological anomaly. This strengthens our hypothesis that the fluorescence signature of pollen is exclusively shaped by a set of light-accessible fluorophores in the pollen sporoderm.

### 3.3 Taxonomic trends in the autofluorescence signature

The mixtures of secondary plant metabolites in the pollen sporoderm, such as phenolics and flavonoids (Bate-Smith, 1962; Molgaard and Ravn, 1988) as well as carotenoids (Schulte et al., 2009) show taxonomic specificity. Thus, it is not surprising that the sporoderm-based fluorescence also exhibits certain taxonomic trends, as observed in our experiments. The Figures 5B-F illustrate differences in fluorescence mode abundance and intensity across pollen species for selected excitation ( $\lambda_{\text{ex}} = 280, 355, 460 \text{ nm}$ ; Fig. 5B-D) and emission wavelengths ( $\lambda_{\text{em}} = 450, \text{ and } 520 \text{ nm}$  Fig. 5F,E). The following general observations were made: (i) grass pollen belonging to the family *Poaceae* (blue) clearly show the highest intensities for both, the phenolic and carotenoid fluorescence modes A - C. This is consistent with studies showing that plant tissue of *Poaceae* shows particularly high contents of phenolic compounds and elevated blue-green fluorescence, compared to other families (Lichtenthaler and Schweiger, 1998). (ii) The shrub pollen belonging to the family *Asteraceae* (red) also show comparably high intensities for all modes. (iii) Medium intensities were found for tree pollen of *Salicaceae* (yellow) and shrub pollen of *Polygonaceae* (cyan). (iv) There is a larger number of (mostly tree) pollen families (e.g. *Betulaceae* in green and *Oleaceae* in violet) which reveal low fluorescence intensities in the entire EEM range. In general, the overall intensity level (averaged intensities of modes A - C) is a distinctive feature across pollen families, with grass pollen (i.e. *Poaceae*) fluorescence being highest and tree pollen (e.g. *Betulaceae*) fluorescence being lowest. Thus, the intensities of the modes A, B, and C are linked and show a clear positive correlation ( $R = 0.74 - 0.87$ ) (see Fig. S3). However, in addition to this general intensity trend, the relative contributions of the individual modes A - C are variable across pollen families, as outlined in the following paragraph.

We utilized principal component analysis (PCA) to visualize general taxonomic trends in pollen fluorescence properties, as observed in Fig. 5. PCA reduces complex datasets to fewer dimensions and preserves most of the variability. It often provides insights into general underlying structures of the dataset in question. Figure 7 displays two PCA bi-plots which illustrate *taxonomic trends* based on fluorescence data only (Fig. 7A) and based on fluorescence data in combination with pollen grain size (Fig. 7B) (Sect. 2.4). In Fig. 7A two principal components (PC) span the fluorescence variability of all analyzed pollen species and the three eigenvectors shown (total intensity, intensity of mode A, and intensity of mode C) represent the main distinctive features. It can be seen that: (i) the intensity eigenvector spreads out the pollen species according to their overall fluorescence intensity, with *Poaceae* being highest, followed by *Asteraceae* as well as *Salicaceae*, and *Betulaceae*

being lowest. (ii) The diametric eigenvectors for mode A and mode C spread the pollen according to their fluorescence mode patterns. For example, the species *J. nigra* and *B. fontinalis* are characterized by a strong fluorescence mode C and the absence of mode A (see Fig. 4D,G). In contrast, *B. papyrifera* exhibits a dominant mode A and a rather weak intensity for mode C (see Fig. 4E). (iii) In addition, a certain clustering of species, which belong to the same family, is observed in the bi-plot, however pollen families are not clearly separated. For comparison, we performed an additional PCA accounting for pollen fluorescence and grains size (Fig. 7B). The eigenvectors for total intensity, intensity of mode A, and average pollen grains size represent the distinctive features. In this PCA bi-plot, the previously observed trends are preserved, however, the clustering becomes clearer and a better separation of pollen families is obtained.

### 3.4 Relevance for ambient pollen measurements

Currently, pollen monitoring and forecasting is still a manual and labor-intensive business based on pollen sampling and microscopy analysis. There is common interest in improving the pollen monitoring strategy in the direction of automated real-time techniques, which can provide statistically reliable and specific pollen measurements. Various approaches from different scientific directions are addressing this aspect (e.g. Ronneberger et al., 2002; Scharring et al., 2006; Ranzato et al., 2007; Skjoth et al., 2013). In the following section, we briefly review and discuss the applicability and limitations of autofluorescence-based techniques to real-time pollen analysis, based on the results of the present and previous studies.

The extent of selectivity that autofluorescence can provide in PBAP detection is still an open question and discussed on three selectivity levels: (i) discrimination between biological and non-biological particles (e.g. PBAP versus mineral dust), (ii) discrimination *among* bioaerosol particles and their *classification* into a certain number of meta-classes (e.g. bacteria, fungal spores, algae, and pollen), and (iii) *identification* of specific organisms on family, genus or even species level (Hill et al., 1999). It is commonly accepted that autofluorescence can reliably distinguish between biological and non-biological particles, in most cases (Pan et al., 2007). On this first level of selectivity, quantification of FBAP and monitoring of its variability in ambient air is feasible, however, mostly without information about FBAP identity (e.g. Huffman et al., 2012; Toprak and Schnaiter, 2013). In this context, single-particle LIF instruments usually rely on the detection of total (spectrally undispersed) fluorescence in comparably broad emission bands from one or two excitation wavelengths (e.g. Hairston et al., 1997; Foot et al., 2008). On the second level of selectivity, classification of bioaerosols is desired and has been addressed in many studies (e.g. Hill et al., 1999; Pinnick et al., 2004; Pan et al., 2009; Sivaprakasam et al., 2009; Pan et al., 2010). An increase of “resolving power” requires recording of a larger array of fluorescence information from single particles. This can be realized either on the excitation (i.e. multi-wavelength excitation) or on the emission axis (i.e. spectral dispersion). Instruments relying on spectrally dispersed fluorescence have proven to provide a stable classification of ambient FBAP with distinct spectral signatures (e.g. Pan et al., 2009; 2010), but are not commercially available and generally extremely expensive. On the third level of selectivity, bioaerosol *identification* is desired, however, several specialists

argue that this is beyond the scope of LIF instruments, with few exceptional cases (Sivaprakasam et al., 2004; Pan et al., 2007). This can be explained by the fact that relatively few fluorophores (i.e. amino acids and coenzymes) determine the shape of the fluorescence signal of many organisms. For instance, a large number of bacterial species exhibits similar and comparably featureless fluorescence spectra and therefore cannot be discriminated (Hill et al., 1999; 2009). Thus, the abundance, diversity and light accessibility of the underlying fluorophores is a crucial and limiting factor for the selectivity of LIF-based techniques.

Autofluorescence based, real-time monitoring of pollen clearly requires taxonomic selectivity for the detection of a minority population of few allergenic pollen species (approx. 10-20) on top of a complex and highly variable aerosol background. Several studies have indicated that the pollen fluorescence signal may be sufficiently specific for pollen differentiation (e.g. Willemse, 1972; Driessen et al., 1989; Satterwhite, 1997; Butkhuzi et al., 2002; O'Connor et al., 2011). Ronneberger et al. (2002) confirmed that *offline* techniques, such as high-resolution fluorescence microscopy, can provide a high pollen recognition rate (> 90 %) based on the 3D fluorescence distribution inside the pollen grains. Mitsumoto et al. (2009; 2010) were the first to confirm the *online* practicality of fluorescence-based pollen recognition for a set of five species. Their experiments are based on pollen sizing (via elastic light-scattering) and determining of the ratio of blue ( $\Delta\lambda_{em,blue} = 400-550$  nm) to red ( $\Delta\lambda_{em,red} = 560-700$  nm) fluorescence when excited with UV-light ( $\lambda_{ex} = 350-380$  nm). Their successful pollen discrimination is consistent with Fig. 7, showing a taxonomic clustering based on grain size and the ratio of fluorescence modes. Pan et al. (2011) reported the *online* detection of emission wavelength dispersed fluorescence spectra from two excitation wavelengths ( $\lambda_{ex,1} = 263$ ,  $\lambda_{ex,2} = 351$  nm) and showed spectral differences across twelve pollen species. Their results are in good agreement with the autofluorescence signature reported here. For instance, a dominant peak at  $\sim 450$  nm (phenolics) occurred for the majority of species and additional signals at  $\sim 340$  nm (protein) and at  $\sim 520$  nm (carotenoid) are observed occasionally. Figure 5C,D confirms that for UV-excitation phenolic fluorescence is predominant. Moreover, the intensities of the online spectra reflect the taxonomic trends reported in Fig. 7: species of the families *Poaceae* (i.e. corn, meadow oat) and *Asteraceae* (e.g. Ragweed) were found to exhibit the highest intensities, whereas *Betulaceae* species (i.e. birch) shows substantially weaker fluorescence. Consequently, the results of these initial online LIF measurements and the offline results reported in this study are in good agreement. This underlines that offline and online instrumentation is measuring the same pollen-specific autofluorescence signature.

We suggest that our study can support the development and operation of LIF instruments for specific pollen monitoring in ambient air. Particularly, Fig. 5 can serve as a roadmap to select the most appropriate excitation wavelengths and emission bands, which provide good signal-to-noise ratios and the highest level of selectivity. In terms of ambient applicability the following aspects can be concluded: (i) Pollen exhibit an autofluorescence fingerprint which is intrinsically different from bacteria and fungal spores (Hill et al., 2009), based on the fact that it does not originate from proteins and other cytosolic compounds, but rather from cell wall associated fluorophores. This enables an autofluorescence-based differentiation of pollen from other PBAP types in the atmos-

phere, particularly when combined with particle sizing. (ii) Moreover, a classification of different pollen species is, in principle, practicable as visualized in Fig. 7. The most distinctive features are the overall fluorescence intensity as well as the occurrence and strength of the phenolic mode A and the carotenoid mode C. In addition, differences in pollen grain size can support a taxonomic discrimination. One remarkable example is the clear separation of grass (*Poaceae*) and tree pollen species (e. g. *Betulaceae*) in Fig. 7, which both represent important aeroallergens. The separation of other pollen families is less clear and the extent of clustering versus overlap has to be addressed in further studies. (iii) It has to be kept in mind that the reported EEMs represent bulk spectra, which average the specific fluorescence properties of individual pollen grains. The fluorescence microscopy analysis in this study has shown a substantial diversity on pollen grain level in terms of fluorescence intensity, intra-cellular fluorophore distribution, and emission wavelength. Therefore, ambient applications, which mostly are operated as single particle detectors, have to account for this heterogeneity. Another layer of complexity opens up, when the influence of environmental factors (e.g. relative humidity or chemical and physical aging) on pollen autofluorescence and morphology is taken into account. Such phenomena are beyond the scope of the present study and will be addressed in a companion paper (Pöhlker et al., 2013).

#### 4. Conclusions

This study provides a characterization of the origin, properties, and selectivity of the autofluorescence from native pollen. It utilizes fluorescence microscopy and spectroscopy for the analysis of 27 pollen species. The experimental results are complemented with a synthesis of related literature knowledge. We show that full-field fluorescence microscopy is a simple and valuable tool for histological studies on single pollen grains. This allows to explore the intra-cellular distribution of intrinsic fluorophores in pollen. We found very diverse morphological fluorescence properties across pollen species with fluorescent emission from the cell wall, the cytosol, and certain organelles. In addition, a remarkable heterogeneity of fluorescence intensity and emission wavelength across grains of the same species has been observed. It can be concluded that the fluorescence micro-architecture of pollen grains is very complex and that maturation and metabolic state likely have a strong influence on it.

Fluorescence spectroscopy was utilized to record EEMs which exhibit a steady-state autofluorescence fingerprint of individual pollen species. The EEMs revealed a characteristic and reproducible signature of five fluorescence modes across all pollen samples which could be attributed to four different fluorophore classes, namely phenolic compounds, carotenoid pigments, proteins and chlorophyll *a*. The most characteristic fluorescence originates from cell wall associated phenolics ( $\lambda_{em} = \sim 280$  and  $355$  nm/ $\lambda_{em} = \sim 450$  nm) and carotenoids ( $\sim 460/520$ ). Weak chlorophyll *a* ( $\sim 350-650/675$ ) and protein ( $\sim 280/340$ ) fluorescence was observed occasionally for certain species. We found that the cell wall associated fluorophores are dominating the fluorescence signature of dry and native pollen. The abundance of fluorophores in the pollen sporoderm is species-specific, and therefore, the sporoderm-related fluorescence signals show certain taxonomic trends. Principal component analysis was used to explore the discrimination potential of pollen autofluorescence and

revealed a differentiation of pollen on family level. We suggest that the results reported here can support the development and application of autofluorescence-based detectors for a specific monitoring of allergenic pollen in the atmosphere. In general, our results help to explore the levels of selectivity that autofluorescence-based techniques can provide in PBAP analysis.

*Acknowledgements.* This work has been funded by the Max Planck Society, the Max Planck Graduate Center and the LEC Geocycles Mainz. J. A. Huffman acknowledges internal faculty funding from the University of Denver. The authors gratefully acknowledge support by M. O. Andreae, A. Zimmer, K. Selzle, J. Fröhlich-Nowoisky and I. Müller-Germann and helpful conversation with D. R. Huffman, B. Weber and W. Elbert.

## References

- Agranovski, V., Ristovski, Z., Hargreaves, M., Blackall, P. J. and Morawska, L.: Performance evaluation of the UVAPS: influence of physiological age of airborne bacteria and bacterial stress, *Journal of Aerosol Science*, 34, 1711-1727, 10.1016/s0021-8502(03)00191-5, 2003.
- Andrada, A. C. and Telleria, M. C.: Pollen collected by honey bees (*Apis mellifera* L.) from south of Calden district (Argentina): botanical origin and protein content, *Grana*, 44, 115-122, 10.1080/00173130510010459, 2005.
- Andrade-Eiroa, A., Canle, M. and Cerda, V.: Environmental Applications of Excitation-Emission Spectrofluorimetry: An In-Depth Review I, *Applied Spectroscopy Reviews*, 48, 1-49, 10.1080/05704928.2012.692104, 2013.
- Asbeck, F.: Fluoreszierender Blütenstaub, *Naturwissenschaften*, 42, 632-632, 1955.
- Barrell, P. J., Wakelin, A. M., Gatehouse, M. L., Lister, C. E. and Conner, A. J.: Inheritance and Epistasis of Loci Influencing Carotenoid Content in Petal and Pollen Color Variants of California Poppy (*Eschscholzia californica* Cham.), *J. Hered.*, 101, 750-756, 10.1093/jhered/esq079, 2010.
- Bate-Smith, E. C.: The phenolic constituents of plants and their taxonomic significance, *Jour. Linn. Soc. London Bot.*, 58, 95-173, 1962.
- Bedinger, P. A., Hardeman, K. J. and Loukides, C. A.: Travelling in style: The cell biology of pollen, *Trends in Cell Biology*, 4, 132-138, 10.1016/0962-8924(94)90068-x, 1994.
- Bernstein, J. A., Alexis, N., Barnes, C., Bernstein, I. L., Nel, A., Peden, D., Diaz-Sanchez, D., Tarlo, S. M. and Williams, P. B.: Health effects of air pollution, *Journal of Allergy and Clinical Immunology*, 114, 1116-1123, 10.1016/j.jaci.2004.08.030, 2004.
- Boavida, L. C., Becker, J. D. and Feijo, J. A.: The making of gametes in higher plants, *International Journal of Developmental Biology*, 49, 595-614, 10.1387/ijdb.05201961b, 2005.
- Brooks, J. and Shaw, G.: Sporopollenin a review of its chemistry paleochemistry and geochemistry, *Grana*, 17, 91-98, 1978.
- Bundke, U., Reimann, B., Nillius, B., Jaenicke, R. and Bingemer, H.: Development of a Bioaerosol single particle detector (BIO IN) for the Fast Ice Nucleus Chamber FINCH, *Atmos. Meas. Tech.*, 3, 263-271, 2010.
- Burrows, S. M., Elbert, W., Lawrence, M. G. and Pöschl, U.: Bacteria in the global atmosphere - Part 1: Review and synthesis of literature data for different ecosystems, *Atmospheric Chemistry and Physics*, 9, 9263-9280, 2009.
- Butkhuzi, T., Kuchukashvili, Z., Sharvashidze, M., Natsvlshvili, G. and Gurabanidze, V.: Cytodiagnostics on intact pollen using photoluminescence, *Journal of Biological Physics and Chemistry*, 2, 53-55, 2002.
- Castro, A. J., Rejón, J. D., Fendri, M., Jiménez-Quesada, M. J., Zafra, A., Jiménez-López, M. I., Rodríguez-García, M. I. and Alché, J. D.: Taxonomical discrimination of pollen grains by using confocal laser scanning microscopy (CLSM) imaging of autofluorescence, in: *Microscopy: Science, Technology, Applications and Education*, edited by: Méndez-Vilas, A. and Díaz Álvarez, J., Formatex Research Center, 607-613, 2010.
- D'Amato, G.: Urban air pollution and plant-derived respiratory allergy, *Clinical and Experimental Allergy*, 30, 628-636, 2000.
- Després, V. R., Huffman, J. A., Burrows, S. M., et al.: Primary biological aerosol particles in the atmosphere: a review, *Tellus B*, 64, 2012.

- Dickinson, H.: Dry stigmas, water and self-incompatibility in *Brassica*, *Sex. Plant Reprod.*, 8, 1-10, 1995.
- Diehl, K., Quick, C., Matthias-Maser, S., Mitra, S. K. and Jaenicke, R.: The ice nucleating ability of pollen - Part I: Laboratory studies in deposition and condensation freezing modes, *Atmospheric Research*, 58, 75-87, 10.1016/s0169-8095(01)00091-6, 2001.
- Diehl, K., Matthias-Maser, S., Jaenicke, R. and Mitra, S. K.: The ice nucleating ability of pollen: Part II. Laboratory studies in immersion and contact freezing modes, *Atmospheric Research*, 61, 125-133, 10.1016/s0169-8095(01)00132-6, 2002.
- Diethart, B., Sam, S. and Weber, M.: Walls of allergenic pollen: Special reference to the endexine, *Grana*, 46, 164-175, 10.1080/00173130701472181, 2007.
- Dingle, A. N.: Pollens as condensation nuclei, *Journal de Recherches Atmospheriques*, 2, 231-237, 1966.
- Driessen, M., Willemse, M. T. M. and Vanluijn, J. A. G.: Grass-pollen grain determination by light-microscopy and UV-microscopy, *Grana*, 28, 115-122, 1989.
- Elbert, W., Taylor, P. E., Andreae, M. O. and Pöschl, U.: Contribution of fungi to primary biogenic aerosols in the atmosphere: wet and dry discharged spores, carbohydrates, and inorganic ions, *Atmospheric Chemistry and Physics*, 7, 4569-4588, 2007.
- Foot, V. E., Kaye, P. H., Stanley, W. R., Barrington, S. J., Gallagher, M. and Gabey, A.: Low-cost real-time multi-parameter bio-aerosol sensors, *Proc. SPIE - Int. Soc. Opt. Eng.*, 7116, 711601 (711612 pp.)-711601 (711612 pp.), 10.1117/12.800226, 2008.
- Franze, T., Weller, M. G., Niessner, R. and Pöschl, U.: Protein nitration by polluted air, *Environmental Science & Technology*, 39, 1673-1678, 10.1021/es0488737, 2005.
- French, C. S., Smith, J. H. C., Virgin, H. I. and Airth, R. L.: Fluorescence-spectrum curves of chlorophylls, pheophytins, phycoerythrins, phycocyanins and hypericin, *Plant Physiol.*, 31, 369-374, 1956.
- Fröhlich-Nowoisky, J., Pickersgill, D. A., Després, V. R. and Pöschl, U.: High diversity of fungi in air particulate matter, *Proceedings of the National Academy of Sciences of the United States of America*, 106, 12814-12819, 10.1073/pnas.0811003106, 2009.
- Gabey, A., Stanley, W. R., Gallagher, M. and Kaye, P. H.: The fluorescence properties of aerosol larger than 0.8  $\mu\text{m}$  in an urban and a PBA-dominated location, *Atmospheric Chemistry and Physics Discussions*, 11, 531-566, 2011.
- Gabey, A. M., Gallagher, M. W., Whitehead, J., Dorsey, J. R., Kaye, P. H. and Stanley, W. R.: Measurements and comparison of primary biological aerosol above and below a tropical forest canopy using a dual channel fluorescence spectrometer, *Atmospheric Chemistry and Physics*, 10, 4453-4466, 10.5194/acp-10-4453-2010, 2010.
- Gorbushina, A. A. and Broughton, W. J.: Microbiology of the Atmosphere-Rock Interface: How Biological Interactions and Physical Stresses Modulate a Sophisticated Microbial Ecosystem, in: *Annu. Rev. Microbiol.*, Annual Review of Microbiology, 431-450, 2009.
- Grienenberger, E., Besseau, S., Geoffroy, P., Debayle, D., Heintz, D., Lapierre, C., Pollet, B., Heitz, T. and Legrand, M.: A BAHD acyltransferase is expressed in the tapetum of Arabidopsis anthers and is involved in the synthesis of hydroxycinnamoyl spermidines, *Plant J.*, 58, 246-259, 10.1111/j.1365-313X.2008.03773.x, 2009.
- Griffiths, P. T., Borlace, J. S., Gallimore, P. J., Kalberer, M., Herzog, M. and Pope, F. D.: Hygroscopic growth and cloud activation of pollen: a laboratory and modelling study, *Atmospheric Science Letters*, 13, 289-295, 10.1002/asl.397, 2012.



- Hairston, P. P., Ho, J. and Quant, F. R.: Design of an instrument for real-time detection of bioaerosols using simultaneous measurement of particle aerodynamic size and intrinsic fluorescence, *Journal of Aerosol Science*, 28, 471-482, 1997.
- Harris, P. J. and Hartley, R. D.: Phenolic constituents of the cell-walls of *Monocotyledons*, *Biochemical Systematics and Ecology*, 8, 153-160, 10.1016/0305-1978(80)90008-3, 1980.
- Hawe, A., Sutter, M. and Jiskoot, W.: Extrinsic fluorescent dyes as tools for protein characterization, *Pharmaceutical Research*, 25, 1487-1499, 10.1007/s11095-007-9516-9, 2008.
- Healy, D. A., O'Connor, D. J. and Sodeau, J. R.: Measurement of the particle counting efficiency of the "Waveband Integrated Bioaerosol Sensor" model number 4 (WIBS-4), *Journal of Aerosol Science*, 47, 94-99, 10.1016/j.jaerosci.2012.01.003, 2012.
- Herbrich, S., Gehder, M., Krull, R. and Gericke, K. H.: Label-Free Spatial Analysis of Free and Enzyme-Bound NAD(P)H in the Presence of High Concentrations of Melanin, *Journal of Fluorescence*, 22, 349-355, 10.1007/s10895-011-0965-5, 2012.
- Hill, S. C., Pinnick, R. G., Niles, S., et al.: Real-time measurement of fluorescence spectra from single airborne biological particles, *Field Anal. Chem. Technol.*, 3, 221-239, 1999.
- Hill, S. C., Mayo, M. W. and Chang, R. K.: Fluorescence of bacteria, pollens, and naturally occurring airborne particles: excitation/emission spectra Army report, ARL-TR-4722, 2009.
- Hipkins, V. D., Krutovskii, K. V. and Strauss, S. H.: Organelle genomes in conifers: Structure, evolution, and diversity, *Forest Genetics*, 1, 179-189, 1994.
- Ho, J.: Future of biological aerosol detection, *Anal. Chim. Acta*, 457, 125-148, 2002.
- Hoose, C., Kristjansson, J. E. and Burrows, S. M.: How important is biological ice nucleation in clouds on a global scale?, *Environ. Res. Lett.*, 5, 10.1088/1748-9326/5/2/024009, 2010.
- Hoose, C. and Möhler, O.: Heterogeneous ice nucleation on atmospheric aerosols: a review of results from laboratory experiments, *Atmospheric Chemistry and Physics*, 12, 9817-9854, 10.5194/acp-12-9817-2012, 2012.
- Hoque, E. and Remus, G.: Natural UV-screening mechanisms of Norway spruce (*Picea abies* L Karst) needles, *Photochem. Photobiol.*, 69, 177-192, 10.1111/j.1751-1097.1999.tb03272.x, 1999.
- Huffman, J. A., Treutlein, B. and Pöschl, U.: Fluorescent biological aerosol particle concentrations and size distributions measured with an Ultraviolet Aerodynamic Particle Sizer (UV-APS) in Central Europe, *Atmospheric Chemistry and Physics*, 10, 3215-3233, 2010.
- Huffman, J. A., Sinha, B., Garland, R. M., Snee-Pollmann, A., Gunthe, S. S., Artaxo, P., Martin, S. T., Andreae, M. O. and Pöschl, U.: Biological aerosol particle concentrations and size distributions measured in pristine tropical rainforest air during AMAZE-08, *Atmos. Chem. Phys.*, 12, 25181-25236, 2012.
- Huffman, J. A., Pöhlker, C., Prenni, A. J., et al.: High concentrations of biological aerosol particles and ice nuclei during and after rain, *Atmos. Chem. Phys. Discuss.*, 13, 1767-1793, 10.5194/acpd-13-1767-2013, 2013.
- Hutzler, P., Fischbach, R., Heller, W., Jungblut, T. P., Reuber, S., Schmitz, R., Veit, M., Weissenböck, G. and Schnitzler, J. P.: Tissue localization of phenolic compounds in plants by confocal laser scanning microscopy, *Journal of Experimental Botany*, 49, 953-965, 10.1093/jexbot/49.323.953, 1998.
- Jacobs, J. F., Koper, G. J. M. and Ursem, W. N. J.: UV protective coatings: A botanical approach, *Progress in Organic Coatings*, 58, 166-171, 10.1016/j.porgcoat.2006.08.023, 2007.

Jeys, T. H., Herzog, W. D., Hybl, J. D., Czerwinski, R. N. and Sanchez, A.: Advanced trigger development, *Linc. Lab. J.*, 17, 29-62, 2007.

Kalman, E. L., Winquist, F. and Lundstrom, I.: A new pollen detection method based on an electronic nose, *Atmospheric Environment*, 31, 1715-1719, 10.1016/s1352-2310(96)00313-5, 1997.

Kanaani, H., Hargreaves, M., Smith, J., Ristovski, Z., Agranovski, V. and Morawska, L.: Performance of UVAPS with respect to detection of airborne fungi, *Journal of Aerosol Science*, 39, 175-189, 10.1016/j.jaerosci.2007.10.007, 2008.

Kano, H. and Hamaguchi, H. O.: Vibrational imaging of a single pollen grain by ultrabroadband multiplex coherent anti-stokes Raman scattering microspectroscopy, *Chem. Lett.*, 35, 1124-1125, 10.1246/cl.2006.1124, 2006.

Kaye, P. H., Stanley, W. R., Hirst, E., Foot, E. V., Baxter, K. L. and Barrington, S. J.: Single particle multichannel bio-aerosol fluorescence sensor, *Optics Express*, 13, 3583-3593, 2005.

Kellogg, C. A. and Griffin, D. W.: Aerobiology and the global transport of desert dust, *Trends in Ecology & Evolution*, 21, 638-644, 10.1016/j.tree.2006.07.004, 2006.

Kiselev, D., Bonacina, L. and Wolf, J.-P.: Individual bioaerosol particle discrimination by multi-photon excited fluorescence, *Optics Express*, 19, 24516-24521, 2011.

Kopczynski, K., Kwasny, M., Mierczyk, Z. and Zawadzki, Z.: Laser induced fluorescence system for detection of biological agents: European project FABIOLA, *Proc. SPIE - Int. Soc. Opt. Eng.*, 5954, 595405-595401-595405-595412, 10.1117/12.623013, 2005.

Kuehn, M. J. and Kesty, N. C.: Bacterial outer membrane vesicles and the host-pathogen interaction, *Genes & Development*, 19, 2645-2655, 10.1101/gad.1299905, 2005.

Kuparinen, A., Katul, G., Nathan, R. and Schurr, F. M.: Increases in air temperature can promote wind-driven dispersal and spread of plants, *Proc. R. Soc. B-Biol. Sci.*, 276, 3081-3087, 10.1098/rspb.2009.0693, 2009.

Lakowicz, J. R.: *Principles of Fluorescence Spectroscopy*, Plenum publishers New York, 1999.

Lang, M., Stober, F. and Lichtenthaler, H. K.: Fluorescence emission-spectra of plant-leaves and plant constituents, *Radiat. Environ. Biophys.*, 30, 333-347, 10.1007/bf01210517, 1991.

Li, Z. H., Wang, Q. A., Ruan, X. A., Pan, C. D. and Jiang, D. A.: Phenolics and Plant Allelopathy, *Molecules*, 15, 8933-8952, 10.3390/molecules15128933, 2010.

Lichtenthaler, H. K. and Schweiger, J.: Cell wall bound ferulic acid, the major substance of the blue-green fluorescence emission of plants, *J. Plant Physiol.*, 152, 272-282, 1998.

Mahowald, N., Ward, D. S., Kloster, S., Flanner, M. G., Heald, C. L., Heavens, N. G., Hess, P. G., Lamarque, J.-F. and Chuang, P. Y.: Aerosol Impacts on Climate and Biogeochemistry, in: *Annual Review of Environment and Resources*, Vol 36, edited by: Gadgil, A. and Liverman, D. M., *Annual Review of Environment and Resources*, 45-74, 2011.

McCauley, D. E., Sundby, A. K., Bailey, M. F. and Welch, M. E.: Inheritance of chloroplast DNA is not strictly maternal in *Silene vulgaris* (Caryophyllaceae): Evidence from experimental crosses and natural populations, *American Journal of Botany*, 94, 1333-1337, 10.3732/ajb.94.8.1333, 2007.

Miko, I.: Non-nuclear Genes and Their Inheritance, *Nature Education*, 1, 2008.

Mitsumoto, K., Yabusaki, K. and Aoyagi, H.: Classification of pollen species using autofluorescence image analysis, *Journal of Bioscience and Bioengineering*, 107, 90-94, 10.1016/j.jbiosc.2008.10.001, 2009.

- Mitsumoto, K., Yabusaki, K., Kobayashi, K. and Aoyagi, H.: Development of a novel real-time pollen-sorting counter using species-specific pollen autofluorescence, *Aerobiologia*, 26, 99-111, 10.1007/s10453-009-9147-1, 2010.
- Moberg, L., Robertsson, G. and Karlberg, B.: Spectrofluorimetric determination of chlorophylls and pheopigments using parallel factor analysis, *Talanta*, 54, 161-170, 2001.
- Möhler, O., DeMott, P. J., Vali, G. and Levin, Z.: Microbiology and atmospheric processes: the role of biological particles in cloud physics, *Biogeosciences*, 4, 1059-1071, 2007.
- Molgaard, P. and Ravn, H.: Evolutionary aspects of caffeoyl ester distribution in Dicotyledons, *Phytochemistry*, 27, 2411-2421, 10.1016/0031-9422(88)87005-5, 1988.
- Morris, C. E., Sands, D. C., Vinatzer, B. A., Glaux, C., Guilbaud, C., Buffiere, A., Yan, S. C., Dominguez, H. and Thompson, B. M.: The life history of the plant pathogen *Pseudomonas syringae* is linked to the water cycle, *Isme J.*, 2, 321-334, 10.1038/ismej.2007.113, 2008.
- Mularczyk-Oliwa, M., Bombalska, A., Kaliszewski, M., Wlodarski, M., Kopczynski, K., Kwasny, M., Szpakowska, M. and Trafny, E. A.: Comparison of fluorescence spectroscopy and FTIR in differentiation of plant pollens, *Spectroc. Acta Pt. A-Molec. Biomolec. Spectr.*, 97, 246-254, 10.1016/j.saa.2012.05.063, 2012.
- Nepi, M. and Franchi, G. G.: Cytochemistry of mature angiosperm pollen, *Plant Systematics and Evolution*, 222, 45-62, 10.1007/bf00984095, 2000.
- O'Connor, D. J., Iacopino, D., Healy, D. A., O'Sullivan, D. and Sodeau, J. R.: The intrinsic fluorescence spectra of selected pollen and fungal spores, *Atmospheric Environment*, 45, 6451-6458, 10.1016/j.atmosenv.2011.07.044, 2011.
- Pacini, E.: From anther and pollen ripening to pollen presentation, *Plant Systematics and Evolution*, 222, 19-43, 10.1007/bf00984094, 2000.
- Pacini, E. and Hesse, M.: Pollenkitt - its composition, forms and functions, *Flora*, 200, 399-415, 10.1016/j.flora.2005.02.006, 2005.
- Pan, Y.-L., Hill, S. C., Pinnick, R. G., Huang, H., Bottiger, J. R. and Chang, R. K.: Fluorescence spectra of atmospheric aerosol particles measured using one or two excitation wavelengths: Comparison of classification schemes employing different emission and scattering results, *Optics Express*, 18, 12436-12457, 10.1364/oe.18.012436, 2010.
- Pan, Y.-L., Hill, S. C., Pinnick, R. G., House, J. M., Flagan, R. C. and Chang, R. K.: Dual-excitation-wavelength fluorescence spectra and elastic scattering for differentiation of single airborne pollen and fungal particles, *Atmospheric Environment*, 45, 1555-1563, 10.1016/j.atmosenv.2010.12.042, 2011.
- Pan, Y. L., Eversole, J. D., Kaye, P. H., et al.: Bio-aerosol fluorescence - Detecting and characterising bio-aerosols via UV light-induced fluorescence spectroscopy, in: *Optics of Biological Particles*, edited by: Hoekstra, A., Maltsev, V. and Videen, G., NATO Science Series, Human Press / Springer, Dordrecht, 63-163, 2007.
- Pan, Y. L., Pinnick, R. G., Hill, S. C. and Chang, R. K.: Particle-Fluorescence Spectrometer for Real-Time Single-Particle Measurements of Atmospheric Organic Carbon and Biological Aerosol, *Environmental Science & Technology*, 43, 429-434, 10.1021/es801544y, 2009.
- Phillips, L.: Application of fluorescence microscopy to problem of derived pollen in British Pleistocene deposits, *New Phytologist*, 71, 755-&, 10.1111/j.1469-8137.1972.tb01286.x, 1972.
- Piffanelli, P., Ross, J. H. E. and Murphy, D. J.: Biogenesis and function of the lipidic structures of pollen grains, *Sex. Plant Reprod.*, 11, 65-80, 10.1007/s004970050122, 1998.

- Pinnick, R. G., Hill, S. C., Pan, Y. L. and Chang, R. K.: Fluorescence spectra of atmospheric aerosol at Adelphi, Maryland, USA: measurement and classification of single particles containing organic carbon, *Atmospheric Environment*, 38, 1657-1672, 10.1016/j.atmosenv.2003.11.017, 2004.
- Pinnick, R. G., Fernandez, E., Rosen, J. M., Hill, S. C., Wang, Y. and Pan, Y. L.: Fluorescence spectra and elastic scattering characteristics of atmospheric aerosol in Las Cruces, New Mexico, USA: Variability of concentrations and possible constituents and sources of particles in various spectral clusters, *Atmospheric Environment*, 65, 195-204, 2013.
- Pöhlker, C., Huffman, J. A. and Pöschl, U.: Autofluorescence of atmospheric bioaerosols - fluorescent biomolecules and potential interferences, *Atmos. Meas. Tech.*, 5, 37-71, 10.5194/amt-5-37-2012, 2012.
- Pöhlker, C., Huffman, J. A., Förster, J.-D. and Pöschl, U.: Autofluorescence of atmospheric bioaerosols – water influence on pollen morphology and autofluorescence. *in preparation*, 2013.
- Pope, F. D.: Pollen grains are efficient cloud condensation nuclei, *Environ. Res. Lett.*, 5, 10.1088/1748-9326/5/4/044015, 2010.
- Pöschl, U.: Atmospheric aerosols: Composition, transformation, climate and health effects, *Angewandte Chemie-International Edition*, 44, 7520-7540, 10.1002/anie.200501122, 2005.
- Pöschl, U., Martin, S. T., Sinha, B., et al.: Rainforest Aerosols as Biogenic Nuclei of Clouds and Precipitation in the Amazon, *Science*, 329, 1513-1516, 10.1126/science.1191056, 2010.
- Pragowski, J.: Effects of pre-treatment and embedding media on shape of pollen grains, *Rev. Palaeobot. Palynology*, 10, 203-&, 10.1016/0034-6667(70)90003-5, 1970.
- Prahl, A. K., Springstube, H., Grumbach, K. and Wiermann, R.: Studies on sporopollenin biosynthesis - the effect of inhibitor of carotenoid biosynthesis on sporopollenin accumulation, *Z.Naturforsch.(C)*, 40, 621-626, 1985.
- Prenni, A. J., Petters, M. D., Kreidenweis, S. M., Heald, C. L., Martin, S. T., Artaxo, P., Garland, R. M., Wollny, A. G. and Pöschl, U.: Relative roles of biogenic emissions and Saharan dust as ice nuclei in the Amazon basin, *Nature Geoscience*, 2, 401-404, 10.1038/ngeo517, 2009.
- Prenni, A. J., Tobo, Y., Garcia, E., et al.: The impact of rain on ice nuclei populations at a forested site in Colorado, *Geophys. Res. Lett.*, 40, 227-231, 10.1029/2012gl053953, 2013.
- Pummer, B. G., Bauer, H., Bernardi, J., Bleicher, S. and Grothe, H.: Suspendable macromolecules are responsible for ice nucleation activity of birch and conifer pollen, *Atmospheric Chemistry and Physics*, 12, 2541-2550, 10.5194/acp-12-2541-2012, 2012.
- Ranzato, M., Taylor, P. E., House, J. M., Flagan, R. C., LeCun, Y. and Perona, P.: Automatic recognition of biological particles in microscopic images, *Pattern Recognition Letters*, 28, 31-39, 2007.
- Razmovski, V., O'Meara, T. J., Taylor, D. J. M. and Tovey, E. R.: A new method for simultaneous immunodetection and morphologic identification of individual sources of pollen allergens, *Journal of Allergy and Clinical Immunology*, 105, 725-731, 10.1067/mai.2000.105222, 2000.
- Reid, C. E. and Gamble, J. L.: Aeroallergens, Allergic Disease, and Climate Change: Impacts and Adaptation, *EcoHealth*, 6, 458-470, 10.1007/s10393-009-0261-x, 2009.
- Reitsma, T.: Size modification of recent pollen grains under different treatments, *Rev. Palaeobot. Palynology*, 9, 175-&, 10.1016/0034-6667(69)90003-7, 1969.
- Ronneberger, O., Schultz, E. and Burkhardt, H.: Automated pollen recognition using 3D volume images from fluorescence microscopy, *Aerobiologia*, 18, 107-115, 10.1023/a:1020623724584, 2002.

- Roshchina, V. V., Melnikova, E. V. and Kovaleva, L. V.: Changes in fluorescence during development of the male gametophyte, *Russ. J. Plant Physiol.*, 44, 36-44, 1997.
- Roshchina, V. V.: Autofluorescence of plant secreting cells as a biosensor and bioindicator reaction, *Journal of Fluorescence*, 13, 403-420, 2003.
- Roshchina, V. V., Yashin, V. A. and Kononov, A. V.: Autofluorescence of developing plant vegetative microspores studied by confocal microscopy and microspectrofluorimetry, *Journal of Fluorescence*, 14, 745-750, 2004.
- Roshchina, V. V.: *Fluorescing world of plant secreting cells*, Science Publishers, 2008.
- Roshchina, V. V.: Vital Autofluorescence: Application to the Study of Plant Living Cells, *Int. J. Spectrosc.*, 124672 (124614 pp.)-124672 (124614 pp.)124672 (124614 pp.), 10.1155/2012/124672, 2012.
- Roulston, T. H. and Cane, J. H.: Pollen nutritional content and digestibility for animals, *Plant Systematics and Evolution*, 222, 187-209, 10.1007/bf00984102, 2000.
- Rozema, J., Broekman, R. A., Blokker, P., Meijkamp, B. B., de Bakker, N., van de Staaij, J., van Beem, A., Ariese, F. and Kars, S. M.: UV-B absorbance and UV-B absorbing compounds (para-coumaric acid) in pollen and sporopollenin: the perspective to track historic UV-B levels, *J. Photochem. Photobiol. B-Biol.*, 62, 108-117, 10.1016/s1011-1344(01)00155-5, 2001.
- Satterwhite, M. B.: Spectral Luminescence Of Plant Pollen, *Geoscience and Remote Sensing Symposium*, 1990. IGARSS '90. 'Remote Sensing Science for the Nineties', 10th Annual International, 1990, 1945-1948,
- Satterwhite, M. B.: Luminescence of some airborne plant materials, *Advances in Laser Remote Sensing for Terrestrial and Oceanographic Applications*, edited by: Narayanan, R. M. and Kalshoven, J. E., *Spie - Int Soc Optical Engineering*, Bellingham, 52-62 pp., 1997.
- Scharring, S., Brandenburg, A., Breitfuss, G., et al.: Online monitoring of airborne allergenic particles (OMNIBUSS), in: *Biophotonics*, edited by: Popp, J. and Strehle, M., *WILEY-VCH*, Weinheim, 31-87, 2006.
- Scheifinger, H., Belmonte, J., Buters, J., et al.: Monitoring, Modelling and Forecasting of the Pollen Season, in: *Allergenic Pollen*, edited by: Sofiev, M. and Bergmann, K.-C., *Springer Netherlands*, 71-126, 2013.
- Schulte, F., Maeder, J., Kroh, L. W., Panne, U. and Kneipp, J.: Characterization of Pollen Carotenoids with in situ and High-Performance Thin-Layer Chromatography Supported Resonant Raman Spectroscopy, *Anal. Chem.*, 81, 8426-8433, 10.1021/ac901389p, 2009.
- Scott, R. J.: Pollen exine - the sporopollenin enigma and the physics of pattern, *Molecular and Cellular Aspects of Plant Reproduction*, edited by: Scott, R. J. and Stead, A. D., 49-81 pp., 1994.
- Shiraiwa, M., Selzle, K., Yang, H., Sosedova, Y., Ammann, M. and Pöschl, U.: Multiphase Chemical Kinetics of the Nitration of Aerosolized Protein by Ozone and Nitrogen Dioxide, *Environmental Science & Technology*, 46, 6672-6680, 10.1021/es300871b, 2012.
- Siljamo, P., Sofiev, M., Severova, E., Ranta, H., Kukkonen, J., Polevova, S., Kubin, E. and Minin, A.: Sources, impact and exchange of early-spring birch pollen in the Moscow region and Finland, *Aerobiologia*, 24, 211-230, 10.1007/s10453-008-9100-8, 2008.
- Sivaprakasam, V., Huston, A. L., Scotto, C. and Eversole, J. D.: Multiple UV wavelength excitation and fluorescence of bioaerosols, *Optics Express*, 12, 4457-4466, 2004.
- Sivaprakasam, V., Pletcher, T., Tucker, J. E., Huston, A. L., McGinn, J., Keller, D. and Eversole, J. D.: Classification and selective collection of individual aerosol particles using laser-induced fluorescence, *Applied Optics*, 48, B126-B136, 2009.

Skjoth, C. A., Orby, P. V., Becker, T., et al.: Identifying urban sources as cause of elevated grass pollen concentrations using GIS and remote sensing, *Biogeosciences*, 10, 541-554, 10.5194/bg-10-541-2013, 2013.

Sofiev, M., Siljamo, P., Ranta, H. and Rantio-Lehtimäki, A.: Towards numerical forecasting of long-range air transport of birch pollen: theoretical considerations and a feasibility study, *Int. J. Biometeorol.*, 50, 392-402, 10.1007/s00484-006-0027-x, 2006.

Sofiev, M., Bousquet, J., Linkosalo, T., Ranta, H., Rantio-Lehtimäki, A., Siljamo, P., Valovirta, E. and Damialis, A.: Pollen, Allergies and Adaptation, *Biometeorology for Adaptation to Climate Variability and Change*, edited by: Ebi, K. L., Burton, I. and McGregor, G. R., Springer, Po Box 17, 3300 Aa Dordrecht, Netherlands, 75-106 pp., 2009.

Sufra, S., Dellepiane, G., Masetti, G. and Zerbi, G.: Resonance Raman-spectrum of beta-carotene, *Journal of Raman Spectroscopy*, 6, 267-272, 10.1002/jrs.1250060602, 1977.

Taiz, L. and Zeiger, E.: *Plant Physiology*, Sinauer Associates, Incorporated, 2010.

Taylor, P. E., Jacobson, K. W., House, J. M. and Glovsky, M. M.: Links between pollen, atopy and the asthma epidemic, *International Archives of Allergy and Immunology*, 144, 162-170, 10.1159/000103230, 2007.

Toprak, E. and Schnaiter, M.: Fluorescent biological aerosol particles measured with the Waveband Integrated Bioaerosol Sensor WIBS-4: laboratory tests combined with a one year field, *Atmos. Chem. Phys.*, 13, 225-243, 2013.

Traidl-Hoffmann, C., Kasche, A., Menzel, A., Jakob, T., Thiel, M., Ring, J. and Behrendt, H.: Impact of pollen on human health: More than allergen carriers?, *International Archives of Allergy and Immunology*, 131, 1-13, 10.1159/000070428, 2003.

Tylianakis, J. M., Didham, R. K., Bascompte, J. and Wardle, D. A.: Global change and species interactions in terrestrial ecosystems, *Ecology Letters*, 11, 1351-1363, 10.1111/j.1461-0248.2008.01250.x, 2008.

von Blohn, N., Mitra, S. K., Diehl, K. and Borrmann, S.: The ice nucleating ability of pollen: Part III: New laboratory studies in immersion and contact freezing modes including more pollen types, *Atmospheric Research*, 78, 182-189, 10.1016/j.atmosres.2005.03.008, 2005.

Wang, Q., Nakamura, S., Lu, S., Xiu, G., Nakajima, D., Suzuki, M., Sakamoto, K. and Miwa, M.: Release behavior of small sized daughter allergens from *Cryptomeria japonica* pollen grains during urban rainfall event, *Aerobiologia*, 28, 71-81, 10.1007/s10453-011-9212-4, 2012.

Welschmeyer, N. A.: Fluorometric analysis of chlorophyll a in the presence of chlorophyll b and pheopigments, *Limnol. Oceanogr.*, 39, 1985-1992, 1994.

Wiermann, R. and Vieth, K.: Outer pollen wall, an important accumulation site for flavonoids, *Protoplasma*, 118, 230-233, 1983.

Willemsse, M. T.: Changes in autofluorescence of pollen wall during microsporogenesis and chemical treatments, *Acta Bot. Neerl.*, 21, 1-&, 1972.

Wilson, A. F., Novey, H. S., Berke, R. A. and Surprena, E.I.: Deposition of inhaled pollen and pollen extract in human airways, *New England Journal of Medicine*, 288, 1056-1058, 10.1056/nejm197305172882006, 1973.

Włodarski, M., Kaliszewski, M., Kwasny, M., Kopczynski, K., Zawadzki, Z., Mierczyk, Z., Mlyńczak, J., Trafny, E. and Szpakowska, M.: Fluorescence excitation-emission matrices of selected biological materials, in: *Optically Based Biological and Chemical Detection for Defence III*, edited by: Carrano, J. C. and Zukauskas, A., Proceedings of the Society of Photo-Optical Instrumentation Engineers (Spie), Spie-Int Soc Optical Engineering, Bellingham, U18-U29, 2006.

Wu, C. H. and Warren, H. L.: Induced autofluorescence in fungi and its correlation with viability - Potential applications of fluorescence microscopy, *Phytopathology*, 74, 1353-1358, 1984a.

Wu, C. H. and Warren, H. L.: Natural autofluorescence in fungi, and its correlation with viability, *Mycologia*, 76, 1049-1058, 1984b.

Yeloff, D. and Hunt, C.: Fluorescence microscopy of pollen and spores: a tool for investigating environmental change, *Rev. Palaeobot. Palynology*, 133, 203-219, 10.1016/j.revpalbo.2004.10.002, 2005.

Zhang, Y., Isukapalli, S. S., Bielory, L. and Georgopoulos, P. G.: Bayesian analysis of climate change effects on observed and projected airborne levels of birch pollen, *Atmospheric Environment*, 68, 64-73, 2013.

**Table A1.** List of frequently used acronyms.

Acronym	Description
BP	band-pass
BSA	bovine serum albumin
BWA	biological warfare agent
CCD	charge-coupled device
CCN	cloud condensation nuclei
DAPI	4',6-diamidino-2-phenylindole
DNA	deoxyribonucleic acid
EEM	excitation-emission-matrix
FBAP	fluorescent biological aerosol particles
FM	fluorescence microscopy
FS	fluorescence spectroscopy
FWHM	full width half max
GFP	green fluorescent protein
IN	ice nuclei
INA	ice nucleation activity
LIF	light/laser induced fluorescence
NF	normalization factor
OVA	ovalbumin
PAH	polycyclic aromatic hydrocarbons
PBAP	primary biological aerosol particles
PC	principal component
PCA	principal component analysis
RNA	ribonucleic acid
UV	ultraviolet
UV-APS	ultraviolet aerodynamic particle sizer
WIBS	wide issue bioaerosol sensor



**Table 1.** Overview of pollen species analyzed in this study. Pollen grain diameters obtained from [a] product information from pollen vendor Allergon AB, [b] microscopy measurements in this study (Sect. 2.2), or [c] database: <http://www.polleninfo.org> (February 23th 2013) (SD = standard deviation). Axis aspect ratios are measured for some species in this study (Sect. 2.2). Last columns indicate if fluorescence microscopy (FM) and fluorescence spectroscopy (FS) data for certain species are shown in this manuscript.

#	Name		Family	Pollination method	Source/ Provider	Size [ $\mu$ m] Mean $\pm$ SD	Aspect ratio major/minor axis	Analysis	
	Latin	Common						FM	FS
1	<i>Agrostis stolonifera</i>	Creeping bentgrass	Poaceae	anemophilous	Allergon AB	23 $\pm$ 1 <sup>[a]</sup>	-	no	yes
2	<i>Alnus glutinosa</i>	Black alder	Betulaceae	anemophilous	Allergon AB	24 $\pm$ 2 <sup>[a]</sup>	-	no	yes
3	<i>Alnus incana</i>	Grey/speckled alder	Betulaceae	anemophilous	Allergon AB	24 $\pm$ 1 <sup>[a]</sup>	-	no	yes
4	<i>Ambrosia artemisiifolia</i>	Common ragweed	Asteraceae	anemophilous	Polyscience, Allergon AB	21 $\pm$ 1 <sup>[a]</sup>	-	yes	yes
5	<i>Artemisia tridentata</i>	Giant sage/sagebrush	Asteraceae	anemophilous	Sigma Aldrich	21 $\pm$ 3 <sup>[b]</sup>	25/18	yes	yes
6	<i>Artemisia vulgaris</i>	Common mugwort	Asteraceae	anemophilous	Allergon AB	19 $\pm$ 1 <sup>[a]</sup> 18 $\pm$ 2 <sup>[b]</sup>	20/17	yes	yes
7	<i>Betula fontinalis</i>	Waterbirch	Betulaceae	anemophilous	Sigma Aldrich	27 $\pm$ 3 <sup>[b]</sup>	30/26	yes	yes
8	<i>Betula pendula</i>	White birch	Betulaceae	anemophilous	Allergon AB	24 $\pm$ 1 <sup>[a]</sup> 24 $\pm$ 3 <sup>[b]</sup>	26/23	no	yes
9	<i>Brassica napus</i>	Rape	Brassicaceae	entomophilous	Allergon AB	28 $\pm$ 1 <sup>[a]</sup>	-	no	yes
10	<i>Broussonetia papyrifera</i>	Paper mulberry	Moraceae	anemophilous	Thermo scientific, Polyscience	12 $\pm$ 2 <sup>[b]</sup>	14/11	yes	yes
11	<i>Carpinus betulus</i>	Hornbeam	Betulaceae	anemophilous	Allergon AB	35 $\pm$ 2 <sup>[a]</sup>	-	yes	yes
12	<i>Corylus avellana</i>	Common hazel	Betulaceae	anemophilous	Allergon AB	23 $\pm$ 1 <sup>[a]</sup>	-	no	yes
13	<i>Cynodon dactylon</i>	Bermuda grass	Poaceae	anemophilous	Sigma Aldrich	25 $\pm$ 3 <sup>[b]</sup>	28/24	no	yes
14	<i>Juglans nigra</i>	Black walnut	Juglandaceae	anemophilous	Sigma Aldrich	37 $\pm$ 4 <sup>b</sup>	41/34	no	yes
15	<i>Lolium perenne</i>	Perennial ryegrass	Poaceae	anemophilous	Allergon AB	40 $\pm$ 3 <sup>[a]</sup>	-	yes	yes
16	<i>Matricaria chamomilla</i>	Chamomile	Asteraceae	entomophilous	Fresh collection	-	-	yes	no
17	<i>Olea europaea</i>	European olive	Oleaceae	anemophilous	Allergon AB	23 $\pm$ 1 <sup>[a]</sup>	-	no	yes
18	<i>Phleum pratense</i>	Timothy grass	Poaceae	anemophilous	Allergon AB	35 $\pm$ 2 <sup>[a]</sup> 34 $\pm$ 4 <sup>[b]</sup>	36/31	yes	yes
19	<i>Pinus sylvestris</i>	Scotch pine	Pinaceae	anemophilous	Allergon AB	51 $\pm$ 4 <sup>[a]</sup>	-	yes	yes
20	<i>Poa pratensis</i>	Kentucky bluegrass	Poaceae	anemophilous	Allergon AB	29 $\pm$ 2 <sup>[a]</sup>	-	no	yes
21	<i>Populus nigra italica</i>	Lombardy poplar	Salicaceae	anemophilous	Sigma Aldrich	25 $\pm$ 2 <sup>[b]</sup>	27/24	no	yes
22	<i>Populus tremuloides</i>	Aspen	Salicaceae	anemophilous	Sigma Aldrich	26 $\pm$ 3 <sup>[b]</sup>	29/24	yes	yes
23	<i>Quercus robur</i>	English oak	Fagaceae	anemophilous	Allergon AB	30 $\pm$ 1 <sup>[a]</sup>	-	yes	yes
24	<i>Rumex acetosa</i>	Common sorrel	Polygonaceae	anemophilous	Allergon AB	19 $\pm$ 2 <sup>[a]</sup>	-	no	yes
25	<i>Sambucus nigra</i>	Elder	Adoxaceae	entomophilous	Fresh collection	18 $\pm$ 1 <sup>[c]</sup>	-	no	yes
26	<i>Secale cereale</i>	Cultivated rye	Poaceae	anemophilous	Sigma Aldrich	48 $\pm$ 4 <sup>[b]</sup>	56/39	yes	yes
27	<i>Symphoricarpos albus</i>	Common snowberry	Caprifoliaceae	entomophilous	Fresh collection	-	-	yes	no

**Table 2.** Summary of fluorescence modes in EEMs of dry and native pollen with wavelength ranges and fluorophore assignment.

<b>Fluorescence mode</b>	<b>Maximum (<math>\lambda_{ex} / \lambda_{em}</math>) [nm]</b>	<b>Fluorophore</b>
A	~ 280 / 450	Phenolics
B	~ 360 / 450	Phenolics
C	~ 460 / 520	Carotenoids
D	~ 280 / 340	Protein
E	~ 350-650 / 675	Chlorophyll $\alpha$

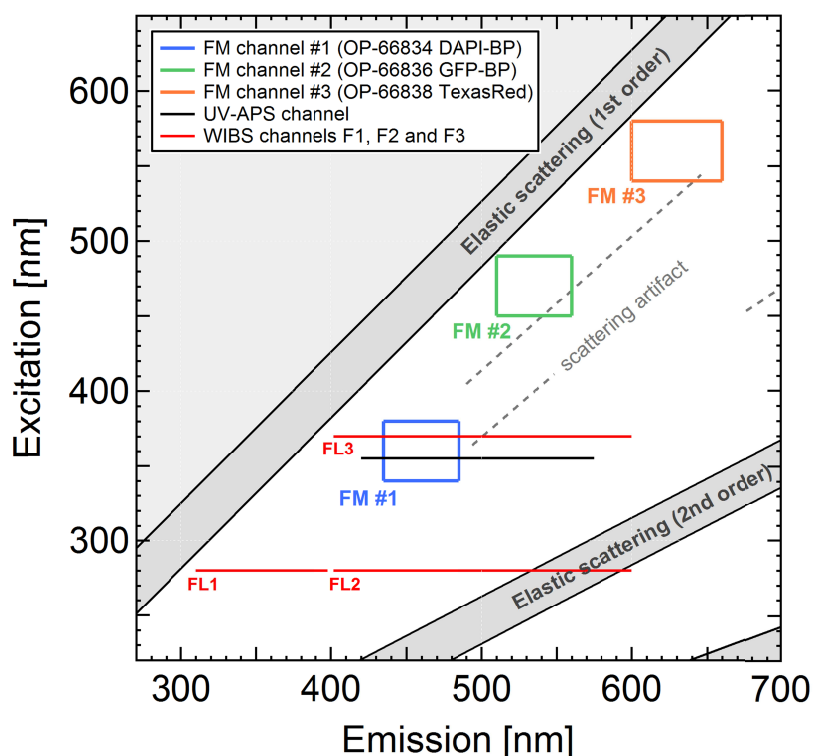


**Figure 1.** Conceptual EEM showing (a) Fluorescence data area (white), areas strongly influenced by elastic (i.e. Rayleigh) light scattering (grey diagonal bars), area without meaningful data (upper left triangle). Dashed lines indicate weak elastic light scattering, probably due to an instrumental artifact which occurs for all dry samples. (b) Operational range of commercially available bioaerosols detectors UV-APS and WIBS (Hairston et al., 1997; Foot et al., 2008). Length of individual lines indicates measured emission band for a certain excitation wavelength shown as sharp line. Instruments spectral specifications: UV-APS (single wavelength laser excitation,  $\lambda_{\text{ex}} = 355$  nm,  $\lambda_{\text{em}} = 420\text{-}575$  nm); WIBS (dual-wavelength Xe-lamp excitation,  $\lambda_{\text{ex},1} = 280$ ,  $\lambda_{\text{em},280} = 310\text{-}400$ ,  $400\text{-}600$ ;  $\lambda_{\text{ex},2} = 370$ ,  $\lambda_{\text{em},370} = 400\text{-}600$ ). (c) Spectral range of three fluorescence microscope (FM) channels used in this study. Spectral specifications of filters: DAPI-BP ( $\lambda_{\text{ex}} = 360/20$  nm,  $\lambda_{\text{Dichroic}} = 400$  nm,  $\lambda_{\text{Absorp}} = 460/25$  nm), GFP-BP ( $\lambda_{\text{ex}} = 470/20$ ,  $\lambda_{\text{Dichroic}} = 495$ ,  $\lambda_{\text{Absorp}} = 535/25$ ), TexasRed ( $\lambda_{\text{ex}} = 560/20$ ,  $\lambda_{\text{Dichroic}} = 595$ ,  $\lambda_{\text{Absorp}} = 630/30$ ). For comparison and further information refer to (Pöhlker et al., 2012; Andrade-Eiroa et al., 2013).

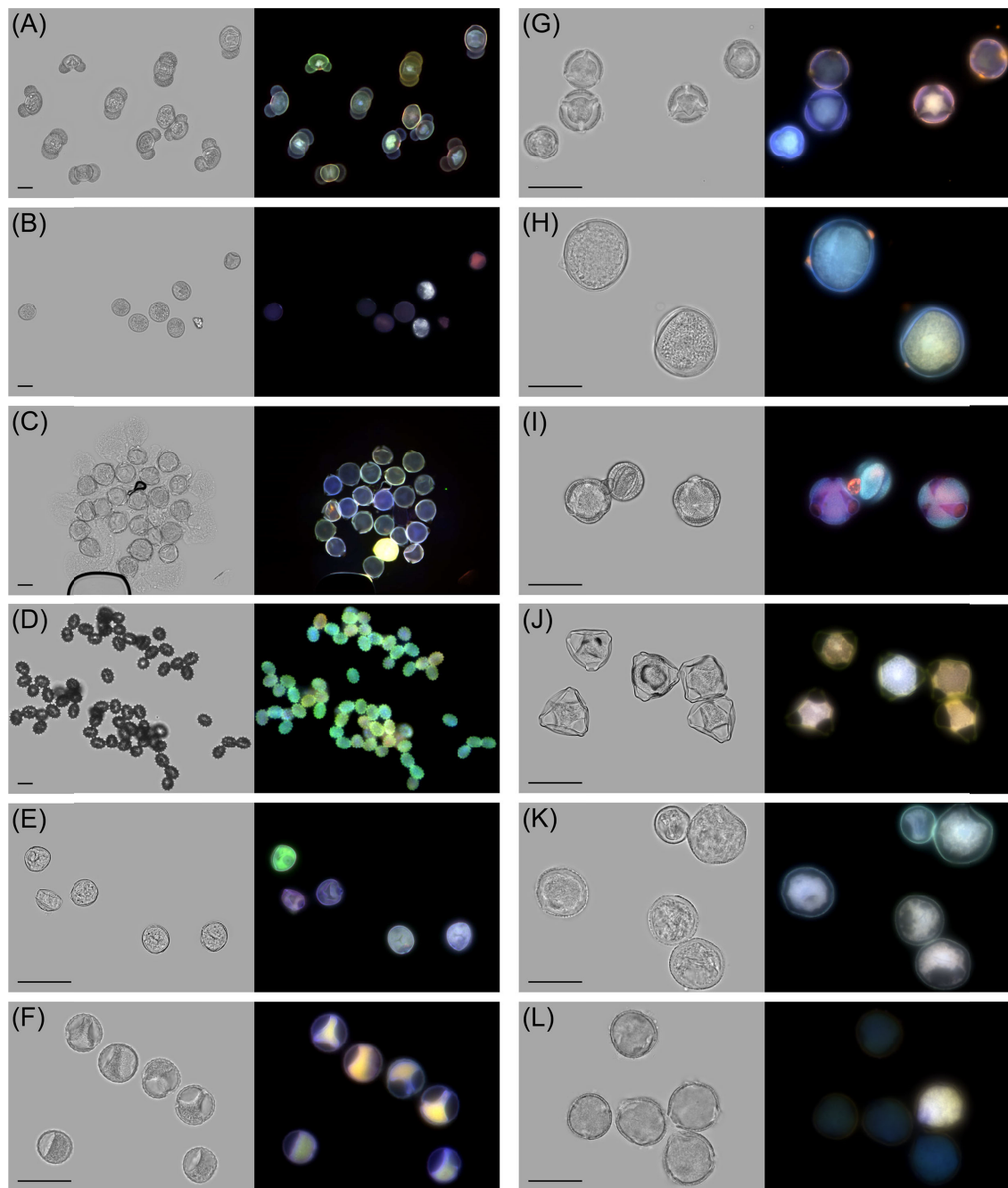


**Figure 2.** Overview panel with fluorescence microscopy images from 12 selected pollen species, shown in bright field (left) and fluorescence mode (right). Fluorescence mode images are displayed as overlay based on three fluorescence channels. Most pollen samples are prepared in moist state, few samples in dry state (see Sect. 2.2). Individual images show: (A) *Pinus sylvestris* in moist state; (B) *Phleum pretense*, moist; (C) *Symphoricarpos albus*, moist, pollen grains are burst due to osmotic pressure (Pöhlker et al., 2013); (D) *Matricaria chamomilla*, dry; (E) *Broussonetia papyrifera*, moist; (F) *Ambrosia artemissifolia*, dry; (G) *Artemisia vulgaris*, moist; (H) *Lolium perenne*, moist; (I) *Artemisia tridentata*, moist; (J) *Betula fontinalis*, in immersion oil; (K) *Populus tremuloides*, moist; (L) *Quercus robur*, moist. All images with focal plane through center of grains - only exception is *A. tridentata* with focal plane through upper part of cell wall. Scale bar = 30  $\mu$ m in all images.

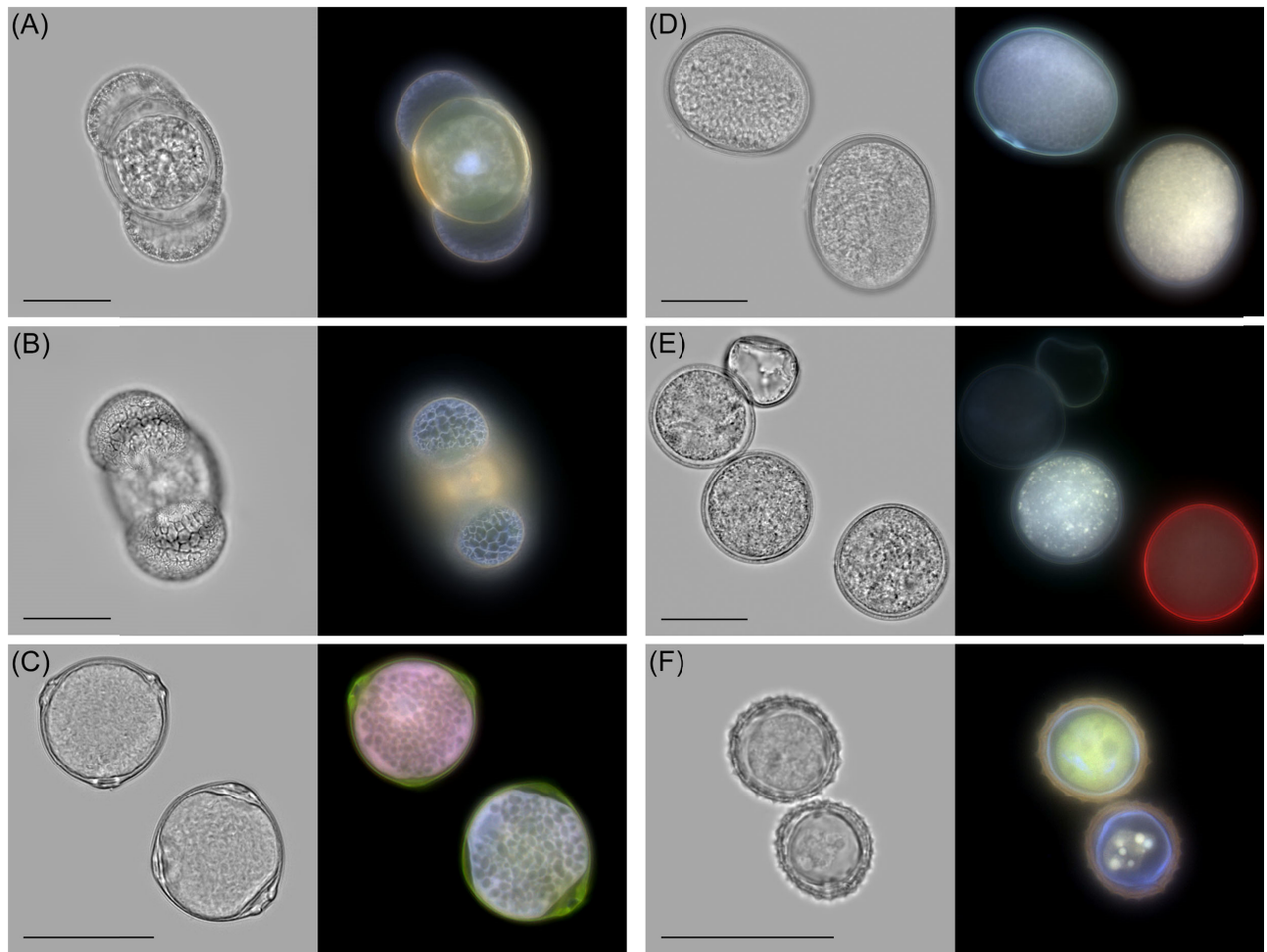


**Figure 3.** High resolution microscopy images of selected pollen species in bright field (left) and fluorescence mode (right). Fluorescence images shown as overlay of three channels. **(A)** *Pinus sylvestris*, moist, with focal plane through center of grain. Image shows red fluorescence from cell wall and bluish cytosolic emission (i.e. from vegetative nucleus). **(B)** *Pinus sylvestris*, moist, with focal plane through air bladders highlighting blue fluorescence from skeleton-like structure inside air bladders with thin reddish cell wall around them. **(C)** *Betula fontinalis*, moist, showing green fluorescence from cell wall and apertures. Also blue-to-red cytosolic emission contrasting with non-fluorescence starch granules. **(D)** *Secale cereale*, moist, showing homogeneous cytosolic fluorescence and thin bluish cell wall. **(E)** *Phleum pratense*, moist, highlighting diverse fluorescence properties without obvious differences in bright field image. **(F)** *Ambrosia artemisiifolia*, moist, with blue fluorescing intine and red fluorescing exine. Also cytosol and strong organelle fluorescence. Scale bar = 30  $\mu\text{m}$  in all images.

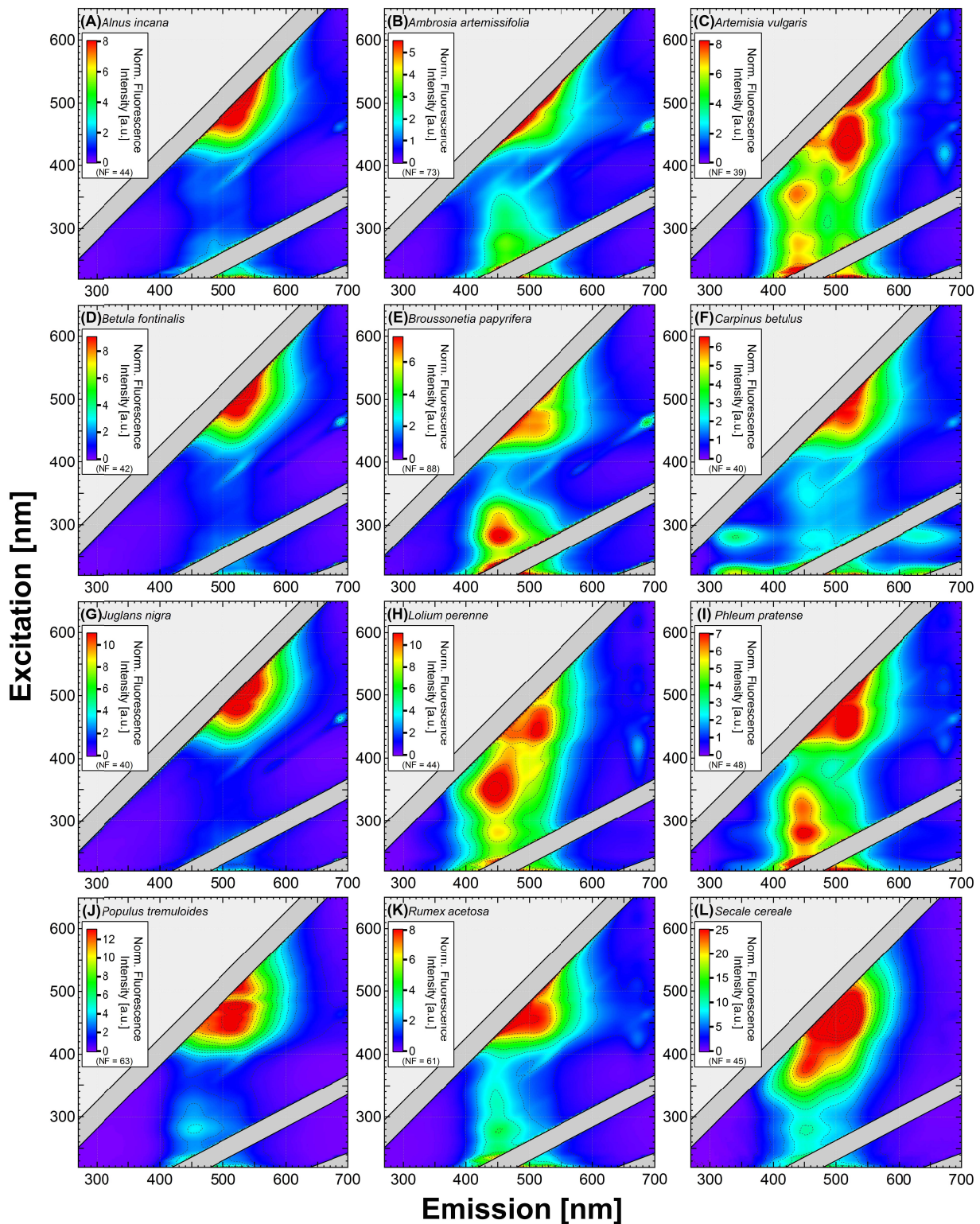


**Figure 4.** Excitation-emission-matrices (EEMs) of selected pollen species in dry and native state. Intensity color code has been adjusted to fluorescence intensity of individual samples. All EEMs are normalized as described in Pöhlker et al. (2012) and a normalization factor (NF) is reported in each panels. EEMs for further pollen species can be found in supplementary Fig. S2.

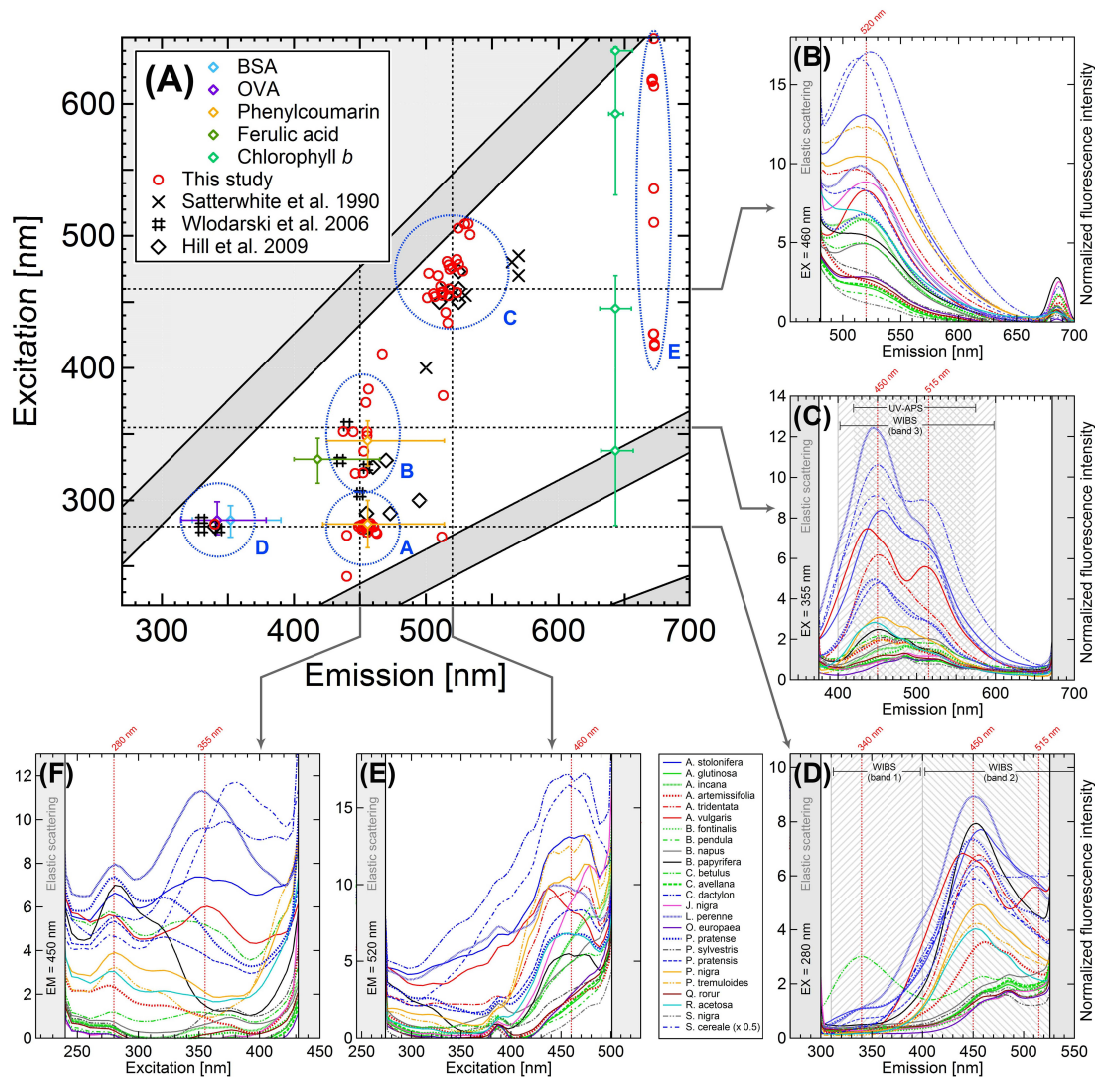


**Figure 5.** Overview figure displaying autofluorescence *fingerprint* of dry and native pollen. (A) EEM summarizes spectral locations of fluorescence modes for all pollen species analyzed in this study (red markers) and data from previous reports (black markers) (Satterwhite, 1990; Wlodarski et al., 2006; Hill et al., 2009). Location of fluorescence modes A - E represented by blue circles. Also shown is spectral location of selected pure fluorophores (proteins BSA and OVA; ferulic acid and phenylcoumarin as phenolic proxies; chlorophyll *b*) for direct comparison. For pure fluorophores, full width half maximum (FWHM) of emission signals is shown as horizontal and vertical bars (see also Pöhlker et al. (2012)). (B-F) Normalized two-dimensional fluorescence spectra for selected excitation ( $\lambda_{\text{ex}} = 280, 355, \text{ and } 460 \text{ nm}$ ) and emission wavelengths ( $\lambda_{\text{em}} = 450 \text{ and } 520 \text{ nm}$ ). These wavelengths have been chosen because (i) they centrally cross the pollen modes A - E, (ii) they cover spectral regions of high biofluorophore density, and (iii) they represent or approximate common excitation sources for FBAP-detection instruments (Pöhlker et al., 2012). Taxonomic affiliation of pollen on family level is represented as color code (see legend here and Fig. 7). Fluorescence spectra are normalized and therefore intensities can be compared across all species. Note that intensity of *S. cereale* is divided by factor 2 in all spectra. Shaded areas in (C) and (D) represent emission bands of LIF detectors UV-APS and WIFS.

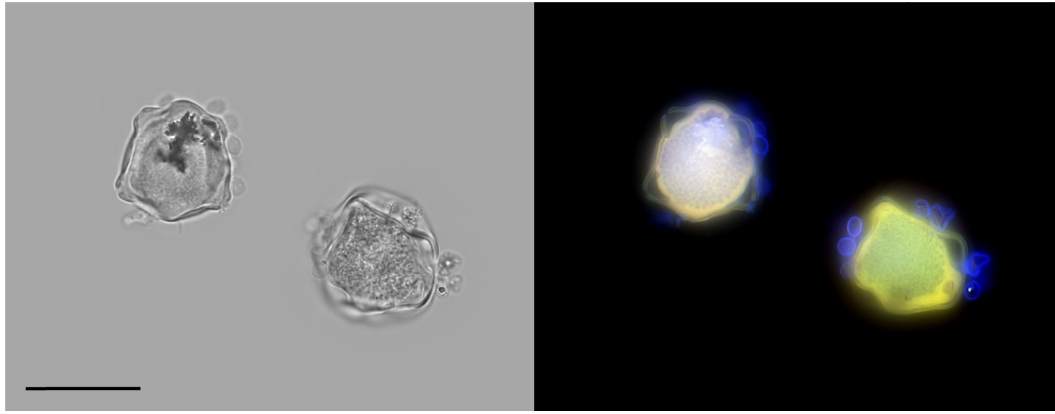


**Figure 6.** Microscopy images of *Carpinus betulus* pollen in bright field (left) and fluorescence mode (right). Fluorescence image shown as overlay of three channels. Pollen are prepared in immersion oil. Micrographs illustrate small blue fluorescing particles adhering to pollen grains. Small particles shown here are representative for entire sample. Scale bar = 30  $\mu\text{m}$ .



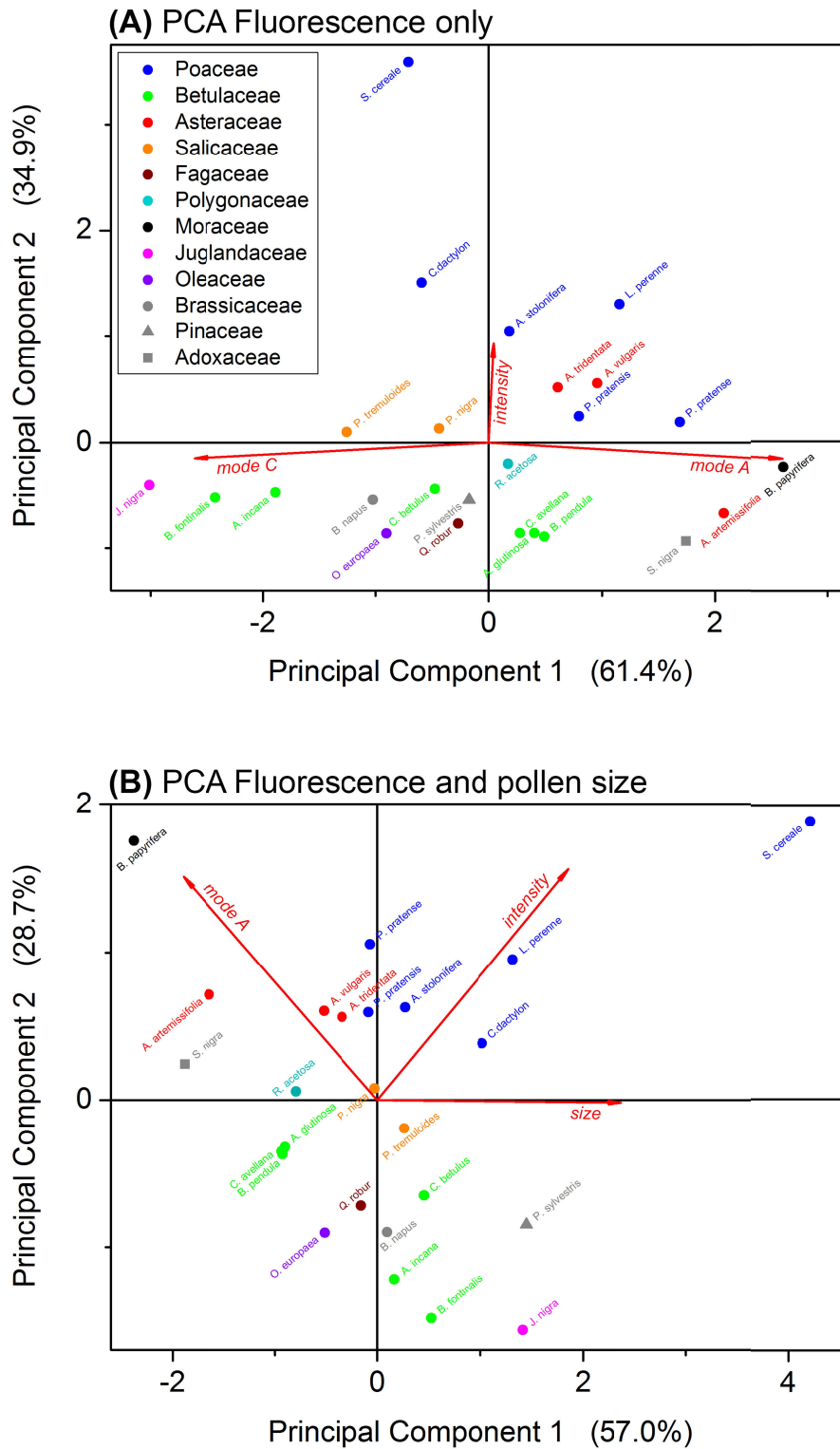


**Figure 7.** Results of principal component analysis (PCA) illustrating taxonomic trends in pollen autofluorescence. **(A)** Bi-plot with scores of PCA based on pollen fluorescence properties only. Eigenvectors (red arrows) represent intensities of modes A and C, as well as total intensity level, as most distinctive features. **(B)** Bi-plot with scores of PCA based on pollen fluorescence properties and grain size. Eigenvectors represent intensity of mode A, total intensity level, and grain size.

## Supporting Online Material

### **Autofluorescence of atmospheric bioaerosols – the spectral fingerprint and taxonomic trends of native pollen**

Christopher Pöhlker<sup>1\*</sup>, J. Alex Huffman<sup>2\*</sup>, Jan-David Förster<sup>1</sup>, and Ulrich Pöschl<sup>1</sup>

<sup>1</sup>*Max Planck Institute for Chemistry, Biogeochemistry Department, P.O. Box 3060, D-55020 Mainz, Germany*

<sup>2</sup>*University of Denver, Department of Chemistry and Biochemistry, 2190 E. Illif, Denver, Colorado 80208, USA*

*\*Corresponding authors: a.huffman@mpic.de, c.pohlker@mpic.de*

**Keywords:** Autofluorescence, bioaerosols, pollen, excitation-emission-matrix, fluorescence spectroscopy, fluorescence microscopy

## Supporting Figures:

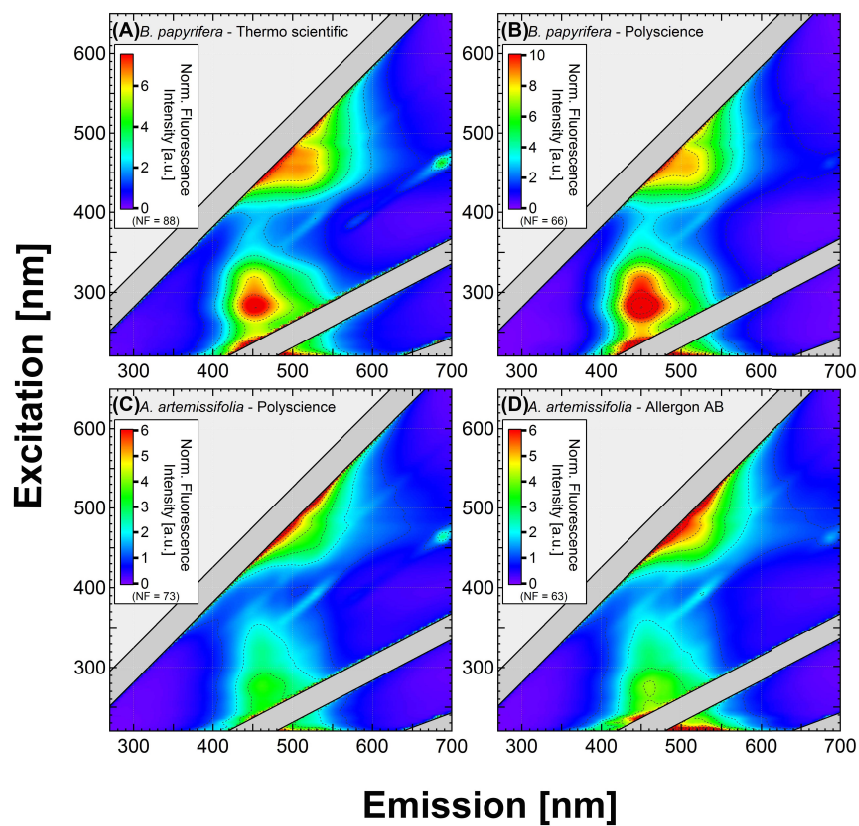


**Figure S1.** Comparison of EEMs of pollen purchased from different vendors: *B. papyrifera* purchased from Thermo Scientific (A) and Polyscience (B). *A. artemisiifolia* purchased from Polyscience (C) and Allergon AB (D). Fluorescence signatures in EEMs are shown to be identical, irrespective of commercial source.

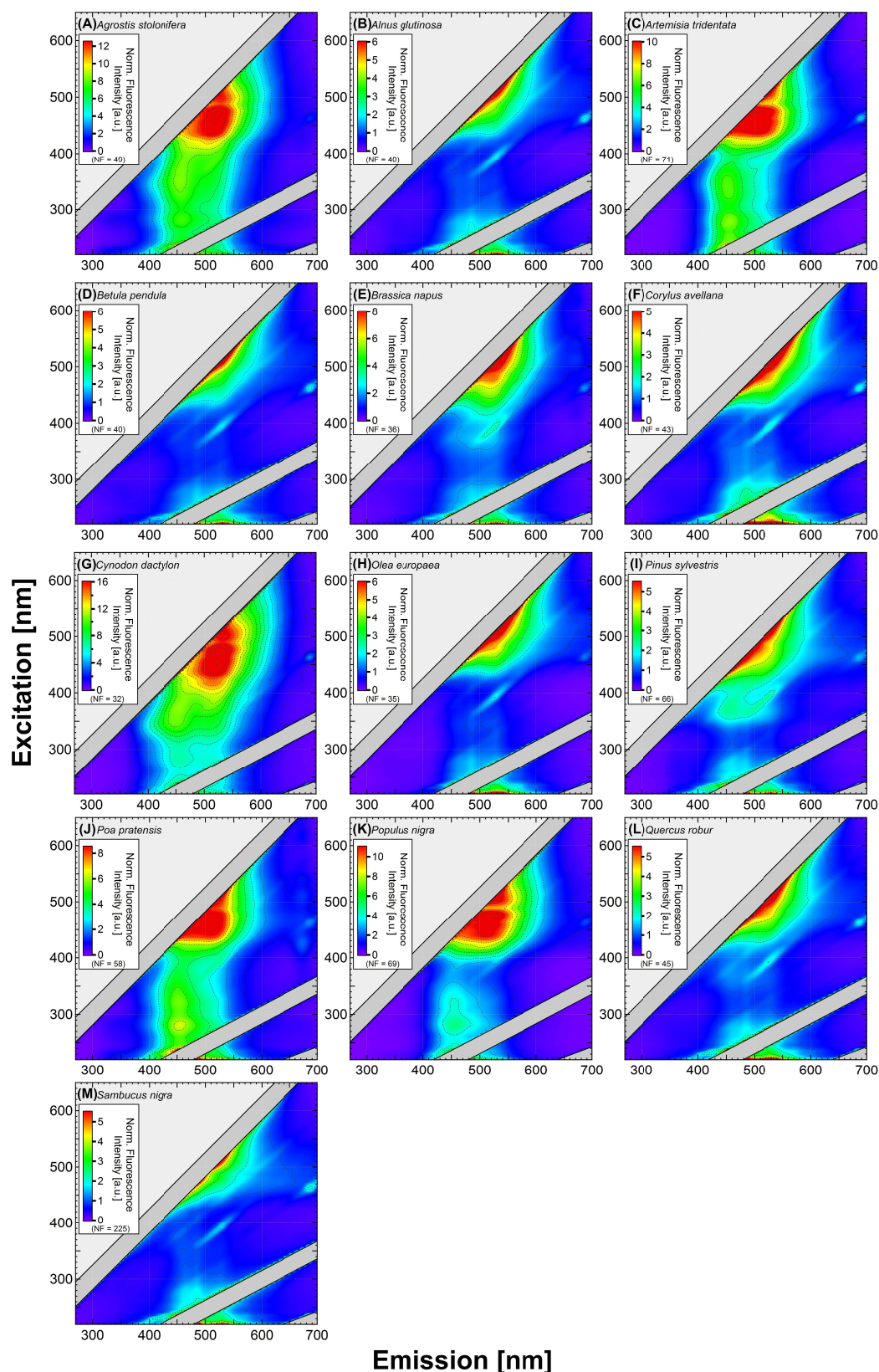


**Figure S2.** Excitation-emission-matrices (EEMs) of pollen in dry and native state. Intensity color code has been adjusted to fluorescence intensity of individual samples. All EEMs are normalized and a normalization factor (NF) is reported in each panels (Sect. 2.3). *Agrostis stolonifera* (A) pollen was treated with acetone for dewaxing after harvest. However, the corresponding EEM does not show substantial alterations.

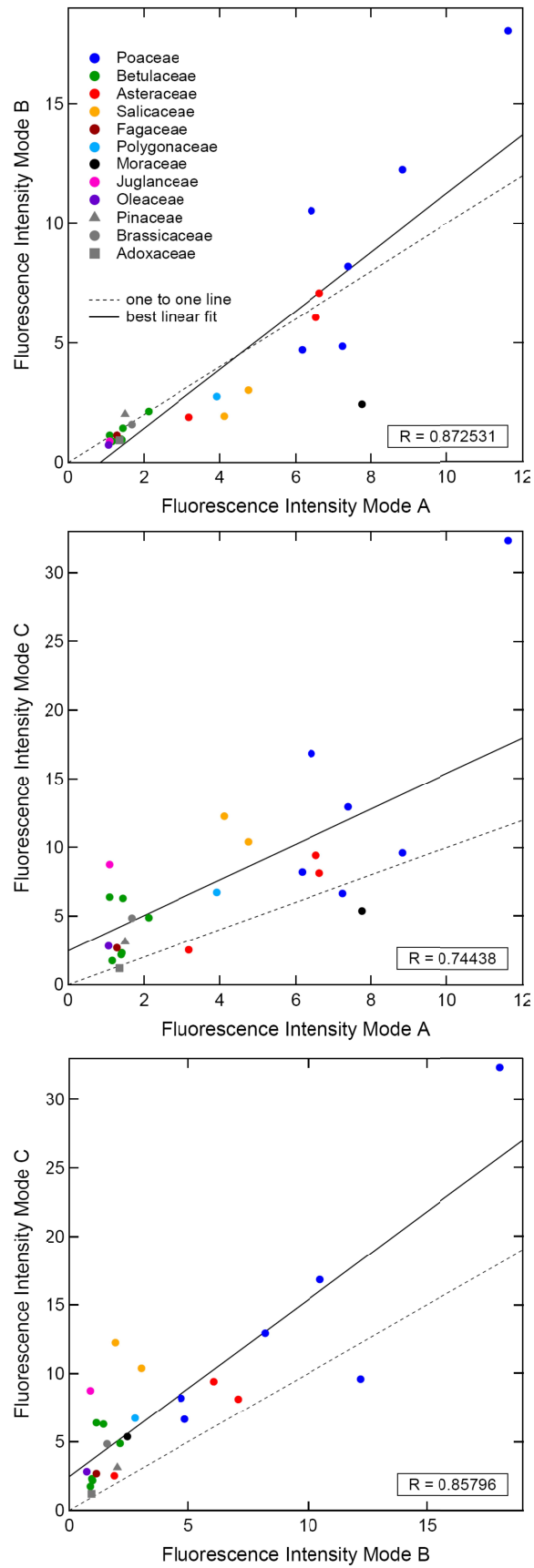


**Figure S3.** Scatter plots showing positive correlation between fluorescence intensities of main fluorescence modes A, B, and C (Fig. 5). Color code represents pollen families.



**B3. Huffman et al., Atmos. Chem. Phys. Discuss., 2013**

**High concentrations of biological aerosol particles and ice nuclei during rain.**

J. Alex Huffman<sup>1</sup>, Christopher Pöhlker<sup>2</sup>, Anthony J. Prenni<sup>3</sup>, Paul J. DeMott<sup>3</sup>, Ryan H. Mason<sup>4</sup>,  
Niall H. Robinson<sup>5</sup>, Janine Fröhlich-Nowoisky<sup>2</sup>, Yutaka Tobo<sup>3</sup>, Viviane R. Després<sup>6</sup>,  
Elvin Garcia<sup>3</sup>, David J. Gochis<sup>7</sup>, Eliza Harris<sup>2</sup>, Isabell Müller-Germann<sup>2</sup>, Cristina Ruzene<sup>2</sup>, Beatrice  
Schmer<sup>2</sup>, Bärbel Sinha<sup>2,8</sup>, Douglas A. Day<sup>9</sup>, Meinrat O. Andreae<sup>2</sup>, Jose-Luis Jimenez<sup>9</sup>, Martin  
Gallagher<sup>5</sup>, Sonia M. Kreidenweis<sup>3</sup>, Allan K. Bertram<sup>4</sup>, and Ulrich Pöschl<sup>2</sup>

*1 University of Denver, Department of Chemistry and Biochemistry, Denver, Colorado, USA*

*2 Max Planck Institute for Chemistry, Biogeochemistry Department, Mainz, Germany*

*3 Colorado State University, Department of Atmospheric Sciences, Fort Collins, CO, USA*

*4 University of British Columbia, Department of Chemistry, Vancouver, BC, Canada*

*5 University of Manchester, Centre for Atmospheric Sciences, Manchester, UK*

*6 Johannes Gutenberg University, Institute for General Botany, Mainz, Germany*

*7 National Center for Atmospheric Research, Boulder, CO, USA*

*8 IISER Mohali, Department of Earth and Environmental Science, Manauli, India*

*9 University of Colorado, Cooperative Institute for Research in the Environmental Sciences and  
Department of Chemistry and Biochemistry, Boulder, CO, USA*

**Atmospheric Chemistry and Physics Discussion 13, 1767-1793, 2013**





This discussion paper is/has been under review for the journal Atmospheric Chemistry and Physics (ACP). Please refer to the corresponding final paper in ACP if available.

# High concentrations of biological aerosol particles and ice nuclei during and after rain

**J. A. Huffman<sup>1</sup>, C. Pöhlker<sup>2</sup>, A. J. Prenni<sup>3</sup>, P. J. DeMott<sup>3</sup>, R. H. Mason<sup>4</sup>, N. H. Robinson<sup>5</sup>, J. Fröhlich-Nowoisky<sup>2</sup>, Y. Tobo<sup>3</sup>, V. R. Després<sup>6</sup>, E. Garcia<sup>3</sup>, D. J. Gochis<sup>7</sup>, E. Harris<sup>2</sup>, I. Müller-Germann<sup>2</sup>, C. Ruzene<sup>2</sup>, B. Schmer<sup>2</sup>, B. Sinha<sup>2,8</sup>, D. A. Day<sup>9</sup>, M. O. Andreae<sup>2</sup>, J. L. Jimenez<sup>9</sup>, M. Gallagher<sup>5</sup>, S. M. Kreidenweis<sup>3</sup>, A. K. Bertram<sup>4</sup>, and U. Pöschl<sup>2</sup>**

<sup>1</sup>Department of Chemistry & Biochemistry, University of Denver, 2190 E. Illif Ave., Denver, CO, 80208, USA

<sup>2</sup>Max Planck Institute for Chemistry, Hahn-Meitner-Weg 1, 55128, Mainz, Germany

<sup>3</sup>Department of Atmospheric Sciences, Colorado State University, 1371 Campus Delivery, Fort Collins, CO, 80523, USA

<sup>4</sup>Department of Chemistry, University of British Columbia, Room D223, 2036 Main Mall, Vancouver, BC, V6T1Z1, Canada

<sup>5</sup>Centre for Atmospheric Sciences, University of Manchester, Simon Building, Oxford Road, Manchester, M139PL, UK

<sup>6</sup>Institute for General Botany, Johannes Gutenberg University, Müllerweg 6, 55099, Mainz, Germany

1767

<sup>7</sup>National Center for Atmospheric Research, P.O. Box 3000, Boulder, CO, 80307, USA

<sup>8</sup>IISER Mohali, Department of Earth and Environmental Science, Sector 81, S. A. S. Nagar, Manauli PO, 140306, India

<sup>9</sup>Cooperative Institute for Research in the Environmental Sciences and Department of Chemistry and Biochemistry, University of Colorado, Boulder, CO, USA

Received: 18 December 2012 – Accepted: 4 January 2013 – Published: 16 January 2013

Correspondence to: J. A. Huffman (alex.huffman@du.edu),  
A. J. Prenni (anthony.prenni@colostate.edu), A. K. Bertram (bertram@chem.ubc.ca),  
and U. Pöschl (u.poschl@mpic.de)

Published by Copernicus Publications on behalf of the European Geosciences Union.





including wavelength ranges, are detailed in the SOM. Scanning electron microscopy (SEM) images were acquired using the secondary electron in-lens detector of a high-performance field emission instrument (LEO 1530 FESEM, EHT 10 keV, WD 9 mm). The elemental composition of inorganic components was characterized using the Oxford Instruments ultra-thin-window energy-dispersive X-ray (EDX) detector.

Optimized methods of DNA extraction, amplification, and sequence analysis of the internal transcribed spacer (ITS) regions were used to determine bacterial and fungal diversity from the high-volume air filter samples (Fröhlich-Nowoisky et al., 2009, 2012). For bacteria, the 16S ribosomal gene was first amplified for taxonomic identification with primer pairs 9/27f and 1492r under PCRs conditions and then cloned and sequenced (Weisburg et al., 1991, 2007). The same primer pair was used for the bacterial lysates obtained from Andersen sampler culture plates. The primer pair ITS4Oo and ITS5 (Nikolcheva and Bärlocher, 2004) was used for amplification of *Peronosporomycetes* (formerly *Oomycota*). Also specific for this study, the ITS regions from fungal lysates, obtained from the cultivation experiments of Andersen impactor samples, were amplified with the primer pair ITS4 and ITS5 (White et al., 1990; Fröhlich-Nowoisky et al., 2009, 2012). The obtained PCR products were sequenced using the primer ITS5 and sequence analysis was performed as described previously (Fröhlich-Nowoisky et al., 2009, 2012). The sequences from the obtained operational taxonomic units have been deposited in the GenBank database under following accession numbers: JX135610–JX136661 (fungi), JX228219–JX228862 (bacteria), and JQ976038–JQ976273 (*Peronosporomycetes*).

Fungal and bacterial colonies were picked and cultured in DPY medium (dextrose  $10\text{ gL}^{-1}$ , peptone  $3\text{ gL}^{-1}$ , yeast extract  $0.3\text{ gL}^{-1}$ ) in 96-well polypropylene plates and incubated at  $16^\circ\text{C}$ . A  $50\ \mu\text{L}$  aliquot of DPY media containing hyphal fragments and fungal spores was tested from each well for ice nucleation activity in a temperature range  $-12^\circ\text{C}$  to  $-2^\circ\text{C}$  (Garcia et al., 2012).

Freezing properties of particles collected on hydrophobic MOUDI slides were determined with an optical microscope and a flow cell with temperature and relative humidity

1773

control (Dymarska et al., 2006; Iannone et al., 2011). The RH was first set to  $> 100\%$  to condense water droplets on the particles. The droplets were grown to approximately  $100\ \mu\text{m}$  in diameter, and after droplet growth was completed each droplet contained between 30 and 100 particles. Then the temperature was decreased at a rate of  $10\text{ Kmin}^{-1}$  until a temperature of  $-40^\circ\text{C}$  was reached. Progression of ice formation was monitored continuously using a camera system.

## 2.5 Real-time IN detection

A ground-based version of the Colorado State University continuous flow diffusion chamber (CFDC) (Rogers et al., 2001) was employed for real-time measurements of IN concentrations. The CFDC permits observation of ice formation on a continuous stream of particles at controlled temperatures and humidities. Physical impaction of larger particles ( $> 2.4\ \mu\text{m}$ ) in advance of the CFDC prevents false detection of large particles as IN. We note that removing these larger particles upstream of the CFDC likely removes some particles that can potentially serve as IN, however, field data suggests that this underestimation is normally less than a factor of two under most sampling situations (Garcia et al., 2012). Water supersaturated conditions (relative humidity  $\sim 105\%$  with respect to water) were typically used for CFDC processing to emphasize ice nucleation predominantly by a condensation/immersion freezing process (Sullivan et al., 2010). Ice crystals activated as IN in the CFDC were collected via impaction at the CFDC outlet (Prezzi et al., 2009, 2013; Garcia et al., 2012).

## 3 Results and discussion

During the field campaign, we observed frequent transitions between dry background conditions and rain events. Figure 1 shows characteristic meteorological parameters and aerosol particle concentrations for seven consecutive days during the campaign (31 July to 6 August 2011). During dry periods we observed low concentrations of both

1774

fluorescent bioparticles ( $N_{F,c} \approx 30 \text{ L}^{-1}$ ) and total aerosol particles ( $N_{T,c} \approx 300 \text{ L}^{-1}$ ) in the supermicrometer size range, as detected by the UV-APS. At the onset of every rain event, the fluorescent bioparticles exhibited an immediate steep increase by as much as 60–160 % per minute during the first ten minutes of precipitation (Fig. 1b). The total concentration of coarse particles ( $> 1 \mu\text{m}$ ), including non-fluorescent material, increased less dramatically but also substantially (by 10–65 % per minute, Fig. 1c), which is in contrast to the traditional view of atmospheric aerosol processing that assumes efficient removal of large aerosol particles by precipitation. Our online measurements, however, show that the concentration of coarse aerosol particles not embedded in rain droplets can rapidly rise by factors as high as  $\sim 4$  to  $\sim 12$  and remain elevated over multiple hours, depending on the intensity and duration of the rain event. Heavy downpours produced a large and extended increase in particle concentration, but even light drizzle led to substantial enhancements (up to factor  $\sim 4$ ). The strong increase of total and biological particle concentrations implies that the precipitation-related enhancements of particle sources as specified and discussed below were substantially stronger than the precipitation-related particle sinks (i.e. precipitation scavenging).

The number fraction of fluorescent bioparticles in total supermicron particles detected by the UV-APS was  $\sim 2$ –6 % under dry conditions (Fig. 1d). It jumped to  $\sim 20$  % at the onset of rainfall, and it increased further to  $\sim 40$  % when humid conditions with elevated leaf wetness persisted beyond the actual rainfall, which was mostly the case during nighttime after strong daytime precipitation (Fig. 1a). The UV-APS, however, provides only a lower limit proxy for the overall abundance of bioparticles, because it is designed for online detection of viable bacteria with strong autofluorescence at specific wavelengths (Huffman et al., 2012; Pöhlker et al., 2012a). Microscopic investigations, making use of a wider range of wavelengths as well as morphological characteristics and elemental composition data (FM, SEM), indicate that the relative abundance of bioparticles in the supermicron size range during rain events (i.e. during or after rainfall) was as high as 55–80 %. In contrast, mineral dust particles prevailed during dry periods (70–80 %, Tables 1–2). Figure 2a, b show microscopic images of aerosol

1775

impactor samples clearly highlighting the contrast between the relatively weak red fluorescence from irregularly shaped dust in a sample collected during dry weather and the intense green and blue fluorescence from cellular structures in a sample collected during a rain event.

During rainfall the median diameter of fluorescent bioparticles was usually 2–3  $\mu\text{m}$ , and the concentration of these particles decayed swiftly after the precipitation had stopped (Fig. 1e). When humid conditions with elevated leaf wetness persisted beyond the actual precipitation, larger fluorescent bioparticles with a median diameter around 4–6  $\mu\text{m}$  appeared ca. 8 h after the beginning of rainfall and persisted for up to 12 more hours (Fig. 1e). Statistical cluster analysis of the size, asymmetry, and multi-channel fluorescence data recorded with the WIBS instrument confirmed that the smaller bioparticles enhanced during rainfall were qualitatively different from the larger ones enhanced after rainfall, implying different sources or physiological states (Pöhlker et al., 2012a; Robinson et al., 2012).

The 2–3  $\mu\text{m}$  bioparticles present through-out the rainfall are likely bacteria or fungal spores released from surrounding vegetation surfaces through mechanical agitation by raindrops (Faulwetter, 1917; Hirst and Stedman, 1963), which is consistent with the observed strong initial enhancement at the onset of rain and a less pronounced enhancement during continued rainfall and immediately following events (e.g.: 2 August, Fig. 1a–c). The increase of relative humidity and leaf wetness can also trigger other bioparticle emission mechanisms like the active wet ejection of fungal spores (Hirst and Stedman, 1963; Elbert et al., 2007; Després et al., 2012) or hygroscopic swelling-induced pollen fragmentation (Taylor et al., 2004; Miguel et al., 2006; Pöhlker et al., 2013; Pummer et al., 2012). Moreover, bioparticles observed during rainfall may also have precipitated from clouds in which some of them served either as giant cloud condensation nuclei (GCCN) or ice nuclei contributing to rain formation (Sands et al., 1982; Morris et al., 2004; Christner et al., 2008; Garcia et al., 2012).

The 4–6  $\mu\text{m}$  bioparticles observed during the humid post-rain periods appear to have been freshly emitted from active biota growing on wetted terrestrial surfaces near the

1776



active as ice nuclei. Convective lofting of biological IN active at temperatures of  $-15^{\circ}\text{C}$  and warmer, where ice mass growth rates maximize (Korolev, 2007) and freezing of larger drops can initiate secondary ice generation (Hallett and Mossop, 1974), may invigorate the glaciation of mixed-phase clouds and thus may strongly contribute to the formation of precipitation.

#### 4 Conclusions

Our observations indicate that rainfall can trigger intense bursts of bioparticle emission and massive enhancements of atmospheric bioaerosol concentrations by an order of magnitude or more, from the onset of precipitation through extended periods of high surface wetness after the rainfall (up to one day). The strong contrast against low background concentrations under dry conditions suggests that the repeated bursts of bioparticle release during and after rain may play an important role in the spread and reproduction of microorganisms in certain environments, and may also contribute to the atmospheric transmission of pathogenic and allergenic agents (Fig. 5). To quantify these effects, we suggest comprehensive metagenomic analyses and dispersion studies of atmospheric bioaerosols contrasting different meteorological conditions. Follow-up studies in other environments shall elucidate whether the observed rain-related bioaerosol increase is a common feature of terrestrial ecosystems or specific for the investigated semi-arid environment.

Three key results of our measurements during rain and dry periods indicate the critical and dynamic role of bioaerosols as IN sources that may strongly influence the evolution of cloud microphysics and precipitation processes: (1) large and closely correlated increases of bioparticles and IN during rain events; (2) similar size distribution patterns of rain-enhanced bioparticles and IN active in the warmest regime of mixed-phase clouds ( $\geq -15^{\circ}\text{C}$ ); and (3) identification of IN-active bioparticles in aerosol and IN samples collected during rain events. Rainfall that triggers bioparticle emission may seed further precipitation (Bigg and Miles, 1964) by convective lifting of bioparticles into

1779

clouds where they can serve as IN, inducing cold rain formation (Hallett and Mossop, 1974; Korolev, 2007), or as GCCN, inducing warm rain formation (Möhler et al., 2007; Pöschl et al., 2010; Després et al., 2012). However, more detailed vertical transport and vertical profile information about rain-related effects will be critical to understanding what the impact of rain-initiated bioaerosol production could mean at the cloud level and for cloud formation. Recent studies suggested that bioaerosols play crucial roles in the hydrological cycle and evolution of pristine tropical rainforest ecosystems (Prenni et al., 2009; Pöschl et al., 2010; Pöhlker et al., 2012b). The measurement results of this study suggest that bioaerosols may also play an important role in mid-latitude semi-arid forest ecosystems, consistent with the recent observation that biogenic emissions significantly impact CCN in the region (Levin et al., 2012). Accordingly, deforestation and changes in land-use and biodiversity might have a significant influence on the abundance of IN, the microphysics and dynamics of clouds and precipitation in these regions, and thus on regional and global climate (DeMott et al., 2010b). In-cloud measurements of aerosol and hydrometeor composition, aerosol- and cloud-resolving process model studies, and earth system model studies capturing potential feedbacks between the atmosphere and biosphere will be required to further quantify the relevance of these effects for climate prediction.

**Supplementary material related to this article is available online at:**

<http://www.atmos-chem-phys-discuss.net/13/1767/2013/acpd-13-1767-2013-supplement.pdf>.

*Acknowledgements.* The BEACHON-RoMBAS campaign was partially supported by an ETBC grant to the National Center for Atmospheric Research (NCAR), the University of Colorado, Colorado State University, and Penn State University (NSF ATM-0919189). J. A. Huffman acknowledges internal faculty funding from the University of Denver. The Mainz team acknowledges financial support from the Max Planck Society (MPG), the Max Planck Graduate Center with the Johannes Gutenberg University Mainz (MPGC), the Geocycles Cluster Mainz (LEC

1780

Rheinland-Pfalz), and the German Research Foundation (DFG PO1013/5-1, FOR 1525 INUIT). R. H. Mason and A. K. Bertram acknowledge financial support from the the National Sciences and Engineering Research Council of Canada. Y. Tobo acknowledges the Japanese Society for the Promotion of Science (JSPS) Postdoctoral Fellowships for Research Abroad. CFDC measurements and analysis were funded by NSF (ATM-0919042, AGS-1036028). J. L. Jimenez and D. A. Day acknowledge US DOE (BER, ASR program) DE-SC0006035. N. H. Robinson and M. Gallagher thank Defence Science and Technology Laboratory (DSTL) for loan of WIBS-4 instrument. The authors wish to thank the USFS, NCAR, R. Oakes, A. Guenther, and J. Smith for providing logistical support and access to the Manitou Experimental Forest field site; A. Turnipseed for providing meteorological data; A. Sun for help with ice nucleation microscopy measurements; J. D. Förster, T. C. J. Hill, S. Lelieveld, T. Pooya, and M. G. Grant for technical assistance in bioaerosol analysis.

## References

- Allitt, U.: Airborne fungal spores and the thunderstorms of 24 June 1994, *Aerobiologia*, 16, 397–406, 2000.
- Bigg, E. K. and Miles, G. T.: The results of large-scale measurements of natural ice nuclei, *J. Atmos. Sci.*, 21, 396–403, doi:10.1175/1520-0469(1964)021<0396:trolmo>2.0.co;2, 1964.
- Burrows, S. M., Butler, T., Jöckel, P., Tost, H., Kerkweg, A., Pöschl, U., and Lawrence, M. G.: Bacteria in the global atmosphere – Part 2: Modeling of emissions and transport between different ecosystems, *Atmos. Chem. Phys.*, 9, 9281–9297, doi:10.5194/acp-9-9281-2009, 2009.
- Christner, B. C., Morris, C. E., Foreman, C. M., Cai, R. M., and Sands, D. C.: Ubiquity of biological ice nucleators in snowfall, *Science*, 319, 1214–1214, doi:10.1126/science.1149757, 2008.
- Connolly, P. J., Möhler, O., Field, P. R., Saathoff, H., Burgess, R., Choularton, T., and Gallagher, M.: Studies of heterogeneous freezing by three different desert dust samples, *Atmos. Chem. Phys.*, 9, 2805–2824, doi:10.5194/acp-9-2805-2009, 2009.
- Constantinidou, H. A., Hirano, S. S., Baker, L. S., and Upper, C. D.: Atmospheric dispersal of ice nucleation-active bacteria – the role of rain, *Phytopathology*, 80, 934–937, doi:10.1094/Phyto-80-934, 1990.

1781

- Dales, R. E., Cakmak, S., Judek, S., Dann, T., Coates, F., Brook, J. R., and Burnett, R. T.: The role of fungal spores in thunderstorm asthma, *Chest*, 123, 745–750, doi:10.1378/chest.123.3.745, 2012.
- DeMott, P. J., Möhler, O., Stetzer, O., Vali, G., Levin, Z., Petters, M. D., Murakami, M., Leisner, T., Bundke, U., Klein, H., Kanji, Z., Cotton, R., Jones, H., Petters, M., Prenni, A., Benz, S., Brinkmann, M., Rzesanke, D., Saathoff, H., Nicolet, M., Gallavardin, S., Saito, A., Nillius, B., Bingemer, H., Abbatt, J., K., A., Ganor, E., Georgakopoulos, D. G., and Saunders, C.: Resurgence in ice nucleation research, *B. Am. Meteorol. Soc.*, 92, 1623–1635, 2010a.
- DeMott, P. J., Prenni, A. J., Liu, X., Kreidenweis, S. M., Petters, M. D., Twohy, C. H., Richardson, M. S., Eidhammer, T., and Rogers, D. C.: Predicting global atmospheric ice nuclei distributions and their impacts on climate, *P. Natl. Acad. Sci. USA*, 107, 11217–11222, doi:10.1073/pnas.0910818107, 2010b.
- Després, V. R., Nowoisky, J. F., Klose, M., Conrad, R., Andreae, M. O., and Pöschl, U.: Characterization of primary biogenic aerosol particles in urban, rural, and high-alpine air by DNA sequence and restriction fragment analysis of ribosomal RNA genes, *Biogeosciences*, 4, 1127–1141, doi:10.5194/bg-4-1127-2007, 2007.
- Després, V. R., Huffman, J. A., Burrows, S. M., Hoose, C., Safatov, A. S., Buryak, G. A., Fröhlich-Nowoisky, J., Elbert, W., Andreae, M. O., Pöschl, U., and Jaenicke, R.: Primary biological aerosol particles in the atmosphere: a review, *Tellus B*, 64, 15598, doi:10.3402/tellusb.v64i0.15598, 2012.
- Diehl, K., Quick, C., Matthias-Maser, S., Mitra, S. K., and Jaenicke, R.: The ice nucleating ability of pollen – Part I: Laboratory studies in deposition and condensation freezing modes, *Atmos. Res.*, 58, 75–87, 2001.
- Dymarska, M., Murray, B. J., Sun, L. M., Eastwood, M. L., Knopf, D. A., and Bertram, A. K.: Deposition ice nucleation on soot at temperatures relevant for the lower troposphere, *J. Geophys. Res.-Atmos.*, 111, D04204, doi:10.1029/2005jd006627, 2006.
- Elbert, W., Taylor, P. E., Andreae, M. O., and Pöschl, U.: Contribution of fungi to primary biogenic aerosols in the atmosphere: wet and dry discharged spores, carbohydrates, and inorganic ions, *Atmos. Chem. Phys.*, 7, 4569–4588, doi:10.5194/acp-7-4569-2007, 2007.
- Elbert, W., Weber, B., Burrows, S. M., Steinkamp, J., Büdel, B., Andreae, M. O., and Pöschl, U.: Contribution of cryptogamic covers to the global cycles of carbon and nitrogen, *Nat. Geosci.*, 5, 459–462, 2012.

1782



- Faulwetter, R. C.: Wind-blown rain, a factor in disease dissemination, *J. Agr. Res.*, 10, 639–648, 1917.
- Fröhlich-Nowoisky, J., Pickersgill, D. A., Després, V. R., and Pöschl, U.: High diversity of fungi in air particulate matter, *P. Natl. Acad. Sci. USA*, 106, 12814–12819, doi:10.1073/pnas.0811003106, 2009.
- Fröhlich-Nowoisky, J., Burrows, S. M., Xie, Z., Engling, G., Solomon, P. A., Fraser, M. P., Mayol-Bracero, O. L., Artaxo, P., Begerow, D., Conrad, R., Andreae, M. O., Després, V. R., and Pöschl, U.: Biogeography in the air: fungal diversity over land and oceans, *Biogeosciences*, 9, 1125–1136, doi:10.5194/bg-9-1125-2012, 2012.
- Garcia, E., Hill, T. C. J., Prenni, A. J., DeMott, P. J., Franc, G. D., and Kreidenweis, S. M.: Biogenic ice nuclei in boundary layer air over two US High Plains agricultural regions, *J. Geophys. Res.-Atmos.*, 117, D18209, doi:10.1029/2012JD018343, 2012.
- Hallett, J. and Mossop, S. C.: Production of secondary ice particles during riming process, *Nature*, 249, 26–28, doi:10.1038/249026a0, 1974.
- Hirst, J. M. and Stedman, O. J.: Dry liberation of fungus spores by raindrops, *J. Gen. Microbiol.*, 33, 335–346, 1963.
- Hoose, C. and Möhler, O.: Heterogeneous ice nucleation on atmospheric aerosols: a review of results from laboratory experiments, *Atmos. Chem. Phys.*, 12, 9817–9854, doi:10.5194/acp-12-9817-2012, 2012.
- Hoose, C., Kristjansson, J. E., and Burrows, S. M.: How important is biological ice nucleation in clouds on a global scale?, *Environ. Res. Lett.*, 5, 024009, doi:10.1088/1748-9326/5/2/024009, 2010.
- Huffman, J. A., Treutlein, B., and Pöschl, U.: Fluorescent biological aerosol particle concentrations and size distributions measured with an Ultraviolet Aerodynamic Particle Sizer (UV-APS) in Central Europe, *Atmos. Chem. Phys.*, 10, 3215–3233, doi:10.5194/acp-10-3215-2010, 2010.
- Huffman, J. A., Sinha, B., Garland, R. M., Snee-Pollmann, A., Gunthe, S. S., Artaxo, P., Martin, S. T., Andreae, M. O., and Pöschl, U.: Size distributions and temporal variations of biological aerosol particles in the Amazon rainforest characterized by microscopy and real-time UV-APS fluorescence techniques during AMAZE-08, *Atmos. Chem. Phys.*, 12, 11997–12019, doi:10.5194/acp-12-11997-2012, 2012.

1783

- Iannone, R., Chernoff, D. I., Pringle, A., Martin, S. T., and Bertram, A. K.: The ice nucleation ability of one of the most abundant types of fungal spores found in the atmosphere, *Atmos. Chem. Phys.*, 11, 1191–1201, doi:10.5194/acp-11-1191-2011, 2011.
- Kaye, P. H., Stanley, W. R., Hirst, E., Foot, E. V., Baxter, K. L., and Barrington, S. J.: Single particle multichannel bio-aerosol fluorescence sensor, *Opt. Express*, 13, 3583–3593, 2005.
- Korolev, A.: Limitations of the Wegener-Bergeron-Findeisen mechanism in the evolution of mixed-phase clouds, *J. Atmos. Sci.*, 64, 3372–3375, doi:10.1175/jas4035.1, 2007.
- Levin, E. J. T., Prenni, A. J., Petters, M. D., Kreidenweis, S. M., Sullivan, R. C., Atwood, S. A., Ortega, J., DeMott, P. J., and Smith, J. N.: An annual cycle of size-resolved aerosol hygroscopicity at a forested site in Colorado, *J. Geophys. Res.*, 117, D06201, doi:10.1029/2011jd016854, 2012.
- Lindemann, J., Constantinidou, H. A., Barchet, W. R., and Upper, C. D.: Plants as sources of airborne bacteria, including ice nucleation-active bacteria, *Appl. Environ. Microbiol.*, 44, 1059–1063, 1982.
- Maki, L. R., Glyan, E. L., Chang-Chien, M. M., and Caldwell, D. R.: Ice nucleation induced by *Pseudomonas syringae*, *Appl. Environ. Microbiol.*, 28, 456–459, 1974.
- Miguel, A. G., Taylor, P. E., House, J., Glovsky, M. M., and Flagan, R. C.: Meteorological influences on respirable fragment release from Chinese elm pollen, *Aerosol Sci. Technol.*, 40, 690–696, doi:10.1080/02786820600798869, 2006.
- Möhler, O., Field, P. R., Connolly, P., Benz, S., Saathoff, H., Schnaiter, M., Wagner, R., Cotton, R., Krämer, M., Mangold, A., and Heymsfield, A. J.: Efficiency of the deposition mode ice nucleation on mineral dust particles, *Atmos. Chem. Phys.*, 6, 3007–3021, doi:10.5194/acp-6-3007-2006, 2006.
- Möhler, O., DeMott, P. J., Vali, G., and Levin, Z.: Microbiology and atmospheric processes: the role of biological particles in cloud physics, *Biogeosciences*, 4, 1059–1071, doi:10.5194/bg-4-1059-2007, 2007.
- Morris, C. E., Georgakopoulos, D. G., and Sands, D. C.: Ice nucleation active bacteria and their potential role in precipitation, *J. Phys. IV*, 121, 87–103, doi:10.1051/jp4:2004121004, 2004.
- Morris, C. E., Sands, D. C., Vinatzer, B. A., Glaux, C., Guilbaud, C., Buffiere, A., Yan, S., Dominguez, H., and Thompson, B. M.: The life history of the plant pathogen *Pseudomonas syringae* is linked to the water cycle, *ISME J.*, 2, 321–334, 2008.
- Morris, C. E., Sands, D. C., Glaux, C., Samsatly, J., Asaad, S., Moukahel, A. R., Gonçalves, F. L. T., and Bigg, E. K.: Urediospores of *Puccinia* spp. and other rusts are

1784

- warm-temperature ice nucleators and harbor ice nucleation active bacteria, *Atmos. Chem. Phys. Discuss.*, 12, 26143–26171, doi:10.5194/acpd-12-26143-2012, 2012.
- Nikolcheva, L. G. and Bärlocher, F.: Taxon-specific fungal primers reveal unexpectedly high diversity during leaf decomposition in a stream, *Mycol. Prog.*, 3, 41–49, 2004.
- 5 Pöhlker, C., Huffman, J. A., and Pöschl, U.: Autofluorescence of atmospheric bioaerosols – fluorescent biomolecules and potential interferences, *Atmos. Meas. Tech.*, 5, 37–71, doi:10.5194/amt-5-37-2012, 2012a.
- Pöhlker, C., Wiedemann, K. T., Sinha, B., Shiraiwa, M., Gunthe, S. S., Smith, M., Su, H., Artaxo, P., Chen, Q., Cheng, Y., Elbert, W., Gilles, M. K., Kilcoyne, A. L. D., Moffet, R. C.,  
10 Weigand, M., Martin, S. T., Pöschl, U., and Andreae, M. O.: Biogenic potassium salt particles as seeds for secondary organic aerosol in the Amazon, *Science*, 337, 1075–1078, 2012b.
- Pöhlker, C., Huffman, J. A., Förster, J. D., and Pöschl, U.: Autofluorescence of pollen, *Atmos. Meas. Tech. Discuss.*, in preparation, 2013.
- Pöschl, U.: Atmospheric aerosols: composition, transformation, climate and health effects, *Angew. Chem. Int. Edit.*, 44, 7520–7540, doi:10.1002/anie.200501122, 2005.
- 15 Pöschl, U., Martin, S. T., Sinha, B., Chen, Q., Gunthe, S. S., Huffman, J. A., Borrmann, S., Farmer, D. K., Garland, R. M., Helas, G., Jimenez, J. L., King, S. M., Manzi, A., Mikhailov, E., Pauliquevis, T., Petters, M. D., Prenni, A. J., Roldin, P., Rose, D., Schneider, J., Su, H., Zorn, S. R., Artaxo, P., and Andreae, M. O.: Rainforest aerosols as biogenic nuclei of clouds and precipitation in the Amazon, *Science*, 329, 1513–1516, doi:10.1126/science.1191056, 2010.
- Pratt, K. A., DeMott, P. J., French, J. R., Wang, Z., Westphal, D. L., Heymsfield, A. J., Twohy, C. H., Prenni, A. J., and Prather, K. A.: In situ detection of biological particles in cloud ice-crystals, *Nat. Geosci.*, 2, 397–400, doi:10.1038/ngeo521, 2009.
- 25 Prenni, A. J., Petters, M. D., Kreidenweis, S. M., Heald, C. L., Martin, S. T., Artaxo, P., Garland, R. M., Wollny, A. G., and Pöschl, U.: Relative roles of biogenic emissions and Saharan dust as ice nuclei in the Amazon basin, *Nat. Geosci.*, 2, 402–405, doi:10.1038/ngeo517, 2009.
- Prenni, A. J., Tobo, Y., Garcia, E., DeMott, P. J., Huffman, J. A., McCluskey, C. S., Kreidenweis, S. M., Prenni, J. E., Pöhlker, C., and Pöschl, U.: The impact of rain on ice nuclei populations at a forested site in Colorado, *Geophys. Res. Lett.*, in press, 2013.
- 30

1785

- Pummer, B. G., Bauer, H., Bernardi, J., Bleicher, S., and Grothe, H.: Suspendable macromolecules are responsible for ice nucleation activity of birch and conifer pollen, *Atmos. Chem. Phys.*, 12, 2541–2550, doi:10.5194/acp-12-2541-2012, 2012.
- Richard, C., Martin, J.-G., and Pouler, S.: Ice nucleation activity identified in some phytopathogenic *Fusarium* species, *Phytoprotection*, 77, 83–92, 1996.
- 5 Robinson, N. H., Allan, J. D., Huffman, J. A., Kaye, P. H., Foot, V. E., and Gallagher, M.: Cluster analysis of WIBS single particle bioaerosol data, *Atmos. Meas. Tech. Discuss.*, 5, 6387–6422, doi:10.5194/amtd-5-6387-2012, 2012.
- Rogers, D. C., DeMott, P. J., Kreidenweis, S. M., and Chen, Y.: A continuous-flow diffusion chamber for airborne measurements of ice nuclei, *J. Atmos. Ocean. Tech.*, 18, 725–741, 2001.
- Sands, D. C., Langhans, V. E., Scharen, A. L., and de Smet, G.: The association between bacteria and rain and possible resultant meteorological implications, *J. Hungarian Meteorol. Serv.*, 86, 148–152, 1982.
- 15 Sullivan, R. C., Petters, M. D., DeMott, P. J., Kreidenweis, S. M., Wex, H., Niedermeier, D., Hartmann, S., Clauss, T., Stratmann, F., Reitz, P., Schneider, J., and Sierau, B.: Irreversible loss of ice nucleation active sites in mineral dust particles caused by sulphuric acid condensation, *Atmos. Chem. Phys.*, 10, 11471–11487, doi:10.5194/acp-10-11471-2010, 2010.
- Taylor, P. and Jonsson, H.: Thunderstorm asthma, *Curr. Allergy Asthm. R.*, 4, 409–413, doi:10.1007/s11882-004-0092-3, 2004.
- 20 Taylor, P. E., Flagan, R. C., Miguel, A. G., Valenta, R., and Glovsky, M. M.: Birch pollen rupture and the release of aerosols of respirable allergens, *Clin. Exp. Allergy*, 34, 1591–1596, doi:10.1111/j.1365-2222.2004.02078.x, 2004.
- Weisburg, W. G., Barns, S. M., Pelletier, D. A., and Lane, D. J.: 16S ribosomal DNA amplification for phylogenetic study, *J. Bacteriol.*, 173, 697–703, 1991.
- 25 White, T. J., Bruns, T., Lee, S., and Taylor, J.: Amplification and direct sequencing of fungal ribosomal RNA genes for phylogenetics, in: *PCR Protocols: a Guide to Methods and Applications*, edited by: Innis, M. A., Gelfand, D. H., Sninsky, J. J., and White, T. J., Academic Press, Inc., New York, 315–322, 1990.

1786

**Table 1.** Number fraction of biological particles and mineral dust particles in aerosol samples collected during dry periods and rain events. The sample numbers S10, S12, S20, S23 refer to Nuclepore<sup>®</sup> filters analyzed by SEM (details specified in Sects. S1.5.1.4 and S1.5.3). The UV-APS data were averaged over periods matching the filter sample collection times. Fluorescent biological aerosol particles (FBAP), primary biological aerosol particles (PBAP).

Method (Particles)	Dry		Rain	
	S10	S12	S20	S23
UV-APS (FBAP/Total)	0.04	0.06	0.28	0.20
SEM (PBAP/Total)	0.03	0.07	0.78	0.56
SEM (Dust/Total)	0.80	0.76	0.08	0.38

1787

**Table 2.** Number fraction of bioparticles on MOUDI stages 4 (3.2–5.6  $\mu\text{m}$ ) and 5 (1.8–3.2  $\mu\text{m}$ ) of aerosol samples collected during a dry period (M28) and a rain event (M10). See Supplement Sect. S1.5.1.1 for sampling dates. Estimates based on fluorescence microscopy.

	Dry (M28)		Rain (M10)	
	Stage 4	Stage 5	Stage 4	Stage 5
Number fraction	0.25	0.22	0.79	0.67

1788



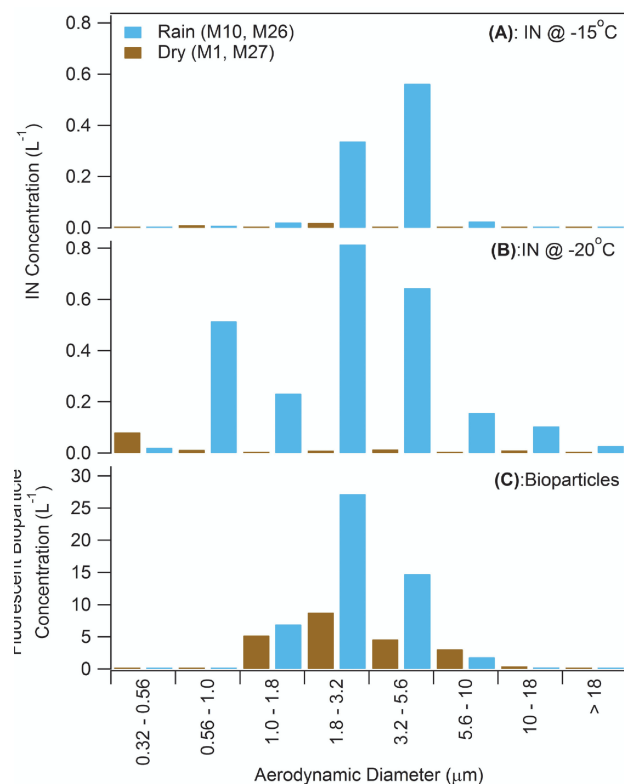


**Fig. 3.** Size distributions of ice nuclei observed in microscopic IN activation experiments **(A)** at  $-15^{\circ}\text{C}$  and **(B)** at  $-20^{\circ}\text{C}$  for aerosol impactor samples collected during dry periods and rain events. **(C)** Size distribution of bioparticles measured by UV-APS during the same periods. See Supplement Sect. S1.5.1.1 for sampling dates.

1791

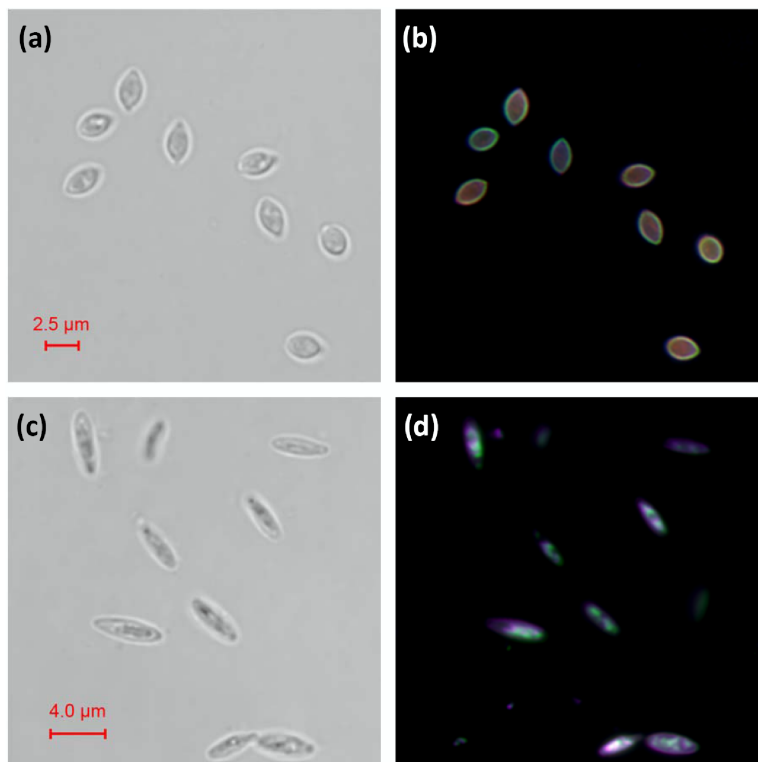


**Fig. 4.** Fluorescence microscopy images of fungal spores from lab cultivation of the two fungi (Ascomycota) with previously unknown IN activity: **(A–B)** *Isaria farinosa*, **(C–D)** *Acremonium implicatum*. Left panels show bright-field image and right panels show overlay of red, green, and blue fluorescence.

1792

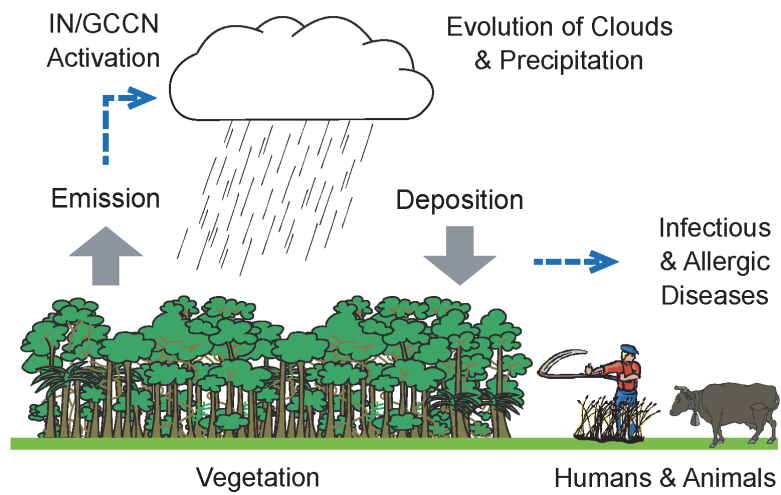


**Fig. 5.** Coupling and effects of biological aerosol particles and precipitation: rain can enhance bioparticle emissions (rain splash, active wet discharge, etc.); bioparticles serving as ice nuclei or giant cloud condensation nuclei (IN/GCCN) can influence the evolution of clouds and precipitation; deposition of pathogenic and allergenic species can trigger human, animal and plant diseases.

1 **Supplementary Online Information (SOM)**

2  
3 **Title: High concentrations of biological aerosol particles and ice nuclei during and**  
4 **after rain**

5 **Authors:** J. A. Huffman<sup>1\*</sup>, C. Pöhlker<sup>2</sup>, A. J. Prenni<sup>3\*</sup>, P. J. DeMott<sup>3</sup>, R. H. Mason<sup>4</sup>, N. H.  
6 Robinson<sup>5</sup>, J. Fröhlich-Nowoisky<sup>2</sup>, Y. Tobo<sup>3</sup>, V. R. Després<sup>6</sup>, E. Garcia<sup>3</sup>, D. J. Gochis<sup>7</sup>, E.  
7 Harris<sup>2</sup>, I. Müller-Germann<sup>2</sup>, C. Ruzene<sup>2</sup>, B. Schmer<sup>2</sup>, B. Sinha<sup>2,8</sup>, D. A. Day<sup>9</sup>, M. O. Andreae<sup>2</sup>,  
8 J. L. Jimenez<sup>9</sup>, M. Gallagher<sup>5</sup>, S. M. Kreidenweis<sup>3</sup>, A. K. Bertram<sup>4\*</sup>, U. Pöschl<sup>2\*</sup>

9 **Affiliations:**

10 <sup>1</sup>Department of Chemistry & Biochemistry, University of Denver, 2190 E. Illif Ave., Denver,  
11 CO, 80208, USA.

12 <sup>2</sup>Max Planck Institute for Chemistry, Hahn-Meitner-Weg 1, D-55128, Mainz, Germany.

13 <sup>3</sup>Department of Atmospheric Sciences, Colorado State University, 1371 Campus Delivery, Fort  
14 Collins, CO, 80523, USA.

15 <sup>4</sup>Department of Chemistry, University of British Columbia, Room D223, 2036 Main Mall,  
16 Vancouver, BC, V6T1Z1, Canada.

17 <sup>5</sup>Centre for Atmospheric Sciences, University of Manchester, Simon Building, Oxford Road,  
18 Manchester, M139PL, UK.

19 <sup>6</sup>Institute for General Botany, Johannes Gutenberg University, Müllerweg 6, D-55099, Mainz,  
20 Germany.

21 <sup>7</sup>National Center for Atmospheric Research, PO Box 3000, Boulder, CO, 80307, USA.

22 <sup>8</sup>IISER Mohali, Department of Earth and Environmental Science, Sector 81, S. A. S. Nagar,  
23 Manauli PO, 140306, India.

24 <sup>9</sup>Cooperative Institute for Research in the Environmental Sciences and Department of Chemistry  
25 and Biochemistry, University of Colorado, Boulder, CO USA.

26 \* Correspondence to: alex.huffman@du.edu (J. A. H.); anthony.prenni@colostate.edu (A. J. P.);  
27 bertram@chem.ubc.ca (A. K. B.); u.poschl@mpic.de (U. P.)  
28

29 **Supplementary Materials:**

30 S1 Materials and Methods

31 Figures S1-S3

32

33 **S1 Materials and Methods**

34 ***S1.1 Site and Campaign Description***

35 The BEACHON-RoMBAS (Bio-hydro-atmosphere interactions of Energy, Aerosols, Carbon,  
36 H<sub>2</sub>O, Organics and Nitrogen – Rocky Mountain Biogenic Aerosol Study) campaign was a  
37 component of the greater BEACHON project sponsored by the National Center for Atmospheric  
38 Research (<http://cires.colorado.edu/jimenez-group/wiki/index.php/BEACHON-RoMBAS>;  
39 <http://web3.acd.ucar.edu/beachon/>). BEACHON-RoMBAS brought together a large,  
40 interdisciplinary set of scientists to address issues surrounding the biogeochemical cycling of  
41 carbon and water at a location representative of the semi-arid Western U.S. The measurements  
42 were located in a part of the Manitou Experimental Forest in a semi-arid, montane ponderosa  
43 pine zone in the Central Rocky Mountains 35 km northwest of Colorado Springs, Colorado and  
44 15 km north of Woodland Park, CO (2370 m elevation, lat. 39°6'0" N, long. 105°5'30" W). All  
45 instruments and samplers were sampled from a height of 1 – 4 m above ground from fixed inlets,  
46 with the exception of the WIBS, high-volume sampler, and biosamplers (details listed below).

47

48 ***S1.2 Meteorological and Leaf Moisture Measurements***

49 Precipitation occurrence, rate and microphysical state (i.e., rain versus hail) were measured using  
50 a laser-optical disdrometer (PARTicle SIZE and VElocity ‘PARSIVEL’ sensor; OTT Hydromet  
51 GmbH, Kempton, Germany). The instrument senses a falling hydrometeor by measuring the  
52 magnitude and duration of attenuation of a temporally continuous 2-dimensional laser beam (780



53 nm) through which the hydrometeor passes. It, therefore, directly detects the presence of falling  
54 hydrometeors without the time delay of typical tipping bucket gauges and with greater particle  
55 size sensitivity than typical weighing gauges. Particle size is estimated from the magnitude of  
56 beam attenuation. Particle fall speed is determined from the duration of beam attenuation while  
57 overall precipitation rate and microphysical classification estimates are generated from a  
58 combination of the size and fall speed measurements. The sensor detects liquid hydrometeor  
59 particles ranging in size from 0.2 to 5 mm in diameter, solid hydrometeors ranging in size from  
60 0.2 to 25 mm and provides estimates of particle velocities from 0.2 to 20 m/s. The stated  
61 accuracy of liquid precipitation rate estimates is +/- 5%. Only the rainfall rate (mm/hr) is  
62 discussed in this text.

63  
64 Leaf wetness state was characterized using a dielectric Leaf Wetness Sensor (LWS; Decagon  
65 Devices, Inc.). The sensor detects and provides a relative measure of the water or ice content on  
66 or near the sensor surface (within ~1 cm) by measuring the dielectric constant of the surface. The  
67 sensor outputs a voltage (measured in millivolts, mV) which is directly proportional to the  
68 amount of water or ice in or near the sensor upper surface. Attribution of the cause of wetness  
69 due to rain or dew formation (i.e. local condensation) is determined by comparing LWS voltage  
70 with optical precipitation measurements and by the pattern of voltage readings from the sensor.  
71 Sharp increases in the mV signal that are concurrent with precipitation events are characterized  
72 as 'rainfall wetness' while slowly increasing mV values that are unaccompanied with  
73 precipitation events are characterized as dew formation.

74

75 Other meteorological parameters such as barometric pressure, air temperature, humidity and  
76 wind speed and direction were measured using a WXT520 Weather Transmitter (Vaisala, Inc.,  
77 Helsinki, Finland). The weather transmitter, the disdrometer and the LWS were all located at the  
78 Manitou Experimental Forest observatory within 100 m of the rest of the particle measurements  
79 described below.

80

### 81 ***SI.3 UV-APS***

82 An ultraviolet aerodynamic particle sizer (UV-APS; TSI Inc. Model 3314, St. Paul, MN) was  
83 utilized for this study following the procedure described by Huffman et al. (Huffman et al.,  
84 2010). Aerodynamic particle diameter ( $D_a$ ) is provided in the range of 0.54 – 19.81  $\mu\text{m}$  by  
85 measuring the time of flight between two continuous-wave red (633 nm) He-Ne lasers. Total  
86 fluorescence of aerosol particles (non-wavelength-dispersed) in the wavelength range of 420 –  
87 575 nm is detected after pulsed excitation by an Nd:YAG laser ( $\lambda_{\text{ex}} = 355 \text{ nm}$ ). UV-APS number  
88 concentrations are reported here as integrated between 1 – 20  $\mu\text{m}$ . Smaller particles are  
89 transmitted within the instrument less efficiently and thus should be considered as lower limit  
90 values. Aerosol sampling was performed with a volumetric flow of 5  $\text{L}\cdot\text{min}^{-1}$  (LPM) at ambient  
91 pressure and temperature, split within the instrument into a sample flow of  $1.0 \pm 0.1$  LPM and a  
92 sheath flow of  $4.0 \pm 0.1$  LPM (pressure difference feedback control). The instrument was  
93 controlled and the measurement data were recorded with an external computer connected via  
94 serial port using the manufacturer's Aerosol Instrument Manager software (TSI AIM).  
95 Measurements were initiated every 5 minutes and integrated over a sample length of 285 s. Five-  
96 minute sample measurements were continuously repeated over a period of five weeks from 20  
97 July to 23 August, 2011 (35 days) and only briefly interrupted for maintenance procedures

98 (usually less than 30 minutes per week). The local time (LT) used for data analysis and plotting  
99 refers to Mountain Daylight Time (MDT). All times reported here are listed as LT.

100

101 Fluorescent particles ( $N_f$ ) detected by the UV-APS can be regarded as a lower limit for the  
102 abundance of primary biological aerosol particles (Huffman et al., 2010; Pöhlker et al., 2012),  
103 utilizing nicotinamide adenine dinucleotide (NADH) and riboflavin as dominant biological  
104 fluorophores. The UV-APS instrument sampled air from a 0.75 inch laminar flow inlet from ~4  
105 m above ground into a climate-controlled trailer at ground level.

106

#### 107 ***SI.4 WIBS***

108 The waveband integrated bioaerosol sensor – model 4 (WIBS4; University of Hertfordshire) is a  
109 dual channel single particle fluorescence spectrometer (Kaye et al., 2005; Foot et al., 2008;  
110 Gabey et al., 2010). Upon detection of a particle, xenon lamps provide two consecutive pulses of  
111 light at 280 nm and 370 nm, in order to stimulate fluorescence of the tryptophan and NADH  
112 biofluorophores respectively. The fluorescence of a particle is measured between 310-400 nm  
113 (the FL1 channel) and 400-600 nm (the FL2 channel), capturing tryptophan fluorescence, and  
114 400-600 nm, capturing NADH fluorescence. This leads to three separate fluorescence channels:  
115 FL1\_280, FL2\_280 and FL2\_370. The forward scattering signal of the particle is also measured  
116 at four angular offsets using a quadrant photo-multiplier tube. This allows for measurements of  
117 size and asymmetry. The WIBS4 model is essentially the same as the WIBS3 model employed  
118 by Gabey et al. (2010), but with improved optics and electronics providing a more precise signal.  
119 Baseline fluorescence is recorded by regularly measuring the internal fluorescence of the  
120 instrument when no particles are present. The increased precision of the model 4 WIBS allows

121 for the detection of more marginally fluorescent particles than was possible using previous  
 122 WIBS models.  
 123  
 124 The WIBS4 was located on an automated profiling system running up the main measurement  
 125 tower, which allowed profile measurements to be made between 3 m and 22 m. Profiles  
 126 consisted of an eight stage profile up, lasting around 45 minutes, and a corresponding continuous  
 127 profile down, lasting about 3 minutes. The WIBS4 total particle size distribution compared well  
 128 with a co-sampling Grimm OPC, particularly in the super-micron regime. A subset of the WIBS4  
 129 single particle data (8000 particles) was analyzed using hierarchical agglomerative cluster  
 130 analysis using a group average distance metric. This clustering was analyzed in five dimensions  
 131 which were z-score normalized before analysis: the three fluorescence channels, size, and  
 132 asymmetry. A suitable solution was assessed by inspecting the coefficient of determination and  
 133 the root mean squared distance between clusters for each (e.g. Robinson et al., 2011).  
 134 Concentration time series for each cluster were established by comparing each of the remaining  
 135 particles to the centroid of each cluster. Each time series was apportioned a fraction of the  
 136 particles' count which was inversely proportional to the distance of the particle from each cluster  
 137 centroid (expressed in number of standard deviations of the centroid).  
 138  
 139 Bioaerosol fluxes were estimated for each cluster by combining the concentration gradient with  
 140 vertical wind speed data using:

141

142 Equation S1 
$$F = -0.16 \left( \frac{\Delta z_u \Delta u}{\left( \ln \frac{z_u z}{z_{u1}} \right)^2} \right) \left( \frac{\Delta c}{\Delta z_c} \right)$$

143

144 Where  $\Delta u$  is the difference between vertical wind speed measurements measured at heights  $z_{u1}$   
145 and  $z_{u2}$  which are  $\Delta z_u$  apart, and  $\Delta c$  is the difference in concentrations between two heights which  
146 are  $\Delta z_c$  apart (Lindemann et al., 1982).

147

## 148 ***S1.5 Filter and Impactor Aerosol Samples***

### 149 ***S1.5.1 Sample Collection***

#### 150 ***S1.5.1.1 Cascade Aerosol Impactor (MOUDI)***

151 Size-resolved particle samples were collected using a micro-orifice uniform deposition impactor  
152 (MOUDI; MSP model 110-R) at a flow-rate of 30 LPM via a dedicated inlet. Samples used for  
153 offline ice nucleation analysis were collected onto hydrophobic, siliconized glass slides  
154 (Hampton Research, HR3-2125). The MOUDI sampler provided aerosol fractionation according  
155 to the following aerodynamic diameter size cuts ( $D_{50}$ ,  $\mu\text{m}$ ) (Marple et al., 1991):

156	Stage 1	18.0
157	Stage 2	10.0
158	Stage 3	5.6
159	Stage 4	3.2
160	Stage 5	1.8
161	Stage 6	1.0
162	Stage 7	0.56
163	Stage 8	0.32
164	Stage 9	0.18
165	Stage 10	0.10

166 Stage 11 0.056

167 Stage 1 is typically referred to as the pre-impactor, and stages 2-11 refer to stages in the MOUDI  
168 impactor. Because we are interested in large particles we refer to the pre-impactor as Stage 1 and  
169 list all stages as 1-11. Thus, the numbering scheme utilized here is shifted lower by one with  
170 respect to the common usage for MOUDI samplers.

171  
172 MOUDI samples collected at the following times were analyzed by fluorescence microscopy and  
173 used for microscopic ice nucleation activation experiments as discussed in the manuscript:

174	M01 (dry period)	7/22 14:29 – 7/23 09:41	(1152 min.)
175	M10 (rain period)	8/2 05:55 – 8/3 05:55	(1440 min.)
176	M26 (rain period)	8/16 20:26 – 8/17 06:32	(606 min.)
177	M27 (dry period)	8/17 06:35 – 8/17 19:46	(791 min.)

178  
179 Size distribution of ice nuclei shown in Figure 2C for dry periods are average of samples M1 and  
180 M27; Figure 2D for rain periods are average of samples M10 and M26. Corresponding time  
181 periods for UV-APS are identical to MOUDI sample periods.

182  
183 ***S1.5.1.2 High-volume Sampler***

184 Total aerosol samples for DNA analysis were collected onto 150 mm glass fiber filters  
185 (Machery-Nagel, Type MN 85/90, 406015) using a self-standing high-volume sampler (Digital  
186 DHA-80) operated at 1000 LPM and located approximately 50 m from the sampling trailer.  
187 Filters were pre-baked at 500 °C (12 h) to remove any contaminant DNA and stored in pre-baked  
188 aluminum bags before and after sampling.

189

190 ***SI.5.1.3 Glass Slide Impactor Samples***

191 Total aerosol samples were collected onto glass cover slides (13 x 13 mm) using a home-built,  
192 single-stage impactor (Flow-rate 1.2 LPM, D<sub>50</sub> cut 0.5 µm). The impactor glass substrates were  
193 coated with a thin layer of high viscosity grease (Baysilone grease, Bayer, Germany) administered  
194 via hexane solution to reduce particle bounce. Single-stage impactor and housing for Nuclepore®  
195 filters (below) sub-sampled from a separate inlet immediately next to MOUDI and UV-APS  
196 inlets.

197

198 Glass slide impactor samples collected at the following times are shown in Figures 2A and 2B  
199 and discussed in the manuscript:

200	G09 (dry period)	7/31 12:17 – 12:49	(32 min.)
201	G21 (rain period)	8/3 23:56 – 8/4 0:27	(31 min.)

202

203 ***SI.5.1.4 Nuclepore® Filters***

204 Aerosol samples for electron microscopy analysis were collected with a stacked filter housing  
205 using 12 mm diameter gold-coated Nuclepore® polycarbonate filters with pore sizes of 2 µm for  
206 coarse particles and 0.2 µm for fine particles, respectively. The volume flow through the stacked  
207 filter unit was nominally 2.0 LPM.

208

209 Stacked filter samples collected at the following times are discussed in the manuscript:

210	S10 (dry period)	7/31 11:57 – 15:58	(241 min.)
211	S12 (dry period)	7/31 19:58 – 23:55	(237 min.)

212	S20 (rain period)	8/4 3:52 – 8:04	(252 min.)
213	S23 (rain period)	8/4 16:23 – 20:24	(261 min.)

214

215 ***SI.5.1.5 Bio-Sampler Impactors***

216 Size-resolved viable bioparticles were collected via two types of impactors directly into growth  
217 media (flow-rate 28 LPM). Andersen cascade impactors (Graseby Andersen; Atlanta, GA)  
218 collect particles onto one of six sequential sample plates designed to collect large particles on  
219 upper plates and smaller particles on lower plates. Slit samplers (New Brunswick Scientific Co.;  
220 Edison, NJ) collect particles without selection due to sizing, but the collection stage rotates such  
221 that particles are deposited in a circular arc to give time resolution of ~2 minutes over the course  
222 of a 60 minute sample time. Samplers were placed ~2 m above ground on a piece of wooden  
223 fencing that allowed air to pass through the support surface above ground and operated at 28  
224 LPM. The surfaces of samplers were sterilized with isopropyl alcohol before each period of  
225 collection to remove contaminant organisms. Samplers were operated separately for optimized  
226 collection of fungi and bacteria. Fungal growth medium (malt extract medium) was prepared by  
227 according to Medelin et al. (Madelin, 1994) with streptomycin (40 units, Sigma Aldrich) and  
228 ampicillin (20 units, Fisher Scientific). Bacterial growth medium (Luria Bertani medium; LB)  
229 was prepared according to Lighthart and Shaffer (Lighthart and Shaffer, 1995) with  
230 cycloheximide (200 µg/mL, Sigma Aldrich). Samples for bacterial analysis were collected for 60  
231 minutes, and samples for fungal analysis were collected for 20 minutes. Collection dishes were  
232 immediately removed from samplers after each use and placed in an incubator (IncuMax,  
233 IC150R) temperature-controlled at 25 °C. Fungal colonies were incubated for ~3 days before  
234 counting and picking into 20 µl of sterile water. Bacterial colonies were incubated for ~7 days



235 before counting and picking into sterile water. The picked colonies were lysed at 95 °C for 10  
236 min.

237

### 238 ***SI.5.2 Fluorescence Microscopy***

239 Fluorescence microscopy images were taken on a BZ-9000 Fluorescence Microscope (Keyence,  
240 Inc., Osaka, Japan). The instrument was equipped with a super high-compression mercury lamp  
241 (120 W) and a 2/3-inch, 1.5 mega pixel monochrome CCD. The following fluorescence filters  
242 were used to take images in different spectral ranges: OP-66834 DAPI-BP ( $\lambda_{\text{ex}} = 360/20$  nm,  
243  $\lambda_{\text{Dichroic}} = 400$  nm,  $\lambda_{\text{Absorp}} = 460/25$  nm), OP-66836 GFP-BP ( $\lambda_{\text{ex}} = 470/20$  nm,  $\lambda_{\text{Dichroic}} = 495$  nm,  
244  $\lambda_{\text{Absorp}} = 535/25$  nm), OP-66838 TexasRed ( $\lambda_{\text{ex}} = 560/20$  nm,  $\lambda_{\text{Dichroic}} = 595$  nm,  $\lambda_{\text{Absorp}} = 630/30$   
245 nm). Filter specifications are represented as wavelength and peak width ( $\lambda/\text{FWHM}$ ).

246

247 In Fig. 2A and 2B an overlay of fluorescent emission from all three fluorescence microscope  
248 channels (DAPI, GFP, TexasRed) onto a brightfield image of the same sample area is shown. For  
249 comparability the exposure times of the individual fluorescence images in Fig. 2A and 2B were  
250 set to the same values. The overlay image Fig. 2B is dominated by “blue-green” fluorescence  
251 indicating strong emissions in the DAPI ( $\lambda_{\text{ex}} = \sim 360$  nm,  $\lambda_{\text{em}} = \sim 460$  nm) and GFP  
252 ( $\lambda_{\text{ex}} = \sim 470$  nm,  $\lambda_{\text{em}} = \sim 535$  nm) channels. Blue-green fluorescence is characteristic for biological  
253 material and mainly originating from protein and coenzyme fluorophores (Pöhlker et al., 2012).  
254 In contrast “red-yellow” fluorescence is predominating in the overlay image in Fig. 2A  
255 indicating strong emission in the TexasRed channel ( $\lambda_{\text{ex}} = \sim 560$  nm,  $\lambda_{\text{em}} = \sim 630$  nm). Red-yellow  
256 fluorescence is regarded to be somewhat characteristic/typical for mineral dust (Bozlee et al.,  
257 2005).

258

### 259 ***S1.5.3 SEM***

260 Scanning electron microscopy (SEM) images of aerosol particles were acquired using the  
261 secondary electron in-lens detector of a high-performance field emission instrument (LEO 1530  
262 FESEM, EHT 10 keV, WD 9 mm). The elemental composition of inorganic components was  
263 characterized using the Oxford Instruments ultra-thin-window energy-dispersive X-ray (EDX)  
264 detector.

265

266 The filter samples were scanned using a semi-automated spot counting technique (Sinha et al.,  
267 2008; Pöschl et al., 2010) at a magnification of  $6500 \times$  (pixel size 88.9 nm) for coarse and  $19500$   
268  $\times$  (pixel size 29.6 nm) for fine particle filters. Particles located on the predefined equidistant  
269 spots of the counting grid were automatically counted, and the recorded data were used to  
270 classify the particles according to size, composition, and mixing state. With spot counting, the  
271 probability for particles of a certain size and type to be counted is directly proportional to the 2-  
272 D surface area of the particles and the fraction of the filter surface covered by such particles.  
273 This relationship is used to upscale the counting results from the investigated filter area to the  
274 total filter area.

275

### 276 ***S1.5.4 DNA Analysis of Aerosol Samples***

277 To determine fungal diversity from the air filter samples (high-volume sampler, S1.5.1.2)  
278 optimized methods of DNA extraction, amplification, and sequence analysis of the internal  
279 transcribed spacer (ITS) regions as described in Fröhlich-Nowoisky et al. (2009; 2012) were  
280 used. In addition to fungi, the primer pair ITS4Oo and ITS5 (Nikolcheva and Bärlocher, 2004)

281 was used for amplification of *Peronosporomycetes* (formerly *Oomycota*). Also specific for this  
282 study, the internal transcribed spacer regions from fungal lysates, obtained from the cultivation  
283 experiments of impactor samples (Anderson Cascade Bio-Sampler Impactors, S1.5.1.5), were  
284 amplified with the primer pair ITS4 and ITS5 (White et al., 1990; Fröhlich-Nowoisky et al.,  
285 2009; Fröhlich-Nowoisky et al., 2012). The obtained PCR products were sequenced using the  
286 primer ITS5 and sequence analysis was performed as described in Fröhlich-Nowoisky et al.  
287 (2009; 2012). The sequences from the obtained operational taxonomic units have been deposited  
288 in the GenBank database under following accession numbers: JX135610 - JX136661 (Fungi) and  
289 JQ976038 - JQ976273 (*Peronosporomycetes*).

290

291 For the determination of bacterial diversity from high-volume aerosol filter samples (see also  
292 S.1.5.1.2) DNA was extracted as described by Després et al. (2007). The 16S ribosomal gene  
293 was first amplified for taxonomic identification with primer pairs 9/27f and 1492r (Weisburg et  
294 al., 1991) with PCRs conditions given by Després et al. (2007), and then cloned and sequenced.  
295 The same primer pair was used for the bacterial lysates obtained from Andersen sampler culture  
296 plates (Anderson Cascade Bio-Sampler Impactors, S1.5.1.5). Sequences are deposited in the  
297 GenBank database under the following accession numbers: JX228219-JX228862.

298

### 299 ***S1.5.5 Freezing Tests***

300 Fungal and bacterial colonies (Andersen Cascade Bio-Sampler Impactor, S1.5.1.5) were picked  
301 and cultured in dextrose-peptone-yeast (DPY) medium (dextrose 10 g/L, peptone 3 g/L, yeast  
302 extract 0.3g/L) in 96-well polypropylene plates and incubated at 16 °C. A 50 µl aliquot of the  
303 inoculated DPY medium containing hyphal fragments and fungal spores was tested from each

304 well for its ice nucleation activity in a temperature range -12 °C to -2 °C. Aliquots were  
305 transferred to a fresh, sterile, 96-well polypropylene PCR tray and these were cooled in a thermal  
306 cycler (MJ Research, PTC-200). Temperature variation across the head was  $\pm 0.2$  °C of the true  
307 temperature measured using a thermistor (Bio-Rad, VPT-0300). The cycler was programmed to  
308 descend in 0.5 or 1 °C increments to -9.0 °C (the limit of the machine). After a 5 min dwell time  
309 at each temperature, the number of frozen wells was counted and the temperature lowered to the  
310 next level. Once at -9 °C, the tray was transferred to a 96-well aluminum incubation block  
311 (VWR, 13259-260) which had been pre-cooled to  $\sim$ -12 °C inside a foam box in a freezer. The  
312 thermistor was inserted into a side well and after 10 min the block temperature and number of  
313 frozen wells was recorded. Aliquots of un-inoculated DPY medium were used as negative  
314 controls. Ice active isolates were then cultured on DPY agar and incubated at RT for  $\sim$  3 days.  
315 Beside microscopic analysis as described under S1.5.2 hyphal fragments and spores were picked  
316 into 20  $\mu$ l water, lysed at 95 °C for 10 min, and identified by DNA analysis as described above.

317

### 318 ***S1.6 Microscopic IN Activation Experiments***

319 Particles were collected on hydrophobic glass slides with a rotating MOUDI, as described above.  
320 The freezing properties of particles collected on the slides were then determined with an optical  
321 microscope and a flow cell with temperature and relative humidity control. The flow cell and  
322 microscope set-up was very similar to the ones used by Iannone et al. (2011) and Dymarska et al.  
323 (2006), to determine the ice nucleation properties of fungal spores and soot particles,  
324 respectively.

325

326 In every IN activation experiment, a hydrophobic slide containing particles was located within  
 327 the flow cell. The RH was first set to > 100% to condense water droplets on the particles. The  
 328 droplets were grown to approximately 100 μm in diameter, and after droplet growth was  
 329 completed each droplet contained between 30 and 100 particles. Next, the temperature was  
 330 decreased at a rate of 10 K/min until a temperature of -40 °C was reached. During the  
 331 experiment, between 11 and 66 droplets (average 36) were continuously monitored with an  
 332 optical microscope coupled to a CCD camera. From the images recorded with the CCD camera,  
 333 the freezing temperatures of the droplets were determined.

334

335 The number of ice nuclei in a freezing experiment,  $\#IN(T)$ , was calculated from the freezing data  
 336 using the following equation (Vali, 1971):

337 Equation S2 
$$\#IN(T) = -\ln\left(\frac{N_{Total} - N_{Frozen}(T)}{N_{Total}}\right) \times N_{Total}$$

338

339 where  $N_{Total}$  is the total number of droplets in a freezing experiment and  $N_{Frozen}(T)$  is the number  
 340 of frozen droplets as a function of temperature in a freezing experiment. Equation S2 accounts  
 341 for the fact that multiple IN can exist in the same droplet (Vali, 1971). The number of ice nuclei  
 342 per volume of air as a function of temperature,  $[IN(T)]$ , was calculated using the following  
 343 equation:

344 Equation S3 
$$[IN(T)] = \frac{\#IN(T)}{VolumeAirSampled} \times \frac{Area_{MOUDIStage}}{Area_{Monitored}}$$

345 where  $VolumeAirSampled$  is the total volume of air sampled by the MOUDI,  $Area_{MOUDIStage}$  is  
 346 the total area covered by particles within a MOUDI stage and  $Area_{Monitored}$  is the area  
 347 monitored with the microscope.

348

349 In the freezing experiments, a majority of the droplets froze by immersion freezing while a  
350 minority froze by contact freezing. Here immersion freezing refers to freezing of droplets by ice  
351 nuclei immersed in the liquid droplets, and contact freezing refers to freezing of liquid droplets  
352 by contact with neighboring frozen droplets (frozen droplets can grow by vapor transfer and  
353 eventually can come in contact with their neighbors). Droplets that froze by contact freezing  
354 were not considered when determining  $N_{Total}$  and  $N_{Frozen}(T)$  from the freezing data. In addition to  
355 immersion freezing and contact freezing, deposition freezing occasionally occurred in the  
356 freezing experiments. Here deposition freezing refers to freezing on a particle not immersed in a  
357 solution droplet. Deposition freezing was included in the calculations of  $[IN(T)]$  by adding the  
358 number of deposition freezing events to  $\#IN(T)$  calculated with Equation S2 above.

359

360 Depending on the experimental conditions, the maximum concentration of ice nuclei,  $[IN(T)]$ ,  
361 that can be detected for any given slide (i.e. size interval sampled with the MOUDI) with the  
362 microscope freezing technique is roughly  $0.6-0.9 \text{ L}^{-1}$  depending on the number of droplets  
363 condensed in an experiment and the total volume of air sampled by the MOUDI. As a result the  
364 maximum concentration of IN determined by the microscope technique is small compared to the  
365 maximum concentration determined with the CFDC method mentioned below.

366

## 367 ***S1.7 Real-Time Ice Nucleation Measurements with CFDC***

### 368 ***S1.7.1 IN Measurements***

369 A ground-based version of the Colorado State University continuous flow diffusion chamber  
370 (CFDC) (Rogers et al., 2001) was employed for real-time measurements of IN concentrations.

371 The CFDC permits observation of ice formation on a continuous stream of particles at controlled

372 temperatures and humidities. In the CFDC, sampled air is directed vertically between two  
373 concentric ice-coated cylinders held at different temperatures, creating a zone supersaturated  
374 with respect to ice in the annular region. The sample air, ~15% of the total flow, is injected  
375 between two particle-free sheath flows. As the particles in the sample flow are exposed to ice  
376 supersaturations for several seconds, those particles active as IN under the sample temperature  
377 and humidity conditions are nucleated and grown to ice crystals larger than a few  $\mu\text{m}$  in size.  
378 These larger particles are distinguished from small non-IN aerosols by an optical particle counter  
379 (OPC) at the outlet of the instrument. Physical impaction of larger aerosols ( $>2.4 \mu\text{m}$ ) in advance  
380 of the CFDC and reduction of humidity conditions to ice saturation in the lower third of the  
381 chamber prevent false detection of large CN or cloud drops as ice nuclei. Temperatures ( $\pm 1^\circ\text{C}$ )  
382 and humidities ( $\pm 3\%$  RH with respect to water maximum uncertainty at  $-30^\circ\text{C}$ ) are well  
383 controlled in the instrument. For data used in this study, measurements were made at  $-25^\circ\text{C}$  at  
384 relative humidity in the range of 103% to 106%. Under these conditions, the CFDC directly  
385 measures IN activating by condensation/immersion freezing, and contributions are expected to  
386 the IN population from both dust and biological particles (Prenni et al., 2009). For the data in  
387 Figures 2E and 2F, particle concentrations were enhanced upstream using an MSP Corporation  
388 (Model 4240) aerosol concentrator. Measurements made using the concentrator were corrected to  
389 ambient concentrations based on the manufacturer's specifications for  $1 \mu\text{m}$  particles, corrected  
390 slightly for the sampling conditions at Manitou, as determined from direct measurements made  
391 approximately every other day. IN number concentrations are reported at standard temperature  
392 and pressure (STP; 1 atm and  $0^\circ\text{C}$ ).

393

394 CFDC measurements were collected at the following times are shown in Figures 2E and 2F E-F  
395 and discussed in the manuscript:

396	C01 (rain period)	8/2 10:27 – 17:57	(450 min.)
397	C02 (dry period)	8/17 16:27 – 23:47	(440 min.)

398

399 Periods C01 and C02 correspond to sub-periods during MOUDI samples M10 and M27,  
400 respectively.

401

#### 402 ***SI.7.2 DNA Analysis of IN Samples***

403 Ice crystals activated as IN in the CFDC were collected via impaction at the CFDC outlet (Prenni  
404 et al., 2009; Garcia et al., 2012). Residual IN were impacted onto a glass slide, which was coated  
405 with 5 mL of molecular grade mineral oil (Bio-Rad). DNA was then enzymatically extracted  
406 using Proteinase K. The extracted DNA was PCR amplified using the universal 515F and 1391R  
407 primers. The presence of biological IN was determined after PCR amplification via acrylamide  
408 gel electrophoresis. PCR products were cloned into a plasmid vector using the TOPO TA  
409 Cloning Kit® for sequencing (Invitrogen). Each clone was sequenced (Sanger method) and  
410 identified via Blast search against the National Center for Biotechnology Information (NCBI)  
411 genome database (2).



412 **References:**

- 413 Bozlee, B. J., Misra, A. K., Sharma, S. K. and Ingram, M.: Remote Raman and fluorescence  
414 studies of mineral samples, *Spectrochimica Acta Part a-Molecular and Biomolecular*  
415 *Spectroscopy*, 61, 2342-2348, 10.1016/j.saa.2005.02.033, 2005.
- 416 Després, V. R., Nowoisky, J. F., Klose, M., Conrad, R., Andreae, M. O. and Pöschl, U.:  
417 Characterization of primary biogenic aerosol particles in urban, rural, and high-alpine air by  
418 DNA sequence and restriction fragment analysis of ribosomal RNA genes, *Biogeosciences*, 4,  
419 1127-1141, 2007.
- 420 Dymarska, M., Murray, B. J., Sun, L. M., Eastwood, M. L., Knopf, D. A. and Bertram, A. K.:  
421 Deposition ice nucleation on soot at temperatures relevant for the lower troposphere, *J. Geophys.*  
422 *Res.-Atmos.*, 111, 10.1029/2005jd006627, 2006.
- 423 Foot, V. E., Kaye, P. H., Stanley, W. R., Barrington, S. J., Gallagher, M. and Gabey, A.: Low-  
424 cost real-time multi-parameter bio-aerosol sensors, *Proceedings of the SPIE - The International*  
425 *Society for Optical Engineering*, 711601 (711612 pp.), 10.1117/12.800226, 2008.
- 426 Fröhlich-Nowoisky, J., Pickersgill, D. A., Després, V. R. and Pöschl, U.: High diversity of fungi  
427 in air particulate matter, *Proceedings of the National Academy of Sciences*, 106, 12814-12819,  
428 10.1073/pnas.0811003106, 2009.
- 429 Fröhlich-Nowoisky, J., Burrows, S. M., Xie, Z., Engling, G., Solomon, P. A., Fraser, M. P.,  
430 Mayol-Bracero, O. L., Artaxo, P., Begerow, D., Conrad, P. G., Andreae, M. O., Després, V. and  
431 Pöschl, U.: Biogeography in the air: fungal diversity over land and oceans, *Biogeosciences*, 9,  
432 1125-1136, 10.5194/bg-9-1125-2012, 2012.
- 433 Gabey, A. M., Gallagher, M. W., Whitehead, J., Dorsey, J. R., Kaye, P. H. and Stanley, W. R.:  
434 Measurements and comparison of primary biological aerosol above and below a tropical forest  
435 canopy using a dual channel fluorescence spectrometer, *Atmospheric Chemistry and Physics*, 10,  
436 4453-4466, 10.5194/acp-10-4453-2010, 2010.
- 437 Garcia, E., Hill, T. C. J., Prenni, A. J., DeMott, P. J., Franc, G. D. and Kreidenweis, S. M.:  
438 Biogenic ice nuclei in boundary layer air over two U.S. High Plains agricultural regions, *Journal*  
439 *of Geophysical Research*, In Review, 2012.
- 440 Huffman, J. A., Treutlein, B. and Pöschl, U.: Fluorescent biological aerosol particle  
441 concentrations and size distributions measured with an Ultraviolet Aerodynamic Particle Sizer  
442 (UV-APS) in Central Europe, *Atmospheric Chemistry and Physics*, 10, 3215-3233, 2010.
- 443 Iannone, R., Chernoff, D. I., Pringle, A., Martin, S. T. and Bertram, A. K.: The ice nucleation  
444 ability of one of the most abundant types of fungal spores found in the atmosphere, *Atmospheric*  
445 *Chemistry and Physics*, 11, 1191-1201, 10.5194/acp-11-1191-2011, 2011.
- 446 Kaye, P. H., Stanley, W. R., Hirst, E., Foot, E. V., Baxter, K. L. and Barrington, S. J.: Single  
447 particle multichannel bio-aerosol fluorescence sensor, *Optics Express*, 13, 3583-3593, 2005.
- 448 Lighthart, B. and Shaffer, B. T.: Airborne bacteria in the atmosphere surface layer: temporal  
449 distribution above a grass seed field, *Applied and Environmental Microbiology*, 61, 1492-1496,  
450 1995.

451 Lindemann, J., Constantinidou, H. A., Barchet, W. R. and Upper, C. D.: Plants as sources of  
452 airborne bacteria, including ice nucleation-active bacteria, *Applied and Environmental*  
453 *Microbiology*, 44, 1059-1063, 1982.

454 Madelin, T. M.: Fungal Aerosols - A Review, *Journal of Aerosol Science*, 25, 1405-1412,  
455 10.1016/0021-8502(94)90216-x, 1994.

456 Marple, V. A., Rubow, K. L. and Behm, S. M.: A microorifice uniform deposit impactor  
457 (MOUDI) - description, calibration, and use, *Aerosol Sci. Technol.*, 14, 434-446,  
458 10.1080/02786829108959504, 1991.

459 Nikolcheva, L. G. and Bärlocher, F.: Taxon-specific fungal primers reveal unexpectedly high  
460 diversity during leaf decomposition in a stream, *Mycological Progress*, 3, 41-49, 2004.

461 Pöhlker, C., Huffman, J. A. and Pöschl, U.: Autofluorescence of atmospheric bioaerosols -  
462 fluorescent biomolecules and potential interferences, *Atmospheric Measurement Techniques*, 5,  
463 37-71, 10.5194/amt-5-37-2012, 2012.

464 Pöschl, U., Martin, S. T., Sinha, B., Chen, Q., Gunthe, S. S., Huffman, J. A., Borrmann, S.,  
465 Farmer, D. K., Garland, R. M., Helas, G., Jimenez, J. L., King, S. M., Manzi, A., Mikhailov, E.,  
466 Pauliquevis, T., Petters, M. D., Prenni, A. J., Roldin, P., Rose, D., Schneider, J., Su, H., Zorn, S.  
467 R., Artaxo, P. and Andreae, M. O.: Rainforest Aerosols as Biogenic Nuclei of Clouds and  
468 Precipitation in the Amazon, *Science*, 329, 1513-1516, 10.1126/science.1191056, 2010.

469 Prenni, A. J., Petters, M. D., Kreidenweis, S. M., Heald, C. L., Martin, S. T., Artaxo, P., Garland,  
470 R. M., Wollny, A. G. and Pöschl, U.: Relative roles of biogenic emissions and Saharan dust as  
471 ice nuclei in the Amazon basin, *Nature Geoscience*, 2, 402-405, 10.1038/ngeo517, 2009.

472 Robinson, N. H., Newton, H. M., Allan, J. D., Irwin, M., Hamilton, J. F., Flynn, M., Bower, K.  
473 N., Williams, P. I., Mills, G., Reeves, C. E., McFiggans, G. and Coe, H.: Source attribution of  
474 Bornean air masses by back trajectory analysis during the OP3 project, *Atmospheric Chemistry*  
475 *and Physics*, 11, 9605-9630, 10.5194/acp-11-9605-2011, 2011.

476 Rogers, D. C., DeMott, P. J., Kreidenweis, S. M. and Chen, Y.: A continuous-flow diffusion  
477 chamber for airborne measurements of ice nuclei, *J. Atmos. Ocean. Tech.*, 18, 725-741, 2001.

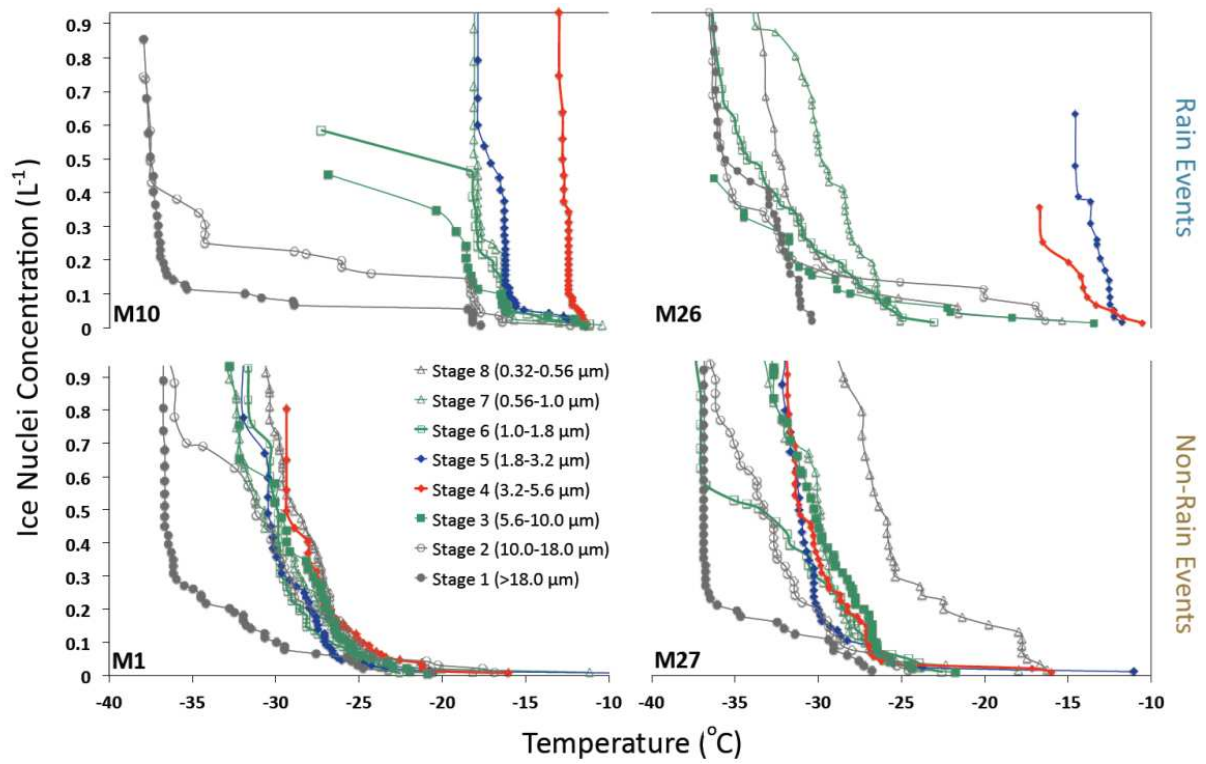
478 Sinha, B. W., Hoppe, P., Huth, J., Foley, S. and Andreae, M. O.: Sulphur isotope analysis of  
479 individual aerosol particles in the urban aerosol at a Central European site (Mainz, Germany),  
480 *Atmospheric Chemistry and Physics*, 8, 7217-7238, 2008.

481 Vali, G.: Quantitative evaluation of experimental results on heterogeneous freezing of  
482 supercooled liquids, *Journal of the Atmospheric Sciences*, 28, 402-&, 10.1175/1520-  
483 0469(1971)028<0402:qoera>2.0.co;2, 1971.

484 Weisburg, W. G., Barns, S. M., Pelletier, D. A. and Lane, D. J.: 16S ribosomal DNA  
485 amplification for phylogenetic study, *J. Bacteriol.*, 173, 697-703, 1991.

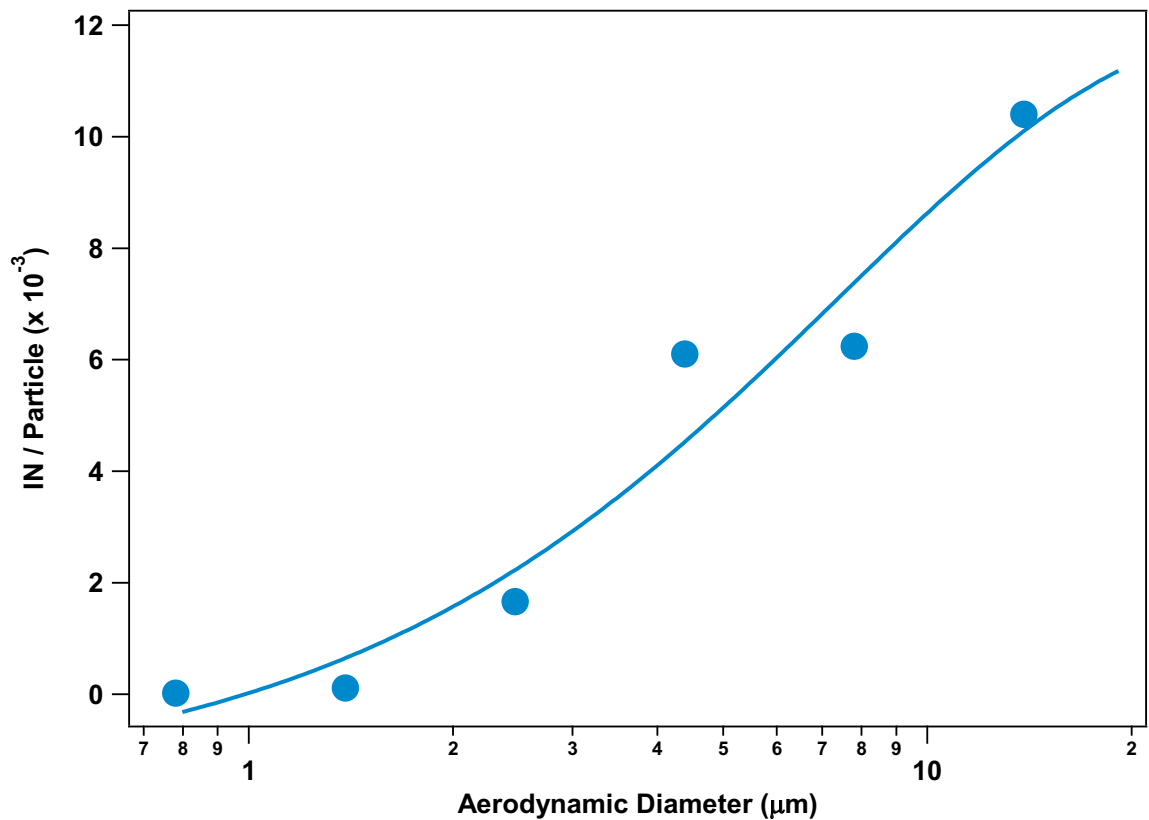
486 White, T. J., Bruns, T., Lee, S. and Taylor, J.: Amplification and Direct Sequencing of Fungal  
487 Ribosomal RNA genes for Phylogenetics, in: *PCR Protocols: a Guide to Methods and*  
488 *Applications*, edited by: Innis, M. A., Gelfand, D. H., Sninsky, J. J. and White, T. J., Academic  
489 Press, Inc., New York, 315-322, 1990.

490



491  
 492  
 493  
 494  
 495  
 496  
 497

**Figure S1:** IN activation curves from microscopic IN activation experiments with size-resolved aerosol samples (MOUDI stages). Upper panels (A,B) for samples collected during rain events, and lower panels (C,D) for samples collected during dry periods. Red traces show Stage 4 (3.2 – 5.6  $\mu\text{m}$ ), blue traces show Stage 5 (1.8 – 3.2  $\mu\text{m}$ ), and light green traces show Stage 3, 6, 7 (5.6-10, 1.0-1.8, and 0.56-1.0  $\mu\text{m}$ , respectively). See SOM section S1.5.1.1 for sampling dates.



498  
499

500 **Figure S2:** An estimate of the fraction of particles collected during rain events (M10, M26) that can serve as IN at  
 501  $-15\text{ }^{\circ}\text{C}$ . IN concentrations were calculated from microscopic IN activation experiments and particle concentrations  
 502 were calculated from UV-APS measurements. See SOM section S1.5.1.1 for sampling dates. Note that the fraction  
 503 of particles with IN activity is greater than 1 in 1000 for all particles  $>2\text{ }\mu\text{m}$  and exceeds 1 in 100 for particles  $>10$   
 504  $\mu\text{m}$ . Exponential curve shown to guide the eye.

**B4. Pöhlker et al., Science, 2012**

**Biogenic potassium salt particles as seeds for secondary organic aerosol in the Amazon**

Christopher Pöhlker<sup>1</sup>, Kenia T. Wiedemann<sup>1</sup>, Bärbel Sinha<sup>1</sup>, Manabu Shiraiwa<sup>1</sup>, Sachin S. Gunthe<sup>1</sup>, Mackenzie Smith<sup>1</sup>, Hang Su<sup>1</sup>, Paulo Artaxo<sup>1</sup>, Qi Chen<sup>1</sup>, Yafang Cheng<sup>1</sup>, Wolfgang Elbert<sup>1</sup>, Mary K. Gilles<sup>1</sup>, Arthur L. D. Kilcoyne<sup>1</sup>, Ryan C. Moffet<sup>1</sup>, Markus Weigand<sup>1</sup>, Scot T. Martin<sup>1</sup>, Ulrich Pöschl<sup>1</sup>, and Meinrat O. Andreae<sup>1</sup>

*1 Max Planck Institute for Chemistry, Biogeochemistry Department, Mainz, Germany*

*2 University of São Paulo, Institute of Physics, São Paulo, Brazil*

*3 Harvard University, School of Engineering and Applied Sciences, Cambridge, MA, USA*

*4 University of Arizona, Ecology and Evolutionary Biology Department, Tucson, AZ, USA*

*5 Max Planck Institute for Chemistry, Particle Chemistry Department, Mainz, Germany*

*6 IISER Mohali, Department of Earth and Environmental Science, Manauli, India*

*7 California Institute of Technology, Department of Chemical Engineering, Pasadena, CA, USA*

*8 Indian Institute of Technology Madras, Department of Civil Engineering, Chennai, India*

*9 Lawrence Berkeley National Laboratory, Chemical Science Division, Berkeley, CA, USA*

*10 Lawrence Berkeley National Laboratory, Advanced Light Source, Berkeley, CA, USA*

*11 University of the Pacific, Department of Chemistry, Stockton, CA, USA*

*12 Max Planck Institute for Intelligent Systems, Stuttgart, Germany*

**Science, 337, 1075-1078, 2012**



# Biogenic Potassium Salt Particles as Seeds for Secondary Organic Aerosol in the Amazon

Christopher Pöhlker,<sup>1\*</sup> Kenia T. Wiedemann,<sup>2,3,4</sup> Bärbel Sinha,<sup>5,6</sup> Manabu Shiraiwa,<sup>1,7</sup> Sachin S. Gunthe,<sup>1,8</sup> Mackenzie Smith,<sup>3</sup> Hang Su,<sup>1</sup> Paulo Artaxo,<sup>2</sup> Qi Chen,<sup>3</sup> Yafang Cheng,<sup>1</sup> Wolfgang Elbert,<sup>1</sup> Mary K. Gilles,<sup>9</sup> Arthur L. D. Kilcoyne,<sup>10</sup> Ryan C. Moffet,<sup>8,11</sup> Markus Weigand,<sup>12</sup> Scot T. Martin,<sup>3</sup> Ulrich Pöschl,<sup>1\*</sup> Meinrat O. Andreae<sup>1</sup>

The fine particles serving as cloud condensation nuclei in pristine Amazonian rainforest air consist mostly of secondary organic aerosol. Their origin is enigmatic, however, because new particle formation in the atmosphere is not observed. Here, we show that the growth of organic aerosol particles can be initiated by potassium-salt-rich particles emitted by biota in the rainforest. These particles act as seeds for the condensation of low- or semi-volatile organic compounds from the atmospheric gas phase or multiphase oxidation of isoprene and terpenes. Our findings suggest that the primary emission of biogenic salt particles directly influences the number concentration of cloud condensation nuclei and affects the microphysics of cloud formation and precipitation over the rainforest.

Organic aerosols are ubiquitous in the atmosphere and play important roles in the climate system. They can cool Earth's surface by scattering sunlight or serve as nuclei for water droplets and ice crystals in clouds and precipitation. The properties and origin of organic aerosol particles are, however, still poorly understood, and their effects are among the largest uncertainties in the current understanding of climate (1–3). For reliable assessment and control of the human influence on climate, it is important to understand the natural background sources of atmospheric aerosols (4). One of the few continental regions where aerosols can be studied under near-natural conditions is the Amazon Basin, which has an aerosol burden that is mainly driven by an intensive biosphere-atmosphere interaction (5). Recent investigations indicate that the fine particles serving as cloud condensation nuclei (CCN) in pristine Amazonian rainforest air consist predominantly of secondary organic aerosol (SOA), formed by oxidation of

volatile organic compounds (VOC) and condensation of low- or semi-volatile oxidation products (6, 7). The actual mechanism of initial particle formation, however, remains unclear. In contrast to other vegetated continental regions, ultrafine particles with diameters < 30 nm (nucleation mode particles), which are characteristic for new particle-formation events in which gaseous species condense to form secondary aerosol particles, are almost never observed in pristine boundary layer air over the Amazonian rainforest (5, 8). One possible explanation for the lack of nucleation mode particles in the Amazonian boundary layer could be that the nucleation and the initial growth of new particles take place in the free troposphere, followed by downward transport in the course of convective overturning (9, 10). Alternatively, as we suggest here, the secondary organic material may condense onto preexisting primary particles directly emitted from the rainforest.

We applied scanning transmission x-ray microscopy with near-edge x-ray absorption fine

structure analysis (STXM-NEXAFS), scanning electron microscopy (SEM), and secondary ion mass spectrometry (NanoSIMS) to determine the microstructure and chemical composition of Amazonian organic aerosol particles in the accumulation mode (0.1 to 1  $\mu\text{m}$  diameter). This size range is most relevant to the activation of cloud condensation nuclei (6). The aerosol samples were collected during the wet season (May 2011) at a remote rainforest site [Amazonian Tall Tower Observatory (ATTO) site] 150 km northeast of Manaus, Brazil. The investigated air masses came with the trade wind circulation from the northeast and traveled over some 1000 km of mostly pristine tropical rainforest. For comparison, we also investigated laboratory-generated SOA reference samples from isoprene and terpene oxidation, as well as reference samples generated by spray-drying of pure organic compounds in aqueous solution (11). We used STXM-NEXAFS for the determination of elemental and functional group composition in individual organic aerosol particles (12, 13) and SEM and NanoSIMS for further morphological characterization and independent confirmation of elemental composition.

The Amazonian aerosol samples comprised a mixture of homogeneous droplets and droplets containing internal structures that may be indicative of their atmospheric aging history (Fig. 1, A and B, and fig. S8). The NEXAFS spectra revealed characteristic similarities and differences between the chemical composition of the Amazonian aerosol and laboratory-generated reference samples. The terpene SOA reference particles exhibit a sharp peak representative of carboxylic acid groups (COOH), as well as shoulders indicating carbonyl groups (C=O) and carbon-carbon double bonds (C=C), but no pronounced signal of hydroxy groups (C-OH). Spectra of the isoprene SOA reference particles show a broad peak resulting from COOH and C-OH signals of comparable intensity, a C=O shoulder, and no C=C signal. Spectra of the carbohydrate reference particles exhibit a sharp C-OH peak, no COOH signal, and very weak C=O and C=C shoulders (Fig. 2A).

<sup>1</sup>Biogeochemistry Department, Max Planck Institute for Chemistry, Mainz 55020, Germany. <sup>2</sup>Institute of Physics, University of São Paulo, São Paulo 05508-900, Brazil. <sup>3</sup>School of Engineering and Applied Sciences, Harvard University, Cambridge, MA 02138, USA. <sup>4</sup>Ecology and Evolutionary Biology Department, University of Arizona, Tucson, AZ 85721, USA. <sup>5</sup>Particle Chemistry Department, Max Planck Institute for Chemistry, Mainz 55020, Germany. <sup>6</sup>Department of Earth and Environmental Science, Indian Institute of Science Education and Research Mohali, S.A.S. Nagar, Manauli PO, India. <sup>7</sup>Division of Chemistry and Chemical Engineering, California Institute of Technology, Pasadena, CA 91125, USA. <sup>8</sup>Environmental and Water Resources Engineering Division, Department of Civil Engineering, Indian Institute of Technology Madras, Chennai 600036, India. <sup>9</sup>Chemical Science Division, Lawrence Berkeley National Laboratory, Berkeley, CA 94720, USA. <sup>10</sup>Advanced Light Source, Lawrence Berkeley National Laboratory, Berkeley, CA 94720, USA. <sup>11</sup>Department of Chemistry, University of the Pacific, Stockton, CA 95211, USA. <sup>12</sup>Max Planck Institute for Intelligent Systems, Stuttgart 70569, Germany.

\*To whom correspondence should be addressed. E-mail: c.pohlker@mpic.de (C.P.); u.poschl@mpic.de (U.P.).

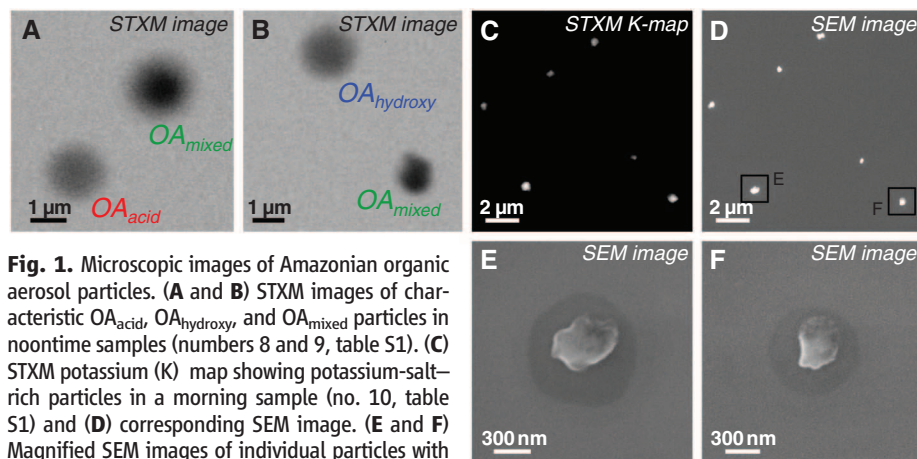


**Fig. 1.** Microscopic images of Amazonian organic aerosol particles. (A and B) STXM images of characteristic  $\text{OA}_{\text{acid}}$ ,  $\text{OA}_{\text{hydroxy}}$ , and  $\text{OA}_{\text{mixed}}$  particles in noontime samples (numbers 8 and 9, table S1). (C) STXM potassium (K) map showing potassium-salt-rich particles in a morning sample (no. 10, table S1) and (D) corresponding SEM image. (E and F) Magnified SEM images of individual particles with salt core and organic coating [black frames in (D)].

In the Amazonian aerosol samples, three chemically distinct types of organic particles could be assigned to the following categories (Fig. 2A): (i)  $OA_{acid}$  particles exhibited spectra with a pronounced COOH peak similar to those of laboratory-generated SOA particles from terpene oxidation; (ii)  $OA_{hydroxy}$  particles showed a strong hydroxy group signal similar to pure carbohydrate particles; and (iii)  $OA_{mixed}$  particles exhibited spectra resembling a mixture of  $OA_{acid}$  and  $OA_{hydroxy}$  spectra. All three particle classes contained variable amounts of potassium. The coexistence of chemically distinct types of organic particles indicates the influence of different sources and formation mechanisms in the Amazonian boundary layer. Categories  $OA_{acid}$  and  $OA_{hydroxy}$  each accounted for about 25% of all particles analyzed in this study, whereas  $OA_{mixed}$  was the most abundant particle type and contributed about 50%. Previous studies in Amazonia had shown that terpene- and isoprene-based SOA dominated the mass of organic aerosol (6, 7, 14), which is consistent with our observation of  $OA_{acid}$ ,  $OA_{hydroxy}$ , and  $OA_{mixed}$  as a mixture of both. In addition to isoprene and terpene oxidation products, carbohydrates associated with primary particle emissions may also contribute to the observed organic matter (15, 16).

The most unexpected finding of our study was the presence of pronounced potassium signals in the NEXAFS spectra of nearly all analyzed organic particles (Fig. 2B). The potassium mass fraction is strongly size-dependent and decreases from ~20% at volume-equivalent particle diameters around 0.15  $\mu\text{m}$  down to ~0.3% for diameters around 1  $\mu\text{m}$  (Fig. 3), with a median value of 2.6% (11) (supplementary text S1.5). This observation suggests that small potassium-salt-rich particles from primary emissions act as seeds for the condensation of organic material and that the primary potassium content is diluted upon particle growth. The occurrence of these potassium-bearing particles has been confirmed by a combination of STXM, SEM, and NanoSIMS. In particular, samples collected during the morning hours show a high abundance of fine particles (~0.2  $\mu\text{m}$ ) with strong potassium signals and a low content of organic matter (Fig. 1, C to F, and fig. S7). The STXM and NanoSIMS results indicate that the potassium-rich particles also contain substantial quantities of ammonium cations as well as chloride and sulfate counteranions (11) (supplementary text S1.7).

Potassium-rich particles, in association with soot carbon, are an important component of biomass-burning smoke (17, 18). In our samples, however, we can exclude biomass burning as a source of the potassium-rich particles, because we did not find any particles containing soot carbon. Also, there were no fires detected in the region along the air mass trajectories during our study period (19, 20). Hence, biogenic emissions are the only potential source. Earlier investigations, including online high-resolution time-of-flight aerosol mass spectrometry (HR-ToF-AMS)

(fig. S12), had already reported substantial amounts of potassium associated with biogenic submicrometer aerosol in the Amazon during the wet season (21–23). They were not able to relate the presence of potassium to specific particle types, but the combination of potassium and sulfur has been attributed to local biogenic sources (24–26), which is consistent with the observation of potassium- and sulfate-rich particles in our study. The median atmospheric potassium concentration estimated from our analysis [ $\sim 50 \text{ ng m}^{-3}$  for particles in the size range of 0.1 to 1  $\mu\text{m}$ , (11) supplementary text S1.5] is consistent with previous measurement results [18 to 220  $\text{ng m}^{-3}$  for particles  $< 2 \mu\text{m}$  (16)]. Several studies show that active biota, such as plants and fungi, can efficiently release salts into the air (15, 16, 27–30). In particular, the active wet discharge of fungal spores is accompanied by the emission of aqueous droplets that contain potassium, chloride, and carbohydrates as the main osmolytes (11, 16) (supplementary text S2.1). STXM and light micrographs of our samples indicate a high abundance of fungal spores in the coarse particle fraction ( $> 1 \mu\text{m}$ , fig. S6), which supports the idea of fungal emissions as a plausible source for the observed potassium-rich particles.

SEM images show that the biogenic salt particles in the early morning samples consist of a

strongly electron-scattering salt core embedded in a thin organic coating (Fig. 1, E and F). However, potassium salt cores are not present in particles collected during the daytime. Instead, many particles show an inorganic microgranular material distributed over the entire particle (fig. S8, A and B). The phase separation observed in our samples follows the same pattern and dependence on oxygen-to-carbon ratio as reported in recent studies of liquid-liquid phase separation in organic and mixed organic-inorganic aerosol particles (31–33):  $OA_{hydroxy}$  particles with high atomic ratios of oxygen to carbon ( $O:C \approx 0.9$  to 1.0) showed no phase separation, whereas  $OA_{acid}$  and  $OA_{mixed}$  particles with  $O:C$  ratios around 0.5 to 0.7 showed internal structures with a COOH-rich core and a C-OH-rich shell (table S4 and fig. S8). These observations indicate a pronounced influence of aqueous processing in deliquesced aerosol particles and cloud or fog droplets on the growth and aging of SOA particles, that is, the formation and evaporation of aqueous droplets in which multiphase chemical reactions can produce secondary organic matter and the inorganic salt seeds can undergo cyclic dissolution and recrystallization. SOA formation by multiphase rather than gas-phase chemistry might also contribute to a suppression of new particle formation (11) (supplementary text S2.3 and S2.4).

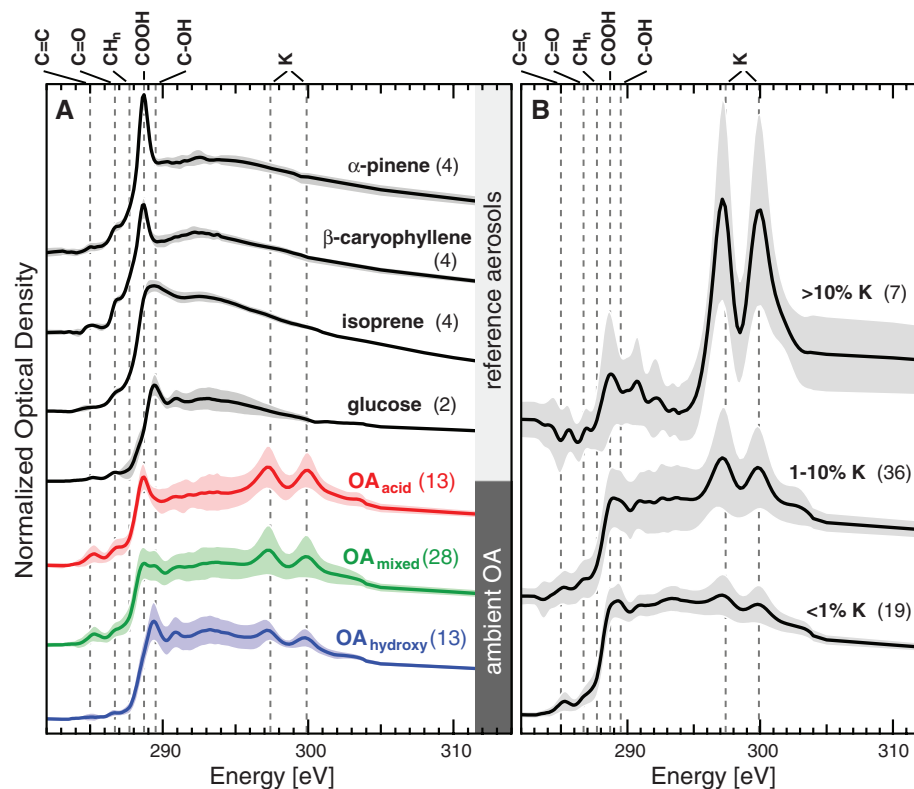


**Fig. 2.** (A) NEXAFS spectra of (i) laboratory-generated SOA from terpene and isoprene oxidation; (ii) glucose as carbohydrate reference compound from spray-drying of aqueous solution; and (iii)  $OA_{acid}$ ,  $OA_{mixed}$ , and  $OA_{hydroxy}$  particles from the Amazon. (B) NEXAFS spectra for Amazonian organic aerosol particles with different potassium (K) mass fractions. Solid lines and shaded areas represent mean spectra and standard deviations. Numbers of analyzed particles are given in parentheses. Vertical lines indicate resonant absorption of organic functional groups and potassium (table S3).



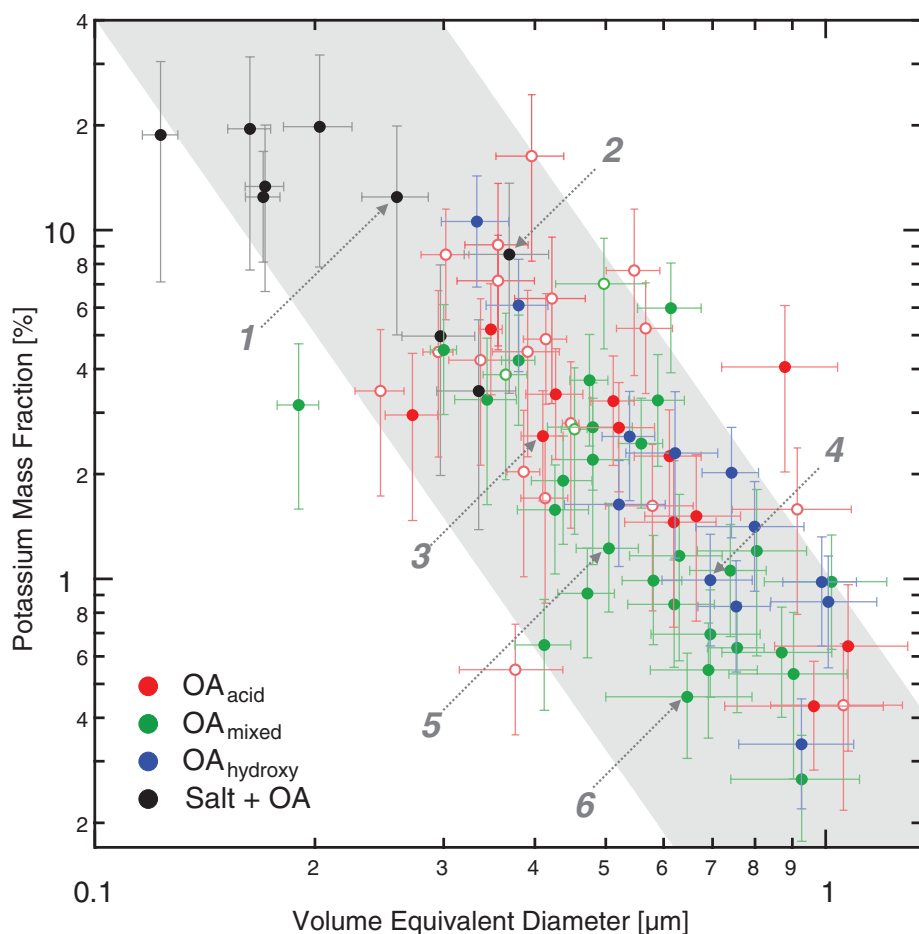
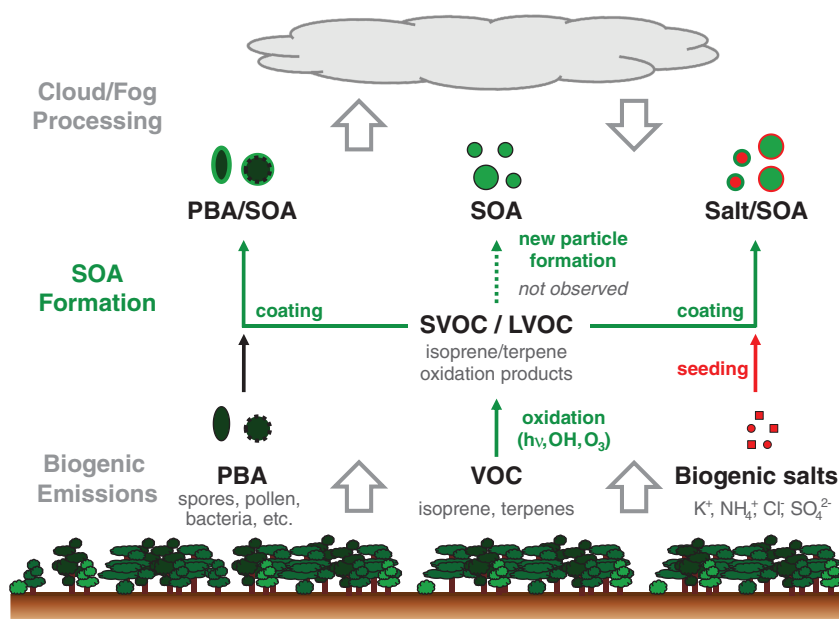


**Fig. 3.** Size dependence of potassium mass fraction in Amazonian organic aerosol particles. Solid markers represent data from samples collected in this study (ATTO site, 2011), and open markers represent additional data from previously collected samples (ZF2 site, 2010) (11). Numbers and arrows identify individual particles from Fig. 1 (1, F; 2, E; 3 and 5, A; and 4 and 6, B). Shaded area illustrates idealized dilution of primary potassium content upon particle growth by condensation of secondary organic material (inverse third-order dependence on particle diameter) (11). Error bars indicate the estimated uncertainty in calculations of particle size and potassium mass content.

**Fig. 4.** Sources and processing of organic aerosol in pristine Amazonian boundary layer air. SOA formation by photooxidation of VOC and condensation of semi- and low-volatile organic compounds (SVOC/LVOC) on primary biological aerosols (PBA) that dominate the coarse particle fraction (>1 μm) (5, 6) and on biogenic salt particles that serve as seeds for organic particles dominating the accumulation size range (0.1 to 1 μm).



Of the 77 Amazonian organic aerosol particles analyzed by STXM-NEXAFS, only 3 contained no detectable amount of potassium (<2 fg). The near-ubiquitous presence of potassium suggests that biogenic salt particles emitted from active biota in the rainforest serve as initial seeds for the condensation of VOC oxidation products. This mechanism appears to dominate the formation of SOA particles in the accumulation size range in pristine Amazonian rainforest air (Fig. 4). It can explain why new particle formation events are not observed, even though the aerosol consists largely of secondary organic material formed from gas-phase precursors (11) (supplementary text S2.4). A major implication is that the number concentration of atmospheric aerosol particles in the accumulation size range is partly regulated by the primary emission of potassium-salt-rich particles from biota in the rainforest. Compared with smaller particles in the nucleation and Aitken size range (<0.1 μm), accumulation mode particles are by orders of magnitude more frequently activated as CCN (11) (supplementary text S2.3 and fig. S11B). Thus, the biological sources and emission rates of potassium-salt-rich particles have a direct influence on the initial droplet number and microphysical evolution of clouds over the rainforest, which in turn influence the dynamics of clouds and precipitation as well as their effects on the hydrological cycle and climate.

Our findings support the hypothesis that the Amazonian rainforest ecosystem can be regarded as a biogeochemical reactor in which the formation of clouds and precipitation in the atmosphere are triggered by particles emitted from the biosphere. The connection between biogenic particle emissions and cloud properties in the tropical rainforest ecosystem appears even stronger and more direct than previously assumed (6, 34). In view of the large impact of tropical rainforests on biogeochemistry and climate, the biological

activity and diversity of particle-emitting organisms seem likely to play important roles in Earth history and future global change.

#### References and Notes

- J. L. Jimenez *et al.*, *Science* **326**, 1525 (2009).
- M. Hallquist *et al.*, *Atmos. Chem. Phys.* **9**, 5155 (2009).
- S. Solomon, *IPCC 4th Assessment Report* (Cambridge Univ. Press, Cambridge, 2007).
- M. O. Andreae, *Science* **315**, 50 (2007).
- S. T. Martin *et al.*, *Rev. Geophys.* **48**, RG2002 (2010).
- U. Pöschl *et al.*, *Science* **329**, 1513 (2010).
- Q. Chen *et al.*, *Geophys. Res. Lett.* **36**, L20806 (2009).
- D. V. Spracklen *et al.*, *Atmos. Chem. Phys.* **6**, 5631 (2006).
- R. Weigel *et al.*, *Atmos. Chem. Phys.* **11**, 9983 (2011).
- A. M. L. Ekman *et al.*, *Geophys. Res. Lett.* **35**, L17810 (2008).
- Materials and methods are available as supplementary materials on *Science Online*.
- A. V. Tivanski, R. J. Hopkins, T. Tyliczszak, M. K. Gilles, *J. Phys. Chem. A* **111**, 5448 (2007).
- S. F. Maria, L. M. Russell, M. K. Gilles, S. C. B. Myneni, *Science* **306**, 1921 (2004).
- M. Claeys *et al.*, *Science* **303**, 1173 (2004).
- J. L. Goatley, R. W. Lewis, *Plant Physiol.* **41**, 373 (1966).
- W. Elbert, P. E. Taylor, M. O. Andreae, U. Pöschl, *Atmos. Chem. Phys.* **7**, 4569 (2007).
- M. O. Andreae, *Science* **220**, 1148 (1983).
- J. Li, M. Posfai, P. V. Hobbs, P. R. Buseck, *J. Geophys. Res.* **108**, 8484 (2003).
- [http://sigma.cptec.inpe.br/queimadas/v\\_anterior/dados\\_ant/dp\\_anteriores.html](http://sigma.cptec.inpe.br/queimadas/v_anterior/dados_ant/dp_anteriores.html).
- <http://firefly.geog.umd.edu/firemap> [accessed 23 March 2012].
- P. Artaxo, H. C. Hansson, *Atmos. Environ.* **29**, 393 (1995).
- M. O. Andreae, P. J. Crutzen, *Science* **276**, 1052 (1997).
- P. Artaxo, W. Maenhaut, H. Storms, R. Vangrieken, *J. Geophys. Res.* **95**, 16971 (1990).
- A. Worobiec *et al.*, *Atmos. Environ.* **41**, 9217 (2007).
- D. R. Lawson, J. W. Winchester, *J. Geophys. Res.* **84**, 3723 (1979).
- D. R. Lawson, J. W. Winchester, *Geophys. Res. Lett.* **5**, 195 (1978).
- G. E. Nemeryuk, *Sov. Plant Physiol.* **17**, 560 (1970).
- G. Crozat, *Tellus* **31**, 52 (1979).
- W. Beauford, J. Barber, A. R. Barringer, *Science* **195**, 571 (1977).
- W. Beauford, J. Barber, A. R. Barringer, *Nature* **256**, 35 (1975).
- A. K. Bertram *et al.*, *Atmos. Chem. Phys.* **11**, 10995 (2011).
- M. Song, C. Marcolli, U. K. Krieger, A. Zuend, T. Peter, *Atmos. Chem. Phys.* **12**, 2691 (2012).
- A. Zuend, J. H. Seinfeld, *Atmos. Chem. Phys.* **12**, 3857 (2012).
- S. S. Gunthe *et al.*, *Atmos. Chem. Phys.* **9**, 7551 (2009).

**Acknowledgments:** This work has been supported by the Max Planck Society, the Max Planck Graduate Center, the Geocycles Cluster Mainz (Landesexzellenzcluster Rheinland-Pfalz),

and the European Community (PEGASOS, FP7-265148). The Harvard Environmental Chamber was supported by the Office of Science, Office of Basic Energy Sciences (BES), U.S. Department of Energy (DOE), grant no. DE-FG02-08ER6452, and the U.S. NSF under grant no. 0925467. The Advanced Light Source is supported by the Director, Office of Science, BES, of the U.S. DOE under contract no. DE-AC02-05CH11231. We thank the Helmholtz-Zentrum Berlin for the allocation of synchrotron radiation beamtime at BESSY II. We thank the Instituto Nacional de Pesquisas da Amazônia (INPA), Manaus, and the ATTO team under the Brazilian coordinator, A. O. Manzi, for their collaboration and field support. We also thank G. R. Carmichael and the Center for Global and Regional Environmental Research at the University of Iowa for support in the Weather Research and Forecasting (WRF) model simulations. We gratefully acknowledge R. Ditz, I. Trebs, X. Chi, J. A. Huffman, J. Kesselmeier, J. Schöngart, M. Kuwata, T. Tyliczszak, J. Huth, G. Schütz, E. Goering, M. Bechtel, J.-D. Förster, and T. Behrendt for support and helpful discussions.

#### Supplementary Materials

[www.sciencemag.org/cgi/content/full/337/6098/1075/DC1](http://www.sciencemag.org/cgi/content/full/337/6098/1075/DC1)

Materials and Methods

Supplementary Text

Figs. S1 to S12

Tables S1 to S9

References (35–106)

12 April 2012; accepted 23 July 2012

10.1126/science.1223264



## Supplementary Materials for

### **Biogenic Potassium Salt Particles as Seeds for Secondary Organic Aerosol in the Amazon**

Christopher Pöhlker,<sup>1\*</sup> Kenia T. Wiedemann,<sup>2,3,4</sup> Bärbel Sinha,<sup>5,6</sup> Manabu Shiraiwa,<sup>1,7</sup>  
Sachin S. Gunthe,<sup>1,8</sup> Mackenzie Smith,<sup>3</sup> Hang Su,<sup>1</sup> Paulo Artaxo,<sup>2</sup> Qi Chen,<sup>3</sup> Yafang  
Cheng,<sup>1</sup> Wolfgang Elbert,<sup>1</sup> Mary K. Gilles,<sup>9</sup> Arthur L. D. Kilcoyne,<sup>10</sup> Ryan C. Moffet,<sup>8,11</sup>  
Markus Weigand,<sup>12</sup> Scot T. Martin,<sup>3</sup> Ulrich Pöschl,<sup>1\*</sup> Meinrat O. Andreae<sup>1</sup>

\*To whom correspondence should be addressed. E-mail: c.pohlker@mpic.de (C.P.); u.poschl@mpic.de (U.P.)

Published 31 August 2012, *Science* **337**, 1075 (2012)  
DOI: 10.1126/science.1123264

#### **This PDF file includes:**

Materials and Methods  
Supplementary Text  
Figs. S1 to S12  
Tables S1 to S9  
References

## **S1 Materials and Methods**

### ***S1.1 Aerosol sampling***

Aerosol samples were collected with a single stage impactor (35) on silicon nitride substrates ( $\text{Si}_3\text{N}_4$ , membrane width 0.5 mm, membrane thickness 100 nm, Silson Ltd, Northampton, UK). The volumetric flow through the impactor was  $1\text{--}1.5\text{ l min}^{-1}$ , corresponding to a nominal cut-off in the range of  $0.5\text{--}0.8\text{ }\mu\text{m}$ . On the  $\text{Si}_3\text{N}_4$  substrate the majority of particles larger than  $1\text{ }\mu\text{m}$  was concentrated in a central impaction spot, whereas smaller particles (down to  $0.1\text{ }\mu\text{m}$ ) were collected via diffusive deposition around this spot. Regions of diffusive deposition have been chosen for STXM analysis because of the relatively high abundance of small particles and appropriate particle coverage. The samples were collected 2–2.5 m above ground level. Sampling times between 30 to 60 min ensured appropriate particle coverage on the substrates. The samples were sealed in air-tight containers, and stored at  $4^\circ\text{C}$  and 20–30 % relative humidity (RH) in the dark. STXM-NEXAFS analysis was done three weeks, and NanoSIMS and SEM analysis four weeks after collection. Several individual particles were investigated with two STXM instruments (ALS-STXM 5.3.2.2 in Berkeley and four months later at the MAXYMUS-STXM in Berlin, Sect. S1.5). The measurements with the two STXM instruments yielded very similar NEXAFS spectra for the investigated Amazonian SOA samples, and the quantitative analysis gave consistent results.

### ***S1.2 Amazonian aerosols and sampling locations***

The samples for this study were collected during the wet season on 13 and 14 May 2011 at a very remote site 150 km NE of the city of Manaus, Brazil, in an untouched forest area (Amazonian Tall Tower Observatory (ATTO) site,  $2.14336^\circ\text{ S}$ ,  $59.00056^\circ\text{ W}$ , 120 m above sea level) (Table S1). The sampled air masses came mainly from the northeast across  $\sim 1000\text{ km}$  of untouched forest areas. Nine-day back trajectories indicated the arrival of air masses from northeastern directions, originating over the Atlantic Ocean in the direction of Cape Verde. Figure S1 shows back trajectories and the cumulative rainfall during this time, which indicates strong wet deposition, and therefore dominance of local and regional aerosol sources. In addition, no soot or other combustion released particles were found in STXM-NEXAFS, SEM, and NanoSIMS analyses. NEXAFS spectra are particularly sensitive to soot and other combustion derived particles that contain a significant amount of aromatic moieties, and therefore, exhibit

strong spectral features at 285 eV (36-38). Hence, the samples are thought to be free of anthropogenic influences such as biomass burning in the Amazon (19-20) and long-range transport of biomass burning emissions from Africa.

An earlier set of samples had been collected on 15 May 2010 at a remote site 60 km NNW of Manaus in Brazil (ZF2 site, 2.59454° S, 60.20929° W, 90 m above sea level) (Table S1). Previously, this site (with K34 and TT34 towers) has been used for field measurement campaigns such as AMAZE-08 (6-7, 34, 39), whereas the ATTO site was established recently (2011). While this study is focused on the samples from the pristine ATTO site, the measurements from the ZF2 samples have been added as independent confirmation for the size dependence of the potassium mass fraction in organic aerosol particles (Fig. 3).

### ***S1.3 Laboratory generated SOA from the Harvard Environmental Chamber***

The Harvard Environmental Chamber (40) was operated under continuous flow conditions to generate particles composed of secondary organic material with ammonium sulfate seeds. For all experiments, the chamber relative humidity was 40 %, the temperature was 25°C, and ammonium sulfate seed particles were injected. The secondary organic material samples were produced by photooxidation of isoprene, dark ozonolysis of  $\alpha$ -pinene, and dark ozonolysis of  $\beta$ -caryophyllene. The oxygen-to-carbon ratio (O:C) and mass loading of the secondary organic material in the chamber outflow was characterized by an Aerodyne high-resolution time-of-flight aerosol mass spectrometer (HR-ToF-AMS) (41). The recent updates of Chen et al. (42) were applied in the analysis of O:C. A summary of the experimental conditions can be found in Table S2.

The  $\alpha$ -pinene and  $\beta$ -caryophyllene ozonolysis experiments largely followed the procedures detailed in Shilling et al. (43) and Chen et al. (44), respectively. Briefly, a solution of  $\alpha$ -pinene in 2-butanol or  $\beta$ -caryophyllene in cyclohexane was continually injected into a gently warmed glass bulb using a syringe pump. The solution evaporated in a pure air flow and was swept into the chamber. Ozone was generated outside the chamber by passing a pure air flow around an ultraviolet light and the resulting flow was injected into the chamber. Within the chamber, the reaction of  $\alpha$ -pinene or  $\beta$ -caryophyllene with ozone formed secondary products, and those of sufficiently low volatility condensed onto the surfaces of the crystalline seed particles.

The generation of isoprene secondary organic material generally followed the method described in King et al. (45). One alteration was that for these experiments the ammonium sulfate seed particles were deliquesced aqueous droplets. Gas-phase isoprene and hydrogen peroxide ( $\text{H}_2\text{O}_2$ ) were injected into the chamber, and isoprene reacted with the OH radicals produced by the photolysis of  $\text{H}_2\text{O}_2$  by irradiation in the chamber. Some of the products of this reaction were of low volatility and partitioned to the seed particles. The laboratory-generated SOA was collected by impaction sampling on silicon nitride substrates using a single stage impactor (see. Sect. S1.1).

#### ***S1.4 Reference aerosols from pure organic compounds***

The following chemicals, purchased from Sigma Aldrich, were used as reference standards: serine, aspartic acid, bovine serum albumin (BSA), glucose, and glucosamine·HCl. Chemicals were used without further purification and dissolved in deionized water (Millipore - Milli Q plus 185, 18.2 M $\Omega$  cm). Reference aerosol was generated by spray-drying of the pure organic compounds in aqueous solution (1 mmol l<sup>-1</sup>) using a constant output atomizer operated with filtered particle-free pressurized air (250 kPa, 3 lpm). The polydisperse aerosol flow was dried to a relative humidity of <15 % (silica-gel diffusion dryer). Further, the generated aerosols were passed through a radioactive neutralizer ( $\text{Kr}^{85}$ , 74 MBq or 2 mCi) to generate charge equilibrium, and then to a differential mobility analyzer (DMA; TSI 3080 electrostatic classifier). This facilitated the selection of particles of suitable size for further analysis (0.35-0.6  $\mu\text{m}$ ). The output from this DMA was split in two for aerosol sampling (1 lpm) and for a condensation particle counter (TSI 3786, 0.6 lpm) to monitor particle concentration. The reference aerosols were collected by: (i) impaction sampling on  $\text{Si}_3\text{N}_4$  substrates using a single stage impactor (see. Sect. S1.1) and (ii) electrostatic precipitation on TEM grids (300-mesh copper mesh, 10-15 nm carbon coating, Plano GmbH, Wetzlar, DE) using an electrostatic sampler (46). The STXM analysis of reference samples on both substrates yielded particle diameters in the expected size range, indicating that no particle fragmentation occurred in the course of sampling (i.e. impaction on  $\text{Si}_3\text{N}_4$  membranes).

### ***S1.5 STXM-NEXAFS measurements and data processing***

STXM-NEXAFS analysis was conducted at the Lawrence Berkeley National Laboratory Advanced Light Source (LBNL ALS), Berkeley, CA, USA, at beamline 5.3.2.2 and at the MAXYMUS beamline (UE46\_PGM-2) at BESSY II, Helmholtz-Zentrum, Berlin, Germany.

The ALS-STXM instrument is located at the bending magnet beamline 5.3.2.2 at the ALS electron storage ring (1.9 GeV, 500 mA stored current in top-off mode) and provides a photon flux of  $\sim 10^7 \text{ s}^{-1}$  in the soft X-ray region (250-800 eV). It is equipped with a spherical grating monochromator (resolving power  $E/\Delta E \leq 5000$ ), a Fresnel zone plate with 25 nm spatial resolution and a phosphor coated Lucite tube coupled with a photomultiplier. Samples are analyzed in a He-filled chamber ( $\sim 30 \text{ kPa}$ ). The accessible energy range (250-800 eV) includes the carbon K-absorption edge (283.8 eV), the potassium  $L_{3,2}$ -edge (294.6 eV), the calcium  $L_{3,2}$ -edge (349.3 eV), the nitrogen K-edge (400.0 eV) and the oxygen K-edge (531.7 eV) (47). Additional technical specifications are given in Kilcoyne et al. (48).

The MAXYMUS-STXM is located at the tunable undulator beamline UE46\_PGM-2 at the BESSY II electron storage ring (1.7 GeV, multibunch mode) and provides a photon flux of  $\sim 5 \cdot 10^8 \text{ s}^{-1}$  in the soft X-ray region. The undulator provides X-ray photons with selectable polarization in the range of 120-1900 eV. The STXM is equipped with a plane grating monochromator using a 600 l/mm blazed grating (resolving power  $E/\Delta E \leq 8000$  at C-K), a Fresnel zone plate with 31 nm spatial resolution and a phosphor coated Lucite tube coupled with a photomultiplier. The samples were placed in an evacuated chamber ( $2\text{-}5 \cdot 10^{-5} \text{ Pa}$ ). Further information can be found in Follath et al. (49).

Single energy images were recorded by raster-scanning the sample in the focused X-ray beam and measuring the intensity of transmitted monochromatic light as a function of sample position. X-ray absorption spectra were obtained either by recording a sequence of energy image scans or an energy line scan that sampled across the particle. For an energy image scan (“stack”) a series of images of a defined region with closely spaced photon energies is recorded over a certain energy range covering peak features, and with a coarser energy grid outside of the regions with fine structure. For line scans, the X-ray spot is scanned across a particle, then the photon energy is changed and the line rescanned. This yields a plot of transmitted light at each position on the scanned line as a function of energy. We used identical energy protocols (number of

energy points and spacings) for stacks and line scans, ranging from 270 to 600 eV, and spanning the carbon, potassium, calcium, nitrogen and oxygen edges (Fig. S2).

Based on the measured transmitted intensity  $I(d)$  the optical density  $OD$  was calculated applying Beer-Lambert's law (50):

$$OD = -\ln\left(\frac{I(d)}{I_0}\right) = \mu\rho d$$

where  $I_0$  represents the incident photon flux,  $\mu$  is the mass absorption coefficient,  $\rho$  is the sample density and  $d$  the sample thickness.  $I_0$  was obtained as the transmission intensity through a particle free region of the substrate. For  $OD < 1.5$ , particle sizes were in the linear absorption regime of the Beer-Lambert's law (12) which was assured for all particles reported in this study.

For the analysis of carbon NEXAFS spectra, the pre-edge absorption (mean value between 275 and 284 eV) was subtracted and the spectra were normalized by the carbon K-edge height (mean value between 305 and 320 eV) (51). We used fine structure features from resonant transitions of core electrons into excited states close to the ionization continuum ( $1s \rightarrow \pi^*, \sigma^*$ ) to characterize the functional group composition of OA particles (50, 52). Characteristic transitions are listed in Table S3.

For the analysis of atomic ratios (i.e., O:C, N:C) the heights of the C, N and O absorption edges  $\Delta OD$  were determined as

$$\Delta OD = OD_{post-edge} - OD_{pre-edge}$$

with carbon post- and pre-edge energies being 320 and 280 eV; nitrogen: 425 and 395 eV; oxygen: 550 and 525 eV (12). The molar ratio of oxygen and carbon  $n_O/n_C$  is calculated as

$$\frac{n_O}{n_C} = \frac{\Delta OD_O M_C \mu_{C, post-pre}}{\Delta OD_C M_O \mu_{O, post-pre}}$$

with  $M$  as the atomic mass and  $\mu_{post-pre}$  as the difference in mass absorption coefficient ( $\mu_{C, 320-280} = 3.8 \cdot 10^4 \text{ cm}^2 \text{ g}^{-1}$ ,  $\mu_{N, 425-395} = 2.8 \cdot 10^4 \text{ cm}^2 \text{ g}^{-1}$ ,  $\mu_{O, 550-525} = 2.0 \cdot 10^4 \text{ cm}^2 \text{ g}^{-1}$ ) (12, 36-37, 47). The ratio  $n_N/n_C$  is obtained in an analogous fashion. The calculation of  $n_O/n_C$  and  $n_N/n_C$  has been verified previously by Moffet et al. (36), and was reconfirmed in this study by means of organic standard compounds and aerosol mass spectrometry data for laboratory-generated SOA. The experimental results show good agreement with the theoretical ratios (see Table S4 and Sect. S2.2).



Based on non-normalized CNO spectra, the potassium mass fraction in organic particles was estimated as described in the following paragraph. In soft X-ray absorption spectra, the potassium L<sub>3,2</sub>-absorption edge occurs as a characteristic double peak superimposed on the carbon K-edge absorption. Both closely spaced potassium L<sub>3</sub>- and L<sub>2</sub>-edges consist of pronounced and sharp peaks at the onset of the edge (at 297.4 eV and 299.9 eV) caused by the resonant electron transition from the ground states (2p<sub>3/2</sub>, 2p<sub>1/2</sub>) into unoccupied states (3d) in addition to the actual absorption step function due to photo-ionization (50).

In spectra of OA particles with high potassium content, the pronounced potassium doublet and the height of the potassium absorption edge (relative to pre-edge absorption) are resolved. For OA particles with low potassium content only the potassium doublet is strong enough to be detected (Fig. S3). The height of the L<sub>3,2</sub>-edge,  $\Delta OD_{edge}$ , is proportional to the number of potassium atoms and can be used to quantify the potassium content. Based on 20 potassium-rich particles the following linear correlation ( $R^2 = 0.85$ ) between  $\Delta OD_{edge}$  and the height of the L<sub>3</sub>-peak  $\Delta OD_{L3}$  was established:

$$\Delta OD_{edge} = 0.235 \cdot \Delta OD_{L3}$$

This correlation allowed a quantitative estimate of  $\Delta OD_{edge}$  even for OA particles with low potassium content. The effective potassium detection limit in individual organic particles is given by the minimum  $\Delta OD_{L3}$  that is resolvable above the spectral noise. It was estimated as  $\sim 2$  fg. Based on Beer-Lambert's law, the following equation was used to calculate the absolute potassium mass,  $m_K$ , in individual aerosol particles:

$$m_K = \frac{\Delta OD_{edge} V}{0.7 \mu_{K, post-pre} h}$$

with  $V$  as the volume of the impacted OA droplets (= spherical cap),  $\mu_{K, 310-292} = 7.0 \cdot 10^4 \text{ cm}^2 \text{ g}^{-1}$  as the difference in potassium L-edge mass absorption coefficient for the pre- and post-edge energies 292 and 310 eV (47, 53),  $h$  as the height of the impacted droplet, and a geometric factor of 0.7 to account for the average light path through the spherical cap (12).  $V$  can be calculated as

$$V = \frac{h\pi}{6} (3a^2 + h^2)$$

with  $a$  as the radius of the spherical cap that was measured for all particles based on STXM images (54). The height,  $h$ , is not directly accessible but can be estimated based on the measured

$OD$  for C, N, and O. According to Pöschl et al. (6), C, N, and O account for ~80 % of the total mass,  $m_{total}$ , of Amazonian aerosol particles in the submicrometer size range. Therefore,

$$m_C + m_N + m_O = 0.8m_{total}$$

with

$$m_X = \frac{OD_X V}{0.7 \mu_{X,post-pre} h}$$

and

$$m_{total} = V \cdot \rho$$

can be converted into

$$h = \frac{1}{0.56\rho} \left( \frac{OD_C}{\mu_C} + \frac{OD_N}{\mu_N} + \frac{OD_O}{\mu_O} \right).$$

Using  $\rho = 1.4 \text{ g cm}^{-3}$  as a characteristic density value for OA particles (2), we obtained the radius-to-height ratio  $a/h$  with a mean value of ~10. Based on  $a$  and  $a/h$ , we calculated a volume equivalent diameter  $D_{ve}$  for each particle:

$$D_{ve} = \sqrt[3]{3ha^2 + h^3}.$$

According to Martin et al. (5), the fine organic aerosol mass concentration (<2  $\mu\text{m}$ ) during the wet season in the Amazon is of the order of ~2  $\mu\text{g m}^{-3}$ . Multiplication of this value with an estimated average potassium mass fraction of ~2.6 % (median of all Amazonian OA particles analyzed in this study), yields an average atmospheric potassium concentration level of ~50  $\text{ng m}^{-3}$  (estimated uncertainty: factor ~2), which is consistent with previous measurements (18-220  $\text{ng m}^{-3}$ , (16)).

### ***S1.6. SEM analysis***

Scanning electron microscopy (SEM) images of aerosol particles were acquired using the secondary electron in-lens detector of a high-performance field emission instrument (LEO 1530 FESEM, EHT 10 keV, WD ~9 mm). The in-lens detector enabled detection of thin organic particles and coatings, which are often difficult to detect. The organic nature of SOA droplets and organic components of mixed SOA-inorganic particles were confirmed by NanoSIMS analysis as detailed below.  $\text{Si}_3\text{N}_4$  windows are mounted on conductive Si wafers; however, the windows

themselves are nonconductive and show strong charging. Therefore, the back of the Si<sub>3</sub>N<sub>4</sub> windows was coated with gold prior to SEM and NanoSIMS analysis to prevent charging and enhance the contrast of SOA particles against the substrate.

### ***SI.7. NanoSIMS measurement and data processing***

Chemical analysis of aerosol particles was performed using a Cameca NanoSIMS 50 ion microprobe in multi-collection detector mode by sputtering the sample with a ~1 pA Cs<sup>+</sup> primary ion beam focused into a spot of ~100 nm diameter. The primary ion beam was scanned several times over an area of 4 μm x 4 μm for the chemical analysis of standards, with a dwell time of 1000 μs pixel<sup>-1</sup>, and images (256 x 256 pixels) were recorded for every scan. The detector dead time was 44 ns and the count rates were corrected accordingly. The energy bandpass slit was set to 20 eV, the entrance slit and aperture slit were decreased to 30 μm x 180 μm and 200 μm x 200 μm, respectively, and the transmission was kept at 50 % to enhance the count rate on small particles. A high transmission is possible because the influence of the quasi simultaneous arrival effect on the quantification of major elements is minor (<1 %) compared to the matrix effects, which introduce a ~20-40 % uncertainty.

On aerosol samples the field of vision was larger (10 μm x 10 μm) to view a representative area of the sample and compare with SEM and STXM images. To remove surface contaminations, all images were pre-sputtered for one cycle. The analysis time varied from 3-20 cycles depending on the number of scans required to collect an appropriate number of counts per pixel on each mass, and on the stability of the compounds investigated.

Secondary ions of <sup>12</sup>C<sup>-</sup>, <sup>16</sup>O<sup>-</sup>, <sup>12</sup>C<sub>2</sub><sup>-</sup>, <sup>12</sup>C<sup>14</sup>N<sup>-</sup>, and <sup>32</sup>S<sup>-</sup> were simultaneously collected in five electron multipliers on standards. For aerosol samples only one proxy for the carbon content of the sample (<sup>12</sup>C<sup>-</sup> or <sup>12</sup>C<sub>2</sub><sup>-</sup>) was selected. Instead, <sup>35</sup>Cl<sup>-</sup> was added to the list in order to allow the detection of a larger variety of inorganic salts. For quantification we compared normalized ion counts to the theoretical concentration of the species of interest in a large number of standards. The observed relationship was then used to calculate the concentration of the element of interest in the aerosol samples. This approach is straightforward for all samples that contain sufficient carbon atoms to ionize all of the nitrogen in the sample to CN<sup>-</sup>. The logarithms of the observed calibration factors show a correlation ( $R^2 = 0.99$ ) with the electron affinity that is similar to that

typically observed between the logarithm of the relative sensitivity factor (RSF) under  $\text{Cs}^+$  bombardment and electron affinity (55).

For 19 salt-rich particles ( $<0.3 \mu\text{m}$ ) from the aerosol samples ATTO\_2011\_#7 and ATTO\_2011\_#10 (Table S1) we determined approximate elemental mole fractions of carbon, nitrogen, oxygen, sulfur and chlorine (C:N:O:S:Cl = 0.01:0.09:0.62:0.17:0.02), indicating a relatively high abundance of sulfate ions in the salt core (Fig. S4, particles 1-3).

### ***S1.8. WRF model simulation***

In order to obtain the probability density distribution of vertical velocities,  $P_w$ , for the Amazonian region during the sampling period, the Weather Research & Forecast model (WRF-ARW-v3.3.1, <http://www.mmm.ucar.edu/wrf/users/>) was applied to simulate the meteorological conditions in the Amazon for the whole of May 2011. The model domain was horizontally configured as  $299 \times 249$  grid cells with a spatial resolution of  $9 \text{ km} \times 9 \text{ km}$ . It was centered near Manaus, Brazil, and covers a large part of the Amazon forest region (Fig. S5). There were 34 vertical layers extending to 100 hPa ( $\sim 15 \text{ km}$ ) with 17 layers below 4 km. To allow sufficient time for the model spin-up, we started the simulation on 26 April 2011. Meteorological initial and boundary conditions were interpolated from the NCEP-FNL Operational Global Analysis data (<http://dss.ucar.edu/datasets/ds083.2/>). The sea surface temperature was updated daily during the model simulation with real-time, global sea surface temperature analysis data (RTG\_SST, <ftp://polar.ncep.noaa.gov/pub/history/sst>). MODIS land-use data with inland lake information were used to feed into the Noah Land Use scheme. Grid nudging was applied only for the spin-up period (April 26-30, 2011), and afterward the WRF model was set to run freely. An overview of the model configuration is given in Table S5.

## S2 Supplementary Text

### S2.1 Observations and sources of biogenic salt particles

The elemental composition of aerosol particles in the Amazon Basin during the wet season has been investigated previously, and a variety of different trace elements have been observed (21, 25, 56-60). In supermicrometer particles, two groups of elements have been found: (i) crustal elements such Si, Al, Ca, and Fe mostly from long range transport of Saharan dust, and (ii) “biogenic” elements such as S, K, and P (25). In submicrometer particles, the elements K, P, S, and Zn are frequently observed and mostly attributable to biogenic sources (21-22, 60-61). These elements often exhibit bimodal mass size distributions with relative maxima at  $\sim 0.3 \mu\text{m}$  and  $\sim 3 \mu\text{m}$  (21, 25-26). The night-time concentrations of K, P, and Zn usually exceed day-time concentrations due to increased microbiological activity (i.e., fungal spore release) during the night (60). Plants, fungi, and other microorganisms are considered to be potential sources of the potassium-salt-rich particles observed in this study (16, 21, 25-26). The following paragraph summarizes current knowledge about biogenic salt emission mechanisms from different organisms.

For the ejection of spores into the air, fungi have developed various active discharge mechanisms that involve hygroscopic water uptake by organic and inorganic solutes to generate osmotic pressure and surface tension effects. The active discharge of spores is accompanied by the emission of a liquid jet which contains inorganic ions and carbohydrates (16). Active wet discharge of *Ascomycota* spores utilizes osmotically pressurized small sacks (asci) which, upon bursting, eject spores and aqueous droplets of the osmotic fluid containing mannitol, potassium and chloride (62). Active wet discharge of *Basidiomycota* spores involves surface tension effects and aqueous droplets containing hexoses, mannitol, phosphate, sodium, and potassium (63-64). Elbert et al. (16) have shown that a major fraction of the potassium concentrations observed in the pristine Amazonian boundary layer can be explained by fungal emissions. X-ray and light microscopic analysis of our samples showed very high abundances of fungal spores in the coarse fraction, supporting the idea that fungal spore ejection is a plausible mechanism for the production of the observed potassium-rich particles (Fig. S6).

In addition to microorganism related emissions, the following plant related salt particle release mechanisms have been described in the literature: (I) transpiration, (II) guttation, (III) leaching of vegetation by rain, and (IV) particle release from leaves due to mechanical abrasion.

Beauford et al. (29-30) suggest that small biogenic salt particles can be released into the air by diffusiophoresis associated with water loss during rapid plant transpiration. Other studies provide experimental evidence that transpiration vapors from different plant species contain salt ions (e.g.,  $\text{Ca}^{2+}$ ,  $\text{Na}^+$ ,  $\text{K}^+$ ,  $\text{NH}_4^+$ ;  $\text{HCO}_3^-$ ,  $\text{Cl}^-$ ,  $\text{SO}_4^{2-}$ ) in considerable concentrations (up to  $5 \text{ mg l}^{-1}$  in the condensate) (27, 65-67).

Guttation is a common water release mechanism of plants when the water supply from the roots exceeds transpiration losses by the leaves. Since transpiration usually does not occur at night, leaf wetness frequently occurs in the morning hours, distinct from dew, depending on physiological and micrometeorological conditions (68-69). Guttation fluids (xylem sap) contain a mixture of sugars, amino acids, and salt ions, with particularly high  $\text{K}^+$ ,  $\text{Ca}^{2+}$ , and  $\text{Mg}^{2+}$  content (15, 70). Accordingly, guttation has been proposed as one potential origin of airborne trace elements in tropical environments (21, 28).

Leaching of soluble compounds from vegetation surfaces by rain, dew, and mist has been described in various studies (71-73). In addition to organic molecules (i.e., carbohydrates), the ions  $\text{K}^+$ ,  $\text{Ca}^{2+}$ ,  $\text{Mg}^{2+}$ , and  $\text{Mn}^{2+}$  are leached in the largest quantities (73-74). It has been suggested that leaching followed by droplet evaporation can generate airborne particles with high trace metal content (66).

Plant surfaces exposed to the atmosphere are covered with waxes that reduce the loss of water and act as a physical defense barrier against pathogens (69). In particular, epicuticular waxes often form the top layer of plant surfaces and are comprised of submicrometer sized, partly crystalline, particles (75). Such particles as small as 200 nm long and 30 nm wide can be released into the air when the plants are mechanically disturbed (e.g., due to rapid growth, surface abrasion by wind, or microbiological activity) (29-30, 76).

The potassium-rich salt particles observed in this study (Fig. 1C-F) were typically in the size range of 0.1-0.3  $\mu\text{m}$ . Figure S7 shows the size distribution obtained by SEM analysis of a morning sample with relatively high salt particle concentration. The maximum around 0.2  $\mu\text{m}$  is in good agreement with the dilution trend of the potassium content in organic particles (Fig. 3). The grey shaded dilution band in Fig. 3 has been calculated assuming that primary biogenic salt particles in the size range of 0.1-0.3  $\mu\text{m}$  with a density of  $2.0\text{-}2.7 \text{ g cm}^{-3}$  ( $\text{KCl}$ ,  $\text{K}_2\text{SO}_4$ ) (77) grew by condensation of SOA with a density of  $1.0\text{-}1.4 \text{ g cm}^{-3}$  (2). The calculated band covers almost

all data points and suggests that the size distribution shown in Fig. S7 is characteristic for the salt particles serving as seeds for the investigated Amazonian SOA.

### ***S2.2 Validation of STXM elemental ratios***

The stoichiometric ratios of organic standard compounds and the STXM elemental ratios for C, N, and O ( $n_O/n_C$  and  $n_N/n_C$ ) generally show good agreement as previously verified by Moffet et al. (36). The results of this study confirm this observation and are summarized in Table S4. The STXM-NEXAFS and AMS derived elemental ratios for laboratory generated SOA show good agreement in  $n_O/n_C$  ratios with deviations up to 20 % (Table S4). For laboratory-generated SOA particles, ammonium sulfate  $[(NH_4)_2SO_4]$  seeds were added to the reaction chamber (Sect. S1.3). For isoprene SOA, ammonium sulfate accounts for a significant mass fraction of the resulting particles (7 % on average), and was observed in the form of a strong ammonium peak at the nitrogen absorption edge (Fig. S2). The mass fraction of ammonium sulfate for terpene SOA (3-4 %; Table S2) is much lower than that for isoprene SOA, corresponding to a weak ammonium peak at the nitrogen absorption edge (Fig. S2). For the STXM analysis, the amount of sulfate was quantified on the basis of the nitrogen content. Accordingly the  $n_O/n_C$  ratios were calculated for total oxygen (organics and sulfate) and for organic oxygen only. For the AMS analysis, the amount of sulfate is known and the  $n_O/n_C$  ratios were also derived for both cases, including and excluding sulfate.

### ***S2.3 Internal structure, cloud/fog processing and CCN activation of aerosol particles***

As discussed in the main text, the investigated Amazonian organic aerosol particles exhibited different types of internal structures that suggest a pronounced influence of cloud and fog processing on SOA formation and aging.

The organic bulk material of many  $OA_{\text{mixed}}$  particles shows a distinct core-shell structure with COOH-rich material in the core and C-OH-rich material in the shell (Fig. S4 and S8). This internal structure may be caused by cloud/fog processing, because  $OA_{\text{acid}}$  and  $OA_{\text{hydroxy}}$ , which are the main constituents of  $OA_{\text{mixed}}$ , have different solubilities in water. Upon evaporation of the cloud droplets, the less soluble  $OA_{\text{acid}}$  material would precipitate first, and the highly soluble hydroxy-rich material (probably sugar- or polyol-like) would form a viscous layer surrounding this core (78). In contrast,  $OA_{\text{hydroxy}}$  occurs as chemically and morphologically homogenous

particles (Fig. S8C). Our findings are consistent with recent studies of liquid-liquid phase separation in organic and mixed organic-inorganic aerosol particles reporting a strong dependence on oxygen-to-carbon ratio of the organic material (31-33): Particles with low atomic ratios of oxygen-to-carbon tend to exhibit phase separation ( $O:C \approx 0.5-0.7$  in  $OA_{acid}$  and  $OA_{mixed}$ ), which is not the case for particles with high O:C ratios ( $O:C \approx 0.9-1.0$  in  $OA_{hydroxy}$ ; Table S4 and Fig. S8). The hygroscopic salt seeds as well as the variable chemical composition and morphology of the SOA particles suggest that aqueous phase reactions play an important role in particle growth and aging (2, 79).

To estimate the frequency of CCN activation and cloud droplet formation on Amazonian aerosol particles, we performed numerical model simulations using input parameters from this and related earlier studies (Sect. S1.8, (6, 34)). The ability of aerosol particles to act as CCN depends on the particle size, hygroscopicity, and water vapor supersaturation. To form cloud droplets, larger particles require a lower supersaturation, which corresponds to a lower updraft velocity (6, 80-81).

Figure S9 shows the critical updraft velocity for CCN activation of aerosol particles as a function of particle diameter. The curve results from cloud parcel model simulations with detailed spectral microphysics using parameters characteristic for pristine Amazonian aerosols during the wet season as determined in the AMAZE-08 campaign (pristine focus period) (6, 39): hygroscopicity parameter  $\kappa = 0.14$ ; particle number concentration  $N = 200 \text{ cm}^{-3}$ ; number size distribution with two log-normal modes with a relative ratio of  $N_2/N_1 = 0.81$  ( $N = N_1 + N_2$ ) and with geometric mean diameter and standard deviation values of  $D_{g,1} = 67 \text{ nm}$  and  $\sigma_{g,1} = 1.32$  (Aitken mode) and  $D_{g,2} = 150 \text{ nm}$  and  $\sigma_{g,2} = 1.43$  (accumulation mode, see Fig. S10A).

As indicated by the dashed lines in Fig. S10A, updraft velocities  $>0.1 \text{ m s}^{-1}$  are sufficient to activate accumulation mode particles at  $\sim 0.15 \text{ }\mu\text{m}$ , whereas the CCN activation of Aitken mode particles at  $\sim 0.07 \text{ }\mu\text{m}$  requires updraft velocities  $>1 \text{ m s}^{-1}$ . Figure S11A shows the probability density function ( $P_w$ ) of atmospheric vertical velocities ( $w$ ) at different altitudes above the Amazonian rainforest during the wet season as calculated with the Weather Research and Forecast model (WRF-ARW-v3.3.1, Sect. S1.8) for the region and period around the aerosol sampling location and time (Fig. S5, May 2011). Combining  $P_w$  from Fig. S11A with  $w_{cri}$  from



Fig. S9, the probability of CCN activation for aerosol particles of a given size,  $P_{\text{act}}(D_p)$ , can be estimated as follows:

$$P_{\text{act}}(D_p) = \int_{w_{\text{cri}}}^{\infty} P_w dw \quad \text{with} \quad w_{\text{cri}} = f(D_p)$$

Figure S11B shows  $P_{\text{act}}$  for different altitudes plotted against the aerosol particle diameter. As expected,  $P_{\text{act}}$  is highest in the upper boundary layer (1-3 km) where the base of convective clouds usually forms. At altitudes  $\geq 1$  km,  $P_{\text{act}}$  is larger than  $\sim 0.5$  % for diameters  $> 0.1$   $\mu\text{m}$ , increases exponentially with increasing diameter, and exceeds 5 % for particles  $> 0.15$   $\mu\text{m}$ , which account for most of the aerosol particle volume and mass (Fig. S10B) (6). In near-surface air (0.1-0.5 km),  $P_{\text{act}}$  is less than  $\sim 0.01$  % for particles  $< 0.1$   $\mu\text{m}$ , but it increases steeply and exceeds 0.5 % for particles  $> 0.15$   $\mu\text{m}$ . The formation of low-lying cloud and fog over the rainforest is a common event in the wet season. The geometric mean value of  $P_{\text{act}}$  for the entire altitude range of 0.1-3 km can be regarded as an estimate for the effective average probability of CCN activation for aerosol particles in pristine Amazonian boundary layer air. It is multiple orders of magnitude higher for accumulation mode particles ( $P_{\text{act}} \approx 2$  % for  $D_p \approx 0.15$   $\mu\text{m}$ ) than for Aitken mode particles ( $P_{\text{act}} < 0.01$  % for  $D_p \approx 0.07$   $\mu\text{m}$ ). This is consistent with the general assumption that the so-called Hoppel minimum around  $\sim 0.1$   $\mu\text{m}$  separating the Aitken mode and the accumulation mode in the size distribution of aged atmospheric aerosols is due to cloud processing (82). In the size range  $> 0.15$   $\mu\text{m}$ , which comprises the particles investigated in this study (Fig. 3) and represents the majority of SOA mass (5-6), the geometric mean value of  $P_{\text{act}}$  exceeds 2 %. The high probability of CCN activation underlines the importance of large accumulation mode particles for the formation of clouds over the rainforest, and it is consistent with the observation of core-shell structures indicating a pronounced influence of aqueous phase processing in clouds or fog on the formation and aging of SOA in the Amazon.

#### ***S2.4 Suppression of new particle formation in the Amazon***

Numerous observations in the planetary boundary layer revealed a consistent correlation between sulfuric acid and the concentration of newly formed particles, and consequently sulfuric acid is thought to be the primary vapor responsible for atmospheric nucleation ((83-86) and references therein). Recent modeling studies argue convincingly that the concentration level of gaseous sulfuric acid in the Amazon region is too low to trigger nucleation and new particle

formation (NPF) events, in contrast to what is observed in relatively clean air over most other vegetated continental regions ((8, 85, 87) and references therein). In line with ambient observations, which consistently show that  $10^6$ - $10^7$  molecules  $\text{cm}^{-3}$  of  $\text{H}_2\text{SO}_4$  are necessary to produce particle formation events, laboratory studies reported that the threshold concentration of sulfuric acid at which newly formed particles ( $>3$  nm) start to appear is approximately  $5$ - $7 \cdot 10^6$  molecules  $\text{cm}^{-3}$  ((85, 88) and references therein). Kanawade et al. (89) calculated a  $\text{H}_2\text{SO}_4$  concentration of about  $1$ - $5 \cdot 10^5$  molecules  $\text{cm}^{-3}$  from the measured  $\text{SO}_2$  (0.02-0.03 ppb) (90) and OH ( $5.5 \cdot 10^6$   $\text{cm}^{-3}$ ) (91) over the Amazon basin, which is nearly one order of magnitude lower than the values observed in boreal forest in Finland (92) and in Michigan forest (89). Low- or semi-volatile organic vapors are also found to be involved in the nucleation and subsequent particle growth (85) and some laboratory studies reported that the presence of organics significantly enhances NPF (93-95). On the other hand, an experimental study showed that homomolecular nucleation of organics, such as aromatic acids, in the absence of  $\text{H}_2\text{SO}_4$  is unlikely to occur under atmospheric conditions (93). In addition, the relatively high isoprene-to-terpene ratio over the Amazon may play a role in suppressing nucleation as discussed by Kiendler-Scharr et al. (96) and Kanawade et al. (89). We assume that these and related issues of atmospheric gas phase chemistry are probably the main reason why NPF is not observed in the Amazon in contrast to boreal forest areas characterized by frequent NPF (97-99).

In addition, the presence of potassium-rich salt particles in a humid environment may indeed enhance the effective condensation sink of organic vapors as outlined below and may thus contribute to suppress new particle formation over the Amazon. The condensation sink (CS) of low-volatile vapors, as determined by the particle size distribution and surface concentration, in pristine Amazonian rainforest air is of the order of  $\sim 1 \cdot 10^{-3} \text{ s}^{-1}$  [based on the size distribution data of Zhou et al. (100) and Pöschl et al. (6)], the influence of hygroscopic growth at average RH of 93 % on the particles size distribution has been taken into account by using the measured average  $\kappa$  value during wet season of Amazon as 0.15 (34)]. Physically, the condensation sink in Amazonia is thus of similar magnitude as in pristine boreal forest air (CS =  $\sim 4 \cdot 10^{-3} \text{ s}^{-1}$  according to Kulmala et al. (98) and Kanawade et al. (89)). From a chemical perspective, however, aqueous droplets formed by hygroscopic growth of the potassium-rich salt particles in tropical rainforest air are not only a condensation sink for low-volatile vapors, they can also absorb volatile and semi-volatile organic compounds and provide a medium for multi-phase chemical reactions that

may be more efficient in converting VOC into SOA than gas phase chemical reactions followed by “dry condensation” of low-volatile vapors (2, 101-102).

Thus, we suggest and intend to pursue further investigations to unravel and quantify how multi-phase chemistry on potassium-rich salt particles may influence the mechanism and rate of SOA formation and the apparent suppression of new particle formation (nucleation events) over the Amazon and other tropical rainforests compared to mid-latitude and boreal forests, which will require comprehensive field measurements of aerosol particle and precursor gas composition as well as kinetic process studies (laboratory experiments and model calculations).

## References and Notes

1. J. L. Jimenez *et al.*, Evolution of organic aerosols in the atmosphere. *Science* **326**, 1525 (2009). [doi:10.1126/science.1180353](https://doi.org/10.1126/science.1180353) [Medline](#)
2. M. Hallquist *et al.*, The formation, properties and impact of secondary organic aerosol: current and emerging issues. *Atmos. Chem. Phys.* **9**, 5155 (2009). [doi:10.5194/acp-9-5155-2009](https://doi.org/10.5194/acp-9-5155-2009)
3. S. Solomon, *IPCC 4th Assessment Report* (Cambridge Univ. Press, Cambridge, 2007).
4. M. O. Andreae, Atmosphere. Aerosols before pollution. *Science* **315**, 50 (2007). [doi:10.1126/science.1136529](https://doi.org/10.1126/science.1136529) [Medline](#)
5. S. T. Martin *et al.*, Sources and properties of Amazonian aerosol particles. *Rev. Geophys.* **48**, RG2002 (2010). [doi:10.1029/2008RG000280](https://doi.org/10.1029/2008RG000280)
6. U. Pöschl *et al.*, Rainforest aerosols as biogenic nuclei of clouds and precipitation in the Amazon. *Science* **329**, 1513 (2010). [doi:10.1126/science.1191056](https://doi.org/10.1126/science.1191056) [Medline](#)
7. Q. Chen *et al.*, Mass spectral characterization of submicron biogenic organic particles in the Amazon Basin. *Geophys. Res. Lett.* **36**, L20806 (2009). [doi:10.1029/2009GL039880](https://doi.org/10.1029/2009GL039880)
8. D. V. Spracklen *et al.*, The contribution of boundary layer nucleation events to total particle concentrations on regional and global scales. *Atmos. Chem. Phys.* **6**, 5631 (2006). [doi:10.5194/acp-6-5631-2006](https://doi.org/10.5194/acp-6-5631-2006)
9. R. Weigel *et al.*, In situ observations of new particle formation in the tropical upper troposphere: the role of clouds and the nucleation mechanism. *Atmos. Chem. Phys.* **11**, 9983 (2011). [doi:10.5194/acp-11-9983-2011](https://doi.org/10.5194/acp-11-9983-2011)
10. A. M. L. Ekman *et al.*, Do organics contribute to small particle formation in the Amazonian upper troposphere? *Geophys. Res. Lett.* **35**, L17810 (2008). [doi:10.1029/2008GL034970](https://doi.org/10.1029/2008GL034970)
11. Materials and methods are available as supplementary material on *Science Online*.
12. A. V. Tivanski, R. J. Hopkins, T. Tyliczszak, M. K. Gilles, Oxygenated interface on biomass burn tar balls determined by single particle scanning transmission X-ray microscopy. *J. Phys. Chem. A* **111**, 5448 (2007). [doi:10.1021/jp070155u](https://doi.org/10.1021/jp070155u) [Medline](#)
13. S. F. Maria, L. M. Russell, M. K. Gilles, S. C. B. Myneni, Organic aerosol growth mechanisms and their climate-forcing implications. *Science* **306**, 1921 (2004). [doi:10.1126/science.1103491](https://doi.org/10.1126/science.1103491) [Medline](#)
14. M. Claeys *et al.*, Formation of secondary organic aerosols through photooxidation of isoprene. *Science* **303**, 1173 (2004). [doi:10.1126/science.1092805](https://doi.org/10.1126/science.1092805) [Medline](#)
15. J. L. Goatley, R. W. Lewis, Composition of guttation fluid from rye, wheat, and barley seedlings. *Plant Physiol.* **41**, 373 (1966). [doi:10.1104/pp.41.3.373](https://doi.org/10.1104/pp.41.3.373) [Medline](#)
16. W. Elbert, P. E. Taylor, M. O. Andreae, U. Pöschl, Contribution of fungi to primary biogenic aerosols in the atmosphere: Wet and dry discharged spores,

- carbohydrates, and inorganic ions. *Atmos. Chem. Phys.* **7**, 4569 (2007).  
[doi:10.5194/acp-7-4569-2007](https://doi.org/10.5194/acp-7-4569-2007)
17. M. O. Andreae, Soot carbon and excess fine potassium: long-range transport of combustion-derived aerosols. *Science* **220**, 1148 (1983).  
[doi:10.1126/science.220.4602.1148](https://doi.org/10.1126/science.220.4602.1148) [Medline](#)
  18. J. Li, M. Posfai, P. V. Hobbs, P. R. Buseck, Individual aerosol particles from biomass burning in southern Africa: 2, Compositions and aging of inorganic particles. *J. Geophys. Res.* **108**, 8484 (2003). [doi:10.1029/2002JD002310](https://doi.org/10.1029/2002JD002310)
  19. [http://sigma.cptec.inpe.br/queimadas/v\\_anterior/dados\\_ant/dp\\_antteriores.html](http://sigma.cptec.inpe.br/queimadas/v_anterior/dados_ant/dp_antteriores.html).
  20. <http://firefly.geog.umd.edu/firemap> [Accessed 23 March 2012].
  21. P. Artaxo, H. C. Hansson, Size distribution of biogenic aerosol particles from the Amazon Basin. *Atmos. Environ.* **29**, 393 (1995). [doi:10.1016/1352-2310\(94\)00178-N](https://doi.org/10.1016/1352-2310(94)00178-N)
  22. M. O. Andreae, P. J. Crutzen, Atmospheric aerosols: Biogeochemical sources and role in atmospheric chemistry. *Science* **276**, 1052 (1997).  
[doi:10.1126/science.276.5315.1052](https://doi.org/10.1126/science.276.5315.1052)
  23. P. Artaxo, W. Maenhaut, H. Storms, R. Vangrieken, Aerosol characteristics and sources for the Amazon Basin during wet season. *J. Geophys. Res.* **95**, 16971 (1990). [doi:10.1029/JD095iD10p16971](https://doi.org/10.1029/JD095iD10p16971)
  24. A. Worobiec *et al.*, Characterisation of Amazon Basin aerosols at the individual particle level by X-ray microanalytical techniques. *Atmos. Environ.* **41**, 9217 (2007). [doi:10.1016/j.atmosenv.2007.07.056](https://doi.org/10.1016/j.atmosenv.2007.07.056)
  25. D. R. Lawson, J. W. Winchester, Sulfur, potassium, and phosphorus associations in aerosols from south-american tropical rain forests. *J. Geophys. Res.* **84**, 3723 (1979). [doi:10.1029/JC084iC07p03723](https://doi.org/10.1029/JC084iC07p03723)
  26. D. R. Lawson, J. W. Winchester, Sulfur and trace-element concentration relationship in aerosols from south-american continent. *Geophys. Res. Lett.* **5**, 195 (1978).  
[doi:10.1029/GL005i003p00195](https://doi.org/10.1029/GL005i003p00195)
  27. G. E. Nemeryuk, Migration of salts into the atmosphere during transpiration. *Sov. Plant Physiol.* **17**, 560 (1970).
  28. G. Crozat, Emission of potassium aerosols in tropical forest. *Tellus* **31**, 52 (1979).  
[doi:10.1111/j.2153-3490.1979.tb00881.x](https://doi.org/10.1111/j.2153-3490.1979.tb00881.x)
  29. W. Beauford, J. Barber, A. R. Barringer, Release of particles containing metals from vegetation into the atmosphere. *Science* **195**, 571 (1977).  
[doi:10.1126/science.195.4278.571](https://doi.org/10.1126/science.195.4278.571) [Medline](#)
  30. W. Beauford, J. Barber, A. R. Barringer, Heavy metal release from plants into the atmosphere. *Nature* **256**, 35 (1975). [doi:10.1038/256035a0](https://doi.org/10.1038/256035a0) [Medline](#)
  31. A. K. Bertram *et al.*, Predicting the relative humidities of liquid-liquid phase separation, efflorescence, and deliquescence of mixed particles of ammonium sulfate, organic material, and water using the organic-to-sulfate mass ratio of the

- particle and the oxygen-to-carbon elemental ratio of the organic component. *Atmos. Chem. Phys.* **11**, 10995 (2011). [doi:10.5194/acp-11-10995-2011](https://doi.org/10.5194/acp-11-10995-2011)
32. M. Song, C. Marcolli, U. K. Krieger, A. Zuend, T. Peter, Liquid-liquid phase separation and morphology of internally mixed dicarboxylic acids/ammonium sulfate/water particles. *Atmos. Chem. Phys.* **12**, 2691 (2012). [doi:10.5194/acp-12-2691-2012](https://doi.org/10.5194/acp-12-2691-2012)
33. A. Zuend, J. H. Seinfeld, Modeling the gas-particle partitioning of secondary organic aerosol: The importance of liquid-liquid phase separation. *Atmos. Chem. Phys.* **12**, 3857 (2012). [doi:10.5194/acp-12-3857-2012](https://doi.org/10.5194/acp-12-3857-2012)
34. S. S. Gunthe *et al.*, Cloud condensation nuclei in pristine tropical rainforest air of Amazonia: Size-resolved measurements and modeling of atmospheric aerosol composition and CCN activity. *Atmos. Chem. Phys.* **9**, 7551 (2009). [doi:10.5194/acp-9-7551-2009](https://doi.org/10.5194/acp-9-7551-2009)
35. L. M. Russell, S. F. Maria, S. C. B. Myneni, Mapping organic coatings on atmospheric particles. *Geophys. Res. Lett.* **29**, 1779 (2002). [doi:10.1029/2002GL014874](https://doi.org/10.1029/2002GL014874)
36. R. C. Moffet, A. V. Tivanski, M. K. Gilles, in *Fundamentals and Applications in Aerosol Apectroscopy*, R. Signorell, J. Reid, Eds. (CRC, Boca Raton, FL, 2010).
37. R. J. Hopkins, A. V. Tivanski, B. D. Marten, M. K. Gilles, Chemical bonding and structure of black carbon reference materials and individual carbonaceous atmospheric aerosols. *J. Aerosol Sci.* **38**, 573 (2007). [doi:10.1016/j.jaerosci.2007.03.009](https://doi.org/10.1016/j.jaerosci.2007.03.009)
38. D. Solomon *et al.*, Carbon (1s) NEXAFS Spectroscopy of biogeochemically relevant reference organic compounds. *Soil Sci. Soc. Am. J.* **73**, 1817 (2009). [doi:10.2136/sssaj2008.0228](https://doi.org/10.2136/sssaj2008.0228)
39. S. T. Martin *et al.*, An overview of the Amazonian aerosol characterization experiment 2008 (AMAZE-08). *Atmos. Chem. Phys.* **10**, 11415 (2010). [doi:10.5194/acp-10-11415-2010](https://doi.org/10.5194/acp-10-11415-2010)
40. S. M. King, T. Rosenoern, J. E. Shilling, Q. Chen, S. T. Martin, Increased cloud activation potential of secondary organic aerosol for atmospheric mass loadings. *Atmos. Chem. Phys.* **9**, 2959 (2009). [doi:10.5194/acp-9-2959-2009](https://doi.org/10.5194/acp-9-2959-2009)
41. P. F. DeCarlo *et al.*, Field-deployable, high-resolution, time-of-flight aerosol mass spectrometer. *Anal. Chem.* **78**, 8281 (2006). [doi:10.1021/ac061249n](https://doi.org/10.1021/ac061249n) [Medline](#)
42. Q. Chen, Y. Liu, N. M. Donahue, J. E. Shilling, S. T. Martin, Particle-phase chemistry of secondary organic material: modeled compared to measured O:C and H:C elemental ratios provide constraints. *Environ. Sci. Technol.* **45**, 4763 (2011). [doi:10.1021/es104398s](https://doi.org/10.1021/es104398s) [Medline](#)
43. J. E. Shilling *et al.*, Particle mass yield in secondary organic aerosol formed by the dark ozonolysis of alpha-pinene. *Atmos. Chem. Phys.* **8**, 2073 (2008). [doi:10.5194/acp-8-2073-2008](https://doi.org/10.5194/acp-8-2073-2008)

44. Q. Chen, Y. L. Li, K. A. McKinney, M. Kuwata, S. T. Martin, Particle mass yield from  $\beta$ -caryophyllene ozonolysis. *Atmos. Chem. Phys.* **12**, 3165 (2012). [doi:10.5194/acp-12-3165-2012](https://doi.org/10.5194/acp-12-3165-2012)
45. S. M. King *et al.*, Cloud droplet activation of mixed organic-sulfate particles produced by the photooxidation of isoprene. *Atmos. Chem. Phys.* **10**, 3953 (2010). [doi:10.5194/acp-10-3953-2010](https://doi.org/10.5194/acp-10-3953-2010)
46. M. Fierz, R. Kaegi, H. Burtscher, Theoretical and experimental evaluation of a portable electrostatic TEM sampler. *Aerosol Sci. Technol.* **41**, 520 (2007). [doi:10.1080/02786820701253327](https://doi.org/10.1080/02786820701253327)
47. B. L. Henke, P. Lee, T. J. Tanaka, R. L. Shimabukuro, B. K. Fujikawa, Low-energy X-ray interaction coefficients: photoabsorption, scattering, and reflection. *At. Data Nucl. Data Tables* **27**, 1 (1982). [doi:10.1016/0092-640X\(82\)90002-X](https://doi.org/10.1016/0092-640X(82)90002-X)
48. A. L. D. Kilcoyne *et al.*, Interferometer-controlled scanning transmission X-ray microscopes at the Advanced Light Source. *J. Synchrotron Radiat.* **10**, 125 (2003). [doi:10.1107/S0909049502017739](https://doi.org/10.1107/S0909049502017739) [Medline](#)
49. R. Follath, J. S. Schmidt, M. Weigand, K. Fauth, in *Sri 2009: The 10th International Conference on Synchrotron Radiation Instrumentation*, R. Garrett, I. Gentle, K. Nugent, S. Wilkins, Eds. (American Institute of Physics, Melville, NY, 2010), vol. 1234, pp. 323–326.
50. J. Stöhr, *NEXAFS Spectroscopy* (Springer-Verlag, Berlin, ed. 1, 2003).
51. S. Takahama, S. Liu, L. M. Russell, Coatings and clusters of carboxylic acids in carbon-containing atmospheric particles from spectromicroscopy and their implications for cloud-nucleating and optical properties. *J. Geophys. Res.* **115**, D01202 (2010). [doi:10.1029/2009JD012622](https://doi.org/10.1029/2009JD012622)
52. S. C. B. Myneni, in *Applications of Synchrotron Radiation in Low-Temperature Geochemistry and Environmental Sciences*, P. A. Fenter, M. L. Rivers, N. C. Sturchio, S. R. Sutton, Eds. (Mineralogical Society of America, Washington, DC, 2002), vol. 49, pp. 485–579.
53. B. L. Henke, E. M. Gullikson, J. C. Davis, X-ray interactions - photoabsorption, scattering, transmission, and reflection at E=50-30,000 eV, Z=1-92. *At. Data Nucl. Data Tables* **54**, 181 (1993). [doi:10.1006/adnd.1993.1013](https://doi.org/10.1006/adnd.1993.1013)
54. L. Råde, B. Westergren, *Mathematics Handbook for Science and Engineering* (Springer, Berlin, ed. 5, 2004).
55. A. Benninghoven, F. G. Rüdener, H. W. Werner, *Secondary Ion Mass Spectrometry: Basic Concepts, Instrumental Aspects, Applications, and Trends* (Wiley, New York, 1987).
56. W. Maenhaut, M. T. Fernandez-Jimenez, I. Rajta, P. Artaxo, Two-year study of atmospheric aerosols in Alta Floresta, Brazil: Multielemental composition and source apportionment. *Nucl. Instrum. Methods Phys. Res. B* **189**, 243 (2002). [doi:10.1016/S0168-583X\(01\)01050-3](https://doi.org/10.1016/S0168-583X(01)01050-3)

57. F. Echalar *et al.*, Long-term monitoring of atmospheric aerosols in the Amazon Basin: Source identification and apportionment. *J. Geophys. Res.* **103**, 31849 (1998). [doi:10.1029/98JD01749](https://doi.org/10.1029/98JD01749)
58. L. Wouters, S. Hagedoren, I. Dierck, P. Artaxo, R. Vangrieken, Laser microprobe mass analysis of Amazon Basin aerosols. *Atmos. Environ.* **27**, 661 (1993). [doi:10.1016/0960-1686\(93\)90184-Z](https://doi.org/10.1016/0960-1686(93)90184-Z)
59. P. Artaxo *et al.*, Physical and chemical properties of aerosols in the wet and dry seasons in Rondonia, Amazonia. *J. Geophys. Res.* **107**, 8081 (2002). [doi:10.1029/2001JD000666](https://doi.org/10.1029/2001JD000666)
60. B. Graham *et al.*, Composition and diurnal variability of the natural Amazonian aerosol. *J. Geophys. Res.* **108**, 4765 (2003). [doi:10.1029/2003JD004049](https://doi.org/10.1029/2003JD004049)
61. S. Matthias-Maser, R. Jaenicke, The size distribution of primary biological aerosol particles with radii >0.2  $\mu\text{m}$  in an urban rural influenced region. *Atmos. Res.* **39**, 279 (1995). [doi:10.1016/0169-8095\(95\)00017-8](https://doi.org/10.1016/0169-8095(95)00017-8)
62. F. Trail, I. Gaffoor, S. Vogel, Ejection mechanics and trajectory of the ascospores of *Gibberella zeae* (anamorph *Fuvarium graminearum*). *Fungal Genet. Biol.* **42**, 528 (2005). [doi:10.1016/j.fgb.2005.03.008](https://doi.org/10.1016/j.fgb.2005.03.008) [Medline](#)
63. J. C. R. Turner, J. Webster, Mushroom Spores - The analysis of Bullers drop. *Chem. Eng. Sci.* **50**, 2359 (1995). [doi:10.1016/0009-2509\(95\)00097-O](https://doi.org/10.1016/0009-2509(95)00097-O)
64. J. Webster *et al.*, Mannitol and hexoses are components of Bullers drop. *Mycol. Res.* **99**, 833 (1995). [doi:10.1016/S0953-7562\(09\)80737-5](https://doi.org/10.1016/S0953-7562(09)80737-5)
65. A. A. Kazarov, L. S. Plieva, Evolution of ions into the atmosphere during transpiration by plants of several zones of the Northern Caucasus. *Sov. Plant Physiol.* **36**, 761 (1989).
66. G. C. Curtin, H. D. King, E. L. Mosier, Movement of elements into the atmosphere from coniferous trees in subalpine forests of Colorado and Idaho. *J. Geochem. Explor.* **3**, 245 (1974). [doi:10.1016/0375-6742\(74\)90025-9](https://doi.org/10.1016/0375-6742(74)90025-9)
67. Y. L. Melchakov, Ecological and geochemical effect of evapotranspiration in the mountain-taiga and subalpine belts of the Northern Urals. *Geochem. Int.* **50**, 84 (2012). [doi:10.1134/S0016702911110073](https://doi.org/10.1134/S0016702911110073)
68. R. N. Hughes, P. Brimblecombe, Dew and guttation - Formation and environmental significance. *Agric. For. Meteorol.* **67**, 173 (1994). [doi:10.1016/0168-1923\(94\)90002-7](https://doi.org/10.1016/0168-1923(94)90002-7)
69. L. Taiz, E. Zeiger, *Plant Physiology* (Sinauer, Sunderland, MA, 2010).
70. N. Mizuno, A. Takahashi, T. Wagatsuma, T. Mizuno, H. Obata, Chemical composition of guttation fluid and leaves of *Petasites japonicus* v. *giganteus* and *Polygonum cuspidatum* growing on ultramafic soil. *Soil Sci. Plant Nutr.* **48**, 451 (2002). [doi:10.1080/00380768.2002.10409225](https://doi.org/10.1080/00380768.2002.10409225)
71. G. M. Will, Removal of mineral nutrients from tree crowns by rain. *Nature* **176**, 1180 (1955). [doi:10.1038/1761180b0](https://doi.org/10.1038/1761180b0)



72. H. B. Tukey, R. A. Mecklenburg, Leaching of metabolites from foliage + subsequent reabsorption + redistribution of leachate in plants. *Am. J. Bot.* **51**, 737 (1964). [doi:10.2307/2440213](https://doi.org/10.2307/2440213)
73. H. B. Tukey, Jr., Leaching of substances from plants. *Annu. Rev. Plant Physiol.* **21**, 305 (1970). [doi:10.1146/annurev.pp.21.060170.001513](https://doi.org/10.1146/annurev.pp.21.060170.001513)
74. G. Stenlid, Salt losses and redistribution of salts in higher plants, in *Encyclopedia of Plant Physiology*, W. Ruhland, Ed. (Springer, Berlin, 1958), vol. 4, pp. 615–637.
75. S. D. Eigenbrode, K. A. Stoner, A. M. Shelton, W. C. Kain, Characteristics of glossy leaf waxes associated with resistance to diamondback moth (Lepidoptera, Plutellidae) in Brassica-oleracea. *J. Econ. Entomol.* **84**, 1609 (1991).
76. J. T. Martin, B. E. Juniper, *The Cuticles of Plants* (Publisher, City, 1970).
77. D. R. Lide, *CRC Handbook of Chemistry and Physics* (CRC, Boca Raton, FL, ed. 92, 2011).
78. M. Shiraiwa, M. Ammann, T. Koop, U. Pöschl, Gas uptake and chemical aging of semisolid organic aerosol particles. *Proc. Natl. Acad. Sci. U.S.A.* **108**, 11003 (2011). [doi:10.1073/pnas.1103045108](https://doi.org/10.1073/pnas.1103045108) [Medline](#)
79. Y. B. Lim, Y. Tan, M. J. Perri, S. P. Seitzinger, B. J. Turpin, Aqueous chemistry and its role in secondary organic aerosol (SOA) formation. *Atmos. Chem. Phys.* **10**, 10521 (2010). [doi:10.5194/acp-10-10521-2010](https://doi.org/10.5194/acp-10-10521-2010)
80. M. O. Andreae, D. Rosenfeld, Aerosol-cloud-precipitation interactions. Part 1. The nature and sources of cloud-active aerosols. *Earth Sci. Rev.* **89**, 13 (2008). [doi:10.1016/j.earscirev.2008.03.001](https://doi.org/10.1016/j.earscirev.2008.03.001)
81. P. Reutter *et al.*, Aerosol- and updraft-limited regimes of cloud droplet formation: influence of particle number, size and hygroscopicity on the activation of cloud condensation nuclei (CCN). *Atmos. Chem. Phys.* **9**, 7067 (2009). [doi:10.5194/acp-9-7067-2009](https://doi.org/10.5194/acp-9-7067-2009)
82. J. H. Seinfeld, S. N. Pandis, *Atmospheric Chemistry and Physics* (Wiley, New York, 1998).
83. M. Sipilä *et al.*, The role of sulfuric acid in atmospheric nucleation. *Science* **327**, 1243 (2010). [doi:10.1126/science.1180315](https://doi.org/10.1126/science.1180315) [Medline](#)
84. J. Kirkby *et al.*, Role of sulphuric acid, ammonia and galactic cosmic rays in atmospheric aerosol nucleation. *Nature* **476**, 429 (2011). [doi:10.1038/nature10343](https://doi.org/10.1038/nature10343) [Medline](#)
85. A. Metzger *et al.*, Evidence for the role of organics in aerosol particle formation under atmospheric conditions. *Proc. Natl. Acad. Sci. U.S.A.* **107**, 6646 (2010). [doi:10.1073/pnas.0911330107](https://doi.org/10.1073/pnas.0911330107) [Medline](#)
86. M. Kulmala, Atmospheric science. How particles nucleate and grow. *Science* **302**, 1000 (2003). [doi:10.1126/science.1090848](https://doi.org/10.1126/science.1090848) [Medline](#)

87. F. Yu, G. Luo, Simulation of particle size distribution with a global aerosol model: contribution of nucleation to aerosol and CCN number concentrations. *Atmos. Chem. Phys.* **9**, 7691 (2009). [doi:10.5194/acp-9-7691-2009](https://doi.org/10.5194/acp-9-7691-2009)
88. T. Berndt, O. Böge, F. Stratmann, J. Heintzenberg, M. Kulmala, Rapid formation of sulfuric acid particles at near-atmospheric conditions. *Science* **307**, 698 (2005). [doi:10.1126/science.1104054](https://doi.org/10.1126/science.1104054) [Medline](#)
89. V. P. Kanawade *et al.*, Isoprene suppression of new particle formation in a mixed deciduous forest. *Atmos. Chem. Phys.* **11**, 6013 (2011). [doi:10.5194/acp-11-6013-2011](https://doi.org/10.5194/acp-11-6013-2011)
90. M. O. Andreae, T. W. Andreae, The cycle of biogenic sulfur-compounds over the Amazon Basin. 1. Dry season. *J. Geophys. Res.* **93**, 1487 (1988). [doi:10.1029/JD093iD02p01487](https://doi.org/10.1029/JD093iD02p01487)
91. M. Martinez *et al.*, Hydroxyl radicals in the tropical troposphere over the Suriname rainforest: Airborne measurements. *Atmos. Chem. Phys.* **10**, 3759 (2010). [doi:10.5194/acp-10-3759-2010](https://doi.org/10.5194/acp-10-3759-2010)
92. T. Petäjä *et al.*, Sulfuric acid and OH concentrations in a boreal forest site. *Atmos. Chem. Phys.* **9**, 7435 (2009). [doi:10.5194/acp-9-7435-2009](https://doi.org/10.5194/acp-9-7435-2009)
93. R. Y. Zhang *et al.*, Atmospheric new particle formation enhanced by organic acids. *Science* **304**, 1487 (2004). [doi:10.1126/science.1095139](https://doi.org/10.1126/science.1095139) [Medline](#)
94. R. Zhang *et al.*, Formation of nanoparticles of blue haze enhanced by anthropogenic pollution. *Proc. Natl. Acad. Sci. U.S.A.* **106**, 17650 (2009). [doi:10.1073/pnas.0910125106](https://doi.org/10.1073/pnas.0910125106) [Medline](#)
95. B. Verheggen *et al.*, Alpha-pinene oxidation in the presence of seed aerosol: estimates of nucleation rates, growth rates, and yield. *Environ. Sci. Technol.* **41**, 6046 (2007). [doi:10.1021/es070245c](https://doi.org/10.1021/es070245c) [Medline](#)
96. A. Kiendler-Scharr *et al.*, New particle formation in forests inhibited by isoprene emissions. *Nature* **461**, 381 (2009). [doi:10.1038/nature08292](https://doi.org/10.1038/nature08292) [Medline](#)
97. M. Dal Maso *et al.*, Formation and growth of fresh atmospheric aerosols: Eight years of aerosol size distribution data from SMEAR II, Hyytiälä, Finland. *Boreal Env. Res.* **10**, 323 (2005).
98. M. Kulmala *et al.*, On the formation, growth and composition of nucleation mode particles. *Tellus* **53**, 479 (2001). [doi:10.1034/j.1600-0889.2001.d01-33.x](https://doi.org/10.1034/j.1600-0889.2001.d01-33.x)
99. M. Kulmala *et al.*, Formation and growth rates of ultrafine atmospheric particles: A review of observations. *J. Aerosol Sci.* **35**, 143 (2004). [doi:10.1016/j.jaerosci.2003.10.003](https://doi.org/10.1016/j.jaerosci.2003.10.003)
100. J. Zhou, E. Swietlicki, H. C. Hansson, P. Artaxo, Submicrometer aerosol particle size distribution and hygroscopic growth measured in the Amazon rain forest during the wet season. *J. Geophys. Res.* **107**, 8055 (2002). [doi:10.1029/2000JD000203](https://doi.org/10.1029/2000JD000203)

101. A. G. Carlton, C. Wiedinmyer, J. H. Kroll, A review of secondary organic aerosol (SOA) formation from isoprene. *Atmos. Chem. Phys.* **9**, 4987 (2009).  
[doi:10.5194/acp-9-4987-2009](https://doi.org/10.5194/acp-9-4987-2009)
102. B. Ervens, B. J. Turpin, R. J. Weber, Secondary organic aerosol formation in cloud droplets and aqueous particles (aqSOA): A review of laboratory, field and model studies. *Atmos. Chem. Phys.* **11**, 11069 (2011). [doi:10.5194/acp-11-11069-2011](https://doi.org/10.5194/acp-11-11069-2011)
103. T. H. Yoon *et al.*, Nanometer-scale chemical heterogeneities of black carbon materials and their impacts on PCB sorption properties: soft X-ray spectromicroscopy study. *Environ. Sci. Technol.* **40**, 5923 (2006).  
[doi:10.1021/es060173+](https://doi.org/10.1021/es060173+) [Medline](#)
104. S. Takahama, S. Gilardoni, L. M. Russell, A. L. D. Kilcoyne, Classification of multiple types of organic carbon composition in atmospheric particles by scanning transmission X-ray microscopy analysis. *Atmos. Environ.* **41**, 9435 (2007). [doi:10.1016/j.atmosenv.2007.08.051](https://doi.org/10.1016/j.atmosenv.2007.08.051)
105. A. P. Serro, A. C. Fernandes, B. Saramago, J. Lima, M. A. Barbosa, Apatite deposition on titanium surfaces—the role of albumin adsorption. *Biomaterials* **18**, 963 (1997). [doi:10.1016/S0142-9612\(97\)00031-8](https://doi.org/10.1016/S0142-9612(97)00031-8) [Medline](#)
106. W. C. Skamarock *et al.*, “A description of the advanced research WRF version 3” [National Center for Atmospheric Research (NCAR) Technical Note, NCAR/TN-475-STR, Boulder, CO, 2008].

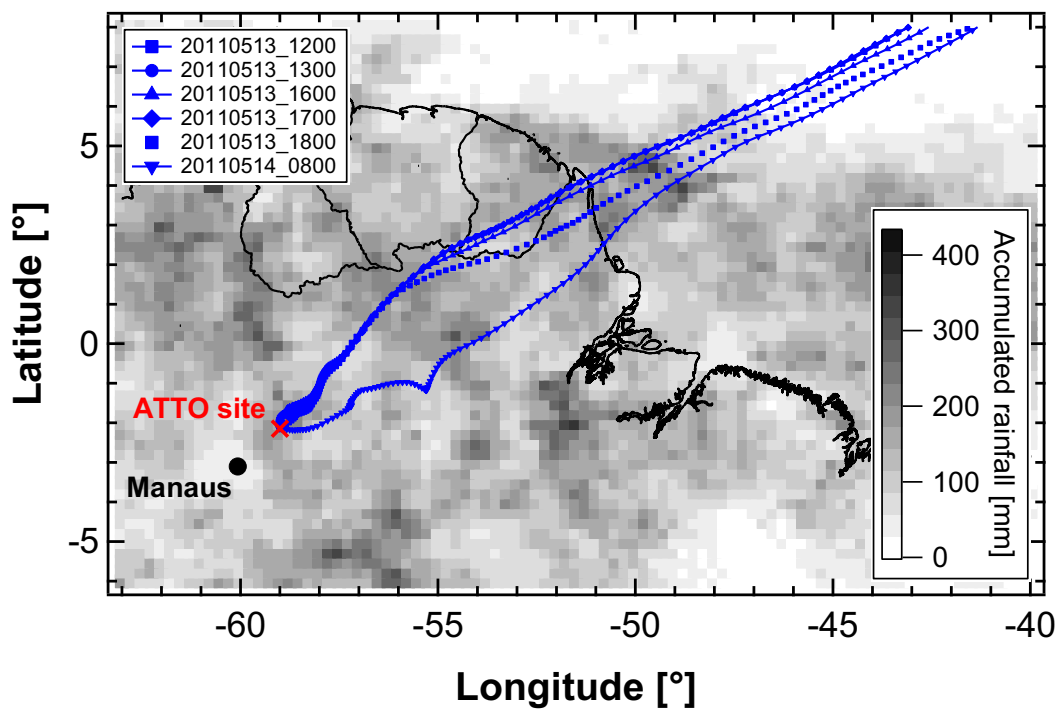


**Figure S1.** Location of the ATTO site in central Amazonia, Brazil, with back trajectories (HYSPLIT, NOAA-ARL, GDAS1 model, start height 100 m) and cumulative rainfall (tropical rainfall measuring mission TRMM) from 13 to 17 May 2011. Back trajectories are simulated for sampling time of individual impactor samples (Table S1).

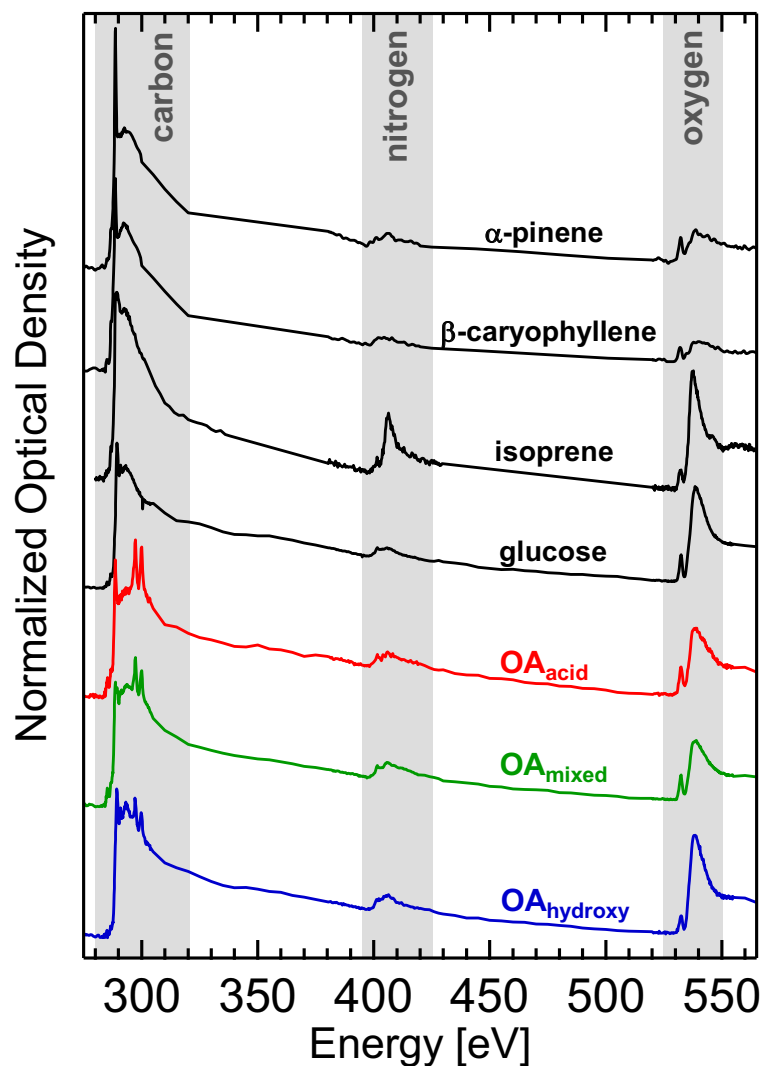


**Figure S2.** CNO X-ray absorption spectra of (i) laboratory-generated SOA from terpene ( $\alpha$ -pinene and  $\beta$ -caryophyllene) and isoprene oxidation, (ii) glucose as reference compound from spray-drying of aqueous solution and (iii) Amazonian OA particles ( $OA_{acid}$ ,  $OA_{mixed}$ ,  $OA_{hydroxy}$ ). The spectra cover the K-edges of carbon (283.8 eV), nitrogen (400.0 eV) and oxygen (531.7 eV) as well as the  $L_{3,2}$ -edges of potassium (294.6 eV) and calcium (349.3 eV). The carbon edge fine structure for the same spectra is shown in Fig. 2A.

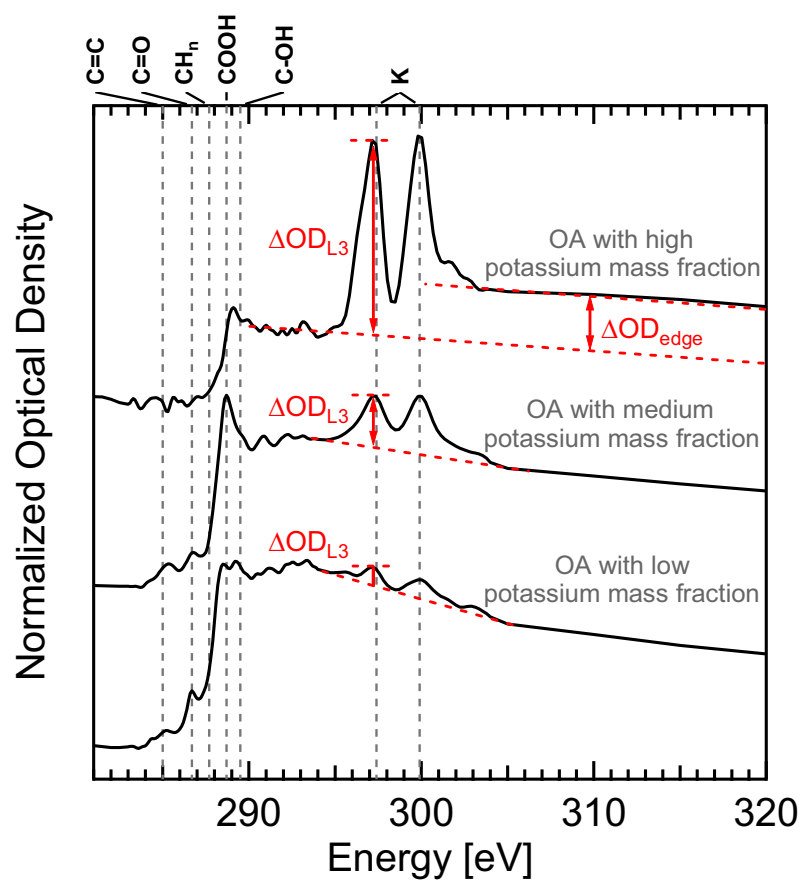


**Figure S3.** Characteristic spectra of individual Amazonian aerosol particles with different potassium mass fractions. Parameters  $\Delta OD_{edge}$  and  $\Delta OD_{L3}$  are used for potassium quantification.

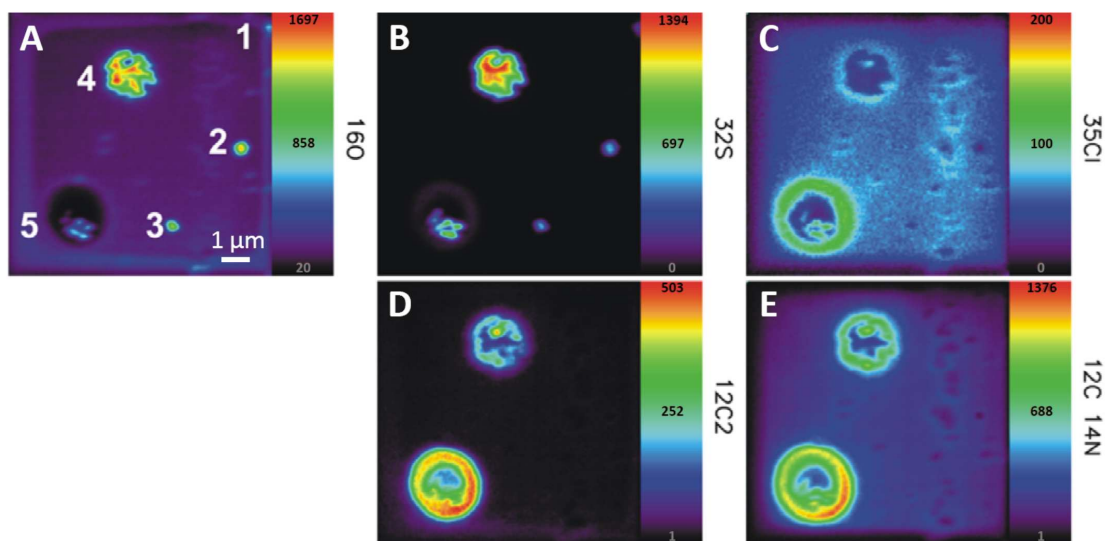


**Figure S4.** NanoSIMS images exhibiting elemental maps for (A) oxygen, (B) sulfur, (C) chlorine, (D) carbon, and (E) nitrogen of Amazonian aerosol particles. 1, 2, and 3 are small salt-rich particles. 4 and 5 are large OA particles exhibiting pronounced core-shell structures. Color code indicates counts of secondary ions.

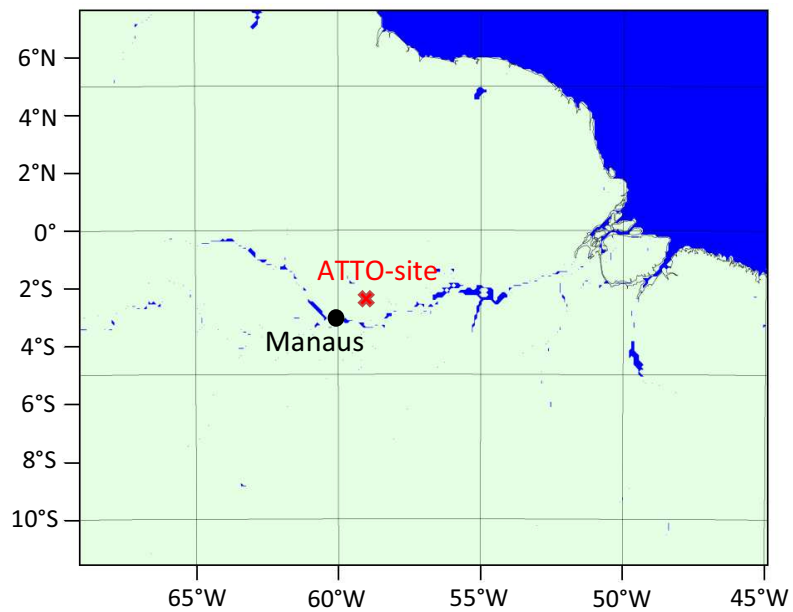


**Figure S5.** WRF model domain around the sampling location (ATTO site). Updraft velocities were calculated for May 2011 and integrated over the entire rainforest area (green shading).



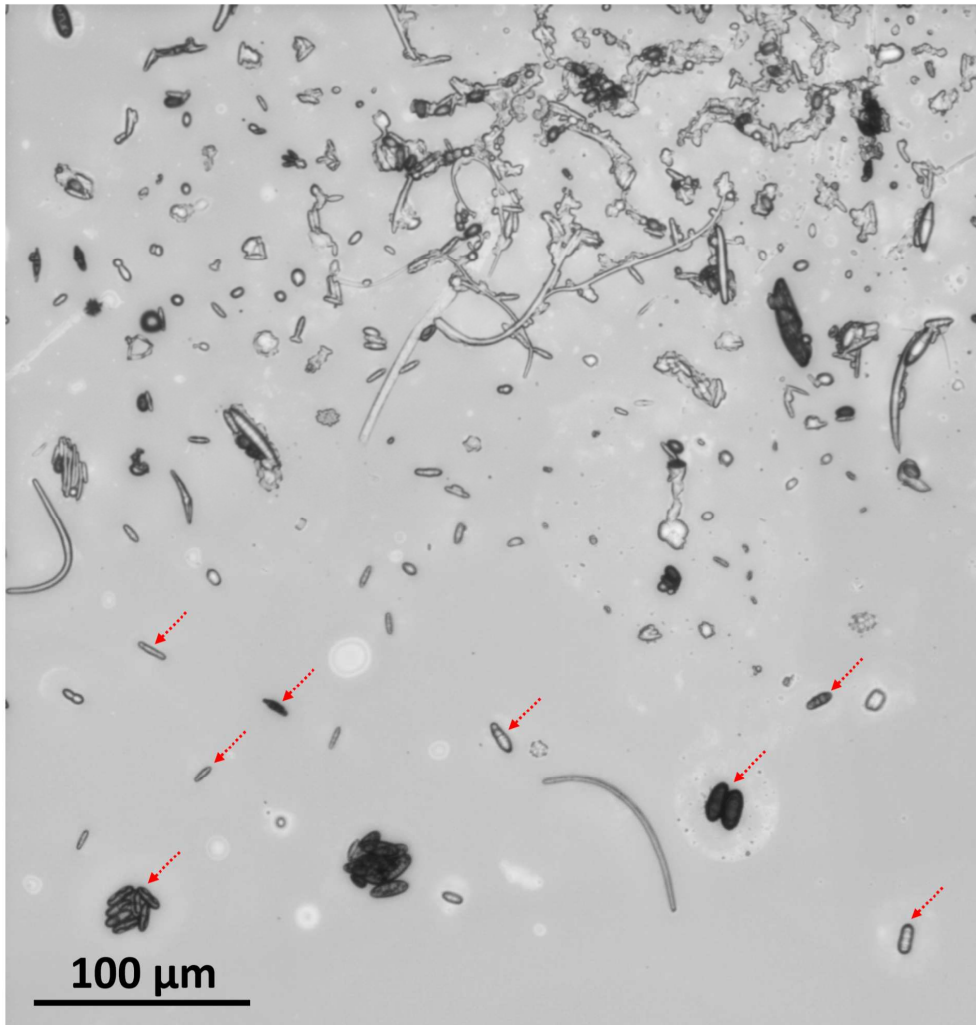


**Figure S6.** Light microscopy image of coarse mode particles in Amazonian aerosol sample (ATTO\_2011\_#2; Table S1). A high abundance and diversity of fungal spores was observed (examples are indicated by red arrows).

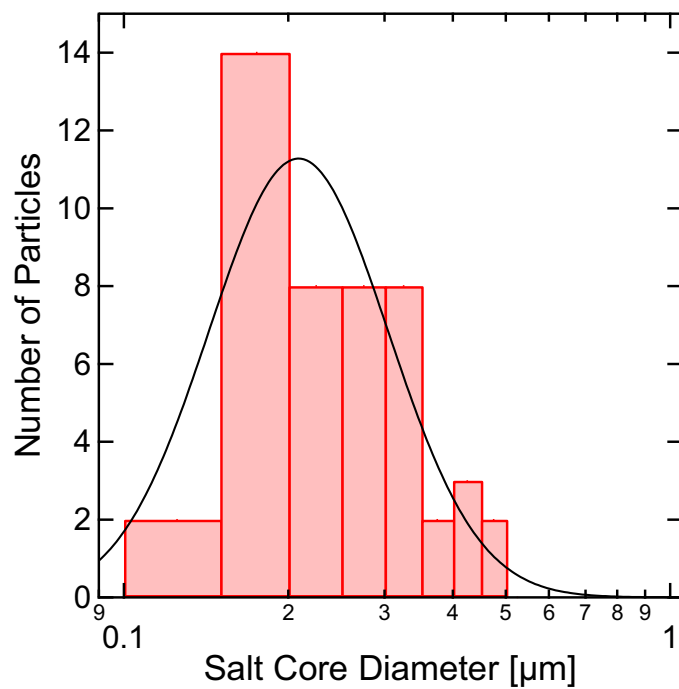


**Figure S7.** Size distribution of salt cores in the Amazonian aerosol sample ATTO\_2011\_#10 collected in the morning of 14 May 2011 (Table S1, Sect. 2.1). SEM measurement data (red bars) and lognormal fit (black line) indicate a peak around  $\sim 0.2 \mu\text{m}$ .

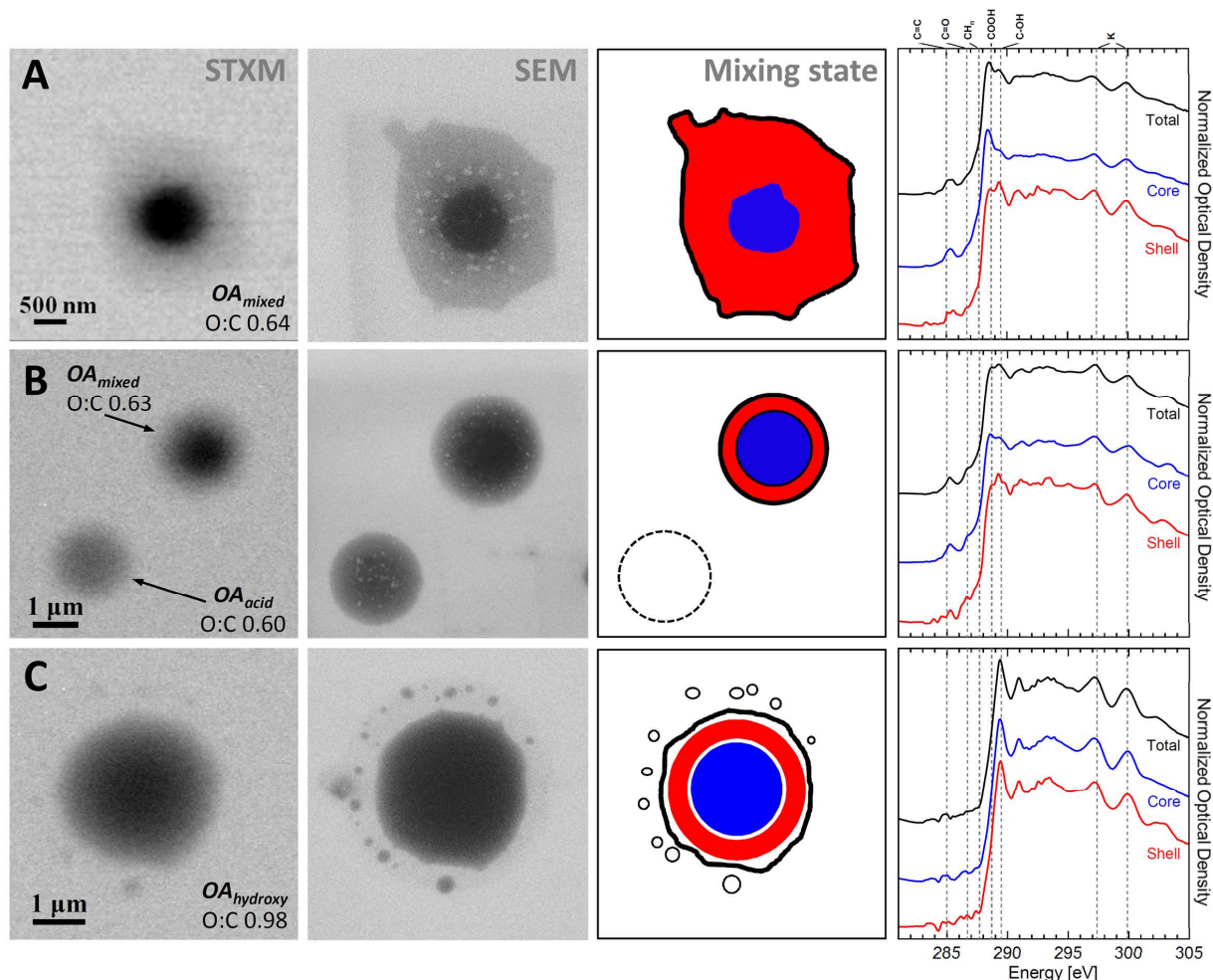


**Figure S8.** Internal structures of Amazonian organic aerosol particles analyzed by STXM-NEXAFS and SEM. Color code indicates integrated region for corresponding NEXAFS spectra. (A)  $OA_{mixed}$  particle with COOH-rich core and thick C-OH-rich coating. (B)  $OA_{mixed}$  particle with COOH-rich core and thin C-OH-rich coating. (C)  $OA_{hydroxy}$  with homogenous chemical composition. Halos of small satellite droplets were observed for  $\sim 50\%$  of  $OA_{hydroxy}$  particles ( $O:C \approx 0.9-1.0$ ) but not for  $OA_{acid}$  and  $OA_{mixed}$  particles ( $O:C \approx 0.5-0.7$ ). The halo satellite droplets were not considered in quantitative analyses of particle size distribution and potassium content.

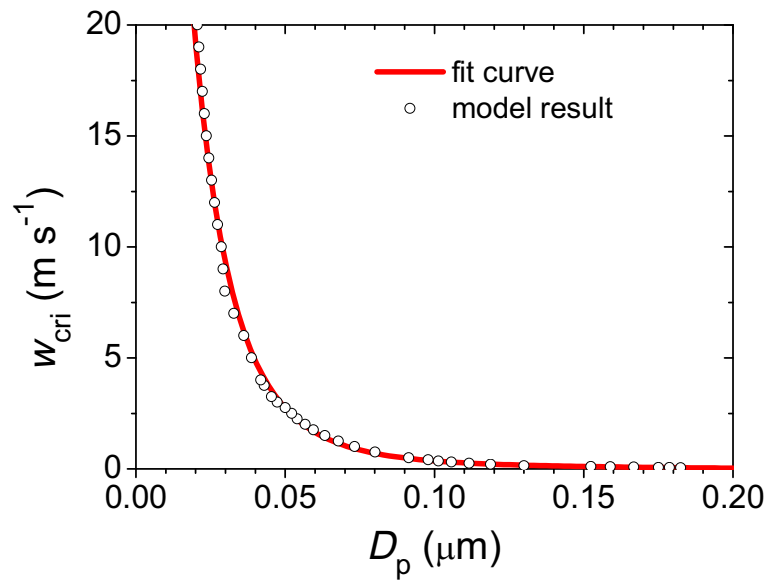


**Figure S9.** Critical updraft velocity for CCN activation of aerosol particles as a function of particle diameter. The data points are the results of cloud parcel model simulations with detailed spectral microphysics using parameters characteristic for pristine Amazonian aerosols (6, 34). The line is a fit of the form  $w_{\text{cri}} = f(D_p) = 10^{(-452 \cdot D_p^3 + 208 \cdot D_p^2 - 40.93 \cdot D_p + 2.021)}$ .

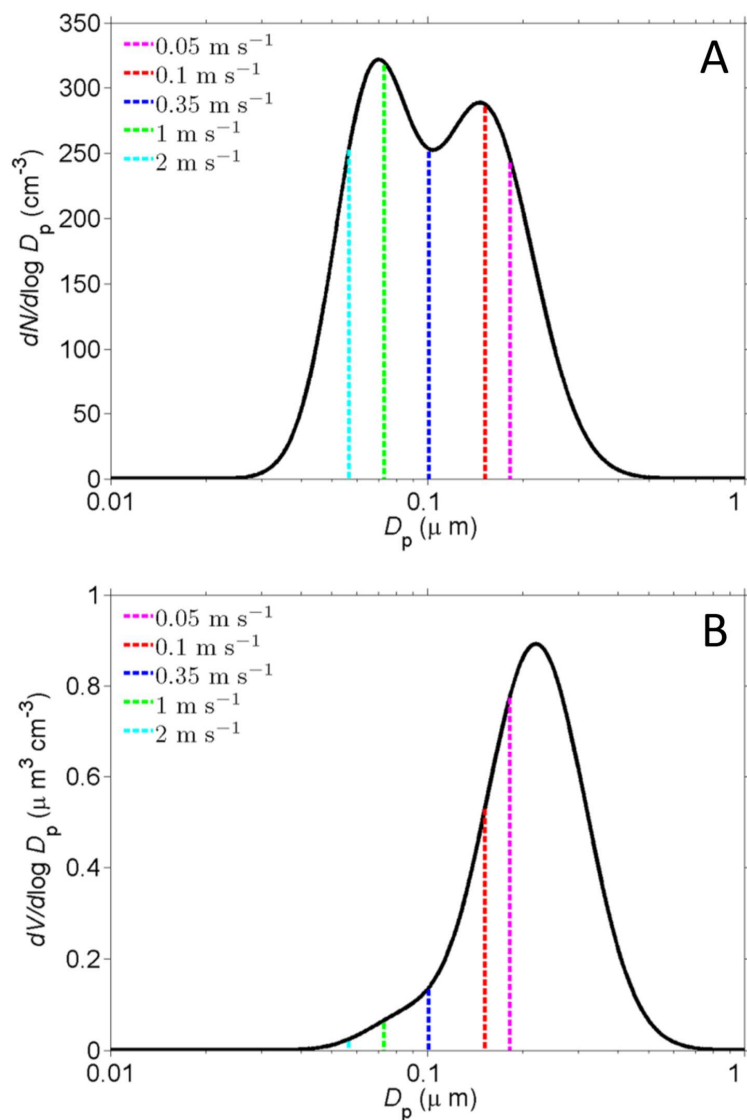


**Figure S10.** Aerosol size distribution and critical diameters of CCN activation for different updraft velocities ( $w = 0.05$  to  $2 \text{ m s}^{-1}$ ) characteristic for pristine Amazonian aerosols. **(A)** Particle number distribution composed of an Aitken mode around  $\sim 0.07 \text{ }\mu\text{m}$  and an accumulation mode around  $\sim 0.15 \text{ }\mu\text{m}$  (6, 34). **(B)** Particle volume distribution corresponding to the bimodal number distribution shown in panel A. Note that the actual volume distribution around  $1 \text{ }\mu\text{m}$  is higher because of coarse particles (primary biological material and mineral dust (6)) that are not included in this analysis, which is focused on the SOA particles dominating the accumulation mode composition.

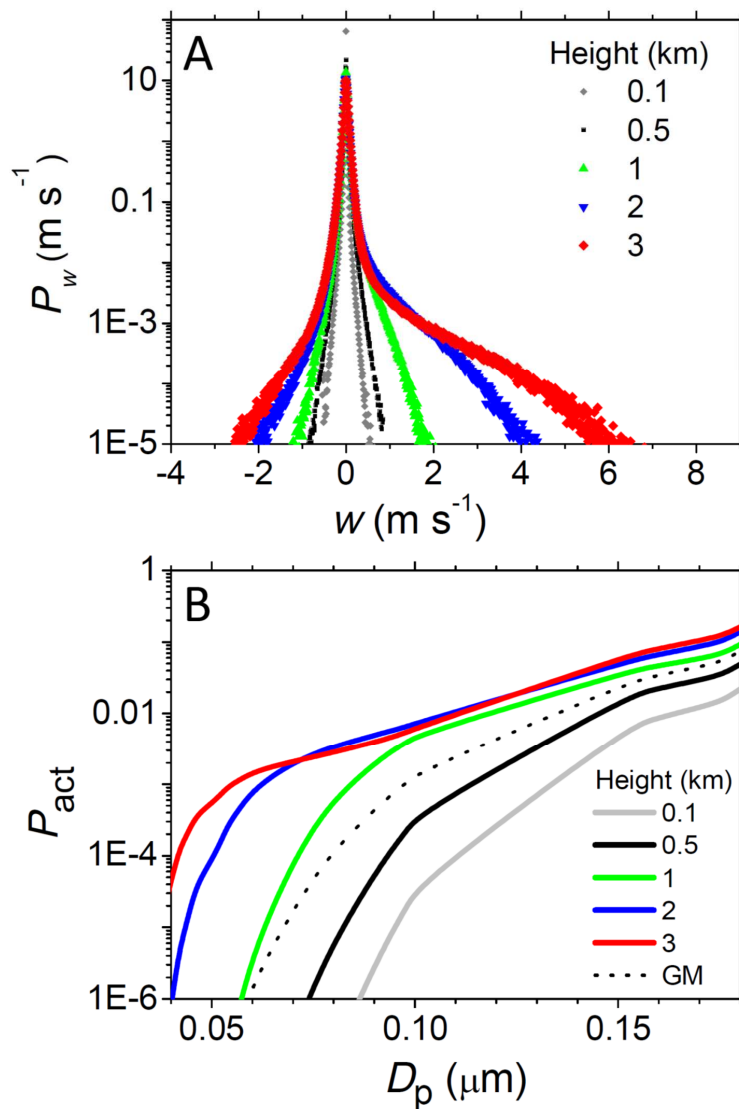


**Figure S11.** (A) Probability density function,  $P_w$ , of atmospheric updraft velocity,  $w$ , at different altitudes above the Amazonian rainforest during the wet season as calculated with the Weather Research and Forecast model (WRF-ARW-v3.3.1, Sect. S1.8) for the region and period around the aerosol sampling location and time (Fig. S5, May 2011). (B) CCN activation probability,  $P_{\text{act}}$ , of particles at diameter  $D_p$ . The lines represent results at different heights (GM = geometric mean value).

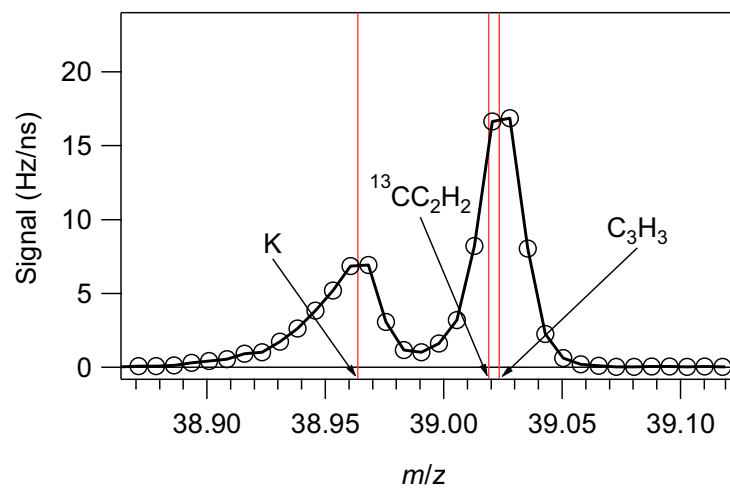


**Figure S12.** Particle mass spectrum averaged for pristine conditions during AMAZE-08 (“class I”), as detected by high-resolution time-of-flight aerosol mass spectrometry (HR-ToF-AMS, unpublished data) (7, 39).

**Table S1.** Characteristics of the analyzed aerosol samples.

<b>Sample Name</b>	<b>Sampling Time</b>		<b>Location</b>	<b>STXM setup</b>
ATTO_2011_#1	2011/05/13	11:30-12:20	ATTO site	ALS, BESSY II
ATTO_2011_#2	2011/05/13	12:35-13:15	ATTO site	ALS
ATTO_2011_#7	2011/05/13	15:50-16:23	ATTO site	ALS
ATTO_2011_#8	2011/05/13	16:27-17:07	ATTO site	ALS
ATTO_2011_#9	2011/05/13	17:15-17:55	ATTO site	ALS, BESSY II
ATTO_2011_#10	2011/05/14	07:42-08:42	ATTO site	ALS
ZF2_2010_#3	2010/05/15	06:20-07:20	ZF2/TT34 site	ALS
ZF2_2010_#4	2010/05/15	08:46-09:46	ZF2/TT34 site	ALS
ZF2_2010_#5	2010/05/15	10:25:11:24	ZF2/TT34 site	ALS



**Table S2.** Experimental parameters for SOA generation in the Harvard Environmental Chamber (GMD = geometric mean diameter, GSD = geometric standard deviation).

VOC	Oxidation	Chamber RH [%]	Ammonium Sulfate Seeds		SOA	
			Dry Diameter [nm]	Concentration [ $\mu\text{g m}^{-3}$ ]	Size Distribution GMD [nm] / GSD	Concentration [ $\mu\text{g m}^{-3}$ ]
Isoprene	photooxidation (H <sub>2</sub> O <sub>2</sub> injected, UV lights on)	40	70	2.4	152.4 / 1.44	32.7
$\alpha$ -pinene (+/-)	dark ozonolysis (O <sub>3</sub> injected, UV lights off)	40	46	1.0	94.2 / 1.58	26.1
$\beta$ -caryophyllene	dark ozonolysis (O <sub>3</sub> injected, UV lights off)	40	46	0.5	95.1 / 1.65	18.2

**Table S3.** Resonance energies of the carbon K-edge NEXAFS features with corresponding functional groups and potassium L-edge transitions. Peak assignments are based on (35, 38, 52, 103-104).

Functionality	Transition	Nominal Energy [eV]
Alkene/aromatic, R(C*=C)R'	1s $\rightarrow$ $\pi^*$	285.0 $\pm$ 0.2
Carbonyl groups, R(C*=O)R'	1s $\rightarrow$ $\pi^*$	286.7 $\pm$ 0.2
Alkyl, C*H <sub>n</sub> (n=1,2,3)	1s $\rightarrow$ $\sigma^*_{\text{C-H}}$	287.7 $\pm$ 0.7
Carboxylic carbonyl, R(C*=O)OH	1s $\rightarrow$ $\pi^*$	288.7 $\pm$ 0.3
Hydroxy/ether, OC*H <sub>2</sub>	1s $\rightarrow$ 3p/ $\sigma^*$	289.3 $\pm$ 0.2
Potassium, K <sub>L3</sub>	2p <sub>3/2</sub> $\rightarrow$ 3d/ $\sigma^*$	297.4 $\pm$ 0.2
Potassium, K <sub>L2</sub>	2p <sub>1/2</sub> $\rightarrow$ 3d/ $\sigma^*$	299.9 $\pm$ 0.2

**Table S4.** Molar elemental ratios for C, N, and O ( $n_{\text{O}}/n_{\text{C}}$  and  $n_{\text{N}}/n_{\text{C}}$ ) for selected standard compounds, laboratory-generated SOA, and Amazonian OA determined by STXM-NEXAFS analysis. The reference data are stoichiometric ratios for pure standard compounds and AMS data for SOA samples. Data for BSA taken from Serro et al. (105). For SOA the ratios for organic plus ammonium sulfate and for organic only (in parentheses) are given.

Compound	$n_{\text{O}}/n_{\text{C}}$		$n_{\text{N}}/n_{\text{C}}$	
	STXM	Reference	STXM	Reference
Glucosamine·HCl ( $\text{C}_6\text{H}_{14}\text{NO}_5\text{Cl}$ )	0.86	0.83	0.17	0.17
Glucose ( $\text{C}_6\text{H}_{12}\text{O}_6$ )	0.90	1.0	0.04	0
Serine ( $\text{C}_3\text{H}_7\text{NO}_3$ )	0.75	1.0	0.28	0.33
Aspartic acid ( $\text{C}_4\text{H}_7\text{NO}_4$ )	1.0	1.0	0.23	0.25
BSA	0.36	0.32	0.17	0.25
Isoprene SOA	0.88 (0.63)	0.70 (0.67)	0.23	0.08 (0.004)
$\alpha$ -pinene SOA	0.42 (0.38)	0.36 (0.34)	0.06	0.04 (0.001)
$\beta$ -caryophyllene SOA	0.35 (0.31)	0.33 (0.32)	0.04	0.02 (0.002)
OA <sub>acid</sub>	0.63	-	0.09	-
OA <sub>mixed</sub>	0.67	-	0.17	-
OA <sub>hydroxyl</sub>	0.92	-	0.18	-

**Table S5.** WRF-ARW-v3.3.1 model configuration (106).

<b>Scheme</b>	<b>Options</b>
Microphysics	WRF Single-Moment 6-class scheme with ice, snow and graupel processes
Long-wave radiation	RRTMG scheme, a new version of RRTM
Short-wave radiation	RRTMG shortwave scheme with the MCICA method of random cloud overlap
Surface layer	Eta similarity used in Eta model and based on Monin-Obukhov with Zilitinkevich thermal roughness length and standard similarity functions from look-up tables
Land surface	Noah Land Surface Model unified NCEP/NCAR/AFWA scheme with soil temperature and moisture in four layers
Boundary layer	Mellor-Yamada-Janjic scheme, an Eta operational scheme; one-dimensional prognostic turbulent kinetic energy scheme with local vertical mixing
Cumulus parameterization	Grell 3D, an improved version of the GD scheme that may also be used on high resolution with subsidence spreading turned on
Diffusion	Full diffusion
6th order horizontal diffusion	Positive definite
Non-hydrostatic	True
PD advection	Positive definite on

**Table S6.** Normalized optical density at carbon absorption edge for reference and ambient aerosols as measured by STXM-NEXAFS and plotted against X-ray photon energy in Fig. 2A.

Energy [eV]	Normalized Optical Density						
	$\alpha$ -pinene SOA	$\beta$ -caryophyllene SOA	isoprene SOA	glucose	OA(acid)	OA(mixed)	OA(hydroxy)
280	-0.03	0.02	0	0	0	-0.01	0
280.5	-0.03	0.02	0	-0.01	0	-0.01	0
281	-0.02	0.01	-0.01	-0.01	0	-0.02	0
281.5	-0.01	0	0	-0.01	0	-0.01	0
282	0	-0.01	0.01	-0.01	-0.01	-0.01	-0.01
282.5	0.01	0	0.01	-0.01	-0.01	-0.01	-0.01
283	0.03	0	0	-0.01	-0.01	-0.01	-0.01
283.1	0.03	0	0	-0.01	-0.01	-0.01	-0.01
283.2	0.02	0	0	-0.01	-0.01	-0.01	-0.01
283.3	0.01	0	0	-0.01	-0.01	0	-0.01
283.4	0.01	0	-0.01	-0.01	-0.01	0	-0.01
283.5	0	0.01	-0.01	-0.01	-0.01	0	-0.01
283.6	0.01	0.01	-0.01	0	0	0	-0.01
283.7	0.01	0	0	0	0	0.01	0
283.8	0.01	-0.01	0	0	0.01	0.01	0
283.9	0	-0.01	0.01	0	0.02	0.01	0
284	-0.01	-0.01	0.02	0.01	0.02	0.01	0.01
284.1	-0.01	-0.01	0.03	0.01	0.03	0.01	0.01
284.2	0	-0.01	0.04	0.01	0.03	0.01	0.01
284.3	0.01	-0.02	0.04	0.01	0.04	0.02	0.01
284.4	0.02	-0.01	0.05	0.02	0.06	0.04	0.01
284.5	0.03	0.03	0.06	0.02	0.07	0.05	0.02
284.6	0.04	0.06	0.06	0.02	0.09	0.07	0.02
284.7	0.06	0.1	0.07	0.03	0.12	0.09	0.02
284.8	0.08	0.12	0.07	0.03	0.14	0.11	0.03
284.9	0.1	0.13	0.08	0.04	0.17	0.14	0.03
285	0.11	0.14	0.08	0.05	0.19	0.16	0.03
285.1	0.11	0.14	0.08	0.06	0.21	0.19	0.03
285.2	0.1	0.14	0.08	0.06	0.22	0.2	0.03
285.3	0.1	0.13	0.09	0.06	0.22	0.21	0.03
285.4	0.11	0.13	0.09	0.06	0.21	0.2	0.03
285.5	0.11	0.12	0.09	0.05	0.2	0.19	0.03
285.6	0.12	0.11	0.1	0.05	0.18	0.18	0.03
285.7	0.12	0.1	0.1	0.04	0.17	0.16	0.03
285.8	0.13	0.09	0.11	0.04	0.15	0.15	0.03
285.9	0.14	0.1	0.12	0.05	0.15	0.14	0.03
286	0.16	0.11	0.14	0.06	0.15	0.13	0.04
286.1	0.19	0.12	0.16	0.07	0.16	0.14	0.05
286.2	0.22	0.15	0.19	0.09	0.18	0.15	0.06
286.3	0.27	0.2	0.22	0.11	0.21	0.17	0.08
286.4	0.33	0.28	0.26	0.13	0.25	0.2	0.09
286.5	0.41	0.4	0.3	0.15	0.28	0.24	0.11
286.6	0.47	0.52	0.34	0.16	0.31	0.27	0.12
286.7	0.51	0.61	0.37	0.17	0.34	0.29	0.12
286.8	0.52	0.65	0.4	0.17	0.35	0.3	0.12
286.9	0.53	0.67	0.41	0.16	0.36	0.31	0.11
287	0.53	0.67	0.43	0.16	0.36	0.32	0.11
287.1	0.54	0.68	0.44	0.16	0.36	0.34	0.12
287.2	0.57	0.71	0.47	0.16	0.37	0.36	0.13
287.3	0.62	0.76	0.5	0.17	0.38	0.38	0.14
287.4	0.68	0.83	0.55	0.19	0.4	0.41	0.16
287.5	0.74	0.92	0.6	0.2	0.43	0.45	0.17
287.6	0.82	1.01	0.66	0.22	0.47	0.49	0.2
287.7	0.9	1.11	0.74	0.24	0.54	0.55	0.23
287.8	1	1.22	0.83	0.27	0.63	0.64	0.28
287.9	1.12	1.33	0.93	0.33	0.75	0.76	0.35

288	1.27	1.44	1.06	0.4	0.9	0.9	0.44
288.1	1.46	1.58	1.21	0.48	1.05	1.06	0.55
288.2	1.73	1.74	1.38	0.57	1.22	1.21	0.67
288.3	2.07	1.96	1.58	0.65	1.39	1.35	0.8
288.4	2.48	2.2	1.78	0.73	1.55	1.47	0.94
288.5	2.87	2.42	1.99	0.82	1.68	1.56	1.07
288.6	3.12	2.56	2.16	0.92	1.76	1.62	1.2
288.7	3.18	2.57	2.3	1.04	1.77	1.63	1.32
288.8	3.05	2.48	2.4	1.19	1.73	1.62	1.44
288.9	2.79	2.33	2.46	1.36	1.65	1.6	1.56
289	2.51	2.17	2.5	1.54	1.57	1.59	1.68
289.1	2.27	2.04	2.52	1.7	1.49	1.58	1.8
289.2	2.08	1.95	2.52	1.82	1.43	1.58	1.9
289.3	1.95	1.89	2.53	1.9	1.38	1.58	1.95
289.4	1.87	1.85	2.53	1.93	1.36	1.59	1.96
289.5	1.82	1.83	2.53	1.92	1.33	1.58	1.93
289.6	1.8	1.83	2.52	1.88	1.31	1.56	1.88
289.7	1.8	1.83	2.51	1.82	1.3	1.54	1.82
289.8	1.81	1.83	2.5	1.76	1.29	1.51	1.75
289.9	1.81	1.83	2.48	1.7	1.28	1.48	1.68
290	1.82	1.83	2.46	1.65	1.29	1.45	1.63
290.1	1.82	1.84	2.44	1.6	1.29	1.44	1.59
290.2	1.83	1.84	2.43	1.57	1.3	1.44	1.57
290.3	1.83	1.86	2.41	1.56	1.31	1.45	1.58
290.4	1.83	1.87	2.4	1.57	1.33	1.47	1.6
290.5	1.81	1.88	2.38	1.59	1.35	1.49	1.64
290.6	1.8	1.89	2.36	1.61	1.36	1.51	1.68
290.7	1.8	1.9	2.35	1.64	1.37	1.53	1.71
290.8	1.81	1.92	2.34	1.65	1.38	1.55	1.74
290.9	1.82	1.92	2.32	1.66	1.38	1.56	1.74
291	1.82	1.92	2.31	1.66	1.38	1.56	1.74
291.1	1.81	1.93	2.31	1.64	1.37	1.57	1.72
291.2	1.81	1.94	2.3	1.63	1.37	1.57	1.69
291.3	1.83	1.95	2.3	1.62	1.37	1.56	1.67
291.4	1.84	1.96	2.3	1.6	1.37	1.56	1.66
291.5	1.85	1.96	2.29	1.6	1.38	1.56	1.66
291.6	1.85	1.96	2.3	1.59	1.4	1.56	1.66
291.7	1.84	1.97	2.3	1.59	1.41	1.56	1.66
291.8	1.85	1.98	2.3	1.59	1.42	1.57	1.66
291.9	1.87	1.99	2.3	1.6	1.42	1.57	1.66
292	1.88	2.01	2.31	1.6	1.41	1.57	1.67
292.1	1.89	2.02	2.31	1.61	1.41	1.57	1.68
292.2	1.9	2.02	2.32	1.63	1.41	1.58	1.7
292.3	1.91	2.01	2.32	1.64	1.42	1.59	1.71
292.4	1.91	2.01	2.32	1.64	1.43	1.6	1.73
292.5	1.92	2	2.32	1.65	1.44	1.61	1.74
292.6	1.92	2.01	2.32	1.65	1.45	1.62	1.76
292.7	1.91	2.01	2.32	1.65	1.45	1.63	1.77
292.8	1.91	2	2.31	1.65	1.45	1.63	1.77
292.9	1.89	2	2.31	1.65	1.45	1.63	1.77
293	1.88	1.99	2.31	1.66	1.45	1.63	1.78
293.1	1.87	1.99	2.3	1.66	1.46	1.64	1.79
293.2	1.86	1.99	2.3	1.66	1.47	1.64	1.79
293.3	1.86	1.97	2.29	1.65	1.46	1.65	1.8
293.4	1.86	1.96	2.29	1.64	1.46	1.65	1.79
293.5	1.86	1.96	2.28	1.64	1.46	1.65	1.78
293.6	1.87	1.96	2.28	1.63	1.46	1.65	1.77
293.7	1.87	1.97	2.27	1.63	1.47	1.65	1.77
293.8	1.87	1.97	2.26	1.62	1.47	1.65	1.77
293.9	1.87	1.96	2.26	1.62	1.46	1.65	1.76
294	1.87	1.93	2.25	1.61	1.45	1.64	1.74
294.5	1.86	1.89	2.21	1.6	1.45	1.63	1.72

294.721	1.85	1.88	2.19	1.59	1.46	1.63	1.7
294.942	1.85	1.86	2.17	1.58	1.47	1.62	1.68
295.163	1.84	1.85	2.14	1.57	1.49	1.62	1.66
295.384	1.83	1.83	2.12	1.55	1.5	1.62	1.65
295.605	1.82	1.82	2.09	1.54	1.53	1.61	1.64
295.826	1.81	1.8	2.07	1.52	1.56	1.62	1.64
296.047	1.8	1.79	2.05	1.5	1.61	1.64	1.64
296.268	1.78	1.77	2.03	1.49	1.67	1.68	1.65
296.489	1.77	1.76	2.01	1.47	1.75	1.73	1.68
296.71	1.75	1.75	1.99	1.45	1.83	1.79	1.71
296.931	1.74	1.73	1.97	1.44	1.92	1.85	1.76
297.152	1.72	1.72	1.95	1.42	1.97	1.9	1.78
297.373	1.7	1.71	1.92	1.4	1.97	1.89	1.77
297.594	1.69	1.7	1.9	1.38	1.9	1.84	1.72
297.815	1.67	1.69	1.88	1.37	1.79	1.76	1.65
298.036	1.66	1.67	1.85	1.35	1.68	1.67	1.59
298.257	1.64	1.66	1.83	1.34	1.61	1.61	1.54
298.478	1.63	1.64	1.81	1.33	1.57	1.57	1.51
298.699	1.61	1.62	1.79	1.32	1.57	1.57	1.5
298.92	1.6	1.6	1.77	1.3	1.6	1.59	1.52
299.141	1.57	1.58	1.76	1.29	1.67	1.63	1.55
299.362	1.55	1.57	1.74	1.28	1.76	1.69	1.59
299.583	1.53	1.55	1.73	1.26	1.85	1.74	1.62
299.804	1.52	1.53	1.71	1.25	1.9	1.77	1.63
300.025	1.52	1.51	1.7	1.22	1.91	1.76	1.61
300.246	1.51	1.5	1.68	1.2	1.85	1.71	1.56
300.467	1.5	1.48	1.66	1.18	1.75	1.64	1.5
300.688	1.49	1.47	1.64	1.18	1.65	1.57	1.44
300.909	1.48	1.46	1.61	1.19	1.57	1.51	1.39
301.13	1.46	1.45	1.58	1.19	1.51	1.47	1.36
301.351	1.45	1.44	1.57	1.19	1.47	1.45	1.33
301.572	1.44	1.43	1.55	1.18	1.45	1.43	1.31
301.793	1.43	1.42	1.53	1.18	1.42	1.42	1.29
302.014	1.42	1.41	1.52	1.17	1.4	1.4	1.28
302.235	1.41	1.4	1.5	1.17	1.38	1.39	1.28
302.456	1.4	1.38	1.49	1.16	1.36	1.38	1.27
302.677	1.38	1.37	1.48	1.16	1.34	1.36	1.27
302.898	1.37	1.36	1.47	1.16	1.33	1.35	1.26
303.119	1.36	1.35	1.46	1.16	1.33	1.34	1.25
303.34	1.35	1.34	1.45	1.16	1.33	1.32	1.24
303.561	1.34	1.33	1.44	1.15	1.32	1.3	1.22
303.782	1.33	1.32	1.43	1.15	1.28	1.27	1.2
304.003	1.32	1.31	1.41	1.13	1.23	1.22	1.16
305	1.27	1.26	1.36	1.09	1.15	1.15	1.1
310	1.09	1.08	1.08	1.03	1.06	1.06	1.03
315	0.91	0.91	0.92	0.97	0.96	0.96	0.96

**Table S7.** Normalized optical density at carbon absorption edge for Amazonian aerosol particles with different potassium contents as measured by STXM-NEXAFS and plotted against X-ray photon energy in Fig. 2B.

Energy [eV]	Normalized Optical Density		
	OA with high K mass fraction (>10%)	OA with medium K mass fraction (1-10%)	OA with low K mass fraction (<1%)
280	0.03	0.02	-0.01
280.5	0.03	0.01	-0.01
281	0.03	0	-0.01
281.5	0.03	0	-0.01
282	0.04	0	-0.01
282.5	0.03	0	-0.02
283	0.03	0	-0.02
283.1	0.02	-0.01	-0.02
283.2	0.02	-0.02	-0.01
283.3	0	-0.03	-0.01
283.4	-0.01	-0.04	0
283.5	-0.02	-0.04	0
283.6	-0.04	-0.05	0
283.7	-0.05	-0.05	0.01
283.8	-0.05	-0.04	0.01
283.9	-0.05	-0.03	0.02
284	-0.05	-0.02	0.02
284.1	-0.05	-0.01	0.02
284.2	-0.06	0.01	0.03
284.3	-0.07	0.02	0.04
284.4	-0.09	0.03	0.05
284.5	-0.12	0.05	0.07
284.6	-0.16	0.06	0.09
284.7	-0.21	0.08	0.11
284.8	-0.25	0.09	0.12
284.9	-0.28	0.11	0.14
285	-0.29	0.12	0.16
285.1	-0.27	0.13	0.18
285.2	-0.24	0.14	0.19
285.3	-0.2	0.14	0.19
285.4	-0.16	0.13	0.18
285.5	-0.13	0.12	0.18
285.6	-0.12	0.12	0.16
285.7	-0.13	0.11	0.15
285.8	-0.17	0.11	0.14
285.9	-0.22	0.12	0.13
286	-0.26	0.13	0.13
286.1	-0.3	0.14	0.14
286.2	-0.31	0.16	0.15
286.3	-0.31	0.19	0.17
286.4	-0.3	0.21	0.19
286.5	-0.26	0.24	0.22
286.6	-0.22	0.25	0.24
286.7	-0.16	0.26	0.26
286.8	-0.12	0.27	0.28
286.9	-0.1	0.27	0.3
287	-0.1	0.27	0.31
287.1	-0.12	0.27	0.33
287.2	-0.13	0.29	0.35
287.3	-0.13	0.31	0.37
287.4	-0.11	0.34	0.4
287.5	-0.08	0.37	0.44
287.6	-0.03	0.42	0.48
287.7	0.03	0.48	0.55
287.8	0.1	0.56	0.64
287.9	0.18	0.65	0.75
288	0.26	0.75	0.88



288.1	0.35	0.86	1.02
288.2	0.43	0.98	1.16
288.3	0.52	1.1	1.3
288.4	0.6	1.22	1.41
288.5	0.66	1.32	1.51
288.6	0.7	1.4	1.59
288.7	0.73	1.45	1.64
288.8	0.73	1.49	1.67
288.9	0.71	1.5	1.69
289	0.68	1.5	1.7
289.1	0.64	1.49	1.71
289.2	0.6	1.48	1.72
289.3	0.55	1.48	1.72
289.4	0.5	1.47	1.72
289.5	0.47	1.46	1.7
289.6	0.45	1.44	1.68
289.7	0.45	1.42	1.65
289.8	0.46	1.4	1.62
289.9	0.47	1.37	1.59
290	0.48	1.34	1.57
290.1	0.48	1.32	1.56
290.2	0.48	1.31	1.55
290.3	0.5	1.31	1.56
290.4	0.53	1.33	1.57
290.5	0.57	1.36	1.59
290.6	0.6	1.4	1.62
290.7	0.62	1.43	1.63
290.8	0.61	1.45	1.65
290.9	0.58	1.46	1.65
291	0.53	1.45	1.66
291.1	0.47	1.45	1.66
291.2	0.41	1.44	1.65
291.3	0.35	1.44	1.65
291.4	0.32	1.44	1.65
291.5	0.3	1.44	1.65
291.6	0.3	1.44	1.66
291.7	0.31	1.44	1.66
291.8	0.33	1.44	1.66
291.9	0.34	1.43	1.66
292	0.35	1.43	1.67
292.1	0.36	1.43	1.67
292.2	0.36	1.44	1.68
292.3	0.36	1.46	1.69
292.4	0.34	1.48	1.7
292.5	0.32	1.49	1.71
292.6	0.29	1.5	1.72
292.7	0.26	1.5	1.73
292.8	0.22	1.49	1.74
292.9	0.19	1.48	1.74
293	0.17	1.48	1.75
293.1	0.16	1.48	1.75
293.2	0.16	1.48	1.76
293.3	0.17	1.48	1.76
293.4	0.19	1.49	1.76
293.5	0.19	1.5	1.76
293.6	0.18	1.5	1.76
293.7	0.16	1.5	1.75
293.8	0.13	1.5	1.75
293.9	0.13	1.5	1.74
294	0.14	1.49	1.73
294.5	0.18	1.48	1.72
294.721	0.23	1.48	1.71
294.942	0.3	1.48	1.7
295.163	0.4	1.49	1.7
295.384	0.55	1.51	1.7
295.605	0.77	1.55	1.7

295.826	1.06	1.61	1.71
296.047	1.41	1.7	1.72
296.268	1.83	1.79	1.74
296.489	2.31	1.9	1.76
296.71	2.8	2	1.79
296.931	3.2	2.08	1.8
297.152	3.39	2.11	1.81
297.373	3.28	2.09	1.8
297.594	2.88	2.01	1.76
297.815	2.33	1.89	1.72
298.036	1.8	1.78	1.67
298.257	1.46	1.69	1.63
298.478	1.36	1.65	1.6
298.699	1.49	1.66	1.59
298.92	1.79	1.71	1.59
299.141	2.2	1.78	1.61
299.362	2.63	1.87	1.64
299.583	2.99	1.93	1.66
299.804	3.21	1.96	1.67
300.025	3.23	1.95	1.66
300.246	3.05	1.89	1.63
300.467	2.76	1.79	1.59
300.688	2.43	1.69	1.55
300.909	2.16	1.6	1.5
301.13	1.95	1.53	1.46
301.351	1.79	1.48	1.43
301.572	1.67	1.45	1.41
301.793	1.56	1.42	1.39
302.014	1.45	1.41	1.37
302.235	1.35	1.4	1.36
302.456	1.26	1.39	1.35
302.677	1.19	1.38	1.34
302.898	1.13	1.37	1.32
303.119	1.08	1.35	1.31
303.34	1.06	1.32	1.3
303.561	1.05	1.28	1.27
303.782	1.06	1.24	1.24
304.003	1.05	1.19	1.19
305	1.03	1.12	1.13
310	0.97	1.05	1.05
315	0.9	0.98	0.97

**Table S8.** Potassium mass fraction for OA particles from ZF2-samples (Sect. S1.1) as plotted against particle volume equivalent diameter ( $D_{ve}$ ) in Fig. 3.

	$D_{ve}$ [ $\mu\text{m}$ ]	Potassium Mass Fraction [%]
OA(acid)	0.40	16.3
	0.36	9.1
	0.30	8.5
	0.55	7.7
	0.36	7.2
	0.42	6.4
	0.57	5.2
	0.41	4.9
	0.39	4.5
	0.30	4.5
	0.34	4.2
	0.25	3.5
	0.45	2.8
	0.39	2.0
	0.41	1.7
	0.58	1.6
	0.91	1.6
	0.38	0.5
	1.06	0.4
0.34	0.0	
OA(mixed)	0.50	7.0
	0.37	3.9
	0.45	2.7
	0.35	0.0
	0.35	0.0

**Table S9.** Potassium mass fraction for OA particles from ATTO-samples (Sect. S1.1) as plotted against particle volume equivalent diameter ( $D_{ve}$ ) in Fig. 3.

	$D_{ve}$ [ $\mu\text{m}$ ]	Potassium Mass Fraction [%]
OA(acid)	0.35	5.2
	0.88	4.1
	0.43	3.4
	0.51	3.2
	0.27	3.0
	0.52	2.7
	0.41	2.6
	0.61	2.2
	0.67	1.5
	0.62	1.5
	1.07	0.6
	0.96	0.4
OA(mixed)	0.61	6.0
	0.30	4.5
	0.38	4.2
	0.48	3.7
	0.34	3.3
	0.59	3.3
	0.19	3.2
	0.48	2.7
	0.56	2.4
	0.48	2.2
	0.44	1.9
	0.43	1.6
	0.51	1.2
	0.80	1.2
	0.63	1.2
	0.74	1.1
	0.58	1.0
	1.02	1.0
	0.47	0.9
	0.62	0.8
	0.70	0.7
	0.41	0.6
	0.76	0.6
	0.87	0.6
	0.69	0.5
0.90	0.5	
0.65	0.5	
0.93	0.3	

OA(hydroxy)	0.33	10.6
	0.38	6.1
	0.54	2.6
	0.62	2.3
	0.74	2.0
	0.52	1.6
	0.80	1.4
	0.70	1.0
	0.99	1.0
	1.01	0.9
	0.75	0.8
	0.93	0.3
	Salts + OA	0.20
0.16		19.5
0.12		18.8
0.17		13.3
0.26		12.4
0.17		12.4
0.37		8.5
0.30		5.0
0.34		3.5









